



**University of
Zurich**^{UZH}

Monitoring coffee forest changes related to Participatory Forest Management in Ethiopia using satellite remote sensing

GEO 511 Master's Thesis

Author

Michelle Müller

15-710-312

Supervised by

Dr. Claudia Rööfli

Dr. Vladimir Wingate

Luca Heim (Caritas Switzerland)

Faculty representative

Prof. Dr. Alexander Damm

29.09.2020

Department of Geography, University of Zurich

Monitoring coffee forest changes related to Participatory Forest Management in Ethiopia using satellite remote sensing

Master Thesis

Michelle Müller

28.09.2020

Supervisor

Dr. Claudia Rösli

Co-Supervisors

Dr. Vladimir Wingate

Luca Heim; Caritas Switzerland

Faculty Member

Prof. Dr. Alexander Damm



Figure 1 Natural forest in Ethiopia containing wild coffee plants (Caritas Switzerland, Philipp Schütz, 2020)

Abstract

Over the last 40 years, Ethiopia has been affected by immense deforestation and forest degradation caused by different drivers. On the one hand, extreme weather events such as droughts, wildfires, or floods lead to strong forest degradation. On the other hand, anthropogenic activities have resulted in large-scale deforestation due to the rapidly increasing population demanding a stable livelihood. Consequently, the wild coffee forest and with it the wild coffee species 'coffea arabica' originating in Ethiopia are threatened.

For this reason, Participatory Forest Management (PFM) has been introduced approximately 20 years ago in wild coffee forest regions. The approach aims for forest conservation while simultaneously strengthen the cooperative's autonomy, facilitate access to the forest product market, and offer a higher price for the wild coffee in comparison to coffee growing on plantations. Therefore, the project leader party, for example Caritas Switzerland, works directly with the local communities and together they establish a forest management plan. The agreement allows for individual farmers to pick the wild coffee fruits and sell them for a raised price to receive a sustainable income and at the same time protect the natural forest.

Satellite remote sensing provides useful methods and interesting datasets to monitor and quantify the ongoing forest loss and document the impact of conservation efforts. Besides, it supports PFM evaluation by providing information on the forest extent and the existing land cover classes in the project regions and further enables understanding the impact of PFM measures on the forest. In this thesis, the applied approaches are supervised land cover classification, post-classification comparison for the change detection and the Continuous Degradation Detection (CODED) algorithm which is used to identify forest degradation. The results reveal less deforestation in PFM than in non-PFM regions over the measurement period of 20 years. Hence, PFM appears to have been applied successfully and it is recommended that more PFM projects are implemented in order to reduce forest loss.

In conclusion, the utilized remote sensing methods seem adequate to measure forest disturbances in coffee forest areas in Ethiopia. However, future research is suggested to include field data, local people's knowledge as well as forest expert opinions for the data validation. Furthermore, specific information on measurable characteristics of the different coffee forest systems, for example of wild and semi-wild coffee forests, would help distinguish them.

Acknowledgements

First, I would like to thank my supervisor, Dr. Claudia Rösli whose expertise influenced my workflow and perspective on the Master Thesis significantly. It is also due to her support that I felt motivated and well coached and benefitted from tips relevant for my future career. I very much appreciate her trust-based approach to this supervision.

Further, I would like to offer my special thanks to Dr. Vladimir Wingate for sharing his technical knowledge on Google Earth Engine and accompanying the progress of my thesis as well as being there for relevant questions.

I wish to acknowledge Luca Heim and Benjamin Schilling from Caritas Switzerland for offering an interesting research question connected to their forest projects in Ethiopia. The thesis improved owing to their project insights and collaboration with the Ethiopian colleagues and forest experts.

In addition, I am particularly grateful for the support provided by my boss Patricia Reichelt for her motivation during stressful times, for encouraging me to follow the time schedule and for pushing me with her critical feedback. Finally, I could not have completed my thesis without the help of my parents, brother and friend from University of Zurich, Alicia Hug.

Table of Contents

Abstract	2
Acknowledgements	2
Table of Contents	3
Abbreviations	6
1 Introduction	7
2 Research Background	8
2.1 Deforestation and forest degradation in Ethiopia	8
2.2 Coffee forest systems.....	9
2.3 Wild coffee conservation and Participatory Forest Management (PFM)	10
2.4 Satellite remote sensing for the monitoring of deforestation and forest degradation	11
3 Study areas and their characteristics.....	12
3.1 Study zones.....	12
3.2 Study kebeles	13
3.3 Typical climate in coffee forest areas	15
4 Data	16
4.1 Input data	16
4.1.1 Satellite data: Landsat 5, 7 and 8 imagery	16
4.1.2 Classifier training data	17
4.2 Supplementary data	18
4.2.1 Precipitation data	18
4.2.2 Data for the water and urban masks.....	18
5 Methods	19
5.1 Processing Tool: Google Earth Engine.....	19
5.2 Unsupervised classification	20
5.3 Supervised classification	21
5.3.1 Class definition	21
5.3.2 Random Forest classifier	22
5.3.3 Accuracy assessment of the classification	22
5.4 Change Detection.....	23
5.4.1 Change detection validation	24
5.4.2 Continuous Degradation Detection (CODED)	27
6 Results	29
6.1 Land cover changes in the study zones over the last 20 years.....	29
6.1.1 Analysis of the main study zone Keffa.....	29
6.1.2 Comparison of all five study zones.....	30
6.2 Forest change detection in the study zones over the last 20 years.....	31
6.2.1 Analysis of the main study zone Keffa.....	31
6.2.2 Comparison of all five study zones.....	33

6.3	Land cover changes, forest change detection and Participatory Forest Management in the kebeles	36
6.3.1	Analysis of Keshi kebele	36
6.3.2	Analysis of Chebere kebele	37
6.3.3	Analysis of Giz Meret kebele	39
6.3.4	Analysis of Soddu Lelaftu kebele.....	41
6.3.5	Comparison of all ten study kebeles	44
7	Discussion.....	46
7.1	Data.....	46
7.2	Methods	46
7.2.1	Unsupervised classification	46
7.2.2	Class definition for the supervised classification	47
7.2.3	Accuracy assessment of the supervised classification	47
7.2.4	Change detection	48
7.2.5	Validation of the change detection	48
7.2.6	Continuous Degradation Detection (CODED)	48
7.3	Results	49
7.3.1	Land cover changes and forest disturbances in the study zones	49
7.3.2	Participatory Forest Management.....	50
7.3.3	Place names	51
7.3.4	Recommendations for Caritas Switzerland.....	51
7.4	Additional topics.....	51
7.4.1	Wild and semi-wild coffee forest	51
7.4.2	Climate.....	51
7.4.3	Sentinel-2.....	52
8	Conclusion and Outlook	52
9	References	53
9.1	Table of figures.....	58
9.2	Table of figures Appendix	60
9.3	List of tables	65
9.4	List of tables Appendix.....	65
10	Appendix I Methods	66
10.1	Study on the land cover classes occurring in the Ethiopian study zones.....	66
10.2	Study on the classifier performance	66
10.3	Supervised classification validation assessment.....	67
10.4	Documentation of the change detection validation.....	68
10.4.1	Keffa zone.....	68
10.4.2	Sheka zone.....	72
10.4.3	Illubabor zone	76
10.4.4	Bench Maji zone	81

10.4.5	Bale zone	85
10.5	Google Earth Engine scripts	91
11	Appendix II Results	92
11.1	Sheka zone	92
11.2	Illubabor zone	94
11.3	Bench Maji zone	96
11.4	Bale zone	98
11.5	Keshi kebele	100
11.6	Chebere kebele	101
11.7	Giz Meret kebele.....	101
11.8	Sodu Lelaftu kebele	102
11.9	Bergi kebele.....	102
11.10	Mankira kebele	104
11.11	Keja Araba kebele.....	106
11.12	Seriti kebele	108
11.13	Muti kebele	109
11.14	Ganga kebele	111
11.15	All study kebeles	112
12	Personal declaration.....	113

Abbreviations

API:	Application Programming Interface
BR:	Biosphere Reserve
CART:	Classification And Regression Tree
CHIRPS:	Climate Hazards Group InfraRed Precipitation with Station Data
CODED:	Continuous Degradation Detection
DEM:	Digital Elevation Model
ETM+:	Enhanced Thematic Mapper Plus
EVI:	Enhanced Vegetation Index
GEE:	Google Earth Engine
GIS:	Geographic Information System
GV:	Green Vegetation
L1T:	Level one terrain corrected
LTS:	Landsat Time Series
LULC:	Land use/land cover
m.a.s.l.:	meters above sea level
NDFI:	Normalized Difference Fraction Index
NDVI:	Normalized Difference Vegetation Index
NDWI:	Normalized Difference Water Index
NPOC:	National Point Of Contact for satellite images
NPV:	Non-Photosynthetic Vegetation
OLI:	Operational Land Imager
PFM:	Participatory Forest Management
RF:	Random Forest
SLC:	Scan Line Corrector
SNNP:	Southern Nations, Nationalities, and Peoples
SVM:	Support Vector Machine
TM:	Thematic Mapper
UZH:	University of Zurich

1 Introduction

The importance of monitoring the Ethiopian tropical forest has increased due to high amounts of deforestation and degradation (DeVries et al. 2016). Since the 1960s, the country has been affected by large-scale forest loss (Gashaw et al. 2014) which resulted in the remaining forest area of 11.4% (Hailemariam et al. 2016). The related land use and land cover (LULC) changes are a major concern (Hailemariam et al. 2016), particularly in the southwestern part of Ethiopia (Wubie 2015). Generally, the drivers can be distinguished in natural causes (Hailemariam et al. 2016) and human-induced forest damage (Wubie 2015). The Afromontane rain forests in Ethiopia are in danger due to the continuing forest loss and degradation (Schmitt et al. 2006). Consequently, the wild coffee species ‘*coffea arabica*’ growing in the rain forests is threatened (Tadesse et al. 2014). Furthermore, the coffee production intensification and the introduction of cultivar species endanger the original arabica coffee (Hylander et al. 2013; Aerts et al. 2017). As the arabica coffee constitutes a quarter of the total export profits of Ethiopia, it is the main agricultural good and crucial for the livelihood of the coffee farmers (Moat et al. 2017). Hence, the wild arabica coffee species must be conserved (Aerts et al. 2017). Participatory Forest Management (PFM) is one example of a sustainable coffee forest management process and has been applied in Ethiopia since the late 1990s (Lemenih et al. 2015). The approach protects the forest environment and simultaneously improves the livelihoods of the community applying it (Winberg 2011). In other words, this coffee certification system attempts to encourage the farmers to manage the forest sustainably and in exchange, they are able to sell the certified wild coffee for a higher price (Bewket 2002; Takahashi et al. 2017). Caritas Switzerland functioning as a leading party in the implementation of PFM projects in southern Ethiopia intends to monitor the PFM areas with satellite data. Therefore, the organization approached the National Point of Contact for satellite images (NPOC) at University of Zurich (UZH) and provided a specified field of research matching their interests. Subsequently, this thesis has been established as a cooperative work between UZH and Caritas Switzerland in order to explore the potential of satellite data and methods for the monitoring of Caritas Switzerland’s forest conservation projects.

In literature, the impacts of forest conservation programs on deforestation and degradation remain largely unexamined (Takahashi et al. 2017). The studies lack of an elaborated monitoring system to understand the performance of the sustainable forest management (Winberg 2011). Generally, research focuses strongly on the analysis of the social aspects and neglects the environmental part of PFM (Winberg 2011). Due to high costs for frequent field trips, forest monitoring is not conducted (Winberg 2011). Although satellite-based remote sensing enables regular forest examination through land cover change and tropical deforestation detection, such observations are limited in Ethiopia (Dupuis et al. 2020). Existing LULC products are not suitable for local scale studies in the mountainous regions of that country and therefore researchers created novel LULC products suiting their need (Hailu et al. 2018). In summary, in depth analysis of the last two decades of coffee forest changes in southern Ethiopia using the full archive of freely available remote sensing data has not yet been undertaken and a thorough evaluation of the PFM impacts on the forest is missing.

Hence, this thesis extends on previous work by exploring the forest and land cover changes in Ethiopian coffee growing areas since 2000. This year has been chosen due to PFM project introductions starting around that time. The goal of the study is to measure the forest cover extent and forest degradation by using satellite remote sensing over the selected timespan and link it to sustainable forest management practices. Accordingly, this research aims to profoundly analyse forest alterations in the study areas over the last 20 years and to measure the rate of forest change, its magnitude and time of occurrence. Moreover, the objective is to find drivers of forest change processes and to compare PFM and non-PFM coffee forest areas. Whether remote sensing approaches can distinguish between the different coffee forest systems is intended to be investigated as an additional research goal.

2 Research Background

This chapter explains in more depth the reasons for deforestation and forest degradation in Ethiopia and describes the connected consequences. Furthermore, the four different coffee forest systems including wild forest, semi-forest, and garden coffee as well as coffee plantations are reviewed. After that, Participatory Forest Management is introduced in the context of coffee conservation. The last subchapter is devoted to previous work and the advantages of the use of satellite remote sensing for the monitoring of deforestation and forest degradation.

2.1 Deforestation and forest degradation in Ethiopia

The drivers of the deforestation and degradation in Ethiopia are diverse and can be categorized into five groups illustrated in Figure 2. First, the rapidly increasing population (Wubie 2015; Gashaw et al. 2014) causes pressure on the forest which is expressed in resettlements (Wubie 2015) and urbanization (Hailemariam et al. 2016). Due to scarcity of forest resources in some parts of Ethiopia, people move to areas where they are still able to sustain their livelihood (Wubie 2015). Usually, the income can be secured by living close to a village or city. Consequently, trees are cut down to create space for the growing towns (Hailemariam et al. 2016). Second, low control of agricultural practices leads to extensive cultivation (Wubie 2015) and overgrazing (Winberg 2011) resulting in increased forest degradation. Commercial farming and agricultural land expansion are typical phenomena to meet the needs of the population and particularly those of the farmers (Winberg 2011). Furthermore, the forest is converted into plantations to reach higher yields and sell more coffee (Hylander et al. 2013). Third, the forest resources in southern Ethiopia are exploited (Wubie 2015) and used unsustainably (Dresen 2011b). Mainly, commercial and informal logging destroy very large forest areas (Dessie et al. 2007; Hailemariam et al. 2016). Equally important, large amounts of wood are collected for household tasks, construction and as firewood (Wubie 2015). Additional examples of resource abuse in the Ethiopian forests are wildlife hunting as well as the illegal extraction of forest products (Winberg 2011). The fourth driver of deforestation and degradation is political instability as it contributes to uncontrolled remote forested regions with changing land property rights and concessions for coffee (Dresen 2011b). The fifth group contains natural causes including floods, intense precipitation (FAO 2011) and wildfires (Pasquarella et al. 2016).

The consequences of forest degradation and deforestation affect multiple fields described in Figure 2. The forest is threatened by a higher probability for landslides (Dresen 2011b) and soil erosion (Hailemariam et al. 2016) because the protective root system has been removed. Moreover, the forest biodiversity and its related ecosystem services are reduced and species become extinct (Hailemariam et al. 2016). In addition, deforestation provokes increasing greenhouse gas emissions (Moges et al. 2010; Hailemariam et al. 2016). Another effect related to a changing climate are extreme weather conditions such as droughts (Hailemariam et al. 2016). The concerned communities rely on a stable income based on the forest resources (Moat et al. 2017) which is not guaranteed in degraded forests. Therefore, the environmental degradation decreases the food security and more forest areas become exploited and damaged (Winberg 2011). Thus, the awareness towards tropical forests in Ethiopia rose as alterations of the ecosystem influence the worldwide climate change and biodiversity loss (DeVries et al. 2016). The future of the forest and the people living there are closely linked and depend on each other (Dresen 2011b).

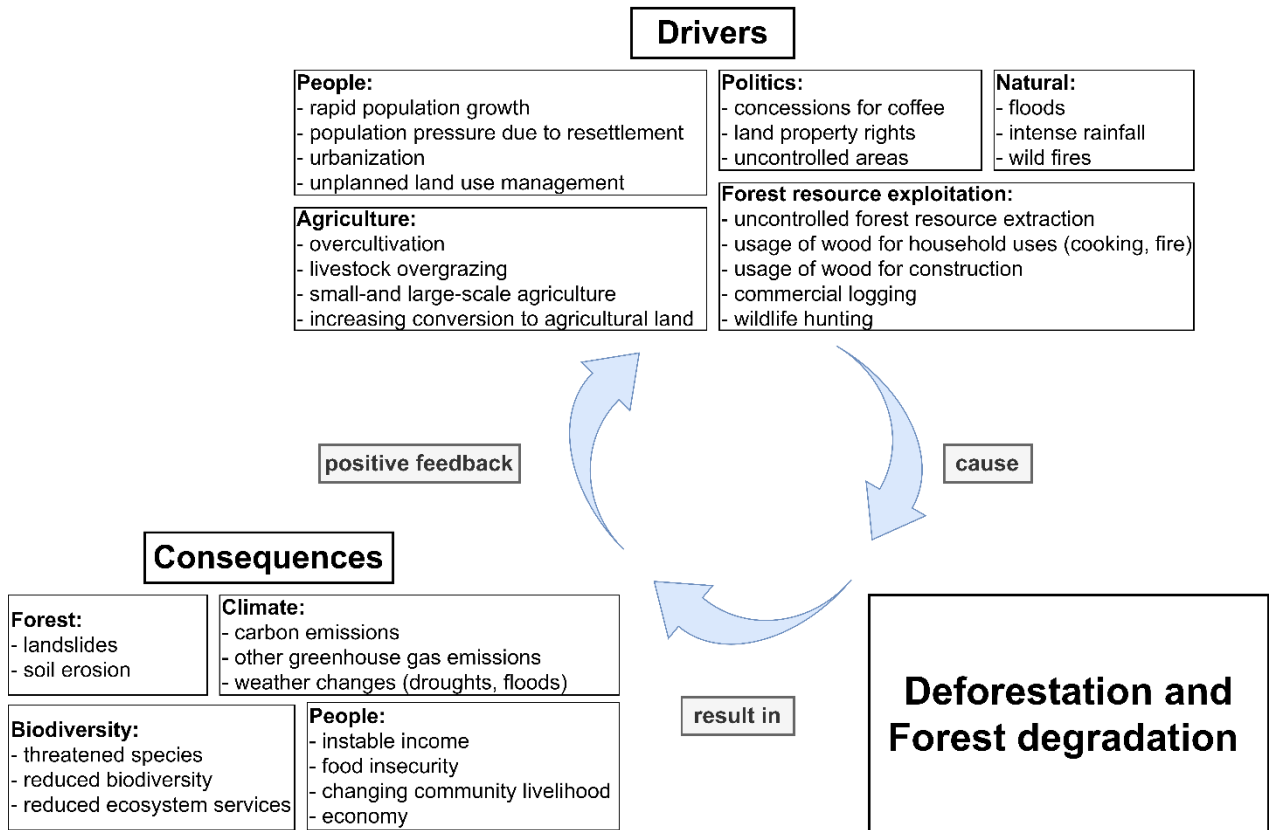


Figure 2 Illustration depicting the drivers of deforestation and forest degradation in Ethiopia as well as the resulting consequences which in turn reinforce the drivers

2.2 Coffee forest systems

Depending on the management type and intensity as well as on the yield, four typical coffee growing systems are distinguished (Hylander et al. 2013) demonstrated in Figure 3. Since the wild forest coffee is unmanaged, the farmers picking the wild coffee fruits is not counted as intervention (Craves 2011). In comparison, the semi-forest coffee is sustainably managed by the farmer cooperatives (Hylander et al. 2013) through the thinning of canopy and removing of competitive undergrowth shrubs (Workie 2015; Craves 2011). These procedures enhance the coffee plant growing conditions (Hylander et al. 2013) and intend to rise the wild arabica coffee yield (Craves 2011). Regions with semi-forest coffee management strategies indicated lower deforestation rates because otherwise the land would be converted to cropland, grazing land or plantations (Aerts et al. 2017; Hylander et al. 2013). Thus, those two coffee growing systems are promoted in protected forest areas (Wiersum et al. 2008). However, as the yield is lower compared to garden coffee or plantations, wild and semi-wild coffee forest is removed in favour of the higher yield growing systems (Takahashi et al. 2017; Moat et al. 2017). Although the modern coffee growing systems increase the sales and therefore the income, the drawbacks are active deforestation, soil erosion and chemical runoff (Takahashi et al. 2017).

	wild forest coffee	semi-forest coffee	garden coffee	coffee plantation
management type	unmanaged	sustainably managed	managed	unsustainably managed
management intensity				
yield				

Figure 3 Visualization of the four different coffee growing systems in Ethiopia emphasizing their differences in management type and intensity as well as in the yield

2.3 Wild coffee conservation and Participatory Forest Management (PFM)

Wild coffee forest conservation is crucial for the natural environment so as to protect the biodiversity and wild species of the forest, such as the wild arabica coffee (Takahashi et al. 2017). However, difficulties and obstacles arise for the implementation of sustainable coffee forest management systems. For instance, the farmers demand a sustainable income and a direct profit from the coffee protection (Aerts et al. 2017). Therefore, adapted measures are proposed to support the farmers' requirements (Hylander et al. 2013). There exist multiple examples of certification systems (Aerts et al. 2017) all having the primary goal to prevent further deforestation and conversions of wild forest into plantations (Hylander et al. 2013).

One commonly applied coffee conservation approach in Ethiopia is called Participatory Forest Management (PFM) (Winberg 2011). A pivotal aspect of that system is the active participation of the village community in the forest conservation process (O'Hara 2013). While participatory managed forests belong to the state (Walle et al. 2019), the individual farmers receive the right to harvest wild coffee in their allocated forest area (Takahashi et al. 2017). When PFM is implemented, the leader party discusses a tailored management plan with the community, illustrated in Figure 4. PFM includes a social and an environmental part (Winberg 2011), however, efforts and time usually concentrate on one depending strongly on the community's essentials (Takahashi et al. 2017). The social part contains for instance improving governmental support and enhancing the communication between stakeholders, whereas the environmental part aims to reduce biodiversity loss, forest degradation and deforestation (Winberg 2011).

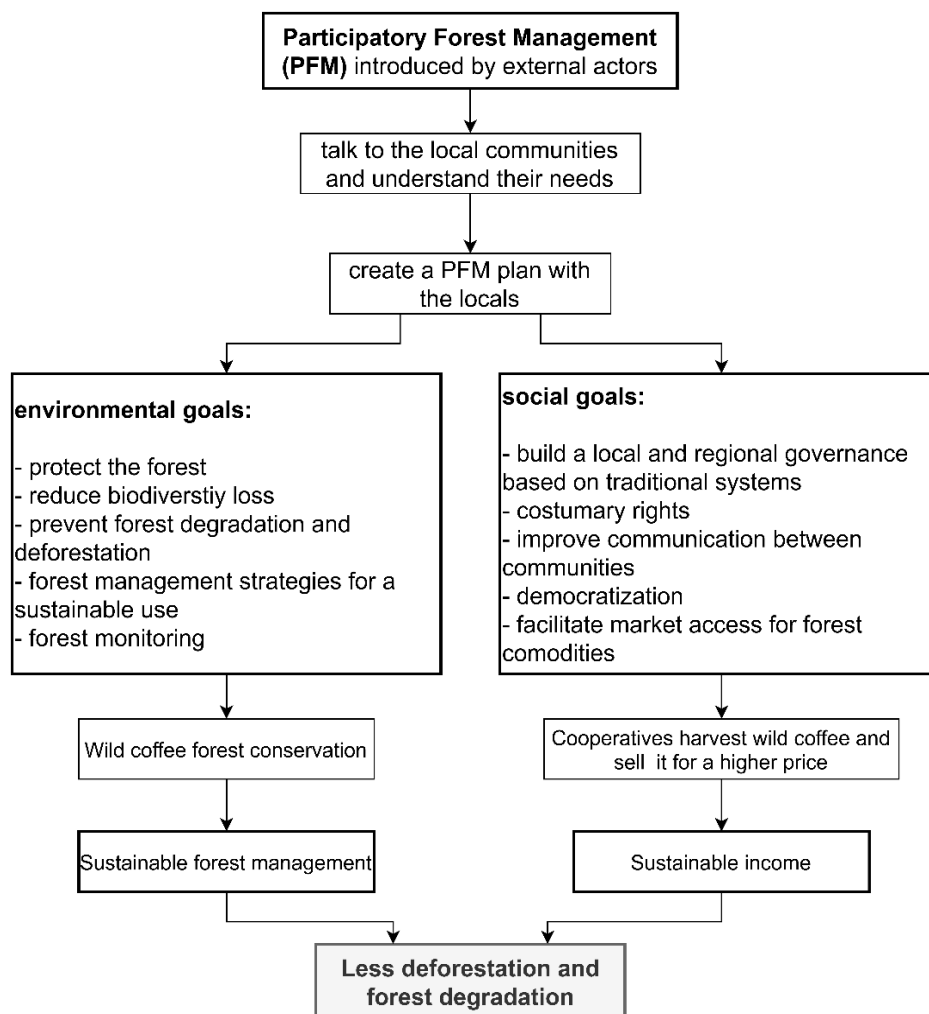


Figure 4 Graphic showing a usual PFM implementation process emphasizing the environmental and social part, their goals, and outcomes

2.4 Satellite remote sensing for the monitoring of deforestation and forest degradation

Sustainable forest management systems such as PFM require a way to monitor and evaluate the applied actions (Winberg 2011; Foody 2003). Primarily, in the beginning of PFM implementation the forest extent needs to be measured and forest maps created (Winberg 2011). Accordingly, satellite remote sensing provides powerful datasets and methods to continuously collect information on deforestation and degradation with high spatial resolution (DeVries et al. 2015; 2016). For its various advantages, remote sensing has been employed in forest-related studies for a long time (Lillesand et al. 2015). For instance, the costs and time investment are lower when using satellite remote sensing instead of gathering field data (Hadi et al. 2018). Another benefit is the small effort necessary to regularly monitor large and remote areas (Hadi et al. 2018).

In Ethiopia, several studies have already used remote sensing and Geographic Information System (GIS) approaches to analyse the land cover transitions in coffee forest areas (Wubie 2015; Gashaw et al. 2014). More specifically, land use and land cover changes (LULC) are observed, quantified and mapped (Hailemariam et al. 2016). These land cover maps provide an informed basis for the decision makers (Aerts et al. 2017). By exploiting space-born data with high temporal resolution, forest disturbances including degradation can be measured (Hansen et al. 2008; DeVries et al. 2016). For this reason, sustainable forest planning is supported by enabling the adaption of sustainable management criteria based on the analysis outputs (Wubie 2015; DeVries et al. 2015).

3 Study areas and their characteristics

The main study zone Keffa and the four additional zones are described in detail in the following section. Thereafter, the ten study kebeles which relate to PFM are specified and mapped. The typical coffee forest environment climate is presented in subsection 3.3.

3.1 Study zones

The main study area is Keffa zone, emphasized in Figure 5, which serves as the pilot region to develop a satellite remote sensing-based coffee forest monitoring approach. It is located in the ‘Southern Nations, Nationalities, and Peoples’ (SNNP) region and has been chosen because sustainable coffee forest management actions have been applied since 2004 (GIZ 2016). The zone covers an area of over 10’500 km² (El Ouaamari et al. 2014) listed in Table 1 and the vegetation consists of evergreen rain forest with optimal coffee plant growing conditions (DeVries et al. 2016). Commonly, the wild coffee grows in the humid mountainous forests in South Ethiopia between 1’000 and 2’000 meters above sea level (m.a.s.l) as an understory tree (Schmitt et al. 2006; Tadesse et al. 2014; Moat et al. 2017; Aerts et al. 2017).

In Keffa an UNESCO Biosphere Reserve (BR) called Kafa was established in 2010 and lies in the northern part of the zone (Dresen 2011b). It promotes forest and wild coffee protection actions, for instance by restoring the natural forest and sensitize people to the sustainable use of forest resources (DeVries et al. 2016). Usually, a BR consists of three different sectors. Namely, a protected core with targeted conservation programs (Aerts et al. 2017), a buffer zone with mixed nature-related land uses, and an agriculturally dominated transition sector (Dresen 2011b).

Bale, Bench Maji, Illubabor and Sheka are the four additional study zones analysed in this thesis (Wubie 2015; Hailemariam et al. 2016). The selection is based on the fact that most PFM intervention areas are located in the Oromia and SNNP regions (Winberg 2011) which are the major coffee growing areas in southern Ethiopia (Moat et al. 2017). Illubabor and Sheka contain UNESCO Biosphere Reserves that were accepted in 2010, respectively 2012 (Aerts et al. 2017).

Table 1 List of the five study zones displaying the region name, zone name, capital city and the zone size. Highlighted with a frame is the main study zone Keffa (OCHA 2017).

Region name	Zone name	Capital city of the zone	Zone size [km ²]
SNNP	Keffa	Bonga	10’520
Oromia	Bale	Robe	54’640
SNNP	Bench Maji	Mizan Teferi	18’990
Oromia	Illubabor	Metu	15’530
SNNP	Sheka	Masha	2’350

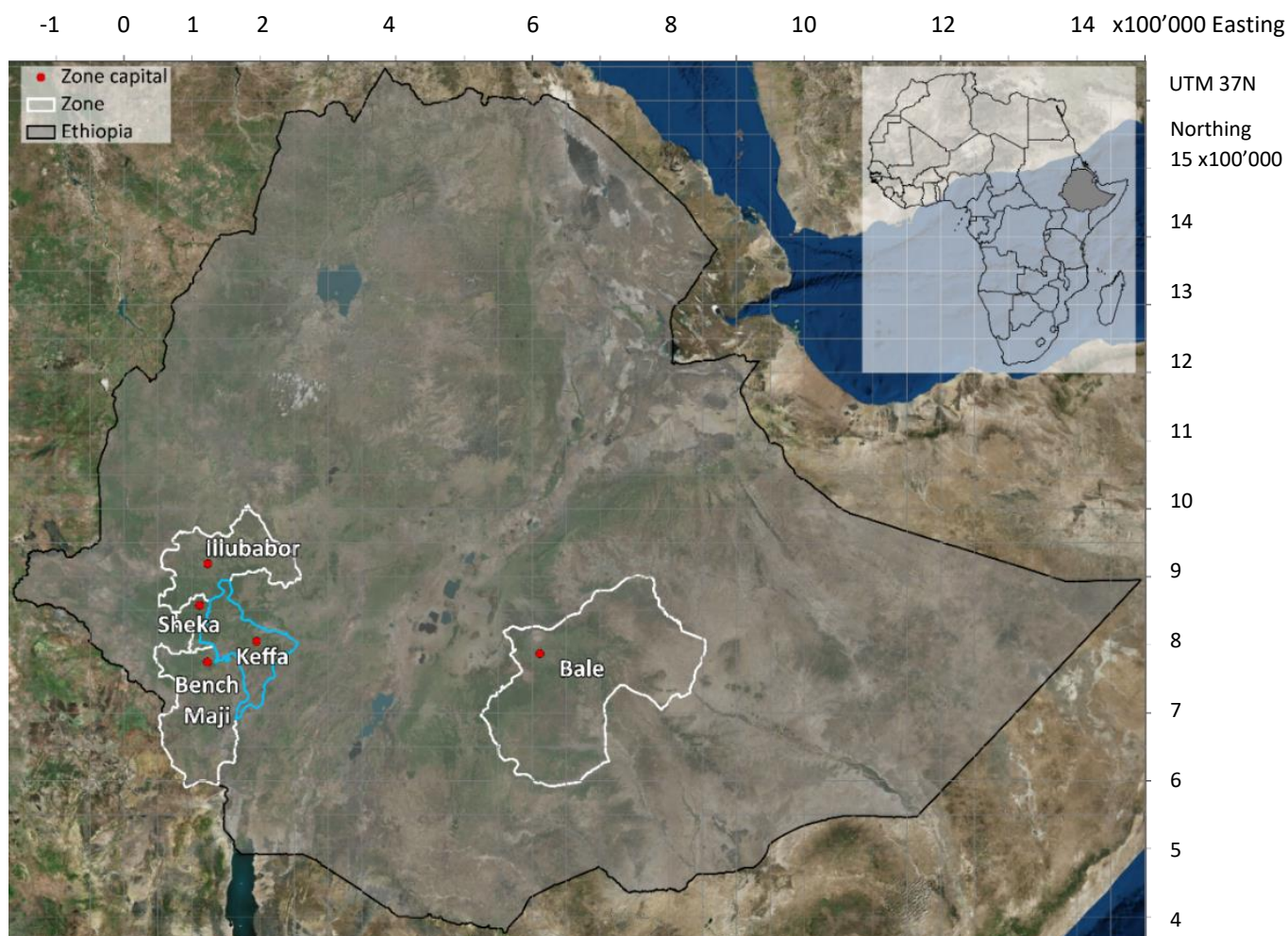


Figure 5 Map illustrating the location of the five study zones and their capital cities in Ethiopia. The main study zone Keffa is highlighted in light blue (openAfrica 2019).

3.2 Study kebeles

In Ethiopia, the smallest administrative unit is called ‘kebele’. Their size varies between 15 and 100 km² and kebeles can be composed of one or more organized cooperatives which are responsible for the sustainable utilization of the community forest (Plan Vivo 2014). For this thesis, ten kebeles listed in Table 2 have been chosen in order to analyse the effect of PFM on the forest (Winberg 2011; Dresen 2011a). Four kebeles will be evaluated in detail and are called Keshi, Giz Meret, Chebere and Sodu Lelaftu mapped in Figure 6.

Table 2 List of the 10 study kebeles displaying information on the zone name, kebele name, PFM status and kebele size. The four kebeles analysed in detail are emphasized with a black frame.

Zone name	Kebele name	PFM (Yes/No)	Kebele size [km ²]
Keffa	Keshi	Yes	35
Bench Maji	Giz Meret	Yes	17
Illubabor	Chebere	No	24
Bale	Sodu Lelaftu	No	167
Keffa	Muti	No	12
Keffa	Keja Araba	Yes	51
Keffa	Mankira	Yes	10
Bench Maji	Bergi	Yes	14
Bench Maji	Seriti	No	23
Sheka	Ganga	No	38

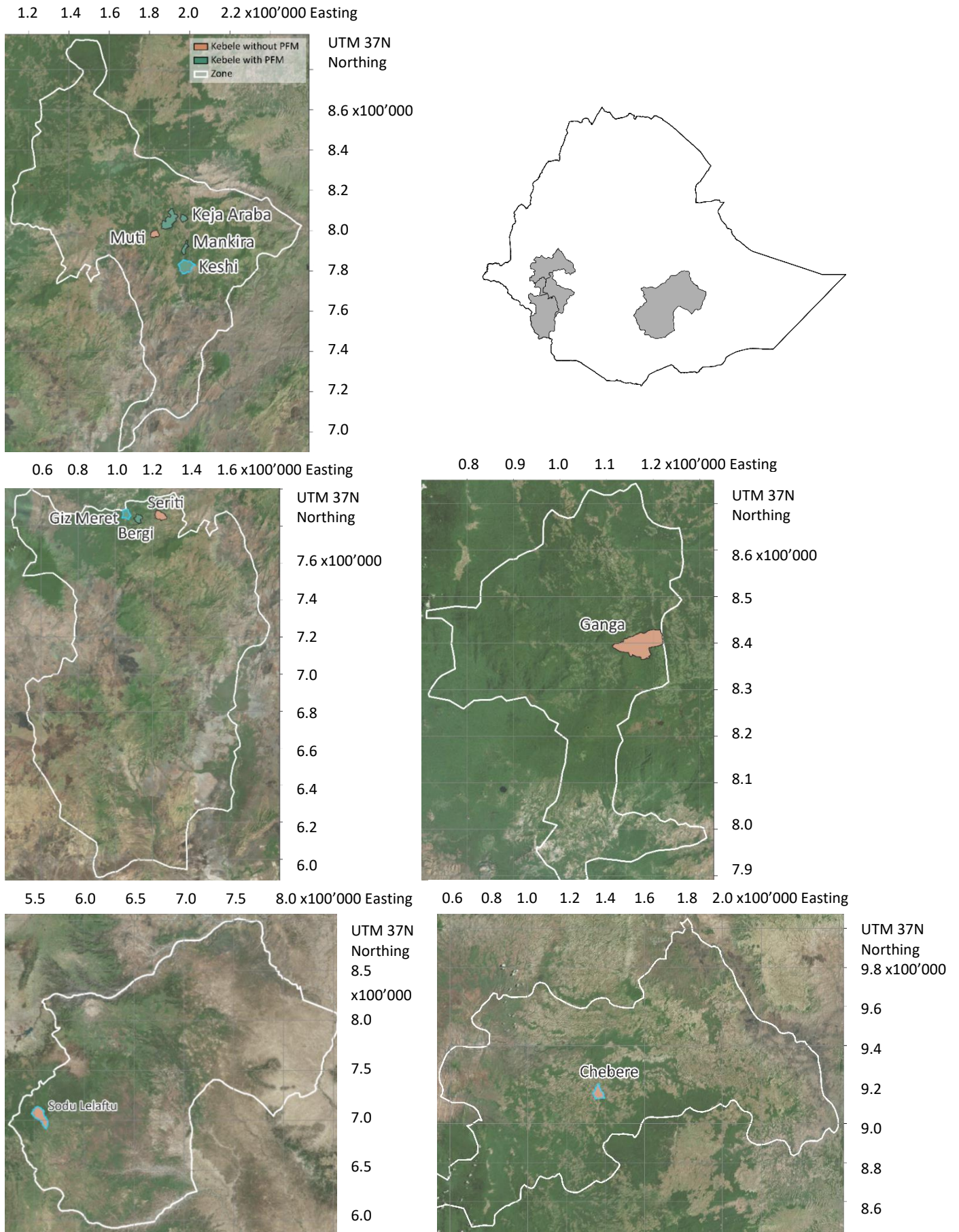


Figure 6 Left: Overview map of all five study zones containing the 10 study kebeles. From top left to bottom right: Keffa zone, location of the study zones in Ethiopia, Bench Maji zone, Sheka zone, Bale zone, Illubabor zone. Marked with a light blue frame are the in depth discussed kebeles (openAfrica 2019; Services ArcGIS 2015).

3.3 Typical climate in coffee forest areas

Generally, the climate in the coffee forest areas is described as cool-tropical and contains three distinct seasons (Hylander et al. 2013) summarized in Figure 7. The dry season lasting from October to February is the coffee harvesting period. The time between February and May is regarded as the start of the wet season if the precipitation pattern is unimodal which refers to one rain season per year. Otherwise the same period represents a distinct short rain season and the rainfall pattern is called bimodal. The subsequent months are the main wet season. In average, the annual precipitation lies between 1'500 and 2'100 mm (Moat et al. 2017) and the ideal coffee growing temperature is around 20° Celsius (Workie 2015).

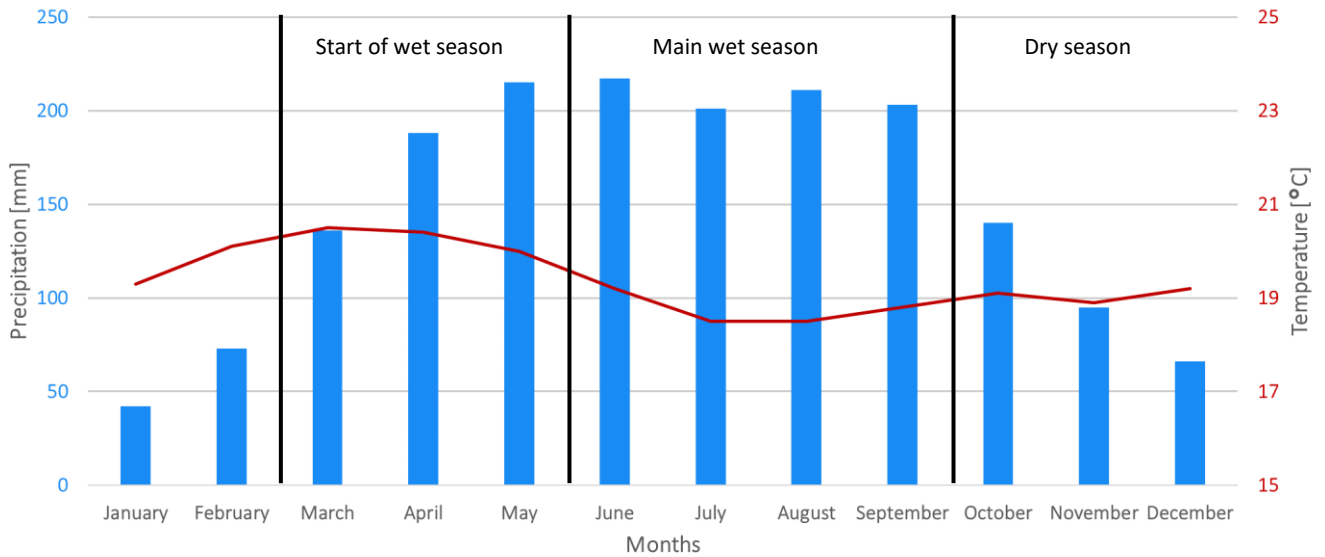


Figure 7 Typical climate diagram for a coffee forest area. This example shows the climate for the zonal capital city Bonga located in Keffa with an unimodal precipitation pattern (World Weather Online 2020).

4 Data

This section starts with a description of the input Landsat images and their compositing followed by the definition of the classifier training data. Subchapter 4.2 considers supplementary data which contains material on the rainfall in Ethiopia and the water and urban masking data used for the supervised classification.

4.1 Input data

4.1.1 Satellite data: Landsat 5, 7 and 8 imagery

Satellite imagery data collected by the Landsat mission 5, 7 and 8 build an earth surface observation time series of over 30 years at moderate temporal and spatial resolution (Roy et al. 2016; Lillesand et al. 2015). Landsat data is commonly used to monitor earth resources and processes (Lillesand et al. 2015) and to analyse land cover changes (Sidhu et al. 2018). Particularly in forest environments, the extracted information supports disturbance detection (Cohen et al. 2017). Different sensor types are mounted on the various satellites. Landsat 5 carries the Thematic Mapper (TM), Landsat 7 the Enhanced Thematic Mapper Plus (ETM+) and Landsat 8 the Operational Land Imager (OLI) (Lillesand et al. 2015; Roy et al. 2016). Due to differences in calibration and wavebands in the spectral resolution, a harmonization between OLI and ETM+/TM is conducted with appropriate statistical transformations between the sensor bands (Roy et al. 2016). Level one terrain corrected (L1T) products are used because they are radiometrically calibrated and georeferenced as well as atmospherically corrected (Pasquarella et al. 2016).

Due to technical problems of the satellite missions 5 and 7, useful Landsat data over Ethiopia is missing between June 2003 and April 2008 (Chen et al. 2012) as well as from November 2011 to February 2013 until Landsat 8 was launched successfully (Roy et al. 2016) visualized in Figure 8. On May 31st, 2003 the scan line corrector (SLC) of Landsat 7 failed which usually shifts the sensor line of sight backwards and thus compensates the satellite's forward movement. All subsequently gathered images show a zig zag pattern along the ground track (Lillesand et al. 2015) and around 22% of the pixels in a scene remain unscanned (Chen et al. 2012). Gap filling algorithms try to overcome this issue (USGS 2004). Nevertheless, the usefulness of recent Landsat 7 data varies greatly depending on the purpose (Chen et al. 2012). At the same time, the solar array drive of Landsat 5 was malfunctioning and therefore affecting the data availability (Chen et al. 2012). Moreover, the Thematic Mapper carried on Landsat 5 was shut down in November 2011 due to an electronic failure (Chen et al. 2012).

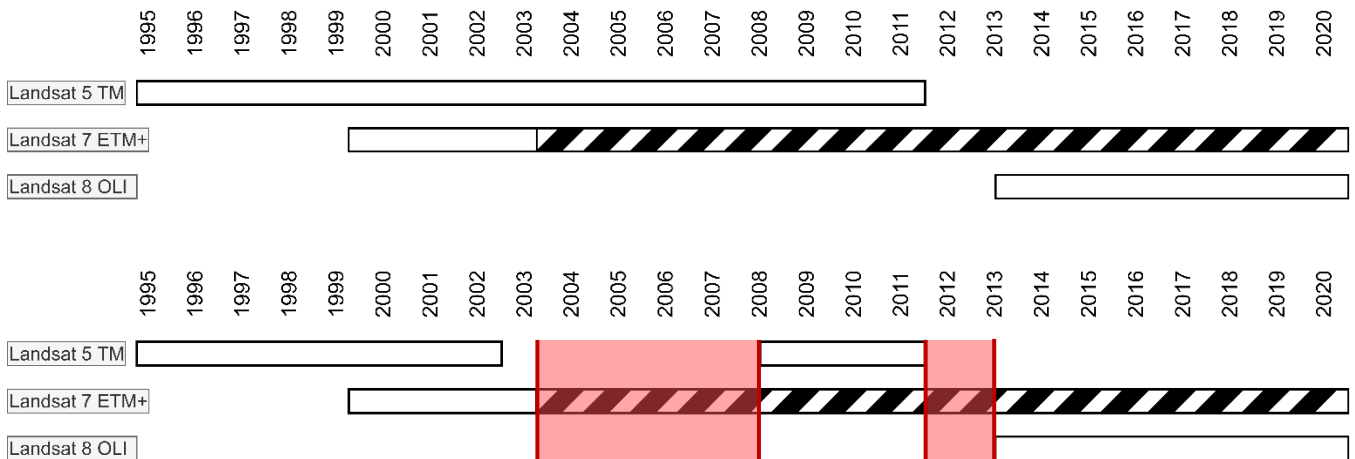


Figure 8 Top: Timeline of the general imagery availability of Landsat 5, 7 and 8 (1995-2020) with the SLC-off status marked as hatched bar, Bottom: Timeline of the Landsat 5, 7 and 8 imagery availability (1995-2020) over the study zones in Ethiopia with the missing years marked in red

Clouds, shadow, haze and missing pixels are typical concerns using optical remote sensing data, principally in tropical forest regions (Pimple et al. 2018) such as over the Ethiopia rain forest (Dorais et al. 2011). Hence, the temporal resolution of Landsat is not high enough to acquire completely disturbance-free scenes (Dorais et al. 2011) which may result in faulty land cover classifications and change detections (Pimple et al. 2018). A common way to minimize the issues is creating median composites (Lillesand et al. 2015; Dorais et al. 2011) although minor disturbances remain. The compositing method stacks multi-temporal satellite data and extracts the median band value per pixel which is then represented in a newly created image (Flood 2013; Lillesand et al. 2015).

With yearly dry season composites covering all years between 2000 and 2020, several problems emerge. For example, composites containing Landsat 7 data show disturbances even though a gap filling algorithm has been applied. Consequently, the classification is disrupted. Furthermore, a dry season of seven months is too long to obtain comparable inter-annual vegetation states. Therefore, another approach has been selected which aggregates five median dry season composites to one collection and after that extract the median band value. With this technique, a shorter dry season of three months is implemented (1st of December to 1st of March). As Landsat 7 generally contaminates the analysis, its data is excluded. Final high-quality composites exist for the years 1995-2000 (Landsat 5), followed by the 2010-2015 composite (Landsat 5 and 8) and the 2015-2020 image composed by Landsat 8 scenes exclusively.

The Normalized Difference Vegetation Index (NDVI) is crucial for vegetation monitoring purposes. Therefore, it is attached as a separated band to the images so as to add valuable information to each pixel. Vegetation commonly represents high NDVI values whereas other land cover types show low values (Lillesand et al. 2015). In some cases, the use of the Enhanced Vegetation Index (EVI) is more appropriate with its adjustment factor that reduces soil background effects (Lillesand et al. 2015).

4.1.2 Classifier training data

The ESA Sentinel-2A land cover product of the year 2016 is utilized as training data for the supervised classification (CCI Land Cover (LC) Team 2016). Having a high spatial resolution of 20 meters and being relatively recent, it suits the purpose. Nonetheless, the thematic map is continuously refined and not yet a finalised product. Table 3 lists the final chosen land cover classes.

Table 3 List of the seven final land cover classes selected based on a pre-study. In addition, their original class value and class name before the reclassification are displayed together with the class definition (CCI Land Cover (LC) Team 2016)

Final class value	Final class name	Original class value and name	Original class definition
0	Forest	1 - Tree cover area	- tree canopy covers more than 15% of the pixel area - tree canopy cover > shrub cover > grassland cover - a tree is a woody plant with a single stem and has a defined crown, the plant is at minimum three meters in height
1	Shrubland	2 - Shrub cover area	- shrubland covers more than 15% of the pixel area - shrub cover > tree canopy cover > grassland cover - a shrub is a woody stemmed plant and is smaller than three meters in height
2	Grassland	3 - Grassland	- grassland covers more than 15% of the pixel area - grassland cover > tree canopy cover > shrub cover - grassland consists of herbaceous plants without stem and no definite firm structure
3	Bare land	7 - Bare areas	- sum of the vegetation canopy cover is less than 4% - no artificial cover made by humans - possible covers include bare rock, sand and deserts
4	Cropland	4 - Cropland	- covers more than 50% of the pixel area - a cropland area is minimal 30 meters wide and sowed or planted - can be harvested at a minimum of once per year - definition from a remote sensing view - can have trees or woody vegetation with less than 20% canopy cover - consists mainly of herbaceous cover
5	Water	10 - Open water	- covers more than 50% of the pixel area - permanent water cover except under particular conditions - based on the Global Surface Water product from JRC/EC
6	Urban	8 - Built-up	- covering more than 50% of the pixel area - defined on the Global Human Settlement Layer from JRC/EC and on the Global Urban Footprint from DLR

4.2 Supplementary data

4.2.1 Precipitation data

In this study, the precipitation data stems from satellite and in-situ measurements merged in the Climate Hazards Group InfraRed Precipitation with Station Data (CHIRPS) dataset (Google Earth Engine 2020). The average daily precipitation is computed for all the five study zones and its capital cities. In addition, world weather (World Weather Online 2020) provides mean monthly rainfall data for the capital cities. Rainfall or its absence might be a reason for forest degradation processes and is therefore included in the analysis of the forest loss results.

4.2.2 Data for the water and urban masks

Water and urban are two classes that are added as masks to the classified land cover map. In other words, the urban mask is integrated first to the thematic map because otherwise urban would obscure parts of the water bodies. The urban mask has been tested with the nightlight dataset which looked promising first but turned out to be inappropriate in rural areas of Ethiopia as they do not show enough light. Therefore, the ‘United Nations adjusted population density’ has finally been chosen (Google Earth Engine 2020). It provides a layer for every five years and the threshold is set to 400 estimated persons per square kilometre to detect the most critical cities and villages. For the water mask, several datasets have been checked. Some already offer ready-to-use mask products, whereas others need some processing first. A mask based on Sentinel-2 was created in the beginning, but it missed vital water bodies and produced noisy results lacking a clear shape visualized in Figure 9. In the end, the Hansen water mask is chosen due to its spatial resolution of 30 meters and the coverage of lakes and larger rivers illustrated in Figure 10. Generally, the chosen study zones contain little water areas.

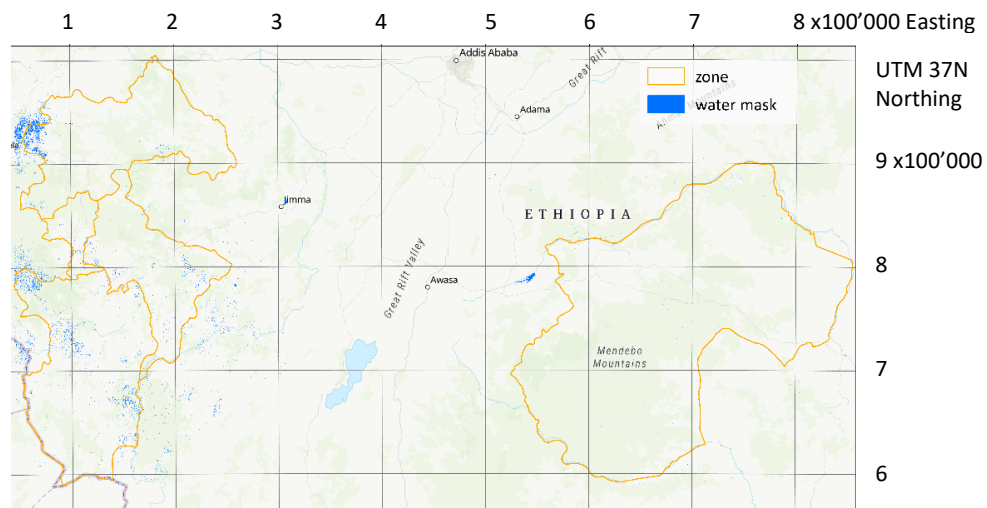


Figure 9 Water mask created with a Sentinel-2 one-year composite. The water mask does not cover the real water areas, for example the lakes in the middle of the scene are not detected.

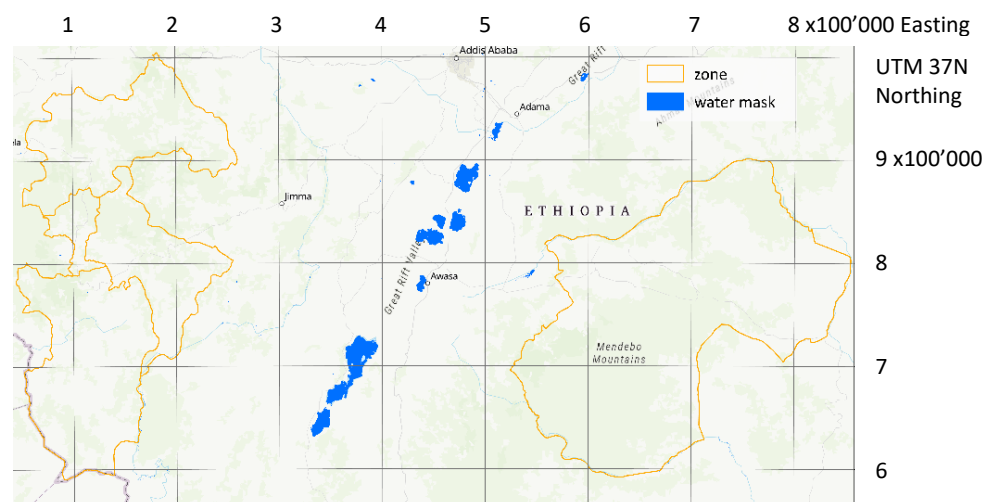


Figure 10 Water mask based on the Hansen dataset. The important water bodies are identified and even smaller water surfaces such as rivers are masked.

5.2 Unsupervised classification

While the unsupervised classification approach aggregates spectral clusters automatically which are labelled by the user in a second step, the supervised classification method trains the classifier with data selected beforehand (Lillesand et al. 2015). An advantage of the unsupervised classification result is that it provides information on the study area for image analysts unfamiliar with the region (Hailemariam et al. 2016).

In this study, the unsupervised classification approach includes the following spectral bands for training: all Landsat satellite bands, a Normalized Difference Vegetation Index (NDVI) band, a Normalized Difference Water Index (NDWI) band, the brightness, greenness and wetness bands of the Tasseled Cap procedure and a Digital Elevation Model (DEM). 5'000 randomly selected points are defined as the input sample for the 'weka means' clusterer which automatically calculates 30 groups based on the spectral properties of the sample points. In order to merge and reduce the groups to eight initially defined land cover classes (forest, woodland, shrubland, grassland, bare land, cropland, water, urban), the resulting cluster map is compared to a Landsat 8 composite for the same year (2016) as the training Landsat imagery.

Multiple detected issues in this process enable the development of an improved supervised classification. In a wide range of places, a discrepancy between the class identified on the Landsat 8 composite and the class displayed on the land cover map exists due to similar spectral properties. For instance, urban and bare land are not separated accurately because of an alike spectral signature particularly in the visible wavelength range demonstrated in Figure 12.

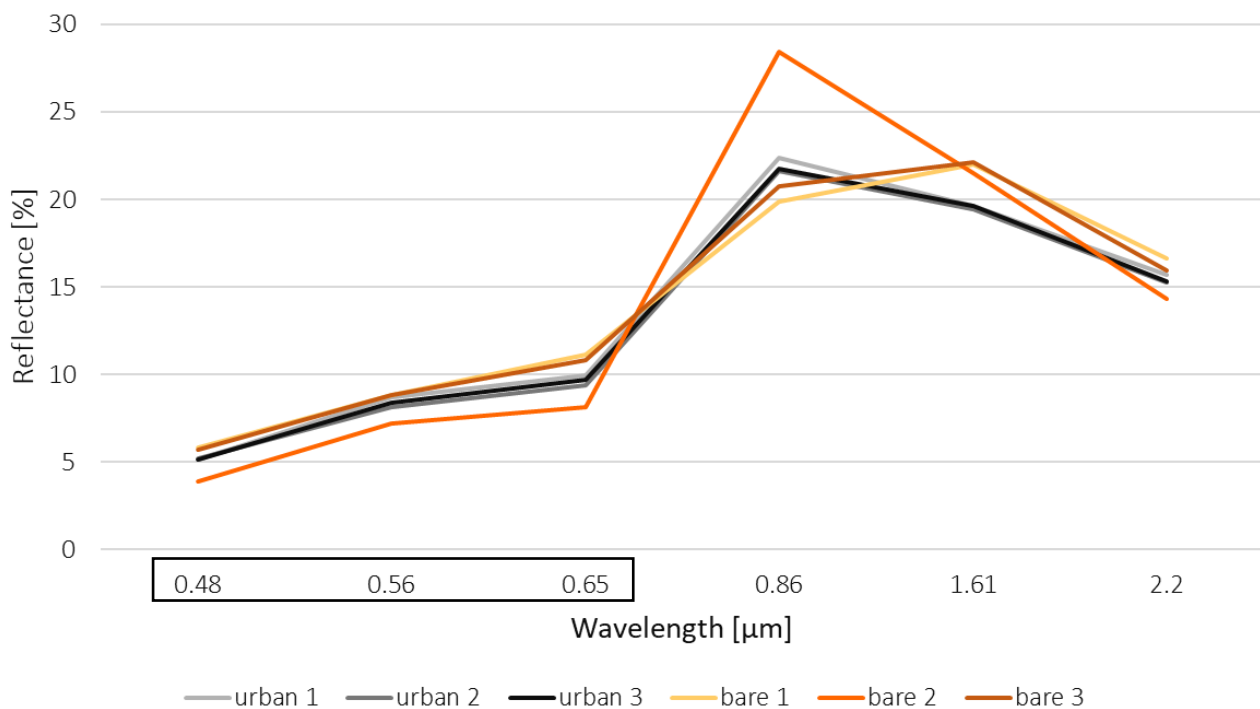


Figure 12 Graphic comparing the spectral signatures of three urban and three bare land examples. The bands of the visible spectrum are marked with a black frame.

Hence, in the supervised classification the urban areas will be masked to avoid confusion with bare land. Similarly, problems with the accurate detection of water occur and consequently this class is masked as well. Furthermore, to better detect cropland, a narrow timeframe with comparable growing conditions in different years is desirable. The final merged map in Figure 13 shows five classes that were distinguishable with visual inspection. Fundamentally, bare land is included even though it is likely a minor class in Keffa but otherwise the classification for Bale zone lacks one of its main classes. The initial idea to train the supervised classification with results from the unsupervised approach is refused. However, the unsupervised classification helps receiving an overview of the class occurrences and distributions over the study area.

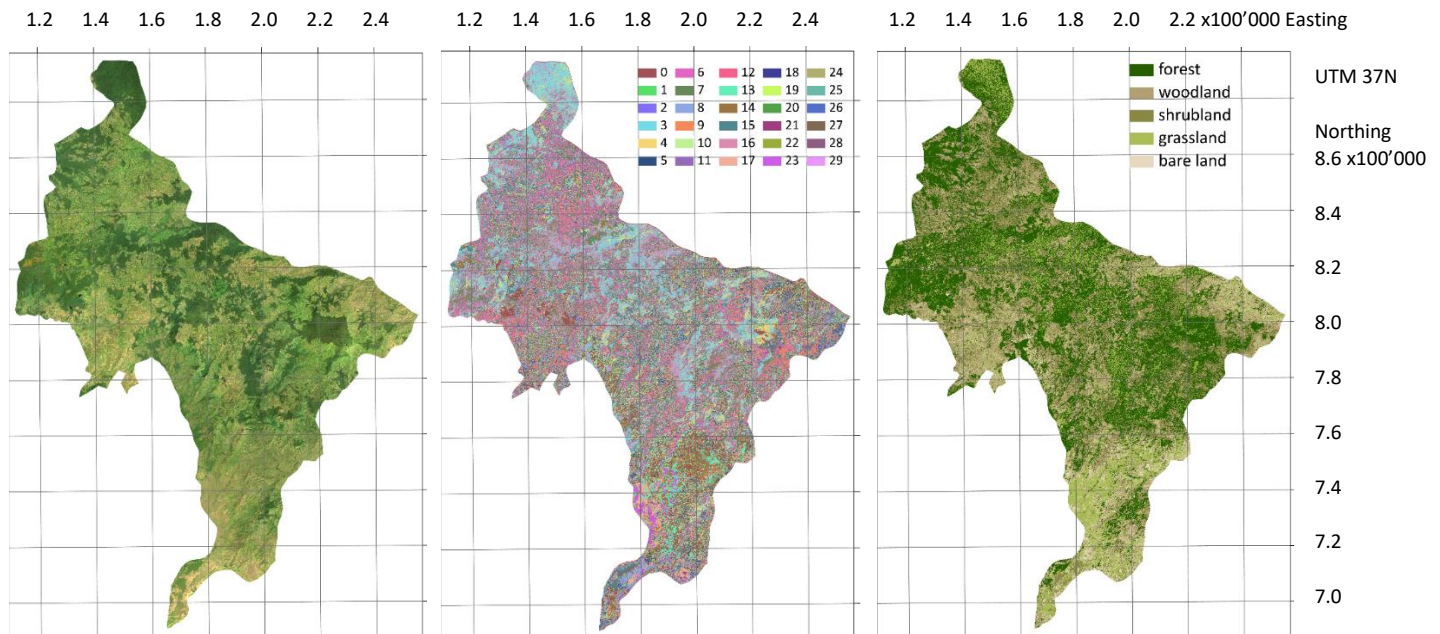


Figure 13 From left to right: Landsat 8 composite (5 month dry season, '2015-11-01', '2016-04-01') of Keffa zone (Google Earth Engine 2020), 30 classes automatically computed by the 'weka means' clusterer and visualized in random colours, map of five distinguishable merged classes

5.3 Supervised classification

The supervised classification is an automated process to identify target features in imagery with the objective to categorize the pixels into pre-defined classes (Lillesand et al. 2015). Accordingly, known land cover types at the sample point location are linked to measured spectral properties in the same place. Subsequently, applied statistical decision rules determine the land cover class in different imagery (Lillesand et al. 2015). Classification results are displayed in thematic land cover maps visualizing the classified surface features (Apan 1997) or the areal extent of individual classes is calculated (Lillesand et al. 2015).

5.3.1 Class definition

Based on diverse sources, such as literature, visual inspection of existing land cover products and the pre-calculated unsupervised classification, major land cover classes for the study zones have been selected. The seven most relevant classes are chosen. A random sample of 5'000 training points is collected over the five study zones because generally large samples are recommended (Banko 1998). Centrally, the sample points are distributed equally over all zones to evenly represent the five study zones and their classes. The Sentinel-2A land cover product is sampled at the location of the 5'000 points and class values are assigned. Water and built-up areas are excluded from the sampling so as to not confuse the classification process because both classes will be masked later. After the first iteration of the entire classification process, noticeably, forest is detected in unobvious places. To check the correctness, the classified forest areas are visually compared to a Landsat 8 composite of 2016. However, those forest samples were not wrong but based on a definition where forest refers to tree cover areas with tree canopy covering 15% of the pixel area. Yet, areas with more than 15% tree cover per pixel are preferred to represent forest areas. Accordingly, the forest sample points are manually relocated to areas with higher tree cover proportions. All land cover classes are systematically controlled to receive as homogeneous classes as possible and the final number of points per class is displayed in Table 4. After the adaptations, the class consistency improved.

Table 4 Table listing the five study zones and the land cover classes with the final number of sample points per class and zone after the manual relocation of some points

	Forest	Shrubland	Grassland	Bare land	Cropland	Sum
Bale	324	932	501	109	268	2'134
Bench Maji	492	196	548	0	200	1'436
Illubabor	708	9	92	1	45	855
Keffa	336	52	36	0	6	430
Sheka	135	4	6	0	0	145
Sum	1'995	1'193	1'183	110	519	5'000

5.3.2 Random Forest classifier

The Random Forest (RF) classifier is frequently used to categorize forest areas (DeVries et al. 2016). Advantages are the high classification accuracy and the possibility to compute various statistical data measurements, for example a regression (Cutler et al. 2007). Due to an ensemble of decision trees, overfitting is eliminated (Pimple et al. 2018). Moreover, the RF is able to classify differently scaled data and analyse large datasets fast (Griffiths et al. 2014). In the standard classification procedure, the observations contain known classes and the classifier establishes rules to predict further observations (Cutler et al. 2007). In the Random Forest model, the novel observations are assessed separately by each of the n-decision trees and the predicted class for a specific observation is based on the majority vote of the n-predictions (Hu et al. 2019; Pimple et al. 2018; Griffiths et al. 2014; Cutler et al. 2007).

In this thesis, the Random Forest classifier is selected based on a classifier performance assessment. Three different classifiers called support vector machine (SVM), CART (Classification and Regression Tree) and RF which are commonly applied in land cover classification have been tested. For the test area, very high-resolution satellite imagery with 2 meters spatial resolution is available (Google Earth Engine 2020) illustrated in Figure 14. 10'000 sample points are collected and compared in their training overall accuracy and the validation overall accuracy which showed no performance difference. Therefore, 13 sample positions are examined and the assigned class of the three classifiers compared to the very-high resolution imagery. The RF classifier performed best in forest areas compared to the other two classifiers which often labelled forest pixels as savanna or grassland.

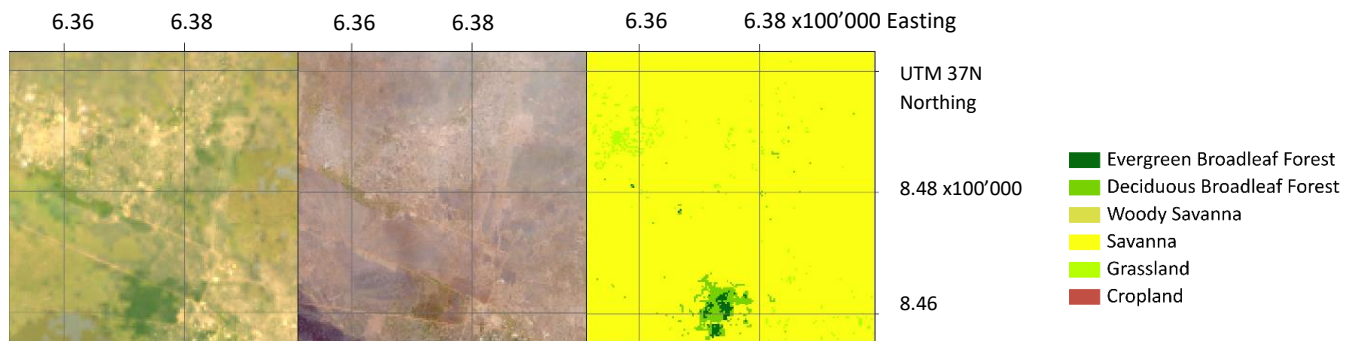


Figure 14 From left to right: Landsat 8 (2015/2016) composite for a forested area, very high-resolution imagery from Planet Sky data (2015/2016) (Google Earth Engine 2020), classification of the Landsat 8 imagery with the Random Forest classifier

In this study, the applied supervised classification procedure, the RF has 10 decision trees and the training land cover data of 2016 is connected to the spectral properties of the three-month dry season composite from the same year.

5.3.3 Accuracy assessment of the classification

The accuracy assessment of the classification is a crucial step before interpreting the results (Banko 1998). Accuracy connected to classifications refers to the degree of exactness, in other words, how much of the resulted land cover map agrees with the 'truth' (Foody 2002; Hailemariam et al. 2016). The reality also called reference data may origin from diverse sources, such as other remote sensing information or field measurements (Lillesand et al. 2015). In addition, an alternative approach to gather reference data is splitting the training data in two groups while one serves training and the other one validation purposes (Hailemariam et al. 2016).

Although multiple accuracy measures have already been applied in classification processes (Banko 1998), typically an 'error matrix' also known as 'confusion matrix' or 'contingency table' is calculated (Banko 1998). This matrix contains the real values in the rows and the classified values in the columns, for instance visible in

Table 6 (Banko 1998). The overall, the producer's and the user's accuracy can be derived from the error matrix (Stehman 1997; Hailemariam et al. 2016). Accordingly, the overall accuracy is the division between the total number of correctly classified pixels and the total number of reference pixels (Hailemariam et al. 2016). As high overall accuracy results represent homogeneous training areas and spectrally separable classes (Lillesand et al. 2015), remote sensing researchers expect a target overall accuracy of over 85% (Foody 2002).

In this thesis, two reference datasets validate the classification. Firstly, the PROBA-V land cover product with 100 meters spatial resolution from 2015 listed in Table 5 represents the reference data because it is close to the training data year and has medium spatial resolution (ESA 2019). 5'000 randomly sampled points were classified from the

land cover map providing the validation dataset. Essentially, only classified pixels are assessed in contrast to masked pixels which could confuse the classification validation. Secondly, the splitting method has been implemented with 70% training and 30% validation data represented in Table 7.

Table 5 PROBA-V dataset (ESA 2019), list of the seven final land cover classes with their original class value and class name before the reclassification to the final values

Final class value	Final class name	Original class value	Original class name
0	Forest	112	Evergreen broadleaf closed forest
		114	Deciduous broadleaf closed forest
		122	Evergreen broadleaf open forest
		124	Deciduous broadleaf open forest
1	Shrubland	20	Shrubs
2	Grassland	30	Herbaceous vegetation
3	Bare land	60	Bare/sparce vegetation
4	Cropland	40	Cropland
5	Water	80	Permanent water bodies
6	Urban	50	Urban

Table 6 Validation error matrix based on the PROBA-V dataset with a validation overall accuracy of approximately 28% ($1'391/5'000=0.2782$). The correctly classified pixels are emphasized in the diagonal.

ground truth	prediction					sum
	0 - forest	1 - shrubland	2 - grassland	3 - bare land	4 - cropland	
0 - forest	694	817	506	98	327	2'442
1 - shrubland	0	238	197	368	330	1'133
2 - grassland	0	68	126	23	167	384
3 - bare land	0	0	0	12	0	12
4 - cropland	18	420	202	68	321	1'029
sum	712	1'543	1'031	569	1'145	5'000

Table 7 Validation error matrix with a validation overall accuracy of around 86% ($1'246/1'447=0.8619$) using 30% of the training sample points for validation. The correctly classified pixels are emphasized in the diagonal.

ground truth	prediction					sum
	0 - forest	1 - shrubland	2 - grassland	3 - bare land	4 - cropland	
0 - forest	557	10	2	0	0	569
1 - shrubland	20	271	46	0	6	343
2 - grassland	12	61	260	0	15	348
3 - bare land	0	1	0	34	1	36
4 - cropland	2	8	15	2	124	151
sum	591	351	323	36	146	1'447

5.4 Change Detection

Change detection in the context of remote sensing refers to quantifying changes in multispectral imagery (Coppin et al. 2004). A land cover conversion means the change from one class into another, in comparison to the land cover modification which is defined as a feature change but not sufficiently that a class change happens (Coppin et al. 2004). Accordingly, deforestation is determined as a land cover conversion from forest to another land cover class while degradation is considered as forest carbon loss resulting from natural or human-induced activities lacking a land cover class change (Bullock, Woodcock, and Olofsson 2020). Change detection analysis attempts to derive multiple outputs, such as the area change, change rate or spatial distribution of the change (Lu et al. 2004).

Various approaches allow change detection (Foody 2002). A frequently used method is the ‘post-classification comparison’ (Foody 2002) defined by the pixel change detection of two classified images gathered on different dates (Lillesand et al. 2015). An important advantage is an enhanced understanding of the type and magnitude of LULC changes over time (Pimple et al. 2018). Furthermore, this technique calculates the matrix of change directions providing information that is less influenced by atmospheric or environmental irritations in the images (Lu et al. 2004).

The post-classification comparison is applied on the five year dry season composites because it is proposed to have a minimum of five years between observations to detect anthropogenic or natural forest disturbances (Coppin et al. 2004). In order to calculate changes happening during the last 20 years, the 1995-2000 composite is compared to the 2015-2020 composite. With focus on the forest changes and to facilitate understanding the results, the values in the change matrix are reclassified in five novel classes: ‘no change’, ‘forest to urban’, ‘to urban’, ‘from forest’ and ‘to forest’. ‘No change’ refers to no class conversion. ‘Forest to urban’ counts exclusively the forest pixels that are transformed to urban, while ‘to urban’ includes all the other classes. ‘From forest’ is the forest loss and ‘to forest’ is defined as forest gain.

5.4.1 Change detection validation

In this study, the change detection is compared and thus validated with the Hansen forest change dataset. The Hansen dataset uses Landsat data at a spatial resolution of 30 meters to quantify global forest changes by applying a consistent method (Hansen et al. 2013). Forest loss in this dataset is defined as the complete removal of tree canopy cover or the replacement by another land cover at a pixel size of 30 meters. The baseline forms the tree cover of the year 2000 (Hansen et al. 2010). For the assessment, six sample regions per study zone illustrated in Figure 15 are examined qualitatively through visual inspection concentrating on the criterion loss detection and loss shape. Out of the 30 investigated regions, our forest loss calculations detected deforestation better than the Hansen dataset in 11 cases while the Hansen global forest change performed better in 2 examples. For the remaining regions both outputs were similar, or it lasts unclear whether loss is detected accurately or not. Figure 16 visualizes one example of an evaluated loss area.

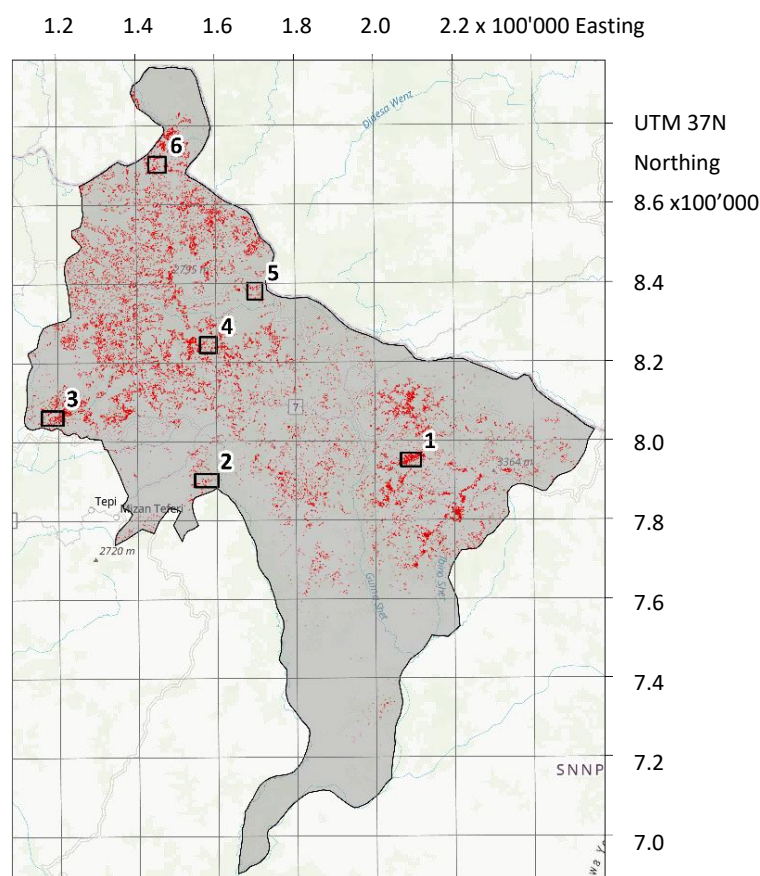


Figure 15 Map of Keffa emphasizing the forest loss areas in red and the validation areas are framed with their corresponding number

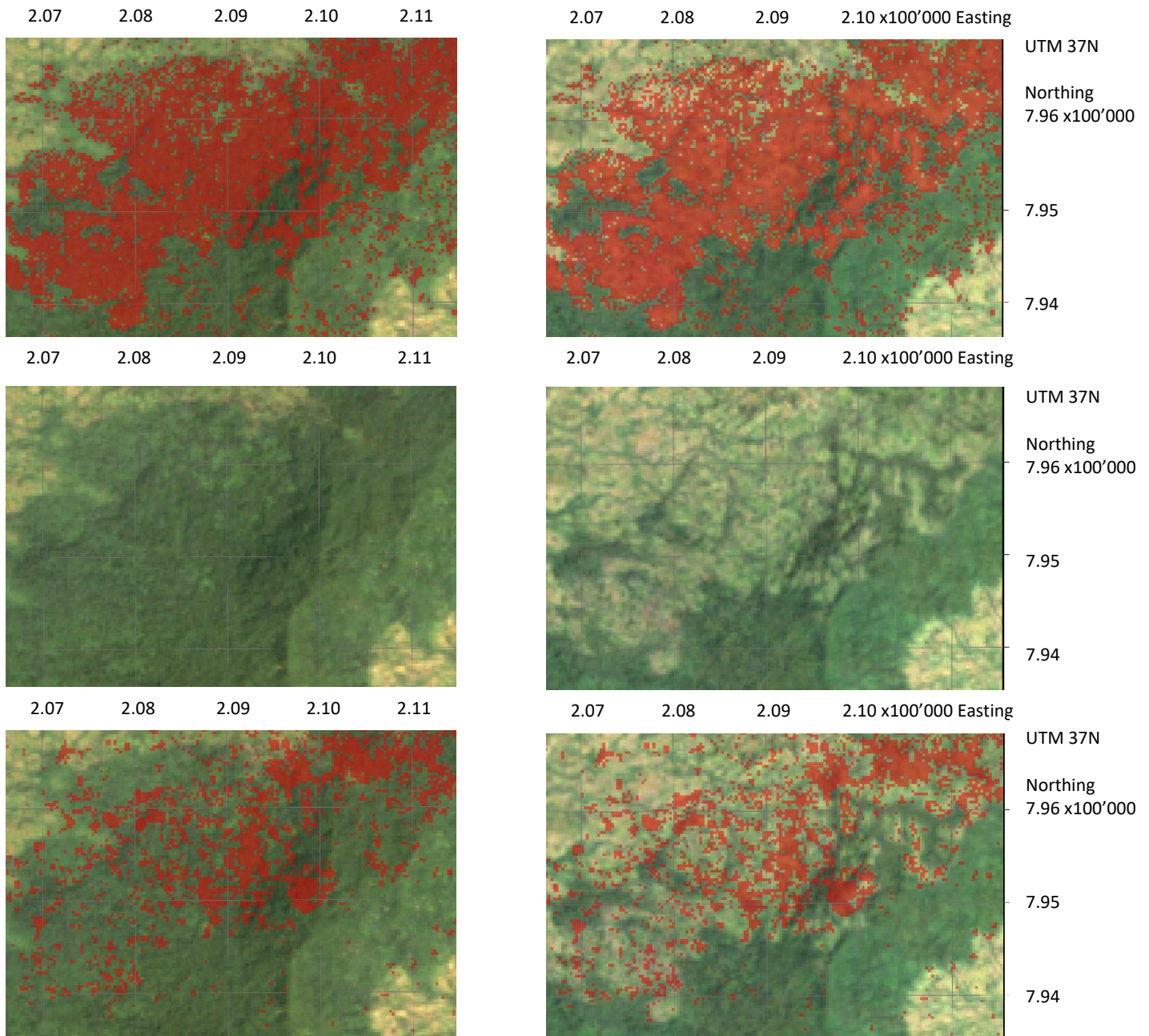


Figure 16 Area 1 forest loss: From top left to bottom right: Calculated forest loss areas in red overlaid on the composite 1995-2000 and on the composite 2015-2020, Landsat imagery composite 1995-2000 and composite 2015-2020, Hansen forest loss in red overlaid on the composite 1995-2000 and on the composite 2015-2020 (Google Earth Engine 2020)

To validate the gain areas the same process was applied with the overview of the gain areas in Keffa visualized in Figure 17 and one example in Figure 18. However, only two validation regions per study zone were chosen and the calculated gain is not compared to the Hansen forest gain because the Hansen dataset seldomly identifies forest gain over the last 20 years in the study zones which leads to incomparability. Special focus lies on the visual inspection of the composites and the corresponding calculated forest gain. Out of the 10 gain areas two cases detected real gain according to our view.

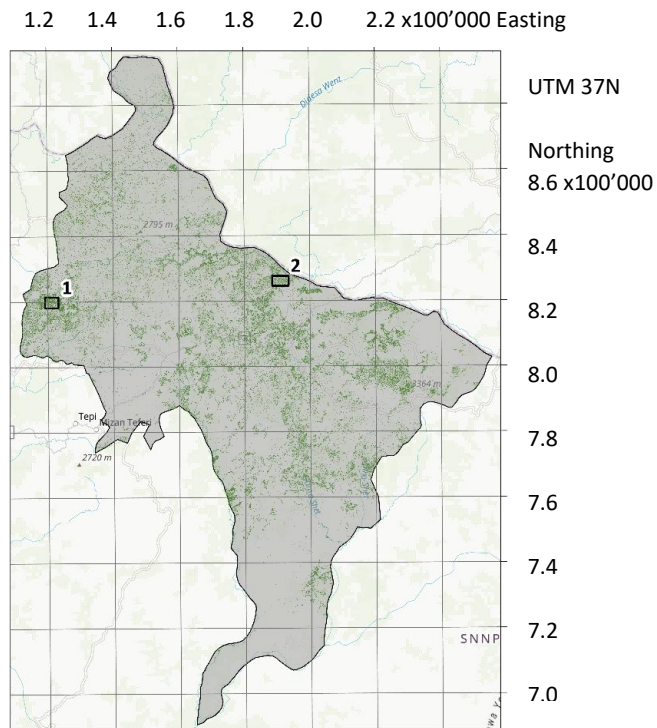


Figure 17 Map of Keffa emphasizing the forest gain areas in green and the validation areas are framed with their corresponding number

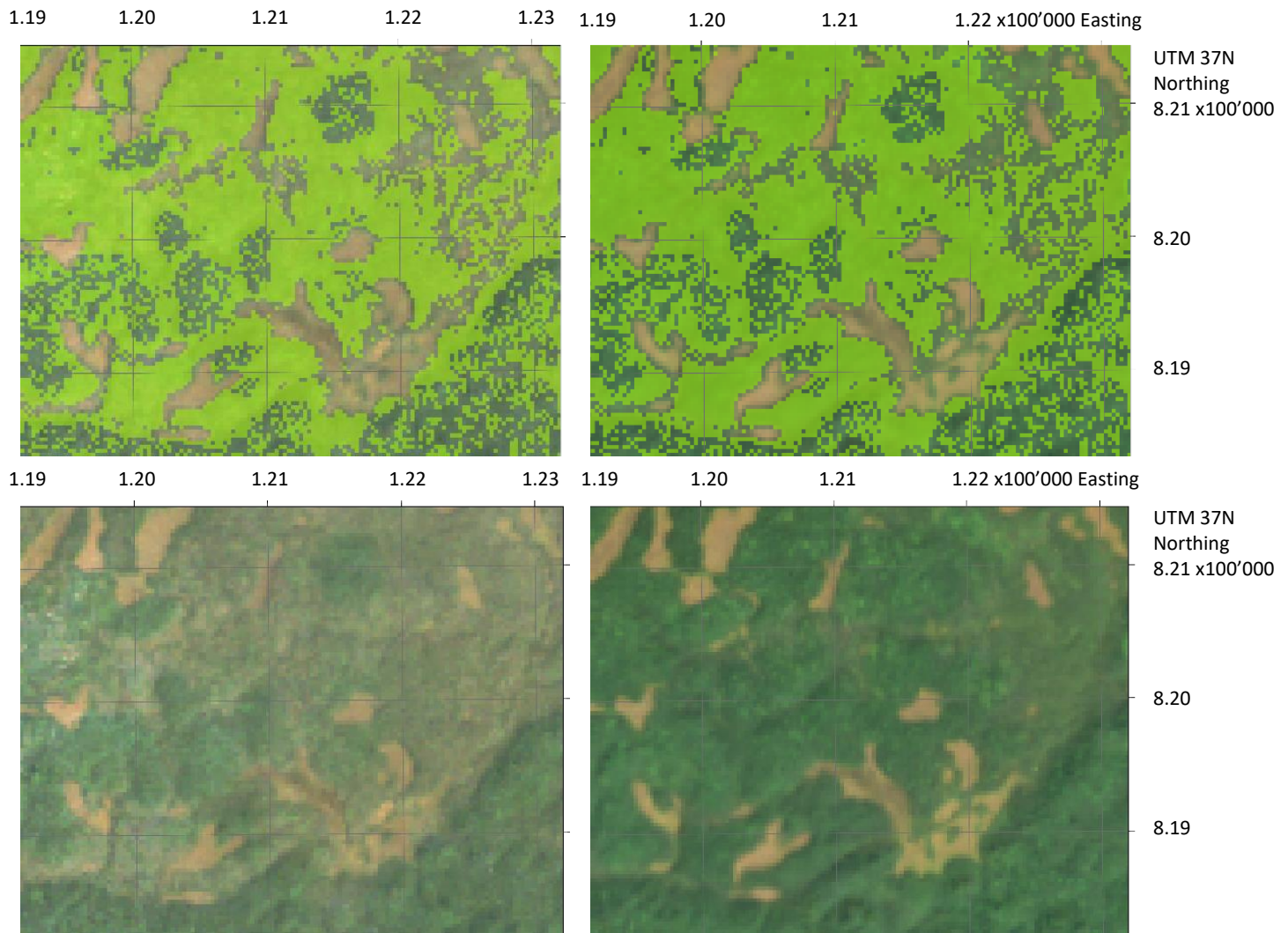


Figure 18 Area 1 forest gain: Top: Calculated forest gain areas in green overlaid on the composite 1995-2000 on the left hand side and on the composite 2015-2020 on the right hand side, Bottom: Landsat imagery composite 1995-2000 and composite 2015-2020 (Google Earth Engine 2020)

5.4.2 Continuous Degradation Detection (CODED)

There has been a gradual shift from traditional image comparison methods, limited to studying particular points in time, to continuous time-series techniques due to an increased amount of available remote sensing data (DeVries et al. 2016) and related to that higher temporal resolutions (Lillesand et al. 2015).

Level one terrain corrected (L1T) products are georeferenced and radiometrically calibrated (Pasquarella et al. 2016). For this reason, they can directly be utilized to compare pixels over time, which is a major advantage for time series analysis (Pasquarella et al. 2016). Effective forest management is based on accurate forest disturbance information extracted from time series exploitation (Shimizu et al. 2019). Landsat Time Series (LTS) are prominent to describe forest change trajectories and frequently used to conduct forest disturbance detection with a temporal segmentation algorithm (DeVries et al. 2016). For example, the frequently mentioned LandTrendR algorithm which works with regression and a point-to-point fitting method to identify linear trends such as disturbance or recovery (Cohen et al. 2010).

The CODED algorithm uses Landsat pixel time series and a spectral mixture analysis to detect forest degradation and deforestation (Bullock, Woodcock, and Olofsson 2020). The spectral endmember fractions green vegetation (GV), non-photosynthetic vegetation (NPV), shade (SHADE) and soil (SOIL) are computed which serve as input for the Normalized Difference Fraction Index (NDFI) calculation (Bullock, Woodcock, and Olofsson 2020; Dupuis et al. 2020). While dense forests show high proportions of GV, and low SOIL and NPV fractions, thinned forest demonstrates decreased GV portions and cleared forest has higher SOIL and NPV fractions (Bullock, Woodcock, and Olofsson 2020; Souza et al. 2013). The NDFI computes values between -1 and 1. Accordingly, a NDFI value of 1 defines dense canopy forest while a value of -1 likely represents a forest clearing (Bullock, Woodcock, and Olofsson 2020).

The change detection is performed by the regression-based break algorithm applied on the time series of the NDFI (Bullock, Woodcock, Souza, et al. 2020). After every detected break a new regression model is calculated along the time series continuing until the end of the imagery series is reached (Bullock, Woodcock, and Olofsson 2020). Subsequently, the trained Random Forest classifier assigns land cover categories to every segment and pixel (Bullock, Woodcock, and Olofsson 2020). After the classification all non-forest classes are merged to one category (Bullock, Woodcock, Souza, et al. 2020). Deforestation is consequently referred to the conversion from the forest class to the non-forest class (Bullock, Woodcock, Souza, et al. 2020). The change threshold value mentioned in Table 8 further classifies the disturbance (Souza et al. 2013). All disturbances have a change date indicated in year information and a change magnitude which refers to a decrease in NDFI and represents an approximation to the amount of tree removal or canopy damage in a pixel (Bullock, Woodcock, and Olofsson 2020).

In this study, the CODED algorithm was used to gather additional information on deforestation and particularly on degradation in the study zones and kebeles. As the Random Forest requires training data, 100 sampling points per class were created supported by a supervised classified image for the year 2016. The outputs of the CODED algorithm are classified maps illustrating the four classes deforestation, forest degradation, forest and non-forest. Furthermore, the change date and change magnitude are computed and mapped separately. Typical deforestation and forest degradation NDFI trajectories are represented in Figure 19, respectively Figure 20. It becomes apparent that forest degradation does not show negative NDFI values, whereas deforestation incorporates values around -1.

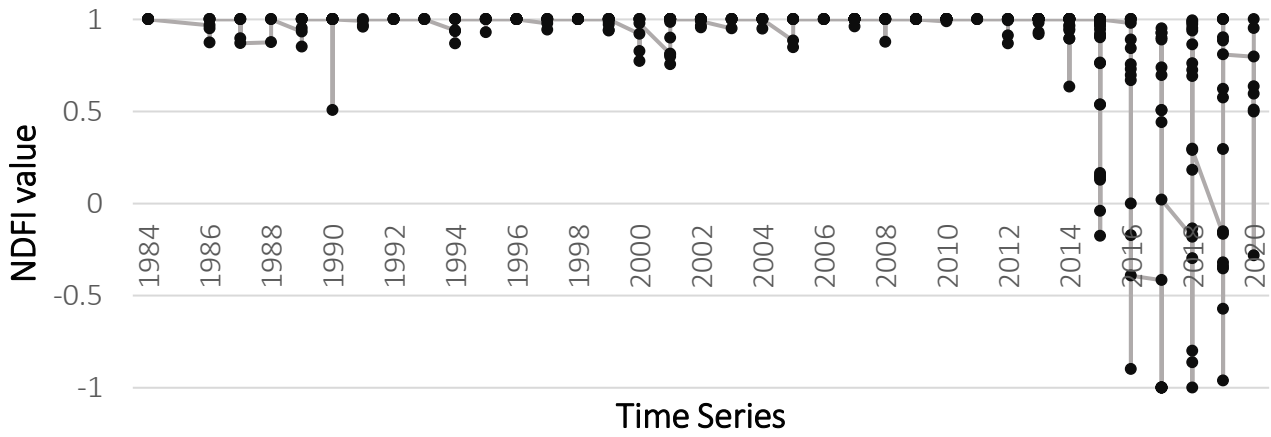


Figure 19 Typical NDFI trajectory for a deforestation pixel over a time series of 36 years

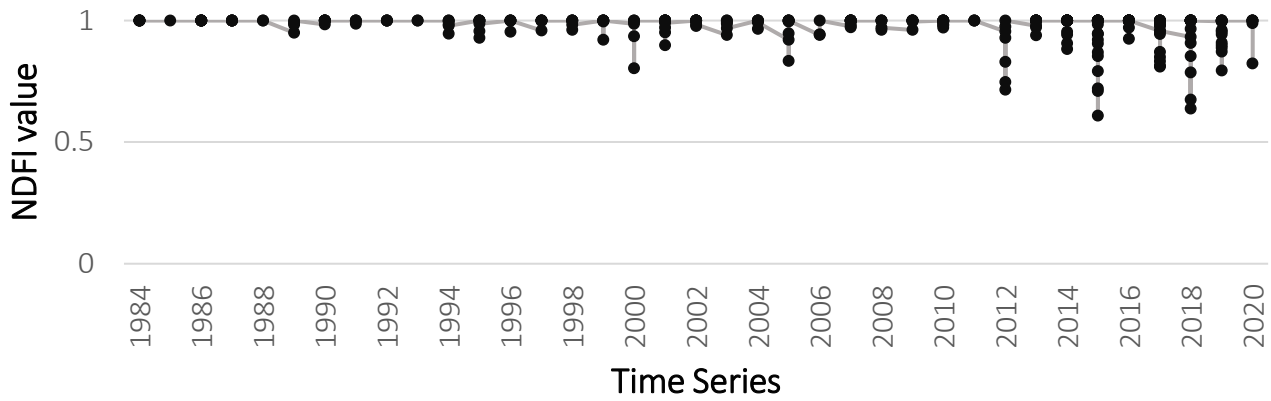


Figure 20 Typical NDFI trajectory for a forest degradation pixel over a time series of 36 years

Table 8 Parameter values entered to the CODED algorithm (Bullock 2018)

Parameter name	Parameter definition	Parameter value
cfThreshold	Minimum cloud fraction threshold	0.05
consec	Consecutive observations to classify a change	3
thresh	Change threshold based on the residual	4
start	Start analysis year	200
end	End analysis year	2019
trainDateEnd	Start year for training period	2016
trainDateStart	End year for training period	2013
trainLenght	Number of years of the training period	3
soil	Endmember 'soil'	2000,3000,3400,5800,6000,5800
gv	Endmember 'green vegetation'	500,900,400,6100,3000,1000
npv	Endmember 'non-photosynthetic vegetation'	1400,1700,2200,3000,5500,3000
shade	Endmember 'shade'	0,0,0,0,0,0
cloud	Endmember 'cloud'	9000,9600,8000,7800,7200,6500
forestLabel	Forest label assigned in the training data	1
window	Maximum number of years in the monitoring period	4
minYears	Minimum number of years between disturbances	3
numChanges	Number of changes to export	3
minObs	Minimum number of observations for model fitting	6
startDOY	Start day of the year	1
endDOY	End day of the year	365

6 Results

6.1 Land cover changes in the study zones over the last 20 years

6.1.1 Analysis of the main study zone Keffa

In the main study zone, clustered forest areas can be found in the northern part and in the central parts mapped in Figure 21. While cropland is mostly found at the zone boundaries, shrubland grows directly at the forest edges. The only classified urban area in Keffa is the city of Bonga lying in the zone centre. Over the 20 years the areal extent of forest seems changing, but the forest locations remain the same. Generally, the forest areas appear more homogeneous and compact in the classifications after 2000.

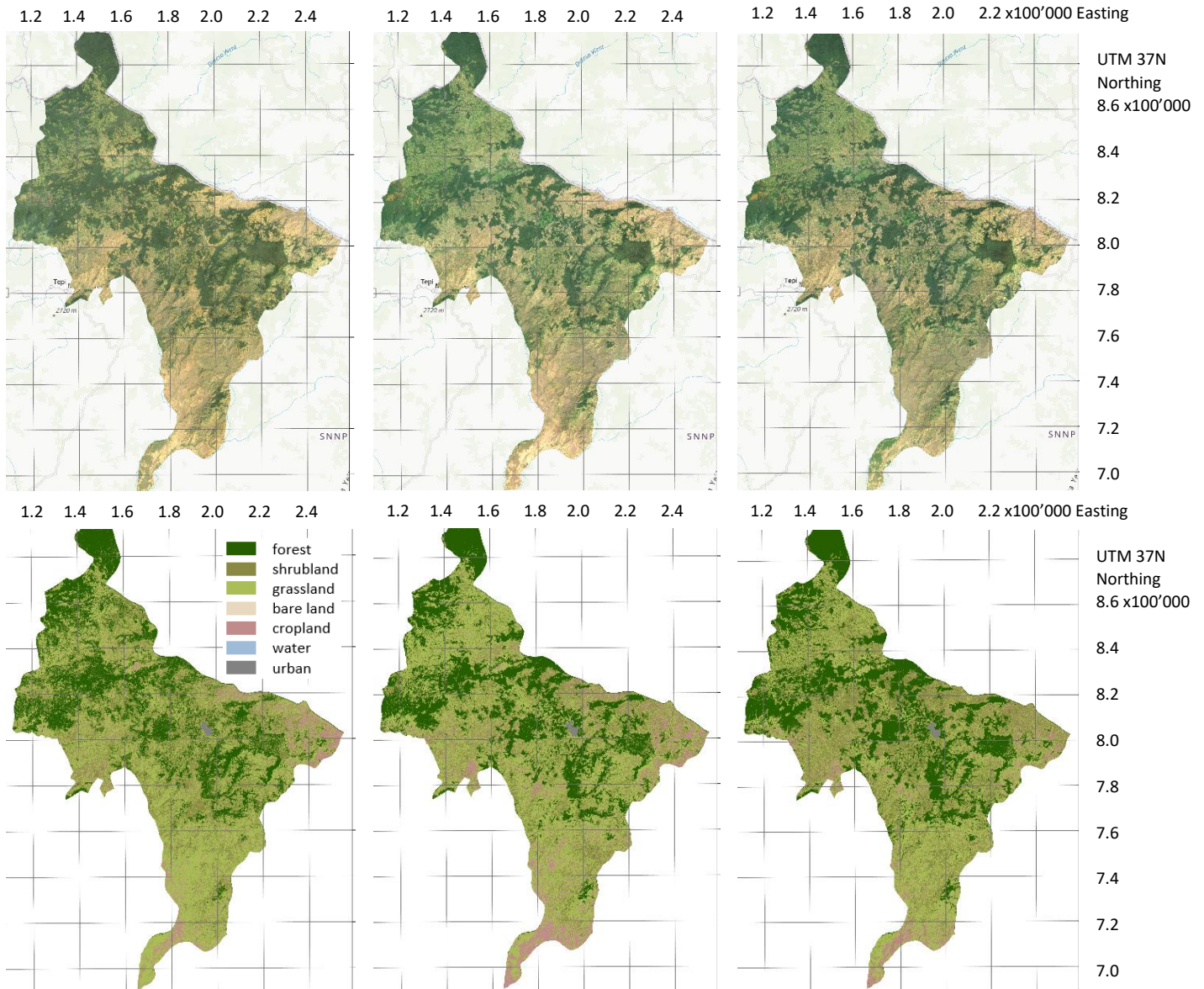


Figure 21 Top: Landsat imagery composites 1995-2000, 2010-2015 and 2015-2020 for Keffa zone (Google Earth Engine 2020), Bottom: Classified composites 1995-2000, 2010-2015 and 2015-2020

Grassland is the biggest land cover class in Keffa, stressed in Figure 22, with an extent of around 3'700 km² in the 2015-2020 composite. It decreased over the last 20 years from an initial extent of 4'400 km² in the 1995-2000 composite. Water is a minor land class in Keffa with 2 km² areal coverage. While shrubland and urban have increased over two decades, cropland remained approximately on the same level. The city of Bonga grew by 2 km². Moreover, bare land does not occur as land cover class in Keffa.

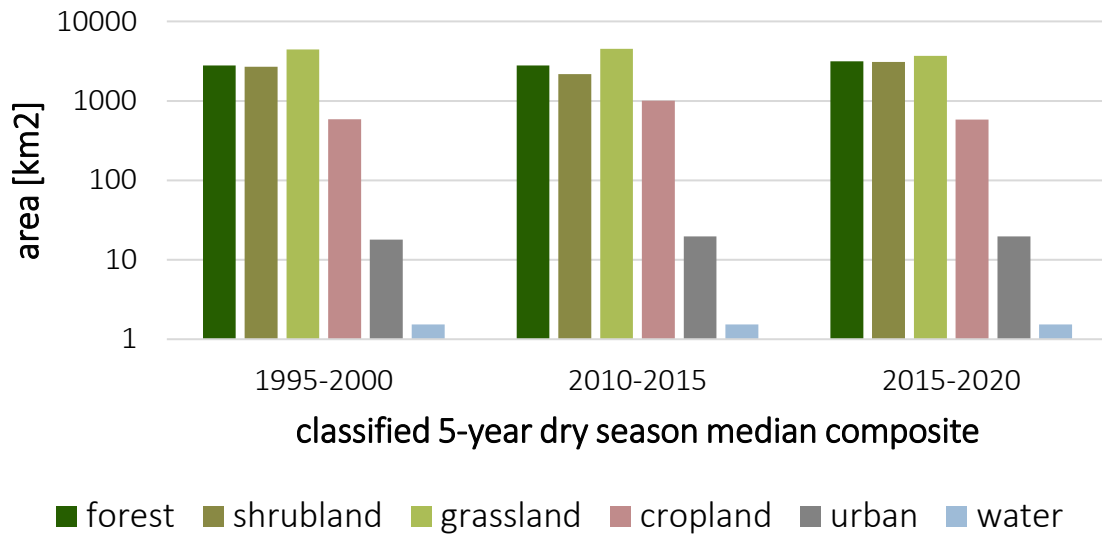


Figure 22 Graphic illustrating the areal size of the different land cover classes per classified composite for Keffa zone

6.1.2 Comparison of all five study zones

Compared to the four other study zones, similarities as well as differences to Keffa are observed. All zones have a small proportion of water which is around 0.01% of the total zone area. Similarly, the classified urban areas cover around 0.1% of the zone area. However, in all study zones with cities the urban area increased over the last 20 years by 2 km² (Keffa, Illubabor), 4 km² (Bench Maji) and 6 km² (Bale). Interestingly, in four zones except Bale, forest increased continuously over the 20 years when considering the areal extent calculations of the classification. In Bale the forest is decreasing, nevertheless, it might be treated as a minor land cover class compared to the whole zone as only some western parts are covered by forest. This class represents in Bale around 5% of the whole zone area. In comparison, bare land plays a major role in Bale as it increased over time and is the third largest class. Grassland mostly decreased except in Bench Maji and shrubland expanded in four zones without Sheka. Differences among the study zones are for example found in the cropland cover. In Sheka and Bench Maji cropland decreased in comparison to the increases in Illubabor and Bale zone illustrated in Figure 23.

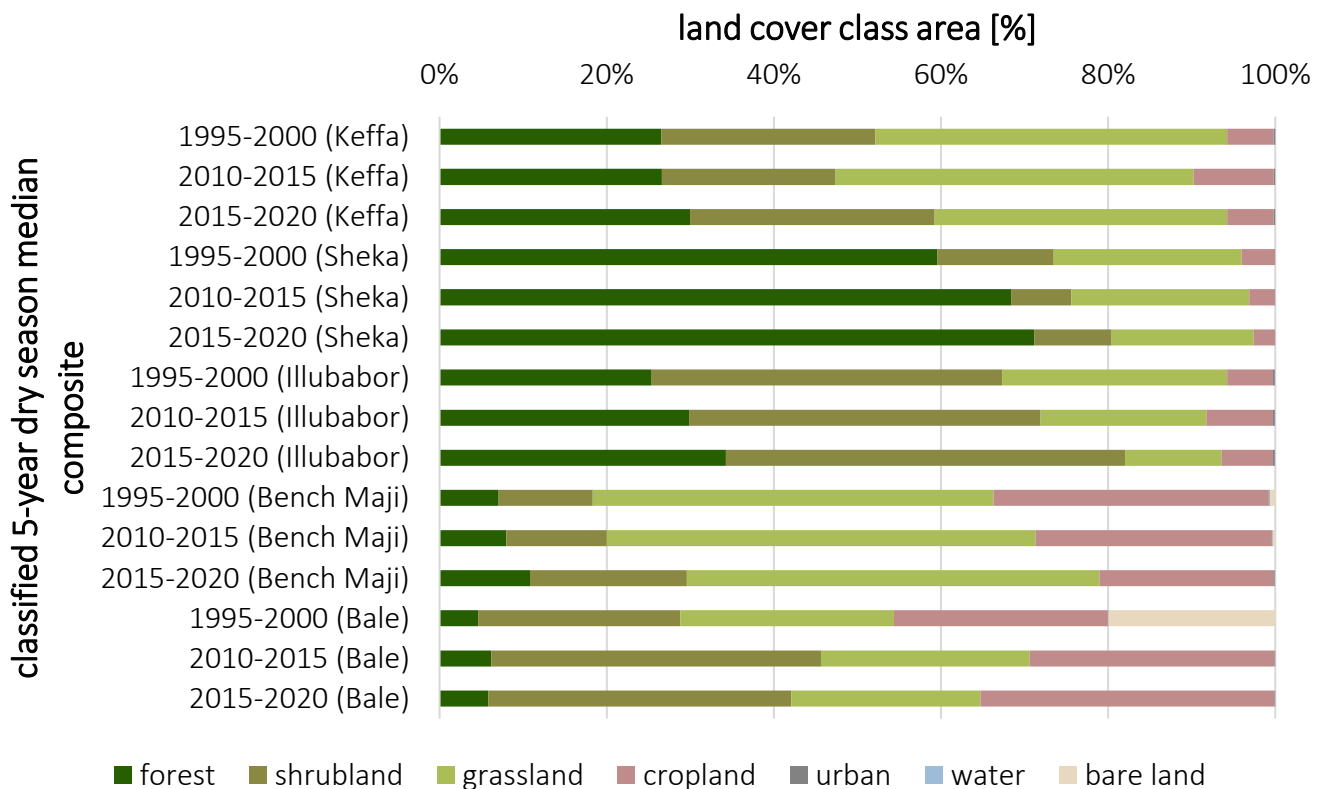


Figure 23 Overview of the percentages of the land cover classes per zone and per classified composite

For the change detection, various novel categories have been created concentrating on forest changes. In order to understand the land cover conversions in more depth, the classes with the major proportion on the change are summed up and plotted in Figure 24. Forest loss happened mostly at cost of increasing shrubland followed by grassland. On the other hand, shrubland often turned to forest as well. Shrubs, grassland and cropland transformed to urban. Undoubtedly, forest was never the class with the highest proportion converting to urban.

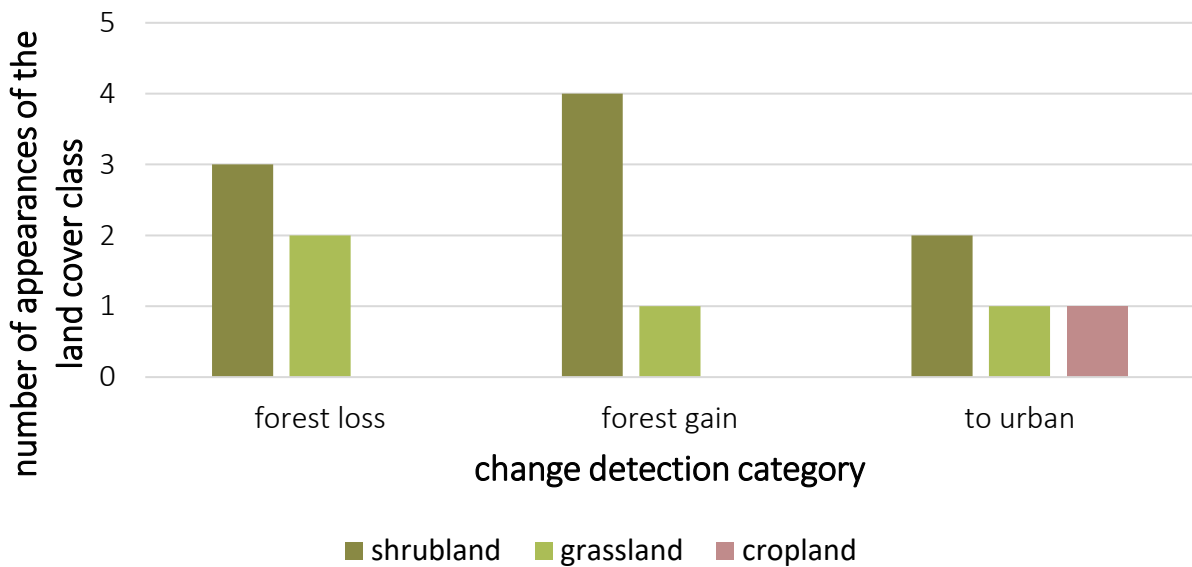


Figure 24 Graphic visualizing the number of appearances of the land cover class with the highest proportion on the categories forest loss, forest gain and to urban

6.2 Forest change detection in the study zones over the last 20 years

6.2.1 Analysis of the main study zone Keffa

In Keffa, forest loss occurs at the forest edges distributed over the whole zone mapped in Figure 25. However, at the northern peak, a connected forest patch seems unaffected compared to other places where large areas are concerned. With the CODED method, deforestation and forest degradation areas are recorded. Most disturbances are categorized as degradation whereas fewer areas are detected as forest loss. The degradation areas are clustered around the forest edges and rarely in the middle of a forest.

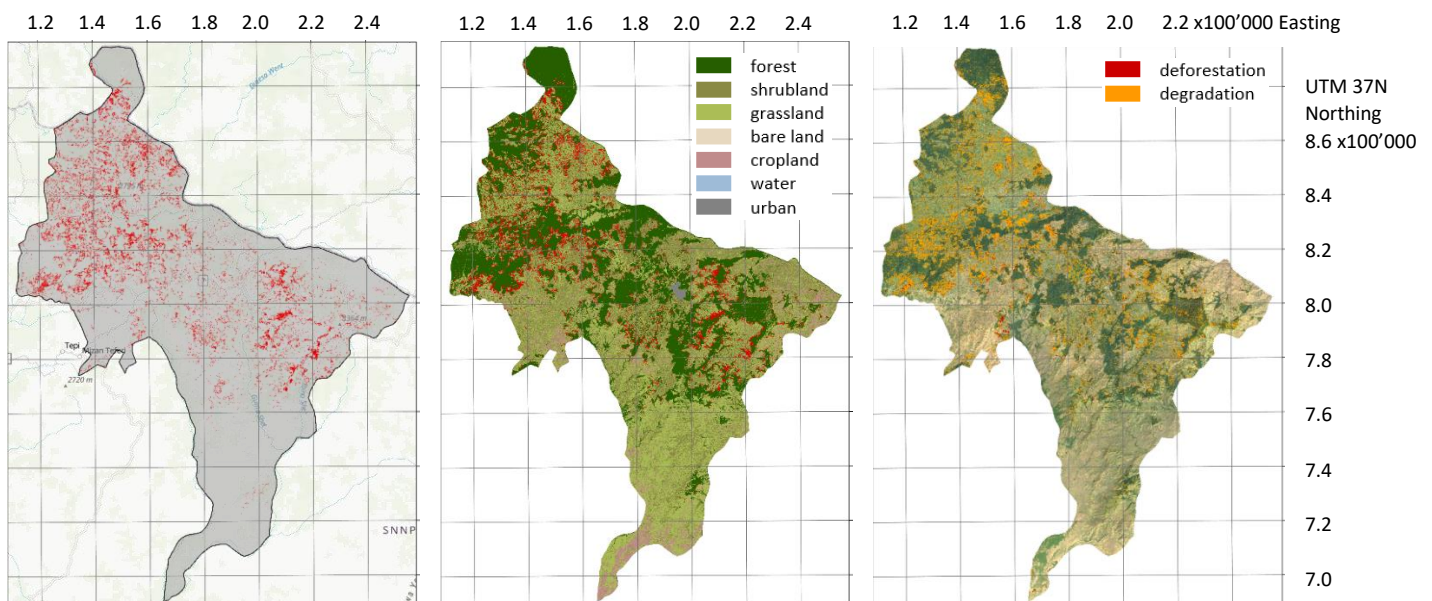


Figure 25 From left to right: Calculated forest loss displayed in red for Keffa zone, calculated loss in red overlaid on the classified composite 2015-2020, degradation in orange and deforestation in red calculated with the CODED algorithm overlaid on the Landsat imagery composite 2015-2020

Considering the disturbance date spread plotted in Figure 26, more disturbances happened after 2010. The exact disturbance years reveal two significant years, namely 2007 and 2011, with the highest number of disturbances. However, also 2012, 2014 and 2017 are years expressing several disturbances. The disturbance magnitudes are concentrated on the lower values visible on the map and confirmed by the histogram in Figure 27 with most pixels between the values 6 and 8.

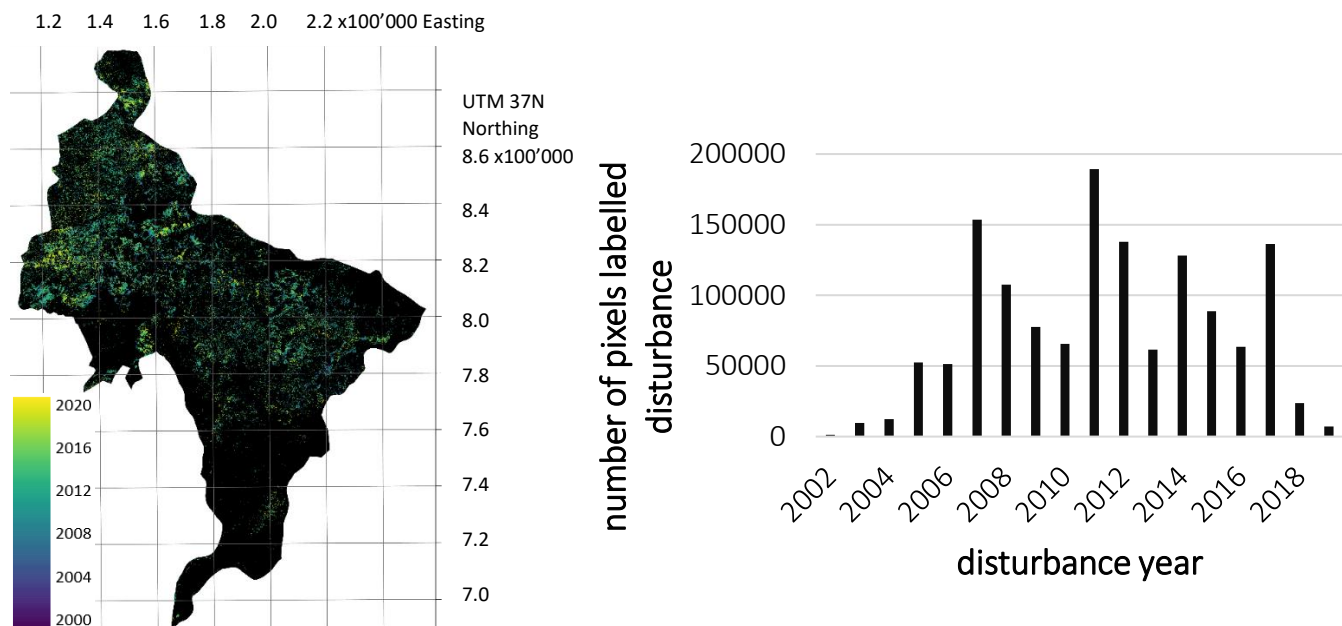


Figure 26 Left: Disturbance dates calculated with the CODED algorithm for Keffa zone, Right: Corresponding histogram showing the number of pixels labelled as disturbance for every year during the study period

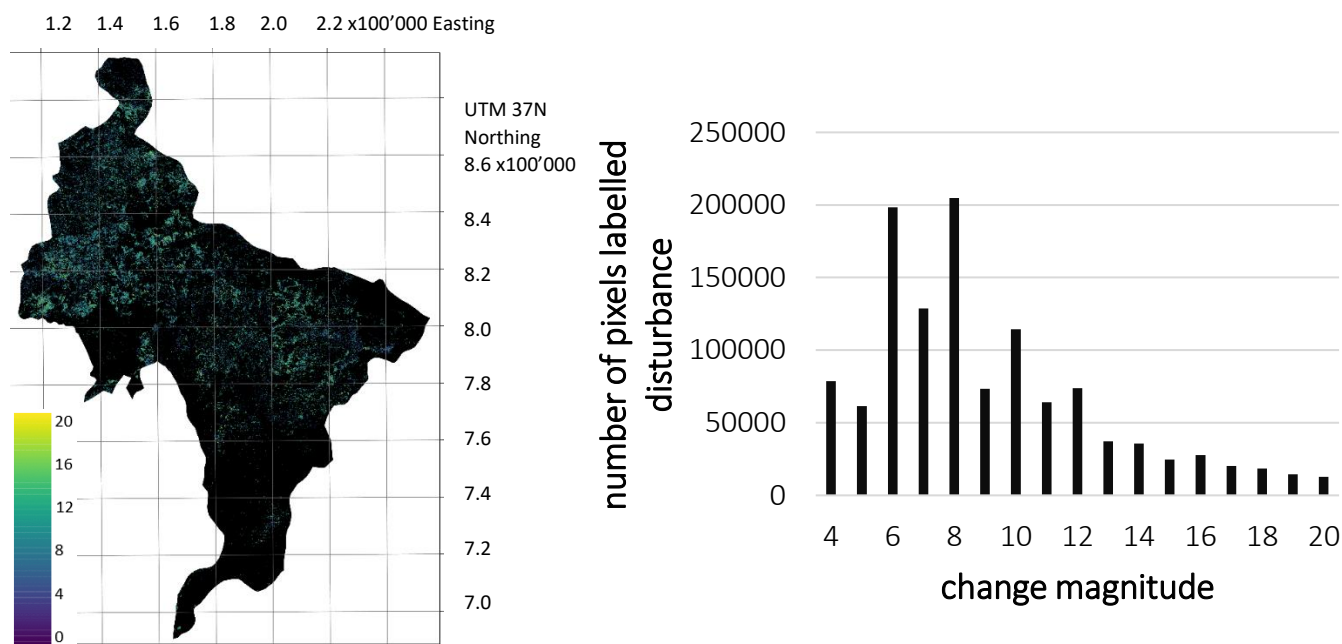


Figure 27 Left: Disturbance magnitudes calculated with the CODED algorithm for Keffa zone, Right: Corresponding histogram showing the number of pixels labelled as disturbance for the different magnitudes

Disturbances may correlate with natural weather phenomena such as the average seasonal precipitation, highlighted in Figure 28. However, in the example of Keffa, neither the average precipitation of the whole zone nor the rainfall in the city of Bonga demonstrate a similar or opposite trend to the number of disturbed pixels per year. Strikingly, the rainfall increased significantly from 2018 to 2019. The same phenomenon has been observed for the four other study zones illustrated in the appendix.

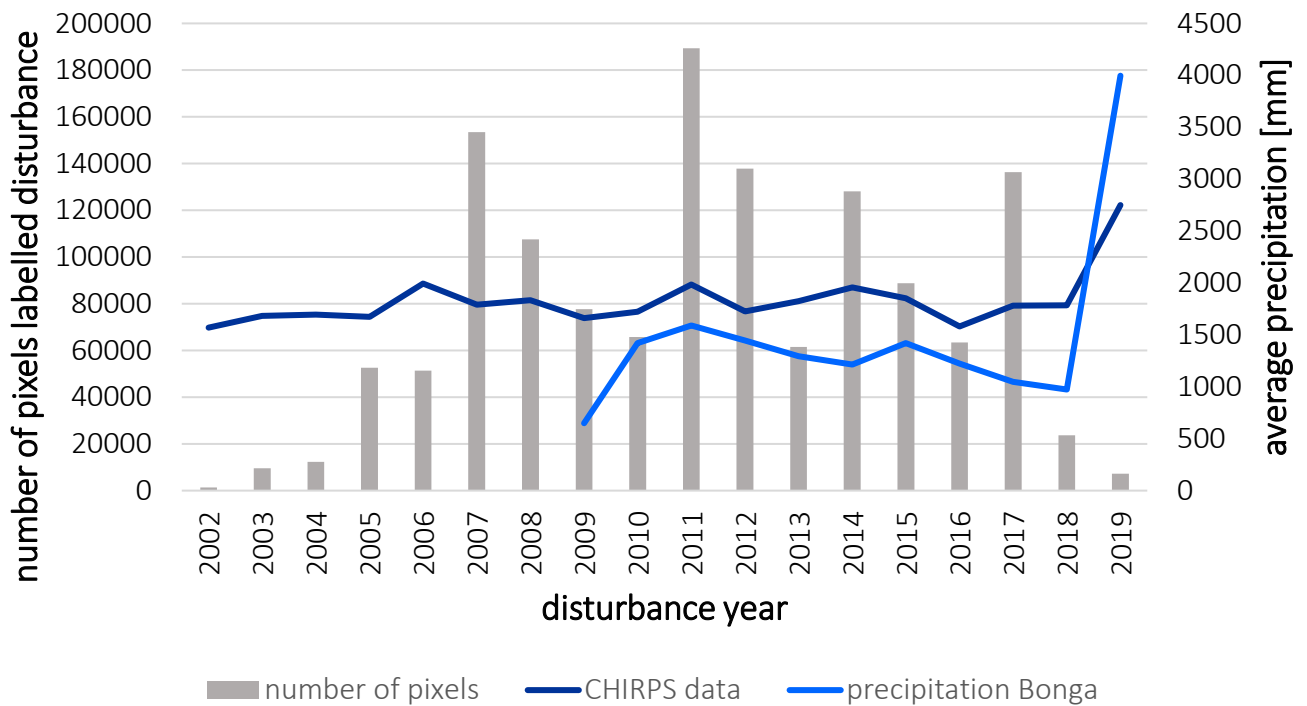


Figure 28 Histogram showing the number of pixels labelled as disturbance for every year during the analysis period for Keffa zone, the light blue line demonstrates the precipitation data from world weather for the city of Bonga (World Weather Online 2020), the dark blue line refers to the average precipitation extracted from the Chirps data (Google Earth Engine 2020)

6.2.2 Comparison of all five study zones

In Bench Maji, the forest loss areas are located in the North, western from the capital city Mizan Teferi shown in Figure 29. Another large loss area is found in the centre of the zone around a relatively small forested region. The CODED disturbances map reveals various degraded forest areas and less forest loss regions. One loss region is the south eastern zone boundary. The histogram in Figure 30 illustrates more disturbances happening in recent years, for instance in 2017 compared to the small number of disturbances in the first decade after 2000. Most magnitude values are rather low with values between 4 and 8.

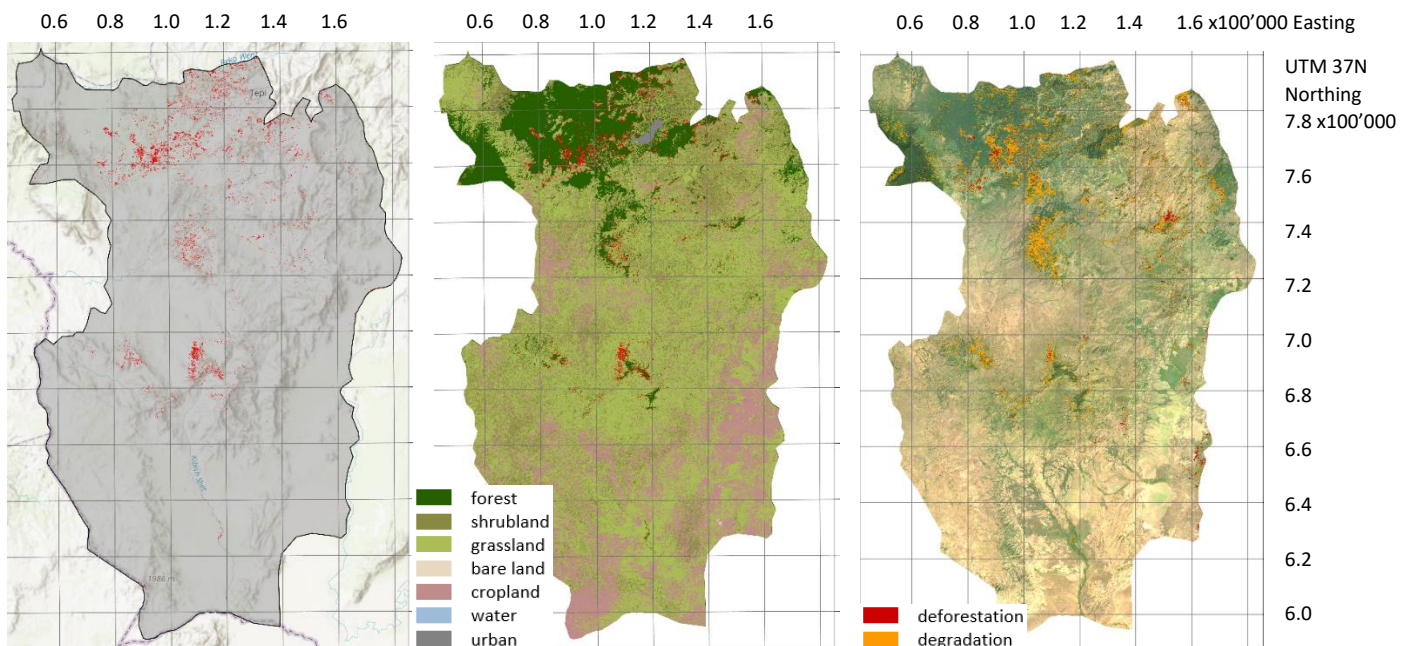


Figure 29 From left to right: Calculated forest loss displayed in red for Bench Maji zone, calculated loss in red overlaid on the classified composite 2015-2020, degradation in orange and deforestation in red calculated with the CODED algorithm overlaid on the Landsat imagery composite 2015-2020

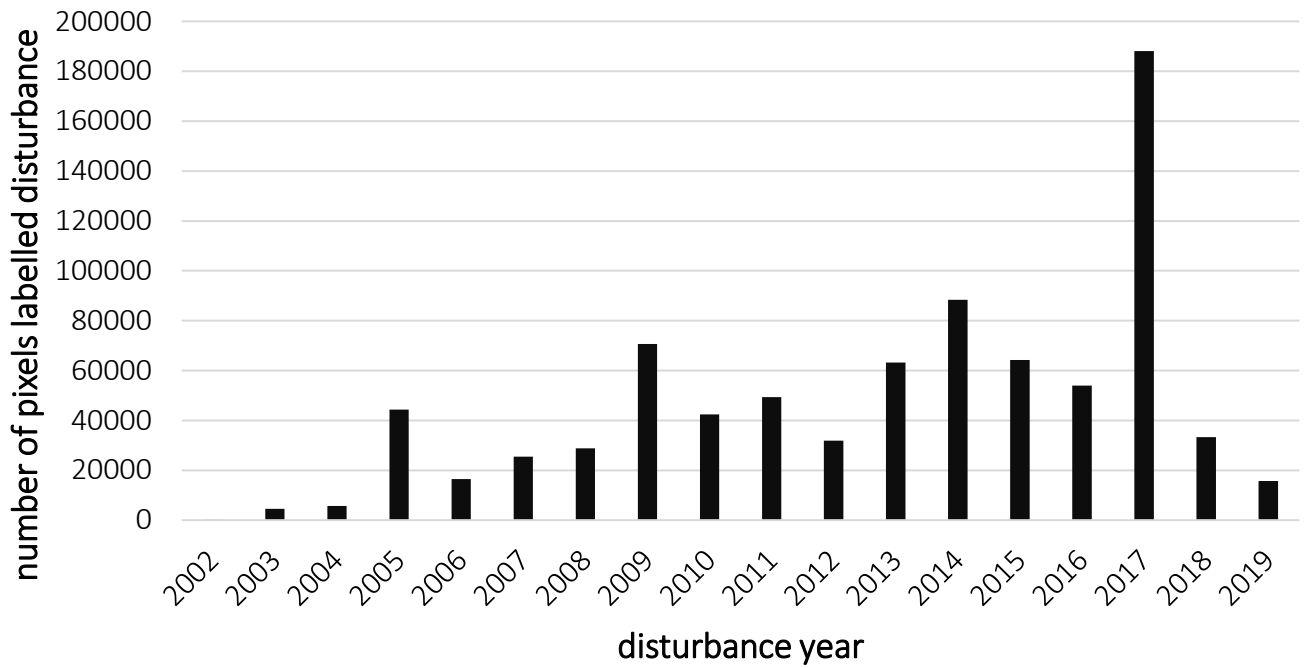


Figure 30 Histogram showing the number of pixels labelled as disturbance for every year during the study period for Bench Maji

Comparing the number of disturbances per year summed up for all zones, Figure 31 shows an increasing trend in disturbances from 2002 to 2009. The following years remain on a high number of disturbances until 2017. Recently, however, a decreasing trend has been computed and less forest areas seem to be lost or degraded. Considering the sum of the disturbance magnitude pixels in Figure 32, all study areas demonstrate low change magnitudes with value of 4 or 8.

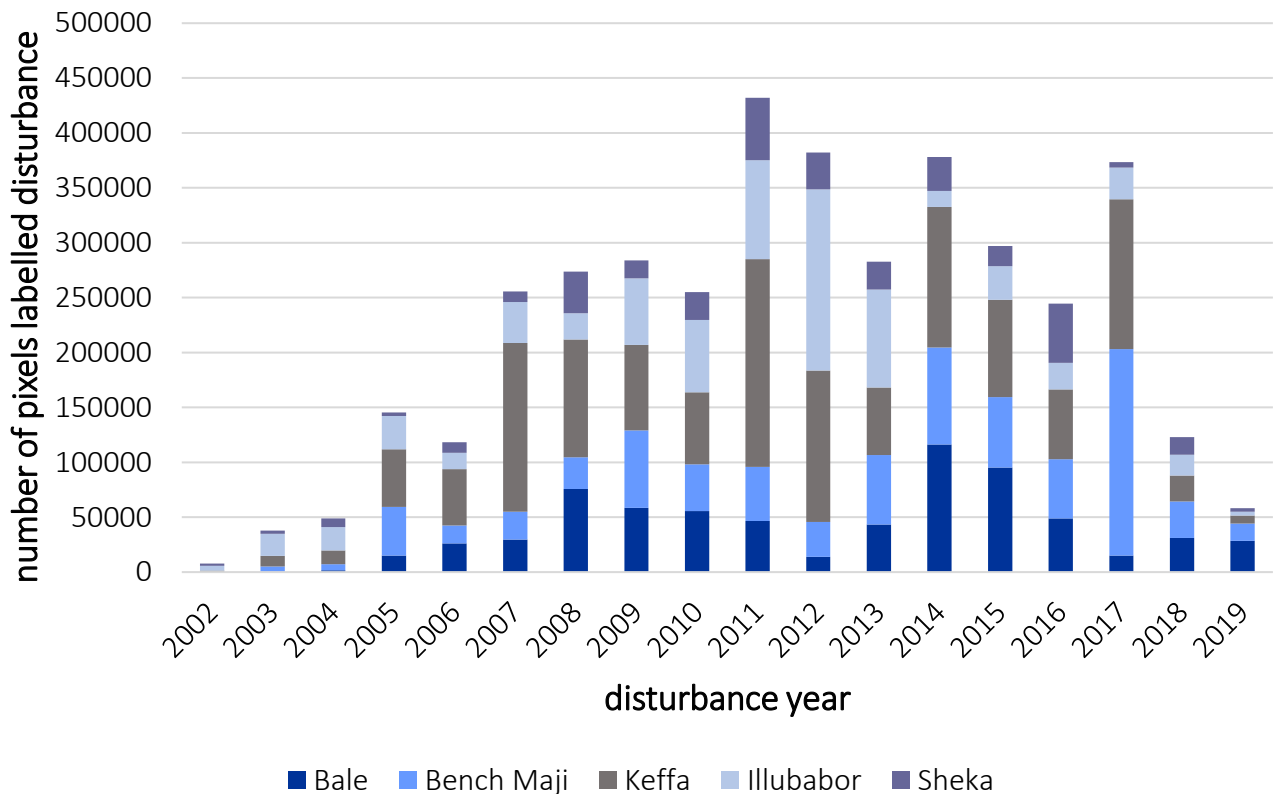


Figure 31 Histogram showing the number of pixels labelled as disturbance for every year during the analysis period summed up for all study zones

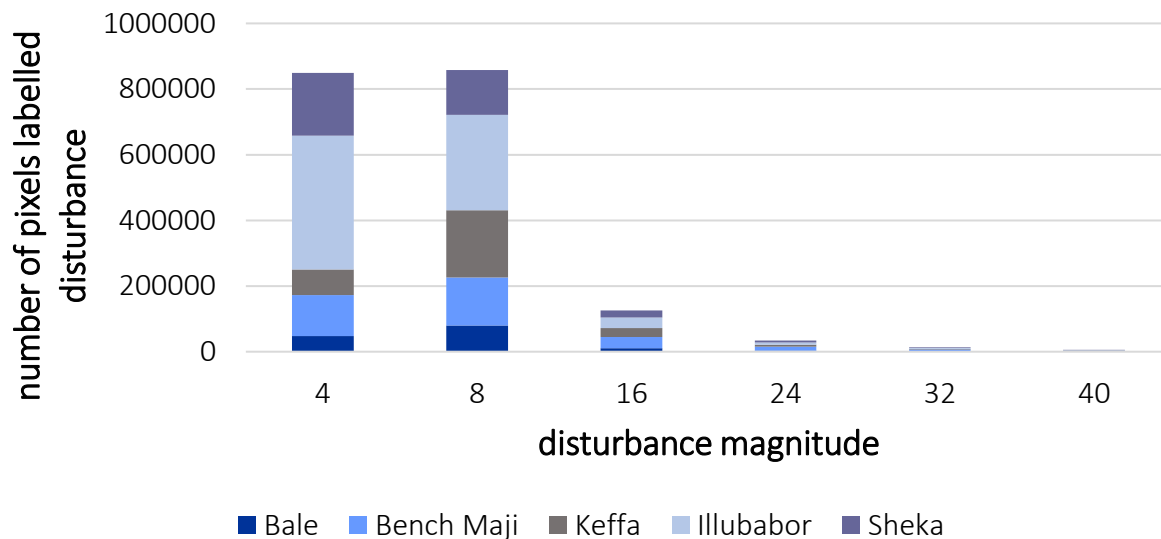


Figure 32 Histogram showing the number of pixels labelled as disturbance for the different disturbance magnitudes summed up for all study zones

Table 9 reveals the highest absolute forest loss over the last 20 years happened in Keffa zone, followed by Illubabor. In general, over all the zones substantial forest areas are lost. However, even more significant in size are the forest gain areas that have been detected, indicating more zones with a net forest gain instead of loss. The relative values illustrated in Figure 33 are defined as the proportion of forest loss area related to the initial forested area in the 1995-2000 composite. Keffa zone is again the region expressing the highest forest loss with the removal of one fourth of the primary forest area. Bench Maji lost around 16% of the forest.

Table 9 Calculated areal forest loss, forest gain and the difference between them for all zones

Zone	Areal forest loss	Areal forest gain	Difference
Keffa	690 km ²	1'052 km ²	362 km ²
Sheka	172 km ²	445 km ²	273 km ²
Illubabor	383 km ²	1'764 km ²	1'381 km ²
Bench Maji	221 km ²	939 km ²	718 km ²
Bale	370 km ²	328 km ²	-42 km ²

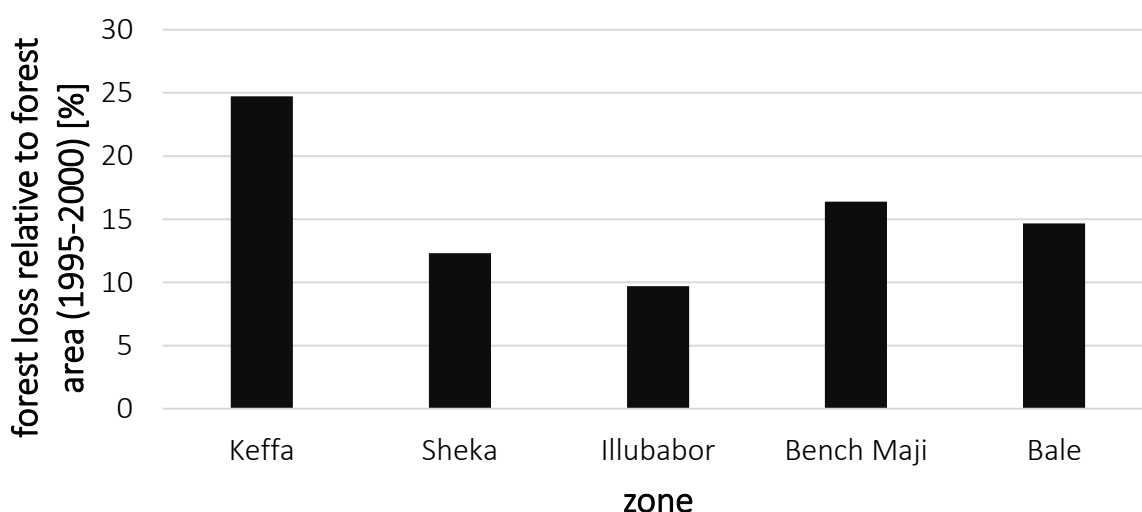


Figure 33 Graphic of the relative forest loss defined as the size of the forest loss area related to the total forested area in 1995-2000 for that zone

6.3 Land cover changes, forest change detection and Participatory Forest Management in the kebeles

Participatory Forest Management is examined detailed with the presented results for four kebeles.

6.3.1 Analysis of Keshi kebele

Keshi kebele is located in Keffa zone and has already implemented a PFM system. The kebele land cover consists mostly of forest and shrubland areas visualized in Figure 34. The total forest area is decreasing over time even though on the classified map the tree cover seems less fragmented. However, particularly along the north eastern boundary forest loss occurred. Grassland and cropland increased over the last 20 years in Keshi plotted in Figure 35. Cropland expanded in the southern part of the kebele.

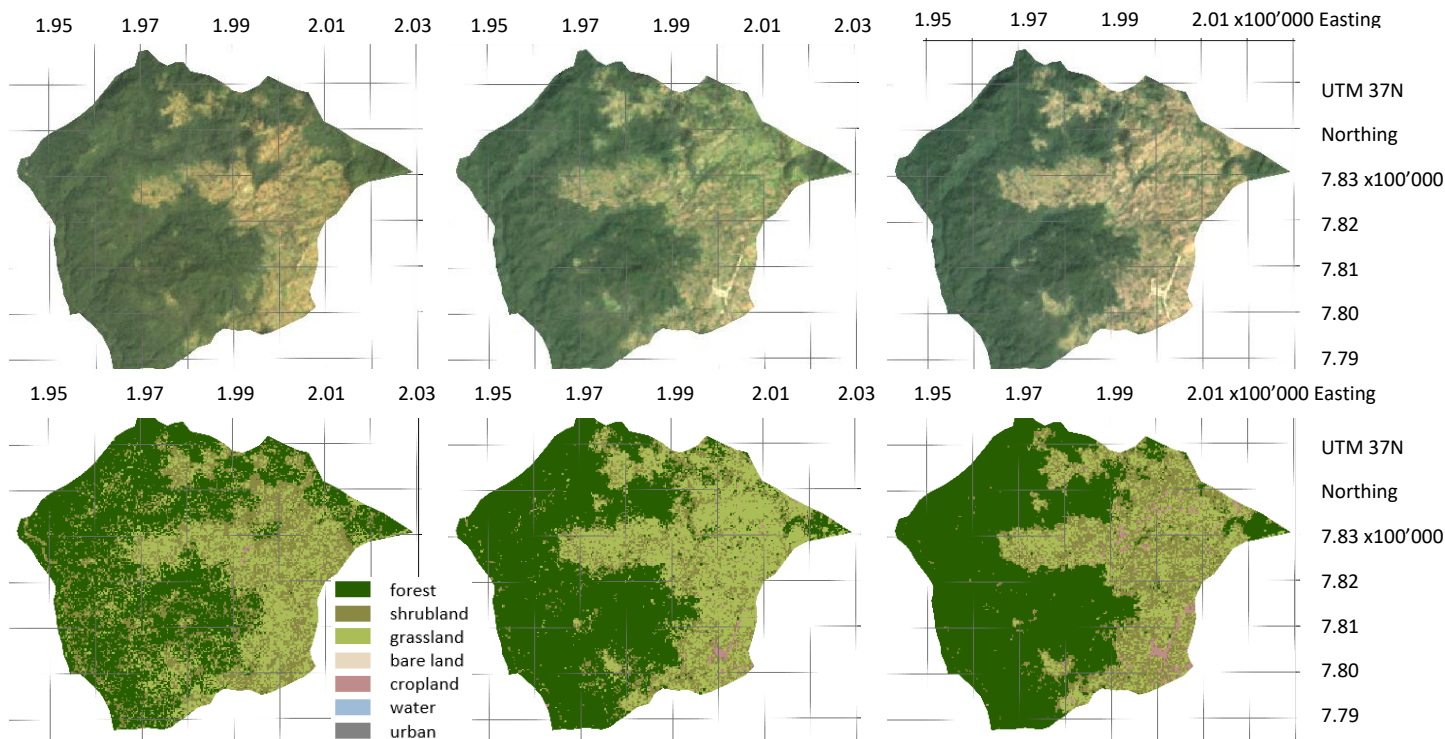


Figure 34 Landsat imagery composites 1995-2000, 2010-2015 and 2015-2020 for Keshi kebele (Google Earth Engine 2020), Bottom: Classified composites 1995-2000, 2010-2015 and 2015-2020

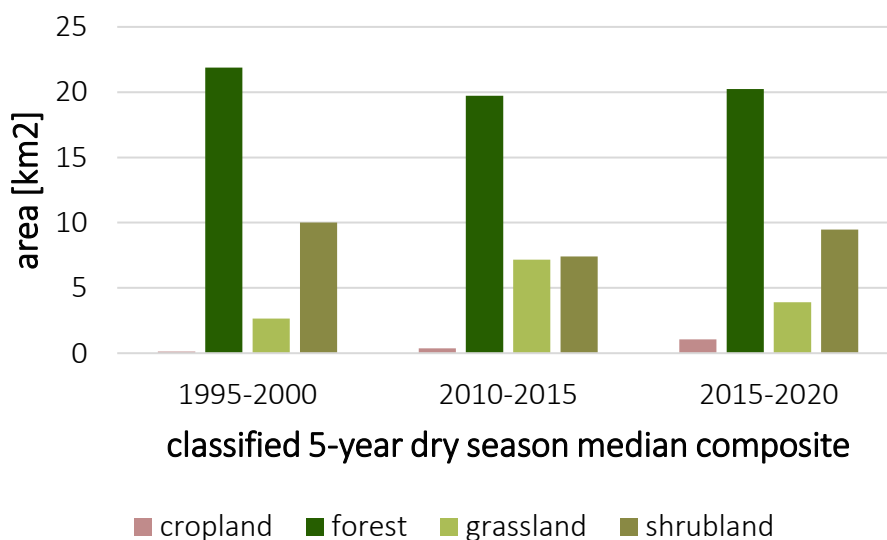


Figure 35 Graphic illustrating the areal size of the different land cover classes per composite for Keshi kebele

On the forest loss change detection scene, it is clearly visible that the north eastern kebele part and the forest edges are affected by deforestation. In other words, Keshi has lost 2,23 km² forest area and the lost areas converted to shrub- or grassland. With the CODED method, the same areas are detected but labelled as degradation rather than deforestation in Figure 36. However, small-scale forest loss has been identified in various places.

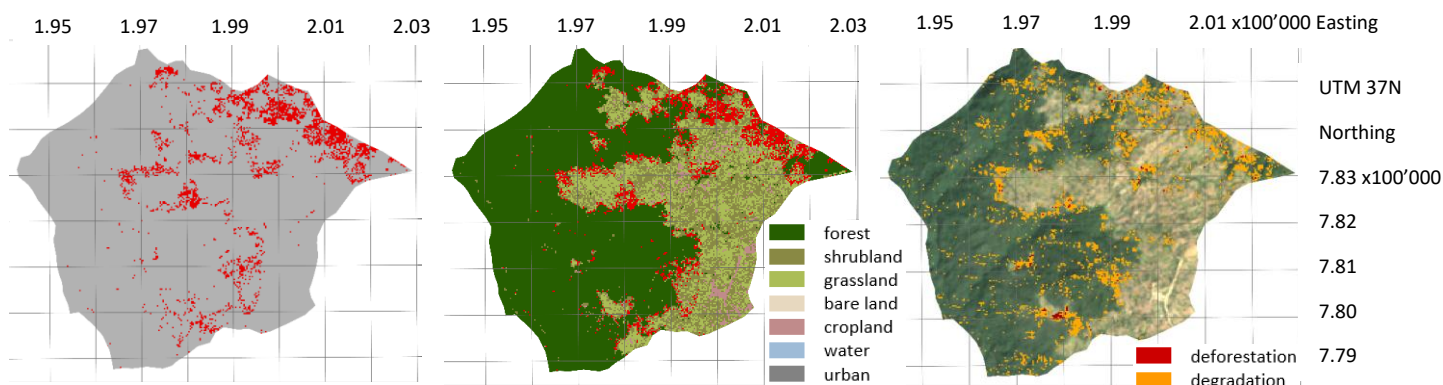


Figure 36 From left to right: Calculated forest loss displayed in red for Keshi kebele, calculated loss in red overlaid on the classified composite 2015-2020, degradation in orange and deforestation in red calculated with the CODED algorithm overlaid on the Landsat imagery composite 2015-2020

The disturbance date histogram in Figure 37 shows several disturbances happened in 2005, 2007 and 2015. While the years in between show a high number of degradation and forest loss, before 2005 and after 2015 less disturbances occurred in Keshi. The majority of the disturbances lie between the values 4 and 8.

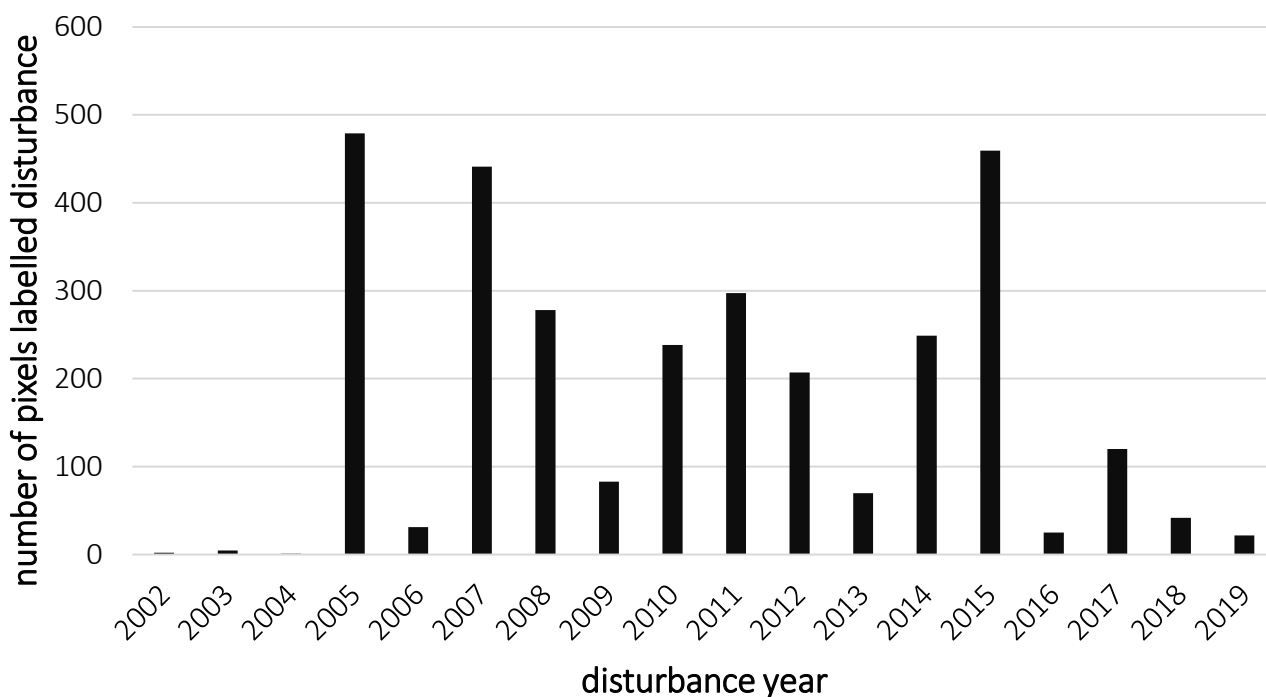


Figure 37 Histogram showing the number of pixels labelled as disturbance for every year during the study period for Keshi kebele

6.3.2 Analysis of Chebere kebele

Chebere kebele which is located in Illubabor zone does not yet have applied PFM projects. The satellite imagery composites and the corresponding classifications in Figure 38 show a clear deforestation region along the south western boundary of the kebele. While in the 1995-2000 composite the forest is still there, it has been removed in subsequent composites. Shrubland being the biggest land cover class in Chebere increased over the two decades time period whereas cropland decreased visualized in Figure 39.

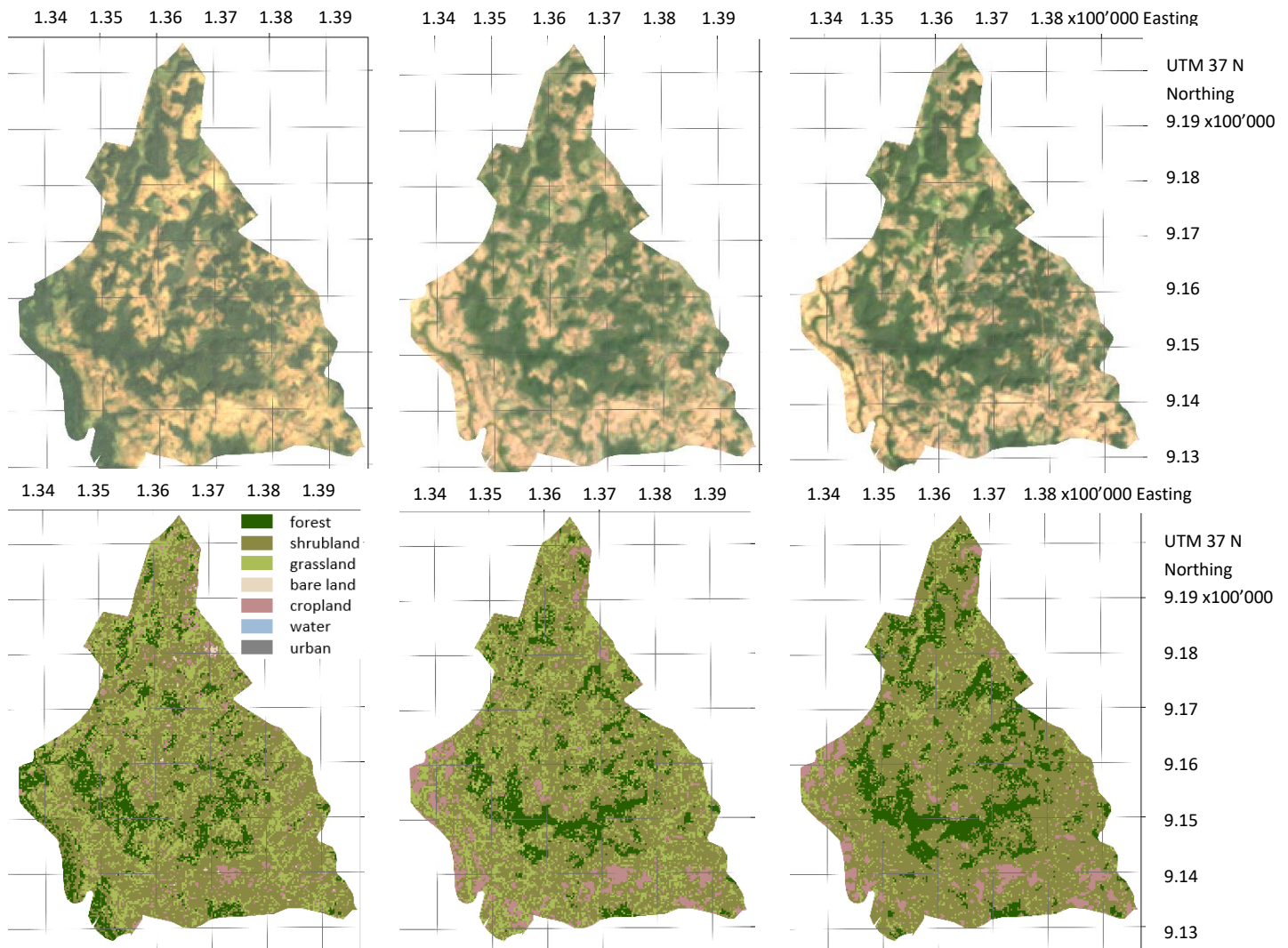


Figure 38 Landsat imagery composites 1995-2000, 2010-2015 and 2015-2020 for Chebere kebele (Google Earth Engine 2020), Bottom: Classified composites 1995-2000, 2010-2015 and 2015-2020

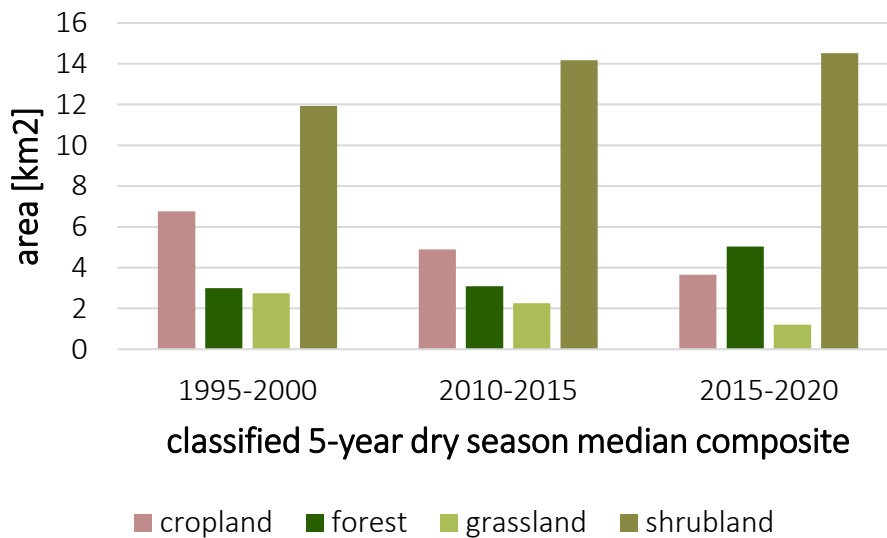


Figure 39 Graphic illustrating the areal size of the different land cover classes per composite for Chebere kebele

In Chebere 1.27 km² forest area has been removed and converted mostly to shrubland or cropland. Clearly, the largest loss occurs at the southwestern border, however, deforestation is distributed over the whole kebele. The CODED approach measures clear deforestation at the boundary as well and degradation processes occurring in several other forested parts mapped in Figure 40.

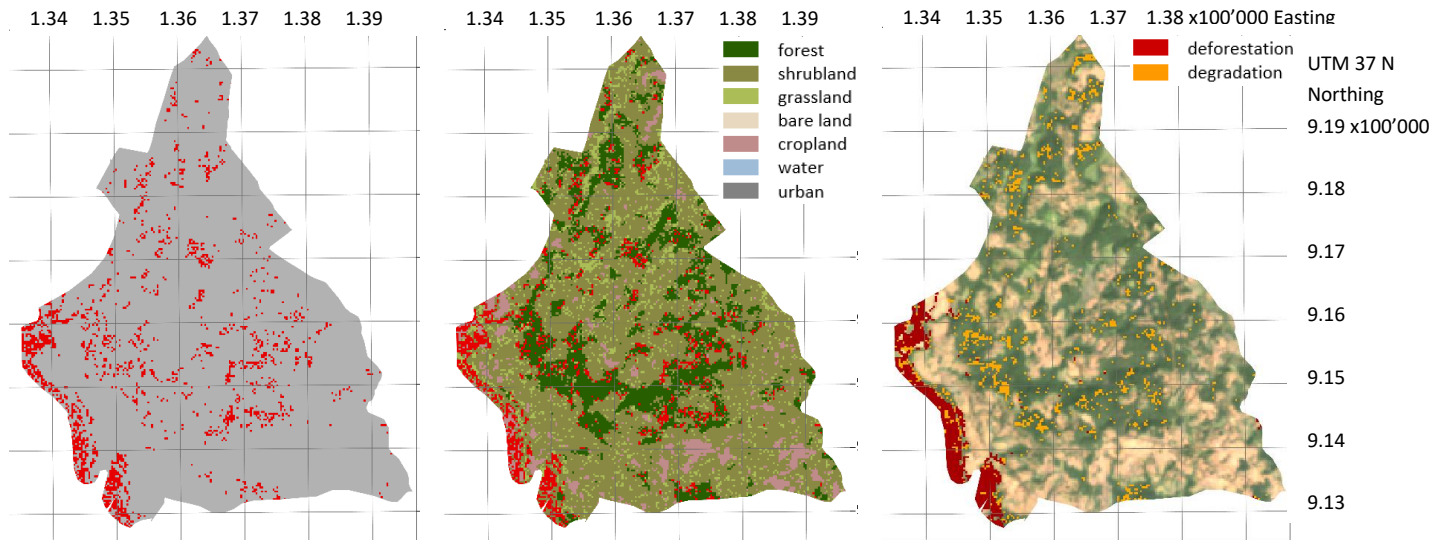


Figure 40 From left to right: Calculated forest loss displayed in red for Chebere kebele, calculated loss in red overlaid on the classified composite 2015-2020, degradation in orange and deforestation in red calculated with the CODED algorithm overlaid on the Landsat imagery composite 2015-2020

The disturbance date distribution expresses numerous disturbances between 2005 and 2012 which correspond to the large loss that happened after 2000 and before 2010 in Figure 41. The change magnitudes lie between 5 and 9.

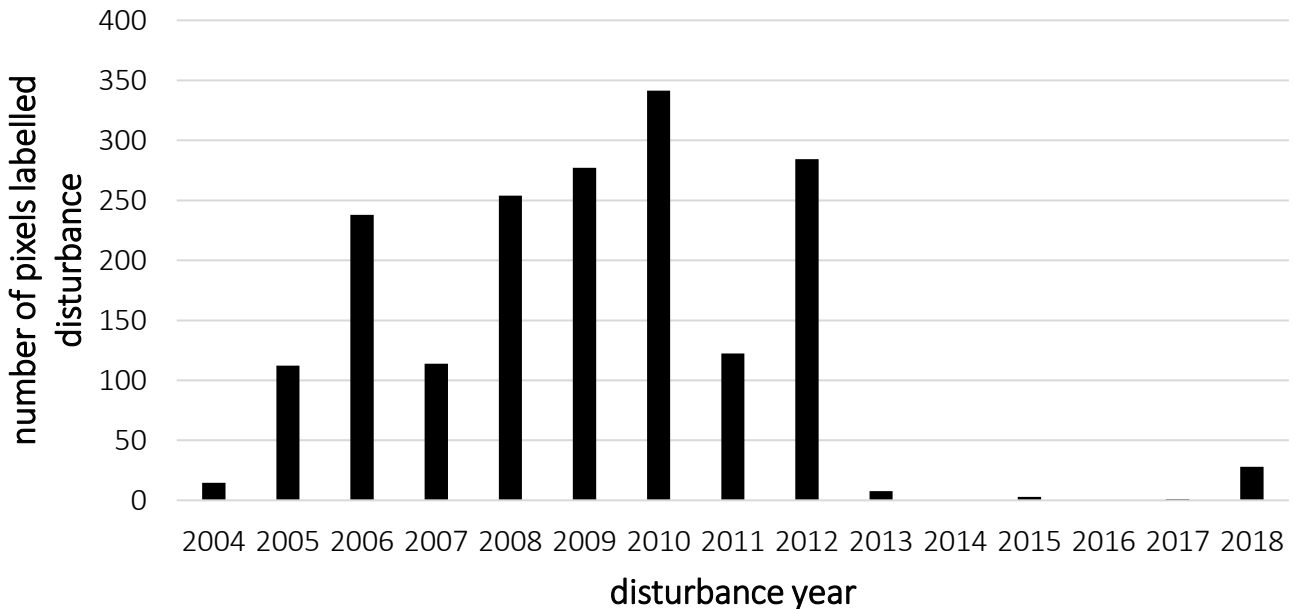


Figure 41 Histogram showing the number of pixels labelled as disturbance for every year during the study period for Chebere kebele

6.3.3 Analysis of Giz Meret kebele

Bench Maji zone contains the Giz Meret kebele which has applied PFM projects. On the satellite imagery composites in Figure 42, apart from the village in the south-central part, the main street running through the kebele stands out. Over the years the street appears developing. On the classified composites, forest area seems relatively stable although it first decreased and after that increased over the course of the last 20 years. The cropland class expands while grassland reduces visible in Figure 43.

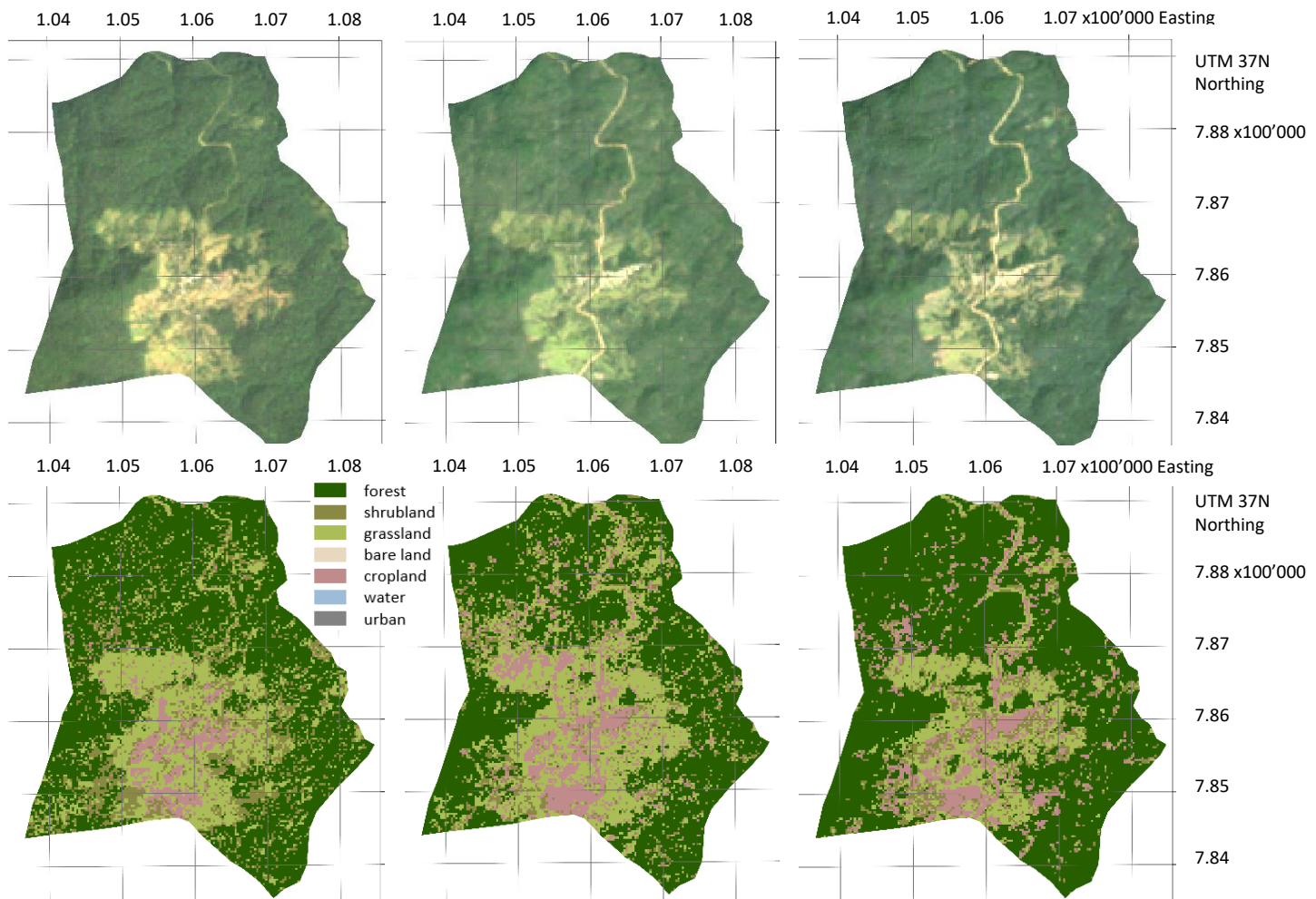


Figure 42 Landsat imagery composites 1995-2000, 2010-2015 and 2015-2020 for Giz Meret kebele (Google Earth Engine 2020), Bottom: Classified composites 1995-2000, 2010-2015 and 2015-2020

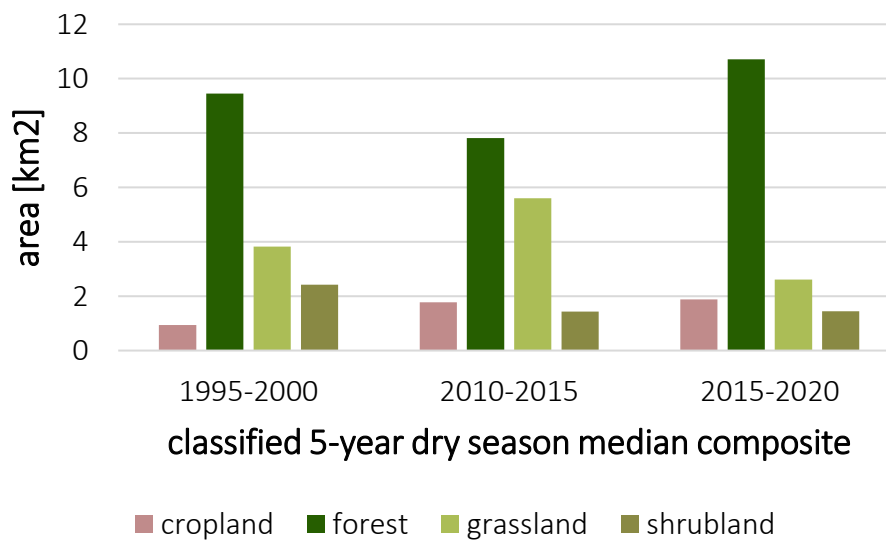


Figure 43 Graphic illustrating the areal size of the different land cover classes per composite for Giz Meret kebele

Giz Meret has lost 1.07 km² forest area and mainly in favour of cropland. In comparison to other kebeles, the loss is low. According to the CODED version, most forest areas appear degraded rather than deforested mapped in Figure 44.

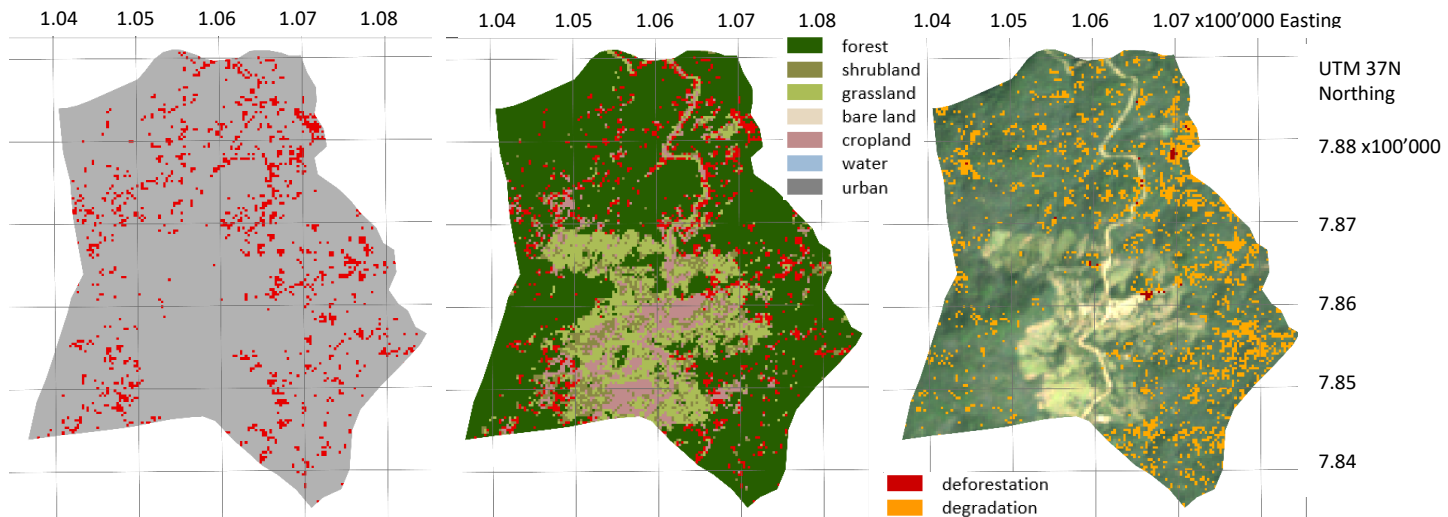


Figure 44 Giz Meret, From left to right: Calculated forest loss displayed in red for Bench Maji zone, calculated loss in red overlaid on the classified composite 2015-2020, degradation in orange and deforestation in red calculated with the CODED algorithm overlaid on the Landsat imagery composite 2015-2020

The disturbance dates visualized in Figure 45 highlight two points in time with an elevated number of disturbances. The years regarded are 2011 and 2014. During the course of the 20 years, the forest in Giz Meret has not been disturbed much despite those two exceptions. The change magnitude varying between the values 5 and 8 is low.

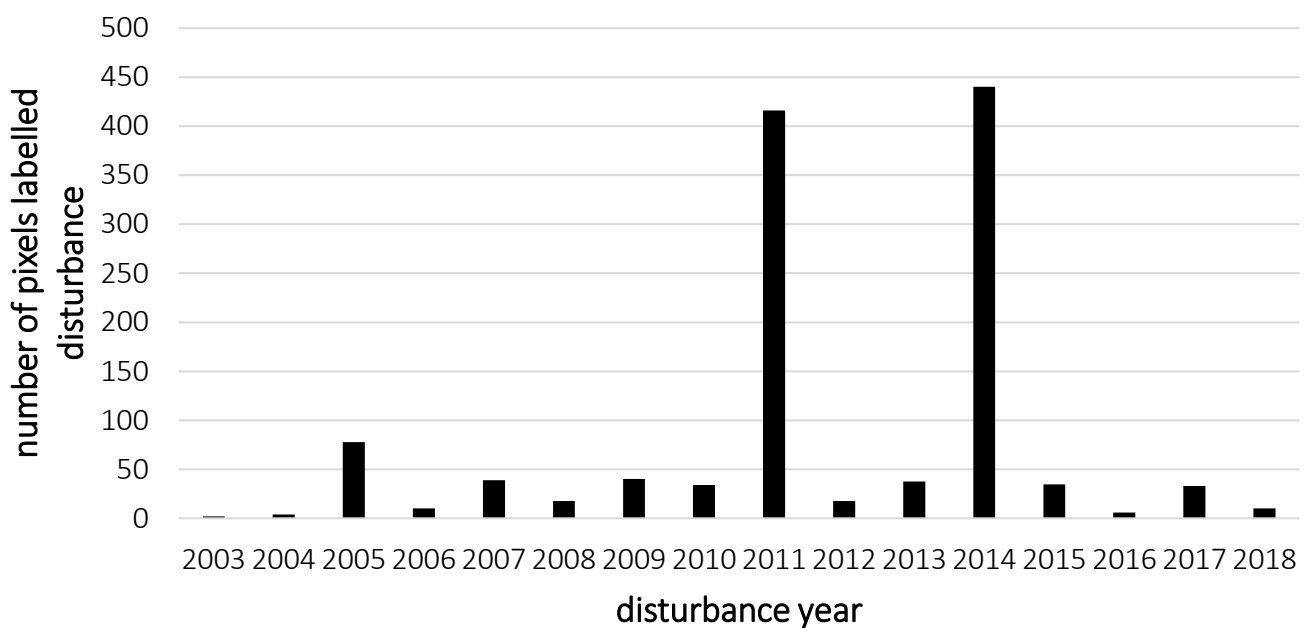


Figure 45 Histogram showing the number of pixels labelled as disturbance for every year during the study period for Giz Meret kebele

6.3.4 Analysis of Sodu Lelaftu kebele

Sodu Lelaftu, a kebele located in Bale zone has not yet implemented PFM strategies. The forest area in that Kebele has been decreasing continuously illustrated in Figure 46. Particularly, areas with already existing forest clearings observed in the 1995-2000 composite are further affected by deforestation. Simultaneously, cropland, shrubland as well as grassland increased gradually in Sodu Lelaftu observed in Figure 47.

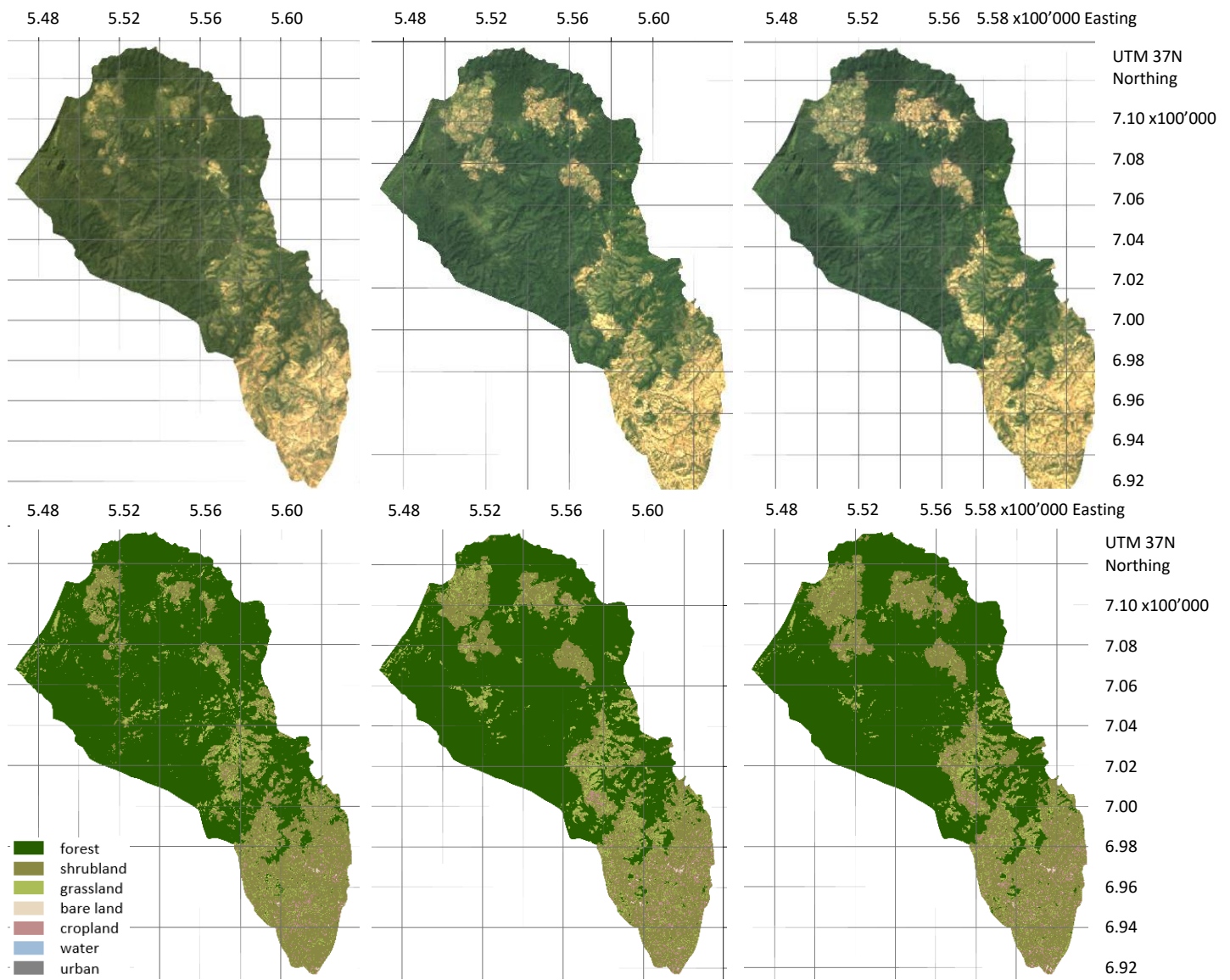


Figure 46 Landsat imagery composites 1995-2000, 2010-2015 and 2015-2020 for Sodu Lelaftu kebele (Google Earth Engine 2020), Bottom: Classified composites 1995-2000, 2010-2015 and 2015-2020

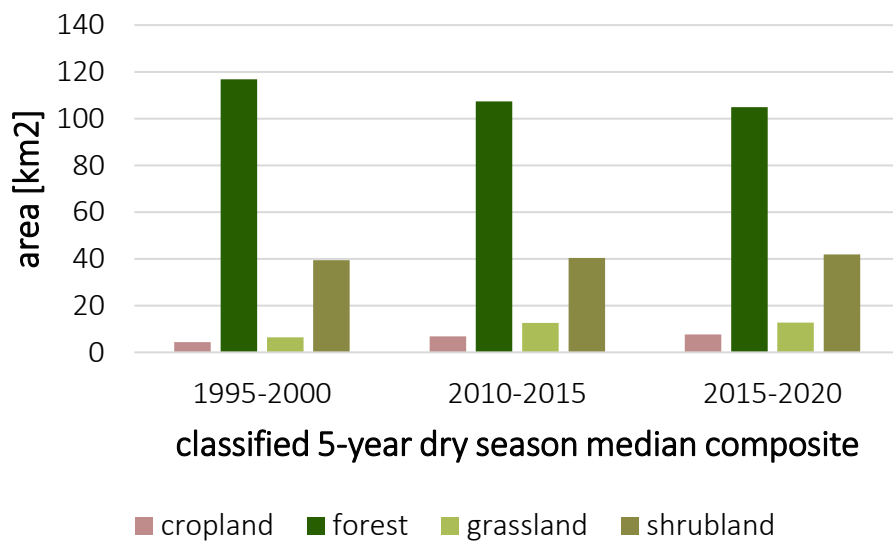


Figure 47 Graphic illustrating the areal size of the different land cover classes per composite for Sodu Lelaftu kebele

Tree cover removal happens largely at the forest boundaries mapped in Figure 48. The CODED degradation detection confirms multiple degraded and deforested areas at the forest edges. In Sodu Lelaftu 16.16 km² forest area has been cut down during the last 20 years. A wide range of those areas transitioned to shrubland or in fewer places to grassland.

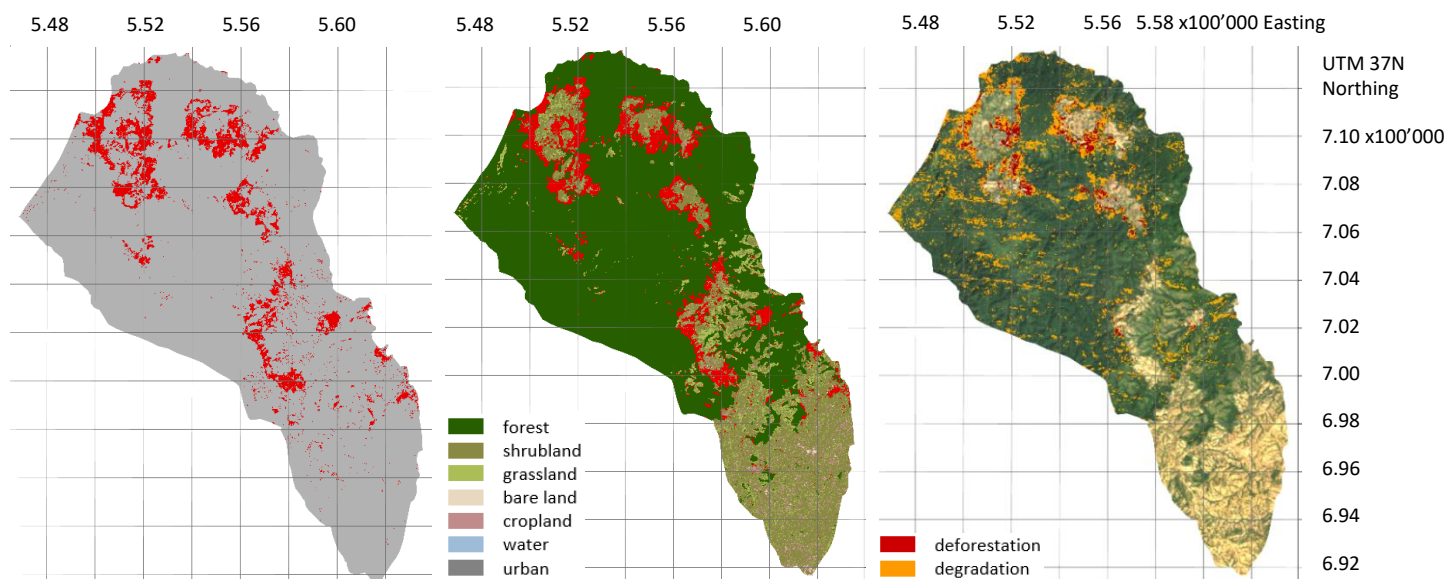


Figure 48 From left to right: Calculated forest loss displayed in red for Sodu Lelaftu kebele, calculated loss in red overlaid on the classified composite 2015-2020, degradation in orange and deforestation in red calculated with the CODED algorithm overlaid on the Landsat imagery composite 2015-2020

The peak expressing most disturbances was reached in 2010 and also the years before show a large number of disturbances visualized in Figure 49. Interestingly, again in the last two years several disturbances have been detected. A substantial number of pixels identified as disturbance belong to a change magnitude category between 5 and 9.

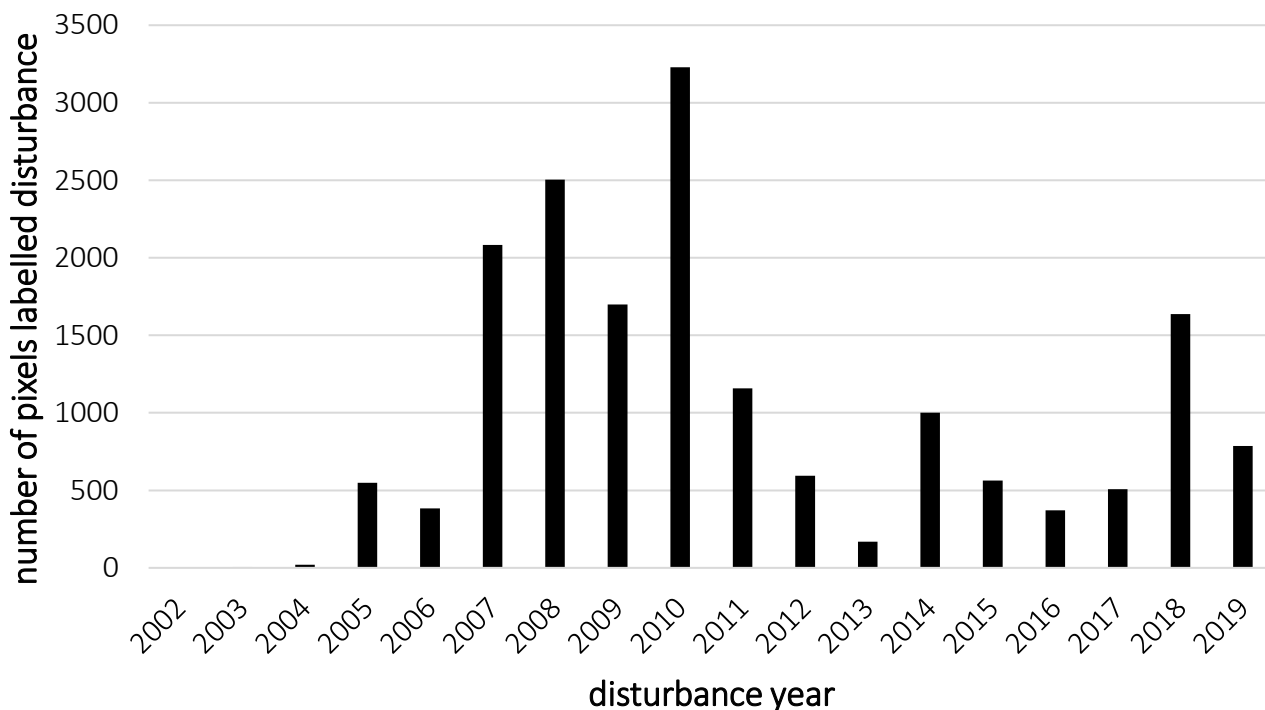


Figure 49 Histogram showing the number of pixels labelled as disturbance for every year during the study period for Sodu Lelaftu

6.3.5 Comparison of all ten study kebeles

In general, the kebeles show diverse deforestation and degradation patterns. For example, Giz Meret having less deforestation and implemented PFM strategies, while Keshi being a PFM Kebele as well still has high deforestation rates. Over all ten study kebeles, the non-PFM areas show higher relative forest loss illustrated in Figure 50. Almost all lost forest areas converted to shrubland.

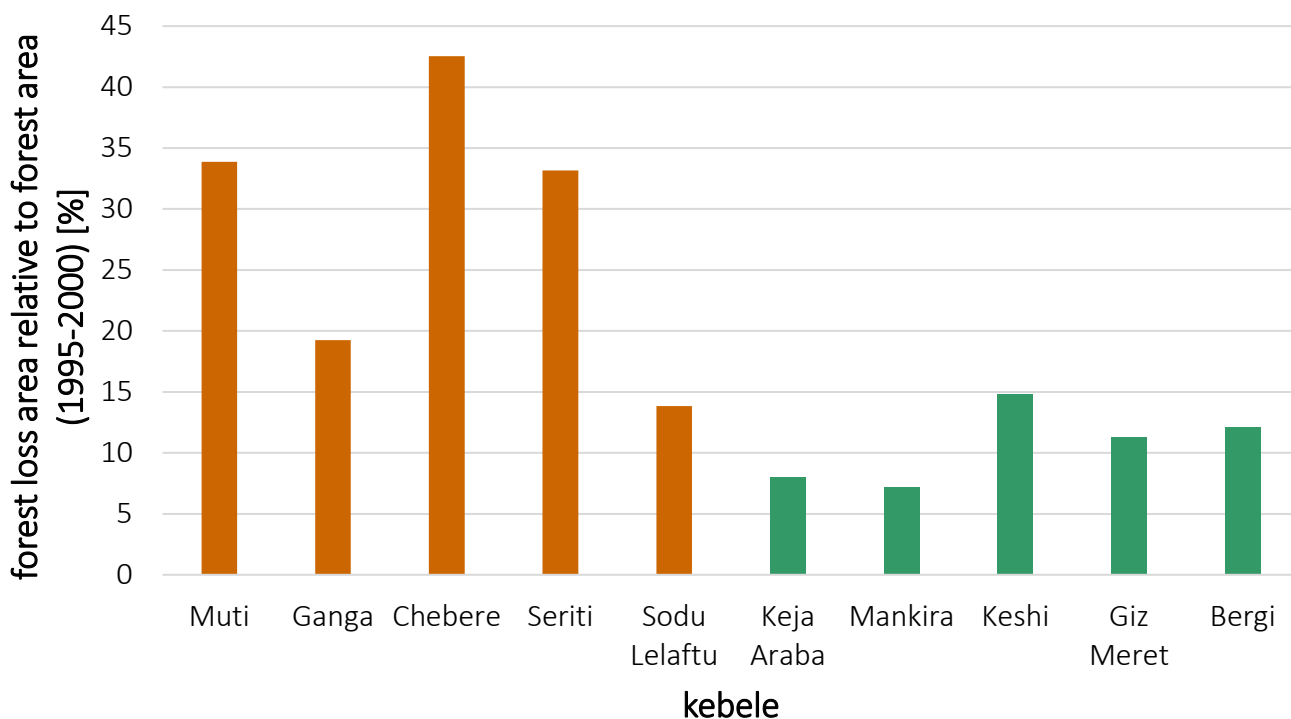


Figure 50 Graphic of the relative forest loss defined as the size of the forest loss area related to the total forested area in 1995-2000 of that kebele, orange-brown coloured are the non-PFM kebeles and green marked are the PFM kebeles

Over the last 20 years, an overview of the forest loss areas in all known kebeles shows that in Keffa the PFM kebeles express less deforested areas than the non-PFM kebeles mapped in Figure 51. Generally, the same is observed in the other four study zones even though in some PFM kebeles exceptions exist. In Illubabor, in the Biosphere Reserve less forest has been removed in comparison to the remaining zone.

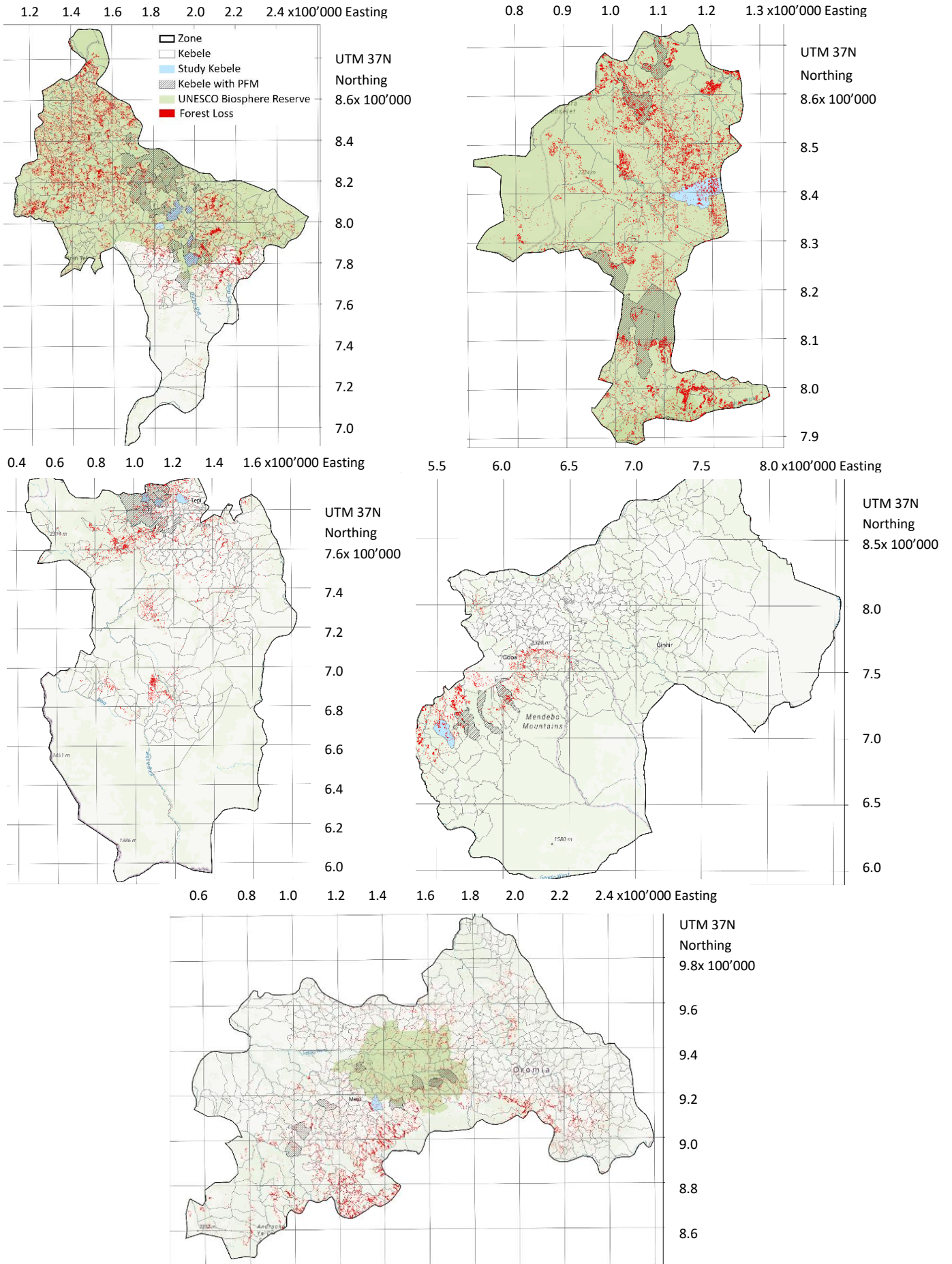


Figure 51 Maps of the study zones highlighting the forest loss to directly compare deforestation in PFM-and non-PFM areas (UNESCO 2020; Dresen 2011a; Plan Vivo 2014)

7 Discussion

The following section discusses the utilized data basis and the applied methods. Furthermore, it reviews the results and outlines additional topics.

7.1 Data

The availability of useful imagery over Ethiopia is limited due to satellite problems explained in section 4.1.1. Moreover, optical satellite data, such as the used Landsat imagery, is affected by environmental and atmospheric factors caused by the tropical climate conditions over the Afromontane rain forest in Ethiopia (Dorais et al. 2011). Examples of atmospheric disturbances are high water vapour content, haze (Sahle et al. 2018), aerosols and clouds (Asner 2009). Furthermore, the measured spectral properties might be affected by the different growing conditions of tropical canopies due to various chemical and structural features originating from different species (Asner 2009). Hence, the recorded spectral information contains an uncertainty and influences the deforestation and degradation measurements (Asner 2009). In this study, compositing aided reducing the effects of clouds, shadow, haze and missing data (Pimple et al. 2018). The application of the median compositing method to extract dry season scenes particularly supported minimizing cloud cover. However, minor imagery disturbances remained and might have resulted in errors in the land cover classification and change detection. Additionally, there exists a data gap of 10 years between the first and second composite due to missing high-quality Landsat imagery over Ethiopia for that period.

The Sentinel-2A land cover product of Ethiopia has been selected as training data. Despite its advantages such as the high spatial resolution and recent release year, it is regarded as a prototype that still needs improvements. Hence, the product possibly causes problems in the classification because it is not specifically developed for Ethiopia or rain forest environments but for land cover maps of the entire continent Africa. Moreover, it is a yearly land cover product not centring particularly on the dry season and has a lower temporal resolution compared to today's possibilities because in 2016 Sentinel-2B imagery was not available.

Overall, the Landsat images of the missions 5 and 8 and the Sentinel-2A land cover product offer interesting information for forest change detection purposes. However, compositing as a way of pre-processing is strongly recommended for the satellite scenes in particular when observing tropical forests and for the training data it is proposed that it should be validated especially if utilizing a not yet finalized product.

7.2 Methods

Generally, the selected approach in this thesis starts with traditional techniques by conducting a supervised classification and applying the post-classification comparison technique, and fluently shifts to modern and more recent methods by using time series to compute the forest degradation. At the same time, in the beginning, the data has been analysed on the zonal level to obtain an overview of the forest loss at a large scale and continued with the examination of the local level (kebeles) to profoundly evaluate PFM impacts on the forest.

7.2.1 Unsupervised classification

Challenges identified in the unsupervised classification approach helped improving the supervised classification process. A major problem detected in the beginning is the transferability from one zone to another because not all five selected study zones contain the same land cover classes. For instance, Keffa does not have bare land and thus Bale zone would not be represented appropriately due to missing land cover categories. Therefore, all zones have been considered when choosing the land cover classes. Based on the gained experience during this research, it is suggested to include all possible classes existing in the different study regions if more than one area of interest is selected. Furthermore, the training data should be sampled in the study areas in order to prevent misclassification due to different spectral properties. Although the unsupervised classification has not been used as training data, it enhanced the class definition process because multiple classes and their distribution are mapped automatically without prior knowledge of the area of interest. It might further support the selection of valuable field data sample locations.

The class woodland was excluded after the application of the unsupervised classification. Usually, it refers to the transition between forest and shrubland and is found in altitudes around 1'300 m.a.s.l (Hylander et al. 2013). However, woodland is not sufficiently defined for remote sensing applications. Consequently, it is hard to detect this class in satellite imagery. Thus, the five study zones contain either the class forest (dense and open) or shrubland and woodland is considered as included in the forest class.

7.2.2 Class definition for the supervised classification

A challenge with the supervised classification is related to finding characteristic feature descriptions in the context of remote sensing because accurate class representations improve the classifiers training data and accordingly the classification. By visual inspection, some sample points are manually relocated to typical locations of the class based on our perspective and knowledge. After this step, the classes appear more homogenous. However, it must be acknowledged that the classifier is trained on the spectral properties of all bands which are not directly visible by researchers and therefore detected classification errors might not be real as a person solely identifies known features observed in a limited number of bands. Nevertheless, the sensor might be influenced as well by diverse types of soil, different topography and vegetation density in the five study zones and therefore the same class might be represented by varying spectral signatures which could result in misclassifications (Hailemariam et al. 2016).

An additional possibility to enhance the class definition is the inclusion of seasonality with NDVI time series. This could support differentiating between cropland and plantations which is useful information to develop forest management strategies. Even though the use of an existing land cover product as training data works, it is vital to check the classification results. Crucially, the supervised classification being based on the training data adopts its quality and expresses similar accuracy.

7.2.3 Accuracy assessment of the supervised classification

The accuracy assessment of the land cover classification in this study is conducted with a confusion matrix. A wide range of factors contribute to an uncertainty in the classification and its validation. For example, imagery interpretation mistakes, data entry errors (Lillesand et al. 2015), distinct sensor properties or ground conditions (Foody 2002). As the validation mostly happens at the final product stage, errors introduced in an earlier step such as an inappropriate sampling method or number of samples are not directly assessed (Banko 1998).

A basic assumption using a contingency table relates to reference data representing reality but in fact, ground truth information is also a classification and may contain errors (Foody 2002). Therefore, it is essential to understand that the quality of the accuracy estimation depends directly on the reference data (Lillesand et al. 2015) which may originate from field trips or might be different remotely sensed information (Lillesand et al. 2015). Two different reference datasets are used in this thesis. First, an independent land cover product was included. The confusion matrix showed very low accuracies around 28% which might be connected to a lower spatial resolution of 100 meters in the PROBA-V dataset or the difference of one year between the training and reference data. Moreover, the initial classes of the training and the validation dataset are not the same, but both are categorized into the previously selected final classes in order to compare them. Another reason for the low accuracy might be the manual relocation process of sample points in the training data which was not conducted with the reference data. Secondly, a confusion matrix with the splitting approach has been computed which uses 30% of the Sentinel-2A training data for the validation. Implementing this approach, the accuracy of the validation error matrix increased to a level of 86% and is therefore over the 85% strived by remote sensing researchers. Essentially, the accuracy assessment method and reference data should appropriately reflect the use of the classification (Lillesand et al. 2015).

Hence, a confusion matrix provides a description of the classification accuracy and serves as an initial information source for the supervised classification validation (Foody 2002) but has to be assessed as well.

7.2.4 Change detection

The timing of the image acquisition plays a role for natural vegetation mapping and change detection (Lillesand et al. 2015) for example in this study the dry season has been chosen to measure the largest possible difference between evergreen forest and dry grassland or cropland. As a rule it is crucial to measure at the same time of the year to ensure alike environmental conditions, such as the atmospheric composition (Lillesand et al. 2015). By using composites with a similar vegetation state but gathered from different years, such as the implemented median compositing approach, significant change detection is enabled (Coppin et al. 2004).

The accuracy of the post-classification comparison technique depends on the quality of the primary training data and the accuracy of the individual classifications which are compared (Coppin et al. 2004; Lu et al. 2004). Therefore, the challenge is to produce consistent and accurate classifications before conducting the change detection as errors might be introduced by misclassifications (Coppin et al. 2004). It is possible that in the calculated change detection contains misclassified pixels and thus incorrectly detects conversions that occur due to the quality of the satellite imagery and the classification.

Through the comparison of two classified images with a time-lag of 20 years, some land cover changes happening in between are missed. For this reason, time series analysis, for example the Continuous Degradation Detection (CODED) algorithm better depicts all conversions and further detects gradual changes. While the post-classification comparison detects deforestation, CODED additionally analyses forest degradation.

7.2.5 Validation of the change detection

Generally, there is a limited number of recent and validated high spatial resolution land cover products for Ethiopia. However, the Hansen forest change product is available for the entire world having a spatial resolution of 30 meters and starting in the year 2000. Therefore, it serves as the validation dataset for the forest loss. Even though the calculated forest loss values and the Hansen dataset show differences, the latter is a global product and not specifically developed for Ethiopia. A visual based validation has been conducted and documented. Nevertheless, image analysts might be biased, and therefore the interpretation underlies an uncertainty. However, the developed change detection algorithm works locally and seems better adapted to the area than the Hansen dataset. While the loss areas are captured very well, the gain areas demonstrate some problems. Mostly, the issues are connected to the first composite 1995-2000 where only Landsat 5 data is included. In the gain areas atmospheric disturbances such as haze, fog, smoke, or cloud rests appear to cover parts of the underlying forest. Therefore, the forest is not identified because the spectral properties do not match the forest training data and the pixels are misclassified as grassland, shrubland or cropland. The newer the imagery, the fewer atmospheric disturbances are visible. In other words, on the Landsat 8 composite 2015-2020, forest seems to be detected correctly. The forest gain depends substantially on the quality of the composite imagery and the classification accuracy. Nonetheless, the same could apply to the forest loss detection as similar problems including atmospheric disturbances could result in misclassifications and thus an inaccurate change detection although in the validated loss areas this issue is not observed.

7.2.6 Continuous Degradation Detection (CODED)

The accuracy of the CODED results depends on the land cover class training data that has been defined manually. Furthermore, the output is also based on the initial parameter setting. An appropriate parameter combination is essential for a successful degradation detection. Analogue numerous other algorithms, the accurate detection of low magnitude disturbances remain a challenge because it cannot be clearly distinguished between spectral noise and real effects (Cohen et al. 2017). This might explain the detection of multiple low magnitude disturbances which are consequently attributed with forest degradation rather than deforestation. Importantly, high magnitude changes are identified with higher certainty (Cohen et al. 2017). Thus, the automated classification conducted by using the CODED method demonstrates limitations and uncertainties (Bullock, Woodcock, and Olofsson 2020). However, this approach can serve in a subsequent step as input for a stratification creating sampling points that are interpreted with the tool and validated by field visits at the sample locations (Bullock 2018). For this step, forest experts and field data collectors are necessary with a view to professionally assessing the selected sample areas.

7.3 Results

7.3.1 Land cover changes and forest disturbances in the study zones

Comparing all study zones with a focus on the forest loss, Keffa shows the highest absolute and relative deforestation rates with almost a quarter of the forested area being removed, although a UNESCO Biosphere Reserve has been established and PFM strategies have been implemented for about 10 years. The other study zones have lost between 10 and 15% of the forested area. It is likely, that without PFM application efforts and lack of the Biosphere Reserve, there would have taken place even more deforestation over the last 20 years. Mostly, forest transitioned to shrubland or grassland which could be due to the fact that the forest is surrounded mainly by those two land cover categories. However, even though the forest has not been lost directly to increasing urban areas or cropland, it is clear when comparing to Google Earth for example that in the Keffa zone multiple deforestation areas are related to the expansion of agricultural activities. Forest might have been cut down to provide wood as construction material for the new inhabitants. A possible explanation for the conversions from shrubland to urban is that the area around the cities has been deforested before the selected analysis period began and is therefore already shrubland. As forest loss commonly happens at the forest boundaries in Keffa, existing forest clearings are extended to support alternative land uses.

In Bench Maji, clearly visible in the northern part close to the capital city Mizan Teferi is an area affected by large-scale deforestation and degradation. Direct communication with Caritas Switzerland revealed that the observed area with an accurate road network and distributed settlements could be transport roads and forest product storages for understory forest products such as coffee. Further research confirms that it is the Bebeke coffee estate being Ethiopia's oldest and largest coffee plantation with a size of about 100 km² (Horizon Plantations 2020). Evidently, forest is lost and degraded in favour of the coffee plantation. Additionally, this sample case proves the importance of forest experts and local people's opinion to examine the reasons for ongoing deforestation detected with satellite imagery since it is valuable information for the researcher as well as for the cooperatives to establish an automated monitoring system approach.

The observed forest gain in multiple study zones can be explained in different ways. Possibly, a real gain is observed owing to the application of forest management strategies or controlled afforestation. Furthermore, other studies demonstrated transitions from shrubland to forest (Kedir et al. 2018) which is alike our findings that mostly shrubland turned to forest which could be connected to a forest regeneration, mainly in PFM areas. Likely, those are abandoned or protected areas transforming back to forest. On the other hand, it could reflect misclassifications in the two first composite which both include Landsat 5 data and as the training of the classifier has been calculated on a Landsat 8 dry season composite of 2016, it could lead to some minor discrepancy due to sensor differences. However, a harmonization was performed particularly for this reason. Moreover, researchers might be biased and perceive forest even though the classifier is perhaps able to better distinguish because it decides based on the measured spectral properties. Despite concentrating on forest changes which include forest gain, this study primarily focused on the forest loss since the validation of various forest gain areas showed confusing results. Therefore, less attention is paid to these outputs. Future research could centre on forest gain regions and validate those by comparison to other datasets or collecting field data.

The precipitation data neither correlates with the number of disturbances over the 20 years in the study zone Keffa nor in the four other study zones. For this reason, it is interpreted that anthropogenic drivers lead to the forest degradation and deforestation instead of natural causes. Interestingly, in 2019 the amount of rainfall significantly increased in all study zones. All diagrams displaying the phenomenon are presented in chapter 11 Appendix II Results.

Regarding the change magnitudes, numerous pixels express low magnitudes and therefore more degradation instead of deforestation areas appear. Nevertheless, it has been discussed in the CODED section that usually more areas with low magnitudes are found due to spectral noise. Reasons for forest degradation in the study areas are probably naturally based such as fires, windfall, flooding and insect damage or human-induced including selective logging or damage from surrounding activities (Bullock, Woodcock, and Olofsson 2020) which should be evaluated in more detail with in-situ data.

Considering the change dates over all zones, the number of forest disturbances increased until 2011 the peak has been reached. Undoubtedly, after 2017 the disturbances decrease. This could be due to PFM and conservation

measures being applied around 2010 and showing their impacts after 2017. In other words, the UNESCO Biosphere Reserves were designated in 2010 in Keffa and Illubabor and 2012 in Sheka (UNESCO 2020).

7.3.2 Participatory Forest Management

In Keshi kebele, a village is detectable on the 5-year dry season composites that seems growing over time following the development of new streets. Therefore, the deforestation in Keshi likely happened due to population growth and agricultural expansion, which is cross validated with Google Earth (Google Earth 2020). The village itself did not directly lead to forest loss but the need for agricultural land put the forest under pressure. Even though Keshi kebele has PFM, large forest areas have been lost over the last 20 years.

In Chebere kebele, various forest areas converted to shrubland or cropland. This is linked to an increasing necessity for agricultural areas. Today, the deforested areas show regions with farmhouses and crop fields distributed over a large region along the river (Google Earth 2020). Interestingly, the same process happened at the other riverbank. Chebere is a non-PFM kebele and expresses several deforestation areas that happened in the beginning of the 20 years measurement period. Probably, Participatory Forest Management could have helped to stop further loss.

The deforestation in Giz Meret kebele is considered as low in comparison to other kebeles. The village Chismariet seems relatively stable in areal size but is better visible on the satellite imagery composites after 2000. Furthermore, the forest loss is distributed around the village and the main street. The forest clearing in the north eastern part of the kebele consists of a community forest pulping station and coffee store (Google Earth 2020) and thus demonstrates applied PFM strategies. The minor forest loss that has happened in Giz Meret might be caused by road developments and urbanization. However, as the deforestation rate is small, it is concluded that PFM actions functioned.

In Sodu Lelaftu, the change dates demonstrate multiple disturbances up to the present. Forest loss in this kebele could be due to the expansion of grazing land and cropland in the forest clearings. The cleared patches in the north show single houses and agriculturally used fields (Google Earth 2020). PFM might be helpful in Sodu Lelaftu in order to reduce the ongoing deforestation.

By comparing the 10 study kebeles, non-PFM kebeles show higher rates of forest loss than PFM areas. Generally, this supports the assumption that PFM aids reducing deforestation, already concluded in earlier studies (Takahashi et al. 2017). Ongoing deforestation in Ethiopian kebeles result from anthropogenic activities due to population growth and related to that expanding villages as well as the need for agricultural land. The introduction of PFM has a wide range of advantages for the forest such as less deforestation and soil erosion (Winberg 2011). It demonstrates slower forest loss rates and in some areas the forest even increases through the conversion of shrubland to forest (Kedir et al. 2018). On the other hand, several obstacles stemming from different sources, hinder the success of PFM projects such as social, administrative or policy related issues (Winberg 2011). Another crucial factor to effectiveness is to measure the environmental impact by understanding the forest extent and its changes (Winberg 2011) for instance with the use of satellite remote sensing.

Analysing all known PFM and non-PFM kebeles located in the five study zones, the PFM kebeles generally show less deforestation on the maps. In the Biosphere Reserves different outputs become apparent. In Illubabor zone, less deforestation is measured in the Biosphere Reserve compared to other places in the zone, while in Keffa and Sheka in the BR still high forest loss amounts are detected. However, the BRs have a zoning system where only the core sector strictly protects the forest and therefore deforestation is still possible. In general, PFM appears to work successfully in the applied kebeles. However, some PFM kebeles still show high amounts of forest loss. The cause might be connected to unconfirmed PFM areas and likely some PFM kebeles have not yet started with their project implementation. Moreover, PFM projects do not always centre on the environmental aspect but rather on the social aims, hence leading to continuing high deforestation rates. Besides, another reason is that after the project ending the PFM kebeles remain uncontrolled and increasing forest loss occurs. Furthermore, coffee producers profit from the certification and therefore intend to increase their coffee area which consequently causes higher amounts of forest degradation (Takahashi et al. 2017).

7.3.3 Place names

The issue of official place names has already been noticed in the beginning. The location naming is confusing because one spot is called differently in various sources. Furthermore, place names sometimes change. Evidently, Ethiopia lacks an official naming system and the boundaries are not fixed, at least not at the smallest administrative unit level (kebele). This topic relates to the basic right about ownership. Holding property is not secured in the country and the rights may change. Since the local government is responsible for the land property, the situation is regarded as complicated. Additionally, in discussion with Caritas Switzerland they also mentioned that problem, mostly connected to maps. For the farmers, the land insecurity is a major problem as they need to know their farm boundaries and coffee picking areas in the forest. For this reason, the introduction of conservation measures is difficult due to ongoing boundary disputes (Winberg 2011).

7.3.4 Recommendations for Caritas Switzerland

In this research, it has been discovered that PFM strategies helped reducing the forest loss. With satellite remote sensing techniques, PFM project leaders for example Caritas Switzerland are able to map the land cover of their regions of interest and measure the forest changes. Another advantage is gaining pre-knowledge of an area and identifying possible zones for actions or field data collection at relatively low cost. In addition, it enables the establishment of a monitoring system which supports the decision on specific environmental PFM goals. Landsat 5 and 8 imagery with a spatial resolution of 30 meters provide a high-quality data basis with a long time-series and PFM is one of the most successful approaches in Ethiopia to motivate communities to actively and sustainably manage their forest areas (O'Hara 2013). Moreover, the communities seem encouraged if they receive the right to sustainably extract alternative forest products which secure a continuous income (O'Hara 2013). Therefore, the evaluation of the environmental side of the PFM project is suggested to be included as much as possible as it partly defines the success of PFM measurements. It is essential to provide a forest observation system, for example based on satellite remote sensing data and methods, that remains after the projects ending to control the forest, its resources as well as the advances happening after PFM implementation. However, the developed process for the automatic forest change detection can be improved using additional available information, for instance collected field data. Crucially, the community stakeholders should be included in the local forest monitoring process and profit from the knowledge of the research and reversed.

7.4 Additional topics

7.4.1 Wild and semi-wild coffee forest

An interesting discussion is about whether satellite imagery allows distinguishing between the wild and semi-wild coffee forest. The arabica coffee species growing in Ethiopia is very difficult to observe from space as the plant is an understory shrub (Hylander et al. 2013). Moreover, plantations or garden coffee might not be differentiated from wild and semi-wild coffee forest based on the spectral signature, particularly on coarse spatial resolution imagery (Hylander et al. 2013). Therefore, in this study forest in general is studied and not coffee forest particularly although the observed forest is assumed to contain coffee forest plants. Another difficulty is the missing official definition of the semi-wild coffee forest for remote sensing applications. For satellite imagery analysis, a definition based on physical or optical measurable plant properties is desirable. Possible approaches debate the exploitation of shape, size or texture in order to detect tree species or to take into account seasonal vegetation differences (Lillesand et al. 2015). However, the plant is still hidden under the larger trees canopy (Lillesand et al. 2015). Therefore, it is crucial to know wild and semi-wild forest locations so as to compare them with multi- or hyperspectral instruments (Lillesand et al. 2015). Field data additionally supports developing a definition based on measurable characteristics (Hylander et al. 2013). Including radar data or very high-resolution data around 0.5 meters are further options to test for the detection of coffee plants (Cho et al. 2015).

7.4.2 Climate

The climate over the last 50 years has shown a mean temperature increase by 1.3 degrees Celsius which may influence the growing condition of the coffee plant (Moat et al. 2017). The climate forecast predicts rising temperatures and rainfall in south western Ethiopia (Hylander et al. 2013). Probably, the coffee forest environment reacts sensitively to climate change (Hylander et al. 2013) which in turn has implications for the coffee farmers. They need to understand the influence of the climate change on coffee production (Moat et al. 2017). Depending on the weather shifts, particular areas become unsuitable for coffee farming and have to be relocated (Moat et al. 2017). Possibly, coffee production moves to higher altitudes due to changing tree cover in lower elevations (Moat

et al. 2017; Hylander et al. 2013). However, in this thesis no influence of a changing climate has been measured although in 2019 it rained significantly more than in the years before.

7.4.3 Sentinel-2

Up to now, Sentinel-2 has been providing imagery since 2015. The temporal resolution improved since the launch of Sentinel-2B in 2017 to a revisit time of 5 days. Due to its high spatial resolution of 10 meters for the visible and near infrared bands, Sentinel-2 is a valuable information source for the coffee forest monitoring in Ethiopia. However, until now the high-quality data availability over Ethiopia is limited (Frampton et al. 2013).

8 Conclusion and Outlook

The purpose of this thesis was to examine the coffee forest changes, its causes and implications for the application of sustainable forest management systems in Ethiopia. Thus, remote sensing approaches were used to create thematic land cover maps in Ethiopian coffee forest areas. Furthermore, change detection methods were applied to analyse the forest changes in Participatory Forest Management (PFM) and non-PFM regions over the last 20 years. It is found that satellite remote sensing techniques are useful for the monitoring of coffee forest and its changes in Ethiopia. Particularly, it saves costs and time as less field trips are necessary, and an automated measuring system can be established to control the remote mountainous forest regions. However, accurate analysis of deforestation and forest degradation remains challenging and requires appropriate validation datasets and assessment methods.

In this study, a process to analyse forest changes was developed and applied which suited the purpose of investigating PFM and non-PFM areas. Nevertheless, further work needs to explore the potential of recent methods in greater detail for instance near real-time monitoring by the fusion of Landsat and MODIS data (Tang et al. 2019) or the use of a mixture of LiDAR, Synthetic Aperture Radar (SAR) and very high-resolution imagery in order to collect available information on tropical forest degradation. These datasets measure for example the forest structure or biomass (Dupuis et al. 2020; Shimizu et al. 2019; Lillesand et al. 2015). Moreover, further techniques suggest implementing an ensemble of change detection algorithms to receive disturbance maps with higher accuracy (Healey et al. 2018). In addition, secondary data such as field information or interviews with farmers is desirable in order to derive deforestation and forest degradation causes. Whether wild and semi-wild coffee forest can be distinguished with satellite remote sensing remains to be determined in future research.

9 References

- Aerts, Raf, Lore Geeraert, Gezahegn Berecha, Kitessa Hundera, Bart Muys, Hanne De Kort, and Olivier Honnay. 2017. "Conserving Wild Arabica Coffee: Emerging Threats and Opportunities." *Agriculture, Ecosystems and Environment* 237: 75–79. <https://doi.org/10.1016/j.agee.2016.12.023>.
- Apan, A. A. 1997. "Land Cover Mapping for Tropical Forest Rehabilitation Planning Using Remotely-Sensed Data." *International Journal of Remote Sensing* 18 (5): 1029–49. <https://doi.org/10.1080/014311697218557>.
- Asner, Gregory P. 2009. "Automated Mapping of Tropical Deforestation and Forest Degradation: CLASlite." *Journal of Applied Remote Sensing* 3 (1): 033543. <https://doi.org/10.1117/1.3223675>.
- Banko, Gebhard. 1998. "A Review of Assessing the Accuracy of Classifications of Remotely Sensed Data and of Methods Including Remote Sensing Data in Forest Inventory." *International Institute for Applied Systems Analysis, Interim Report IT-98-081*.
- Bewket, Woldeamlak. 2002. "Land Cover Dynamics Since the 1950s in Chemoga Watershed, Blue Nile Basin, Ethiopia." *Mountain Research and Development* 22 (3): 263–69. <https://doi.org/10.1016/j.rsase.2019.100249>.
- Bullock, Eric. 2018. "Continuous Degradation Detection (CODED)." 2018. <https://coded.readthedocs.io/en/latest/index.html>.
- Bullock, Eric, Curtis Woodcock, and Pontus Olofsson. 2020. "Monitoring Tropical Forest Degradation Using Spectral Unmixing and Landsat Time Series Analysis." *Remote Sensing of Environment* 238: 1–16. <https://doi.org/10.1016/j.rse.2018.11.011>.
- Bullock, Eric, Curtis Woodcock, Carlos Souza, and Pontus Olofsson. 2020. "Satellite-Based Estimates Reveal Widespread Forest Degradation in the Amazon." *Global Change Biology* 26 (5): 2956–69. <https://doi.org/10.1111/gcb.15029>.
- CCI Land Cover (LC) Team. 2016. "ESA CCI Land Cover - S2 Prototype Land Cover 20m Map of Africa 2016." 2016. <http://2016africalandcover20m.esrin.esa.int/>.
- Chen, Feng, Xiaofeng Zhao, and Hong Ye. 2012. "Making Use of the Landsat 7 SLC-off ETM+ Image Through Different Recovering Approaches." In *Data Acquisition Applications*, 317–42. <https://doi.org/10.1016/j.colsurfa.2011.12.014>.
- Cho, Moses Azong, Oupa Malahlela, and Abel Ramoelo. 2015. "Assessing the Utility WorldView-2 Imagery for Tree Species Mapping in South African Subtropical Humid Forest and the Conservation Implications: Dukuduku Forest Patch as Case Study." *International Journal of Applied Earth Observation and Geoinformation* 38: 349–57. <https://doi.org/10.1016/j.jag.2015.01.015>.
- Cohen, Warren B., Sean P. Healey, Zhiqiang Yang, Stephen V. Stehman, C. Kenneth Brewer, Evan B. Brooks, Noel Gorelick, et al. 2017. "How Similar Are Forest Disturbance Maps Derived from Different Landsat Time Series Algorithms?" *Forests* 8 (4): 1–19. <https://doi.org/10.3390/f8040098>.
- Cohen, Warren B., Zhiqiang Yang, and Robert Kennedy. 2010. "Detecting Trends in Forest Disturbance and Recovery Using Yearly Landsat Time Series: 2. TimeSync - Tools for Calibration and Validation." *Remote Sensing of Environment* 114 (12): 2911–24. <https://doi.org/10.1016/j.rse.2010.07.010>.
- Coppin, P., I. Jonckheere, K. Nackaerts, B. Muys, and E. Lambin. 2004. "Digital Change Detection Methods in Ecosystem Monitoring: A Review." *International Journal of Remote Sensing* 25 (9): 1565–96. <https://doi.org/10.1080/0143116031000101675>.
- Craves, Julie. 2011. "How 'Wild' Is Ethiopian Forest Coffee?" 2011. <https://www.coffeehabitat.com/2011/02/ethiopia-wild-forest-coffee/>.
- Cutler, D. Richard, Thomas C. Edwards, Karen H. Beard, Adele Cutler, Kyle T. Hess, Jacob Gibson, and Joshua J. Lawler. 2007. "Random Forests for Classification in Ecology." *Ecology* 88 (11): 2783–92. <https://doi.org/10.1890/07-0539.1>.
- Dessie, Gessesse, and Johan Kleman. 2007. "Pattern and Magnitude of Deforestation in the South Central Rift Valley Region of Ethiopia." *Mountain Research and Development* 27 (2): 162–68. <https://doi.org/10.1659/mrd.0730>.

- DeVries, Ben, Arun Kumar Pratihast, Jan Verbesselt, Lammert Kooistra, and Martin Herold. 2016. "Characterizing Forest Change Using Community-Based Monitoring Data and Landsat Time Series." *PLoS ONE* 11 (3). <https://doi.org/10.1371/journal.pone.0147121>.
- DeVries, Ben, Jan Verbesselt, Lammert Kooistra, and Martin Herold. 2015. "Robust Monitoring of Small-Scale Forest Disturbances in a Tropical Montane Forest Using Landsat Time Series." *Remote Sensing of Environment* 161: 107–21. <https://doi.org/10.1016/j.rse.2015.02.012>.
- Dorais, Alexis, and Jeffrey Cardille. 2011. "Strategies for Incorporating High-Resolution Google Earth Databases to Guide and Validate Classifications: Understanding Deforestation in Borneo." *Remote Sensing* 3 (6): 1157–76. <https://doi.org/10.3390/rs3061157>.
- Dresen, Elisabeth. 2011a. "Climate Protection and Primary Forest Preservation - A Management Model Using the Wild Coffee Forests in Ethiopia as an Example." NABU. <https://doi.org/10.1515/9783035607840-007>.
- . 2011b. "Forest Status of Kafa Biosphere Reserve."
- Dupuis, Chloé, Philippe Lejeune, Adrien Michez, and Adeline Fayolle. 2020. "How Can Remote Sensing Help Monitor Tropical Moist Forest Degradation?—A Systematic Review." *Remote Sensing* 12 (7): 1087. <https://doi.org/10.3390/rs12071087>.
- ESA. 2019. "Proba-V News." 2019. <https://earth.esa.int/web/guest/missions/esa-operational-eo-missions/proba-v/news/-/article/proba-v-global-land-cover-maps-released>.
- "Ethiopia's Forest Reference Level Submission to the UNFCCC." 2017.
- FAO. 2011. "Assessing Forest Degradation: Towards the Development of Globally Applicable Guidelines." *Forest Resources Assessment*. <https://doi.org/10.1023/B:VEGE.0000029381.63336.20>.
- Flood, Neil. 2013. "Seasonal Composite Landsat TM/ETM+ Images Using the Medoid (a Multi-Dimensional Median)." *Remote Sensing* 5: 6481–6500. <https://doi.org/10.3390/rs5126481>.
- Foody, Giles M. 2002. "Status of Land Cover Classification Accuracy Assessment." *Remote Sensing of Environment* 80 (1): 185–201. [https://doi.org/10.1016/S0034-4257\(01\)00295-4](https://doi.org/10.1016/S0034-4257(01)00295-4).
- . 2003. "Remote Sensing of Tropical Forest Environments: Towards the Monitoring of Environmental Resources for Sustainable Development." *International Journal of Remote Sensing* 24 (20): 4035–46. <https://doi.org/10.1080/0143116031000103853>.
- Frampton, William James, Jadunandan Dash, Gary Watmough, and Edward James Milton. 2013. "Evaluating the Capabilities of Sentinel-2 for Quantitative Estimation of Biophysical Variables in Vegetation." *ISPRS Journal of Photogrammetry and Remote Sensing* 82: 83–92. <https://doi.org/10.1016/j.isprsjprs.2013.04.007>.
- Gashaw, Temesgen, Amare Bantider, and Abraham Mahari. 2014. "Evaluations of Land Use/Land Cover Changes and Land Degradation in Dera District, Ethiopia: GIS and Remote Sensing Based Analysis." *International Journal of Scientific Research in Environmental Sciences* 2 (6): 199–208. <https://doi.org/10.12983/ijres-2014-p0199-0208>.
- GIZ. 2016. "Schätze Des Waldes - Wildkaffee Und Honig: Nachhaltiger Schutz Der Letzten Äthiopischen Wälder."
- Google Earth. 2020. "Google Earth." 2020. <https://earth.google.com/web>.
- Google Earth Engine. 2020. "Earth Engine Data Catalog." 2020. <https://developers.google.com/earth-engine/datasets>.
- Gorelick, Noel, Matt Hancher, Mike Dixon, Simon Ilyushchenko, David Thau, and Rebecca Moore. 2017. "Google Earth Engine: Planetary-Scale Geospatial Analysis for Everyone." *Remote Sensing of Environment* 202: 18–27. <https://doi.org/10.1016/j.rse.2017.06.031>.
- Griffiths, Patrick, Tobias Kuemmerle, Matthias Baumann, Volker C. Radeloff, Ioan V. Abrudan, Juraj Lieskovsky, Catalina Munteanu, Katarzyna Ostapowicz, and Patrick Hostert. 2014. "Forest Disturbances, Forest Recovery, and Changes in Forest Types across the Carpathian Ecoregion from 1985 to 2010 Based on Landsat Image Composites." *Remote Sensing of Environment* 151: 72–88. <https://doi.org/10.1016/j.rse.2013.04.022>.

- Hadi, Andrey Krasovskii, Victor Maus, Ping Yowargana, Stephan Pietsch, and Miina Rautiainen. 2018. "Monitoring Deforestation in Rainforests Using Satellite Data: A Pilot Study from Kalimantan, Indonesia." *Forests* 9 (7): 1–26. <https://doi.org/10.3390/f9070389>.
- Hailemariam, Sisay Nune, Teshome Soromessa, and Demel Teketay. 2016. "Land Use and Land Cover Change in the Bale Mountain Eco-Region of Ethiopia during 1985 to 2015." *Land* 5 (41): 1–22. <https://doi.org/10.3390/land5040041>.
- Hailu, Binyam Tesfaw, Mekbib Fekadu, and Thomas Naus. 2018. "Availability of Global and National Scale Land Cover Products and Their Accuracy in Mountainous Areas of Ethiopia: A Review." *Preprints*, 1–16. <https://doi.org/10.1117/1.jrs.12.041502>.
- Hansen, Matthew C., P V Potapov, R Moore, M Hancher, S A Turubanova, A Tyukavina, D Thau, et al. 2013. "High-Resolution Global Maps of 21st-Century Forest Cover Change." *Science* 342: 850–53. <https://doi.org/10.1126/science.1244693>.
- Hansen, Matthew C., Stephen V. Stehman, and Peter V. Potapov. 2010. "Quantification of Global Gross Forest Cover Loss." *Proceedings of the National Academy of Sciences of the United States of America* 107 (19): 8650–55. <https://doi.org/10.1073/pnas.0912668107>.
- Hansen, Matthew C., Stephen V. Stehman, Peter V. Potapov, Thomas R. Loveland, John R.G. Townshend, Ruth S. DeFries, Kyle W. Pittman, et al. 2008. "Humid Tropical Forest Clearing from 2000 to 2005 Quantified by Using Multitemporal and Multiresolution Remotely Sensed Data." *Proceedings of the National Academy of Sciences of the United States of America* 105 (27): 9439–44. <https://doi.org/10.1073/pnas.0804042105>.
- Healey, Sean P., Warren B. Cohen, Zhiqiang Yang, C. Kenneth Brewer, Evan B. Brooks, Noel Gorelick, Alexander J. Hernandez, et al. 2018. "Mapping Forest Change Using Stacked Generalization: An Ensemble Approach." *Remote Sensing of Environment* 204: 717–28. <https://doi.org/10.1016/j.rse.2017.09.029>.
- Horizon Plantations. 2020. "Bebeka Coffee Estate PLC." 2020. <https://www.horizonplantations.com/enterprisedetail.php?enterpriseID=32>.
- Hu, Yunfeng, and Yang Hu. 2019. "Land Cover Changes and Their Driving Mechanisms in Central Asia from 2001 to 2017 Supported by Google Earth Engine." *Remote Sensing* 11 (554): 1–21. <https://doi.org/10.3390/rs11050554>.
- Hylander, Kristoffer, Sileshi Nemomissa, Josefien Delrue, and Woldeyohannes Enkosa. 2013. "Effects of Coffee Management on Deforestation Rates and Forest Integrity." *Conservation Biology* 27 (5): 1031–40. <https://doi.org/10.1111/cobi.12079>.
- Institute of Biodiversity Conservation (IBC). 2012. "The State of the World's Forest Genetic Resources."
- Kedir, Haji, Mesele Negash, Fantaw Yimer, and Mulugeta Limenih. 2018. "Contribution of Participatory Forest Management towards Conservation and Rehabilitation of Dry Afromontane Forests and Its Implications for Carbon Management in the Tropical Southeastern Highlands of Ethiopia." *Journal of Sustainable Forestry* 37 (4): 357–74. <https://doi.org/10.1080/10549811.2017.1414614>.
- Kennedy, Robert E., Zhiqiang Yang, Noel Gorelick, Justin Braaten, Lucas Cavalcante, Warren B. Cohen, and Sean Healey. 2018. "Implementation of the LandTrendr Algorithm on Google Earth Engine." *Remote Sensing* 10 (691): 1–10. <https://doi.org/10.3390/rs10050691>.
- Kibret, Kefyalew Sahle, Carsten Marohn, and Georg Cadisch. 2016. "Assessment of Land Use and Land Cover Change in South Central Ethiopia during Four Decades Based on Integrated Analysis of Multi-Temporal Images and Geospatial Vector Data." *Remote Sensing Applications: Society and Environment* 3: 1–19. <https://doi.org/10.1016/j.rsase.2015.11.005>.
- Kindu, Mengistie, Thomas Schneider, Demel Teketay, and Thomas Knoke. 2013. "Land Use/Land Cover Change Analysis Using Object-Based Classification Approach in Munessa-Shashemene Landscape of the Ethiopian Highlands." *Remote Sensing* 5: 2411–35. <https://doi.org/10.3390/rs5052411>.
- . 2016. "Changes of Ecosystem Service Values in Response to Land Use/Land Cover Dynamics in Munessa-Shashemene Landscape of the Ethiopian Highlands." *Science of the Total Environment* 547: 137–47. <https://doi.org/10.1016/j.scitotenv.2015.12.127>.

- Lemenih, M., C. Allan, and Y. Biot. 2015. "Making Forest Conservation Benefit Local Communities : Participatory Forest Management in Ethiopia." *Farm Africa*.
- Lillesand, Thomas M., Ralph W. Kiefer, and Jonathan W. Chipman. 2015. *Remote Sensing and Image Interpretation*. Edited by Ryan Flahive, Marian Provenzano, and Christina Volpe. 7th ed. John Wiley & Sons, Inc.
- Lu, D., P. Mausel, E. Brondízio, and E. Moran. 2004. "Change Detection Techniques." *International Journal of Remote Sensing* 25 (12): 2365–2401. <https://doi.org/10.1080/0143116031000139863>.
- Mekonnen, Mulatie, Tsegaye Sewunet, Mulu Gebeyehu, Bayleyegn Azene, and Assefa M. Melesse. 2016. "GIS and Remote Sensing-Based Forest Resource Assessment, Quantification, and Mapping in Amhara Region, Ethiopia." In *Landscape Dynamics, Soils and Hydrological Processes in Varied Climates*, 9–29. <https://doi.org/10.1007/978-3-319-18787-7>.
- Minale, Amare Sewnet. 2013. "Retrospective Analysis of Land Cover and Use Dynamics in Gilgel Abbay Watershed by Using GIS and Remote Sensing Techniques, Northwestern Ethiopia." *International Journal of Geosciences* 4: 1003–8. <https://doi.org/10.2478/jlecol-2018-0005>.
- Moat, J., J. Williams, S. Baena, T. Wilkinson, S. Demissew, Challa Z.K., T.W. Gole, and Davis. 2017. "Coffee Farming and Climate Change in Ethiopia: Impacts, Forecasts, Resilience and Opportunities. – Summary."
- Moges, Y, Z Eshetu, and S Nune. 2010. "Ethiopian Forest Resources: Current Status and Future Management Options in View of Access to Carbon Finances."
- O'Hara, Peter. 2013. "Participatory Forest Management Learning Paper; Reflections on Key Lessons, Challenges and Recommendations."
- OCHA. 2017. "Ethiopia: Administrative Map (August 2017)."
- openAfrica. 2019. "Ethiopia Shapefiles." 2019. <https://africaopendata.org/dataset/ethiopia-shapefiles>.
- Ouaamari, Samir El, and Hubert Cochet. 2014. "The Role of Coffee in the Development of Southwest Ethiopia's Forests: Farmers' Strategies, Investor Speculation, and Certification Projects." *Society and Natural Resources* 27 (2): 200–214. <https://doi.org/10.1080/08941920.2013.847997>.
- Pasquarella, Valerie J., Christopher E. Holden, Les Kaufman, and Curtis E. Woodcock. 2016. "From Imagery to Ecology: Leveraging Time Series of All Available Landsat Observations to Map and Monitor Ecosystem State and Dynamics." *Remote Sensing in Ecology and Conservation* 2 (3): 152–70. <https://doi.org/10.1002/rse2.24>.
- Pimple, Uday, Dario Simonetti, Asamaporn Sitthi, Sukan Pungkul, Kumron Leadprathom, Henry Skupek, Jaturong Som-ard, Valery Gond, and Sirintornthep Towprayoon. 2018. "Google Earth Engine Based Three Decadal Landsat Imagery Analysis for Mapping of Mangrove Forests and Its Surroundings in the Trat Province of Thailand." *Journal of Computer and Communications* 6: 247–64. <https://doi.org/10.4236/jcc.2018.61025>.
- Plan Vivo. 2014. "Wild Coffee Conservation by PFM through Communities and Government Institutions Capacity Building Project." Addis Ababa. http://wetlandsandforests.hud.ac.uk/forests/index_forests.html.
- Roy, D. P., V. Kovalskyy, H. K. Zhang, E. F. Vermote, L. Yan, S. S. Kumar, and A. Egorov. 2016. "Characterization of Landsat-7 to Landsat-8 Reflective Wavelength and Normalized Difference Vegetation Index Continuity." *Remote Sensing of Environment* 185: 57–70. <https://doi.org/10.1016/j.rse.2015.12.024>.
- Sahle, Mesfin, and Kumelachew Yeshitela. 2018. "Dynamics of Land Use Land Cover and Their Drivers Study for Management of Ecosystems in the Socio-Ecological Landscape of Gurage Mountains, Ethiopia." *Remote Sensing Applications: Society and Environment* 12 (April): 48–56. <https://doi.org/10.1016/j.rsase.2018.09.002>.
- Schmitt, C, and U Grote. 2006. "Wild Coffee Production in Ethiopia: The Role of Coffee Certification for Forest Conservation."
- Services ArcGIS. 2015. "Kebeles (Level 4)." 2015. https://hub.arcgis.com/datasets/98602254daac431799db5ffbf82c6547_0?geometry=0.502%2C1.602%2C75.517%2C16.740.

- Shimizu, Katsuto, Tetsuji Ota, and Nobuya Mizoue. 2019. "Detecting Forest Changes Using Dense Landsat 8 and Sentinel-1 Time Series Data in Tropical Seasonal Forests." *Remote Sensing* 11: 1–22. <https://doi.org/10.3390/rs11161899>.
- Sidhu, Nanki, Edzer Pebesma, and Gilberto Câmara. 2018. "Using Google Earth Engine to Detect Land Cover Change: Singapore as a Use Case." *European Journal of Remote Sensing* 51 (1): 486–500. <https://doi.org/10.1080/22797254.2018.1451782>.
- Souza, Carlos M., João V. Siqueira, Marcio H. Sales, Antônio V. Fonseca, Júlia G. Ribeiro, Izaya Numata, Mark A. Cochrane, Christopher P. Barber, Dar A. Roberts, and Jos Barlow. 2013. "Ten-Year Landsat Classification of Deforestation and Forest Degradation in the Brazilian Amazon." *Remote Sensing* 5: 5493–5513. <https://doi.org/10.3390/rs5115493>.
- Stehman, Stephen V. 1997. "Selecting and Interpreting Measures of Thematic Classification Accuracy." *Remote Sensing of Environment* 62: 77–89.
- Tadesse, Getachew, Erika Zavaleta, Carol Shennan, and Margaret FitzSimmons. 2014. "Policy and Demographic Factors Shape Deforestation Patterns and Socio-Ecological Processes in Southwest Ethiopian Coffee Agroecosystems." *Applied Geography* 54: 149–59. <https://doi.org/10.1016/j.apgeog.2014.08.001>.
- Takahashi, Ryo, and Yasuyuki Todo. 2017. "Coffee Certification and Forest Quality: Evidence from a Wild Coffee Forest in Ethiopia." *World Development* 92 (25): 158–66. <https://doi.org/10.1016/j.worlddev.2016.12.001>.
- Tang, Xiaojing, Eric L. Bullock, Pontus Olofsson, Stephan Estel, and Curtis E. Woodcock. 2019. "Near Real-Time Monitoring of Tropical Forest Disturbance: New Algorithms and Assessment Framework." *Remote Sensing of Environment* 224: 202–18. <https://doi.org/10.1016/j.rse.2019.02.003>.
- UNESCO. 2020. "Biosphere Reserves in Africa." 2020. <https://en.unesco.org/biosphere/africa#ethiopia>.
- USGS. 2004. "SLC-off Gap-Filled Products: Gap-Fill Algorithm Methodology."
- Walle, Yibeltal, and Diptimayee Nayak. 2019. "How Can Participatory Forest Management Cooperatives Be Successful In Forest Resources Conservation? An Evidence From Ethiopia." *Journal of Sustainable Forestry* 39 (7): 655–73. <https://doi.org/10.1080/10549811.2019.1684950>.
- Wiersum, K. F., T. W. Gole, F. Gatzweiler, J. Volkmann, E. Bognetteau, and O. Wirtu. 2008. "Certification of Wild Coffee in Ethiopia: Experiences and Challenges." *Forests Trees and Livelihoods* 18 (1): 1–13. <https://doi.org/10.1080/14728028.2008.9752614>.
- Winberg, Ellen. 2011. "Participatory Forest Management in Ethiopia, Practices and Experiences."
- Workie, Melkamu. 2015. "Ethiopian Highlands: Home for Arabica Coffee (Coffea Arabica L.)." *Bahir Dar Universtiy, College of Agriculture and Environmental Sciences*. https://www.researchgate.net/publication/317231826_Ethiopian_Highlands_Home_for_Arabica_Coffee_Coffea_arabica_L.
- World Weather Online. 2020. "Bonga Historical Weather." 2020. <https://www.worldweatheronline.com/bonga-weather-history/et.aspx>.
- Wubie, Abebe Mengaw. 2015. "GIS and Remote Sensing Based Forest Change Detection for Sustainable Forest Management in Bench Maji Zone, Ethiopia." *International Journal of Remote Sensing & Geoscience* 4 (3). www.ijrsg.com.

9.1 Table of figures

Figure 1 Natural forest in Ethiopia containing wild coffee plants (Caritas Switzerland, Philipp Schütz, 2020)	1
Figure 2 Illustration depicting the drivers of deforestation and forest degradation in Ethiopia as well as the resulting consequences which in turn reinforce the drivers	9
Figure 3 Visualization of the four different coffee growing systems in Ethiopia emphasizing their differences in management type and intensity as well as in the yield	9
Figure 4 Graphic showing a usual PFM implementation process emphasizing the environmental and social part, their goals, and outcomes.....	10
Figure 5 Map illustrating the location of the five study zones and their capital cities in Ethiopia. The main study zone Keffa is highlighted in light blue (openAfrica 2019).	13
Figure 6 Left: Overview map of all five study zones containing the 10 study kebeles. From top left to bottom right: Keffa zone, location of the study zones in Ethiopia, Bench Maji zone, Sheka zone, Bale zone, Illubabor zone. Marked with a light blue frame are the in depth discussed kebeles (openAfrica 2019; Services ArcGIS 2015).....	14
Figure 7 Typical climate diagram for a coffee forest area. This example shows the climate for the zonal capital city Bonga located in Keffa with an unimodal precipitation pattern (World Weather Online 2020).	15
Figure 8 Top: Timeline of the general imagery availability of Landsat 5, 7 and 8 (1995-2020) with the SLC-off status marked as hatched bar, Bottom: Timeline of the Landsat 5, 7 and 8 imagery availability (1995-2020) over the study zones in Ethiopia with the missing years marked in red.....	16
Figure 9 Water mask created with a Sentinel-2 one-year composite. The water mask does not cover the real water areas, for example the lakes in the middle of the scene are not detected.	18
Figure 10 Water mask based on the Hansen dataset. The important water bodies are identified and even smaller water surfaces such as rivers are masked.	18
Figure 11 Flowchart of the used data and applied methods. The blue boxes indicate the main applied methods while the grey boxes are either the processing tool or final outputs.	19
Figure 12 Graphic comparing the spectral signatures of three urban and three bare land examples. The bands of the visible spectrum are marked with a black frame.....	20
Figure 13 From left to right: Landsat 8 composite (5 month dry season, '2015-11-01', '2016-04-01') of Keffa zone (Google Earth Engine 2020), 30 classes automatically computed by the 'weka means' clusterer and visualized in random colours, map of five distinguishable merged classes	21
Figure 14 From left to right: Landsat 8 (2015/2016) composite for a forested area, very high-resolution imagery from Planet Sky data (2015/2016) (Google Earth Engine 2020), classification of the Landsat 8 imagery with the Random Forest classifier	22
Figure 15 Map of Keffa emphasizing the forest loss areas in red and the validation areas are framed with their corresponding number.....	24
Figure 16 Area 1 forest loss: From top left to bottom right: Calculated forest loss areas in red overlaid on the composite 1995-2000 and on the composite 2015-2020, Landsat imagery composite 1995-2000 and composite 2015-2020, Hansen forest loss in red overlaid on the composite 1995-2000 and on the composite 2015-2020 (Google Earth Engine 2020).....	25
Figure 17 Map of Keffa emphasizing the forest gain areas in green and the validation areas are framed with their corresponding number.....	26
Figure 18 Area 1 forest gain: Top: Calculated forest gain areas in green overlaid on the composite 1995-2000 on the left hand side and on the composite 2015-2020 on the right hand side, Bottom: Landsat imagery composite 1995-2000 and composite 2015-2020 (Google Earth Engine 2020)	26
Figure 19 Typical NDFI trajectory for a deforestation pixel over a time series of 36 years.....	28
Figure 20 Typical NDFI trajectory for a forest degradation pixel over a time series of 36 years.....	28
Figure 21 Top: Landsat imagery composites 1995-2000, 2010-2015 and 2015-2020 for Keffa zone (Google Earth Engine 2020), Bottom: Classified composites 1995-2000, 2010-2015 and 2015-2020	29
Figure 22 Graphic illustrating the areal size of the different land cover classes per classified composite for Keffa zone	30
Figure 23 Overview of the percentages of the land cover classes per zone and per classified composite	30
Figure 24 Graphic visualizing the number of appearances of the land cover class with the highest proportion on the categories forest loss, forest gain and to urban.....	31
Figure 25 From left to right: Calculated forest loss displayed in red for Keffa zone, calculated loss in red overlaid on the classified composite 2015-2020, degradation in orange and deforestation in red calculated with the CODED algorithm overlaid on the Landsat imagery composite 2015-2020.....	31
Figure 26 Left: Disturbance dates calculated with the CODED algorithm for Keffa zone, Right: Corresponding histogram showing the number of pixels labelled as disturbance for every year during the study period	32
Figure 27 Left: Disturbance magnitudes calculated with the CODED algorithm for Keffa zone, Right: Corresponding histogram showing the number of pixels labelled as disturbance for the different magnitudes	32

Figure 28 Histogram showing the number of pixels labelled as disturbance for every year during the analysis period for Keffa zone, the light blue line demonstrates the precipitation data from world weather for the city of Bonga (World Weather Online 2020), the dark blue line refers to the average precipitation extracted from the Chirps data (Google Earth Engine 2020)	33
Figure 29 From left to right: Calculated forest loss displayed in red for Bench Maji zone, calculated loss in red overlaid on the classified composite 2015-2020, degradation in orange and deforestation in red calculated with the CODED algorithm overlaid on the Landsat imagery composite 2015-2020	33
Figure 30 Histogram showing the number of pixels labelled as disturbance for every year during the study period for Bench Maji	34
Figure 31 Histogram showing the number of pixels labelled as disturbance for every year during the analysis period summed up for all study zones	34
Figure 32 Histogram showing the number of pixels labelled as disturbance for the different disturbance magnitudes summed up for all study zones	35
Figure 33 Graphic of the relative forest loss defined as the size of the forest loss area related to the total forested area in 1995-2000 for that zone	35
Figure 34 Landsat imagery composites 1995-2000, 2010-2015 and 2015-2020 for Keshi kebele (Google Earth Engine 2020), Bottom: Classified composites 1995-2000, 2010-2015 and 2015-2020	36
Figure 35 Graphic illustrating the areal size of the different land cover classes per composite for Keshi kebele	36
Figure 36 From left to right: Calculated forest loss displayed in red for Keshi kebele, calculated loss in red overlaid on the classified composite 2015-2020, degradation in orange and deforestation in red calculated with the CODED algorithm overlaid on the Landsat imagery composite 2015-2020	37
Figure 37 Histogram showing the number of pixels labelled as disturbance for every year during the study period for Keshi kebele	37
Figure 38 Landsat imagery composites 1995-2000, 2010-2015 and 2015-2020 for Chebere kebele (Google Earth Engine 2020), Bottom: Classified composites 1995-2000, 2010-2015 and 2015-2020	38
Figure 39 Graphic illustrating the areal size of the different land cover classes per composite for Chebere kebele	38
Figure 40 From left to right: Calculated forest loss displayed in red for Chebere kebele, calculated loss in red overlaid on the classified composite 2015-2020, degradation in orange and deforestation in red calculated with the CODED algorithm overlaid on the Landsat imagery composite 2015-2020	39
Figure 41 Histogram showing the number of pixels labelled as disturbance for every year during the study period for Chebere kebele	39
Figure 42 Landsat imagery composites 1995-2000, 2010-2015 and 2015-2020 for Giz Meret kebele (Google Earth Engine 2020), Bottom: Classified composites 1995-2000, 2010-2015 and 2015-2020	40
Figure 43 Graphic illustrating the areal size of the different land cover classes per composite for Giz Meret kebele	40
Figure 44 Giz Meret, From left to right: Calculated forest loss displayed in red for Bench Maji zone, calculated loss in red overlaid on the classified composite 2015-2020, degradation in orange and deforestation in red calculated with the CODED algorithm overlaid on the Landsat imagery composite 2015-2020	41
Figure 45 Histogram showing the number of pixels labelled as disturbance for every year during the study period for Giz Meret kebele	41
Figure 46 Landsat imagery composites 1995-2000, 2010-2015 and 2015-2020 for Sodu Lelaftu kebele (Google Earth Engine 2020), Bottom: Classified composites 1995-2000, 2010-2015 and 2015-2020	42
Figure 47 Graphic illustrating the areal size of the different land cover classes per composite for Sodu Lelaftu kebele	42
Figure 48 From left to right: Calculated forest loss displayed in red for Sodu Lelaftu kebele, calculated loss in red overlaid on the classified composite 2015-2020, degradation in orange and deforestation in red calculated with the CODED algorithm overlaid on the Landsat imagery composite 2015-2020	43
Figure 49 Histogram showing the number of pixels labelled as disturbance for every year during the study period for Sodu Lelaftu	43
Figure 50 Graphic of the relative forest loss defined as the size of the forest loss area related to the total forested area in 1995-2000 of that kebele, orange-brown coloured are the non-PFM kebeles and green marked are the PFM kebeles	44
Figure 51 Maps of the study zones highlighting the forest loss to directly compare deforestation in PFM-and non-PFM areas (UNESCO 2020; Dresen 2011a; Plan Vivo 2014)	45

Figure 11-1 Top: Landsat imagery composites 1995-2000, 2010-2015 and 2015-2020 for Sheka zone (Google Earth Engine 2020), Bottom: Classified composites 1995-2000, 2010-2015 and 2015-2020	92
Figure 11-2 Graphic illustrating the areal size of the different land cover classes per classified composite for Sheka zone	92
Figure 11-3 From left to right: Calculated forest loss displayed in red for Sheka zone, calculated loss in red overlaid on the classified composite 2015-2020, degradation in orange and deforestation in red calculated with the CODED algorithm overlaid on the Landsat imagery composite 2015-2020.....	93
Figure 11-4 Left: Disturbance dates calculated with the CODED algorithm for Sheka zone, Right: Corresponding histogram showing the number of pixels labelled as disturbance for every year during the study period	93
Figure 11-5 Left: Disturbance magnitudes calculated with the CODED algorithm for Sheka zone, Right: Corresponding histogram showing the number of pixels labelled as disturbance for the different magnitudes	93
Figure 11-6 Histogram showing the number of pixels labelled as disturbance for every year during the analysis period for Sheka zone, the light blue line demonstrates the precipitation data from world weather for the city of Masha (World Weather Online 2020), the dark blue line refers to the average precipitation extracted from the Chirps data (Google Earth Engine 2020)	94
Figure 11-7 Top: Landsat imagery composites 1995-2000, 2010-2015 and 2015-2020 for Illubabor zone (Google Earth Engine 2020), Bottom: Classified composites 1995-2000, 2010-2015 and 2015-2020	94
Figure 11-8 Graphic illustrating the areal size of the different land cover classes per classified composite for Illubabor zone	95
Figure 11-9 From left to right: Calculated forest loss displayed in red for Illubabor zone, calculated loss in red overlaid on the classified composite 2015-2020, degradation in orange and deforestation in red calculated with the CODED algorithm overlaid on the Landsat imagery composite 2015-2020.....	95
Figure 11-10 Left: Disturbance dates calculated with the CODED algorithm for Illubabor zone, Right: Corresponding histogram showing the number of pixels labelled as disturbance for every year during the study period	95
Figure 11-11 Left: Disturbance magnitudes calculated with the CODED algorithm for Illubabor zone, Right: Corresponding histogram showing the number of pixels labelled as disturbance for the different magnitudes	96
Figure 11-12 Histogram showing the number of pixels labelled as disturbance for every year during the analysis period for Illubabor zone, the light blue line demonstrates the precipitation data from world weather for the city of Metu (World Weather Online 2020), the dark blue line refers to the average precipitation extracted from the Chirps data (Google Earth Engine 2020)	96
Figure 11-13 Graphic illustrating the areal size of the different land cover classes per classified composite for Bench Maji zone	96
Figure 11-14 Disturbance dates calculated with the CODED algorithm for Bench Maji zone	97
Figure 11-15 Left: Disturbance magnitudes calculated with the CODED algorithm for Bench Maji zone, Right: Corresponding histogram showing the number of pixels labelled as disturbance for the different magnitudes	97
Figure 11-16 Histogram showing the number of pixels labelled as disturbance for every year during the analysis period for Bench Maji zone, the light blue line demonstrates the precipitation data from world weather for the city of Mizan Teferi (World Weather Online 2020), the dark blue line refers to the average precipitation extracted from the Chirps data (Google Earth Engine 2020).....	97
Figure 11-17 Top: Landsat imagery composites 1995-2000, 2010-2015 and 2015-2020 for Bale zone (Google Earth Engine 2020), Bottom: Classified composites 1995-2000, 2010-2015 and 2015-2020	98
Figure 11-18 Graphic illustrating the areal size of the different land cover classes per classified composite for Bale zone..	98
Figure 11-19 From left to right: Calculated forest loss displayed in red for Bale zone, calculated loss in red overlaid on the classified composite 2015-2020, degradation in orange and deforestation in red calculated with the CODED algorithm overlaid on the Landsat imagery composite 2015-2020.....	99
Figure 11-20 Left: Disturbance dates calculated with the CODED algorithm for Bale zone, Right: Corresponding histogram showing the number of pixels labelled as disturbance for every year during the study period	99
Figure 11-21 Left: Disturbance magnitudes calculated with the CODED algorithm for Bale zone, Right: Corresponding histogram showing the number of pixels labelled as disturbance for the different magnitudes	99
Figure 11-22 Histogram showing the number of pixels labelled as disturbance for every year during the analysis period for Bale zone, the light blue line demonstrates the precipitation data from world weather for the city of Robe (World Weather Online 2020), the dark blue line refers to the average precipitation extracted from the Chirps data (Google Earth Engine 2020)	100
Figure 11-23 Left: Disturbance dates calculated with the CODED algorithm for Keshi kebele	100
Figure 11-24 Left: Disturbance magnitudes calculated with the CODED algorithm for Keshi kebele, Right: Corresponding histogram showing the number of pixels labelled as disturbance for the different magnitudes	100
Figure 11-25 Disturbance dates calculated with the CODED algorithm for Chebere kebele	101
Figure 11-26 Left: Disturbance magnitudes calculated with the CODED algorithm for Chebere kebele, Right: Corresponding histogram showing the number of pixels labelled as disturbance for the different magnitudes	101
Figure 11-27 Disturbance dates calculated with the CODED algorithm for Giz Meret kebele.....	101

Figure 11-28 Left: Disturbance magnitudes calculated with the CODED algorithm for Giz Meret kebele, Right: Corresponding histogram showing the number of pixels labelled as disturbance for the different magnitudes	101
Figure 11-29 Disturbance dates calculated with the CODED algorithm for Sodu Lelaftu kebele	102
Figure 11-30 Left: Disturbance magnitudes calculated with the CODED algorithm for Sodu Lelaftu kebele, Right: Corresponding histogram showing the number of pixels labelled as disturbance for the different magnitudes	102
Figure 11-31 Top: Landsat imagery composites 1995-2000, 2010-2015 and 2015-2020 for Bergi kebele (Google Earth Engine 2020), Bottom: Classified composites 1995-2000, 2010-2015 and 2015-2020	102
Figure 11-32 Graphic illustrating the areal size of the different land cover classes per classified composite for Bergi kebele	103
Figure 11-33 From left to right: Calculated forest loss displayed in red for Bergi kebele, calculated loss in red overlaid on the classified composite 2015-2020, degradation in orange and deforestation in red calculated with the CODED algorithm overlaid on the Landsat imagery composite 2015-2020.....	103
Figure 11-34 Disturbance dates calculated with the CODED algorithm for Bergi kebele, Right: Corresponding histogram showing the number of pixels labelled as disturbance for every year during the study period	103
Figure 11-35 Left: Disturbance magnitudes calculated with the CODED algorithm for Keffa zone, Right: Corresponding histogram showing the number of pixels labelled as disturbance for the different magnitudes	104
Figure 11-36 Top: Landsat imagery composites 1995-2000, 2010-2015 and 2015-2020 for Mankira kebele (Google Earth Engine 2020), Bottom: Classified composites 1995-2000, 2010-2015 and 2015-2020	104
Figure 11-37 Graphic illustrating the areal size of the different land cover classes per classified composite for Mankira kebele	105
Figure 11-38 From left to right: Calculated forest loss displayed in red for Mankira kebele, calculated loss in red overlaid on the classified composite 2015-2020, degradation in orange and deforestation in red calculated with the CODED algorithm overlaid on the Landsat imagery composite 2015-2020.....	105
Figure 11-39 Left: Disturbance dates calculated with the CODED algorithm for Mankira kebele, Right: Corresponding histogram showing the number of pixels labelled as disturbance for every year during the study period	105
Figure 11-40 Left: Disturbance magnitudes calculated with the CODED algorithm for Mankira kebele, Right: Corresponding histogram showing the number of pixels labelled as disturbance for the different magnitudes	106
Figure 11-41 Top: Landsat imagery composites 1995-2000, 2010-2015 and 2015-2020 for Keja Araba kebele (Google Earth Engine 2020), Bottom: Classified composites 1995-2000, 2010-2015 and 2015-2020.....	106
Figure 11-42 Graphic illustrating the areal size of the different land cover classes per classified composite for Keja Araba kebele	106
Figure 11-43 From left to right: Calculated forest loss displayed in red for Keja Araba kebele, calculated loss in red overlaid on the classified composite 2015-2020, degradation in orange and deforestation in red calculated with the CODED algorithm overlaid on the Landsat imagery composite 2015-2020	107
Figure 11-44 Left: Disturbance dates calculated with the CODED algorithm for Keja Araba kebele, Right: Corresponding histogram showing the number of pixels labelled as disturbance for every year during the study period	107
Figure 11-45 Left: Disturbance magnitudes calculated with the CODED algorithm for Keja Araba kebele, Right: Corresponding histogram showing the number of pixels labelled as disturbance for the different magnitudes	107
Appendix Figure 11-46 Top: Landsat imagery composites 1995-2000, 2010-2015 and 2015-2020 for Seriti kebele (Google Earth Engine 2020), Bottom: Classified composites 1995-2000, 2010-2015 and 2015-2020.....	108
Figure 11-47 Graphic illustrating the areal size of the different land cover classes per classified composite for Seriti kebele	108
Figure 11-48 From left to right: Calculated forest loss displayed in red for Seriti kebele, calculated loss in red overlaid on the classified composite 2015-2020, degradation in orange and deforestation in red calculated with the CODED algorithm overlaid on the Landsat imagery composite 2015-2020.....	108
Figure 11-49 Disturbance dates calculated with the CODED algorithm for Seriti kebele, Right: Corresponding histogram showing the number of pixels labelled as disturbance for every year during the study period	109
Figure 11-50 Left: Disturbance magnitudes calculated with the CODED algorithm for Seriti kebele, Right: Corresponding histogram showing the number of pixels labelled as disturbance for the different magnitudes	109
Figure 11-51 Top: Landsat imagery composites 1995-2000, 2010-2015 and 2015-2020 for Muti kebele (Google Earth Engine 2020), Bottom: Classified composites 1995-2000, 2010-2015 and 2015-2020	109
Figure 11-52 Graphic illustrating the areal size of the different land cover classes per classified composite for Muti kebele	110
Figure 11-53 From left to right: Calculated forest loss displayed in red for Muti kebele, calculated loss in red overlaid on the classified composite 2015-2020, degradation in orange and deforestation in red calculated with the CODED algorithm overlaid on the Landsat imagery composite 2015-2020.....	110
Figure 11-54 Left: Disturbance dates calculated with the CODED algorithm for Muti kebele, Right: Corresponding histogram showing the number of pixels labelled as disturbance for every year during the study period	110

Figure 11-55 Left: Disturbance magnitudes calculated with the CODED algorithm for Muti kebele, Right: Corresponding histogram showing the number of pixels labelled as disturbance for the different magnitudes	111
Figure 11-56 Top: Landsat imagery composites 1995-2000, 2010-2015 and 2015-2020 for Ganga kebele (Google Earth Engine 2020), Bottom: Classified composites 1995-2000, 2010-2015 and 2015-2020	111
Figure 11-57 Graphic illustrating the areal size of the different land cover classes per classified composite for Ganga kebele	111
Figure 11-58 From left to right: Calculated forest loss displayed in red for Ganga kebele, calculated loss in red overlaid on the classified composite 2015-2020, degradation in orange and deforestation in red calculated with the CODED algorithm overlaid on the Landsat imagery composite 2015-2020.....	112
Figure 11-59 Left: Disturbance dates calculated with the CODED algorithm for Ganga kebele, Right: Corresponding histogram showing the number of pixels labelled as disturbance for every year during the study period	112
Figure 11-60 Left: Disturbance magnitudes calculated with the CODED algorithm for Ganga kebele, Right: Corresponding histogram showing the number of pixels labelled as disturbance for the different magnitudes	112
Figure 11-61 Graphic visualizing the number of appearances of the land cover class with the highest proportion on the categories forest loss, forest gain and to urban.....	112

9.3 List of tables

Table 1 List of the five study zones displaying the region name, zone name, capital city and the zone size. Highlighted with a frame is the main study zone Keffa (OCHA 2017).	12
Table 2 List of the 10 study kebeles displaying information on the zone name, kebele name, PFM status and kebele size. The four kebeles analysed in detail are emphasized with a black frame.	13
Table 3 List of the seven final land cover classes selected based on a pre-study. In addition, their original class value and class name before the reclassification are displayed together with the class definition (CCI Land Cover (LC) Team 2016).....	17
Table 4 Table listing the five study zones and the land cover classes with the final number of sample points per class and zone after the manual relocation of some points	21
Table 5 PROBA-V dataset (ESA 2019), list of the seven final land cover classes with their original class value and class name before the reclassification to the final values.....	23
Table 6 Validation error matrix based on the PROBA-V dataset with a validation overall accuracy of approximately 28% (1'391/5'000= 0.2782). The correctly classified pixels are emphasized in the diagonal.	23
Table 7 Validation error matrix with a validation overall accuracy of around 86% (1'246/1'447= 0.8619) using 30% of the training sample points for validation. The correctly classified pixels are emphasized in the diagonal.	23
Table 8 Parameter values entered to the CODED algorithm (Bullock 2018).....	28
Table 9 Calculated areal forest loss, forest gain and the difference between them for all zones	35

9.4 List of tables Appendix

Table 10-1 Table displaying the number of times each land cover class has been mentioned in 19 used sources (Bewket 2002; Gashaw et al. 2014; Hailemariam et al. 2016; Minala 2013; Tadesse et al. 2014; Wubie 2015; Kindu et al. 2013; Mekonnen et al. 2016; Kibret et al. 2016; Kindu et al. 2016; Sahle et al. 2018; Moges et al. 2010; "Ethiopia's Forest Reference Level Submission to the UNFCCC" 2017; Google Earth Engine 2020; CCI Land Cover (LC) Team 2016; ESA 2019; Institute of Biodiversity Conservation (IBC) 2012).....	66
Table 10-2 Thirteen test areas to assess the performance of three different classifiers (Random Forest, Classification and Regression Tree, Support Vector Machine) by comparing the classified locations to the real value on the very high resolution imagery. Emphasized with a black frame are the correctly classified forest locations by the Random Forest classifier	66
Table 10-3 Training resubstitution error matrix using the Sentinel-2 land cover dataset with a training overall accuracy of over 97% (4'867/5'000= 0.9734). Highlighted with a black frame are the correctly classified pixels.	67
Table 10-4 Training resubstitution error matrix with a training overall accuracy of around 97% (3'450/3'553= 0.971) using 70% of the sample points for training. Highlighted with a black frame are the correctly classified pixels.....	67
Table 10-5 List depicting the loss validation areas with the zone name, their performance and related to that the explanation. Highlighted with a frame are the areas where the calculated loss performed better than the Hansen forest loss.	90
Table 10-6 List depicting the gain validation areas with the zone name, their performance and related to that the explanation. Highlighted with a frame are the two real gain areas.....	90

10 Appendix I Methods

10.1 Study on the land cover classes occurring in the Ethiopian study zones

Table 10-1 Table displaying the number of times each land cover class has been mentioned in 19 used sources (Bewket 2002; Gashaw et al. 2014; Hailemariam et al. 2016; Minale 2013; Tadesse et al. 2014; Wubie 2015; Kindu et al. 2013; Mekonnen et al. 2016; Kibret et al. 2016; Kindu et al. 2016; Sahle et al. 2018; Moges et al. 2010; "Ethiopia's Forest Reference Level Submission to the UNFCCC" 2017; Google Earth Engine 2020; CCI Land Cover (LC) Team 2016; ESA 2019; Institute of Biodiversity Conservation (IBC) 2012)

Number of occurrences	Land cover class	Alternative names mentioned
19	forest	primary forest, afroalpine forest, natural forest, high forest, evergreen broadleaf open/closed forest, montane forest, submontane forest, lowland forest
9	woodland	dense woodland, open woodland
12	shrubland	bushland, different shrublands
17	grassland	grazing lands, different grasslands
11	urban area	built up, settlements
13	bare land	soil, rock, sparse vegetation, degraded land
14	water	open water, water body
18	agriculture	cultivated land, farmland, cropland, plantation

10.2 Study on the classifier performance

Table 10-2 Thirteen test areas to assess the performance of three different classifiers (Random Forest, Classification and Regression Tree, Support Vector Machine) by comparing the classified locations to the real value on the very high resolution imagery. Emphasized with a black frame are the correctly classified forest locations by the Random Forest classifier

Location	Real value (very high resolution imagery)	Random Forest (RF)	Classification and Regression Tree (CART)	Support Vector Machine (SVM)
34.2607, 7.62905	Forest	Forest	Savanna	Grassland
34.26035, 7.6202	Forest	Forest	Forest	Savanna
34.21564, 7.61723	Forest	Forest	Savanna	Grassland
34.21632, 7.62029	Forest	Forest	Savanna	Forest
34.25799, 7.59968	Forest	Forest	Savanna	Savanna
34.24087, 7.63003	Water	Savanna	Savanna	Forest
34.20817, 7.62586	Water	Savanna	Grassland	Forest
34.26091, 7.61991	Forest	Savanna	Forest	Grassland
34.21589, 7.61786	Forest	Forest	Savanna	Grassland
34.26048, 7.62931	Forest	Forest	Savanna	Savanna
34.21126, 7.62373	Water	Savanna	Forest	Savanna
34.22443, 7.62548	Savanna	Grassland	Savanna	Forest
34.22263, 7.65778	Grassland	Grassland	Savanna	Savanna

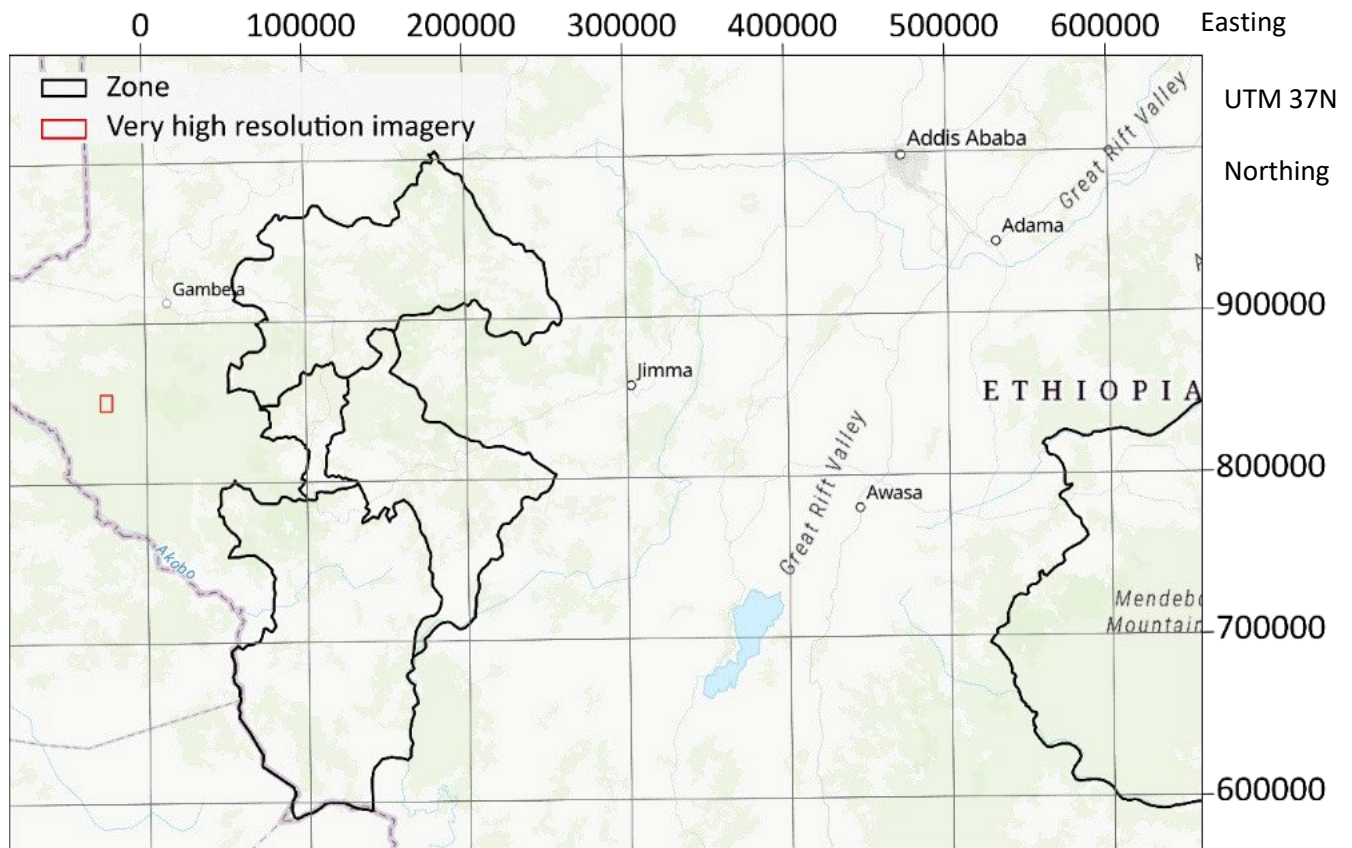


Figure 10-1 Location and extent of the very high resolution satellite data in red in comparison to the study zones (Google Earth Engine 2020)

10.3 Supervised classification validation assessment

Table 10-3 Training resubstitution error matrix using the Sentinel-2 land cover dataset with a training overall accuracy of over 97% ($4'867/5'000=0.9734$). Highlighted with a black frame are the correctly classified pixels.

ground truth	prediction					sum
	0 - forest	1 - shrubland	2 - grassland	3 - bare land	4 - cropland	
0 - forest	1'990	3	2	0	0	1'995
1 - shrubland	25	1'150	16	0	2	1'193
2 - grassland	11	40	1'127	0	5	1'183
3 - bare land	0	0	0	109	1	110
4 - cropland	5	12	10	1	491	519
sum	2'031	1'205	1'155	110	499	5'000

Table 10-4 Training resubstitution error matrix with a training overall accuracy of around 97% ($3'450/3'553=0.971$) using 70% of the sample points for training. Highlighted with a black frame are the correctly classified pixels.

ground truth	prediction					sum
	0 - forest	1 - shrubland	2 - grassland	3 - bare land	4 - cropland	
0 - forest	1'424	2	0	0	0	1'426
1 - shrubland	14	816	19	0	1	850
2 - grassland	4	42	784	0	5	835
3 - bare land	0	0	0	74	0	74
4 - cropland	4	6	4	2	352	368
sum	1'446	866	807	76	358	3'553

10.4 Documentation of the change detection validation

10.4.1 Keffa zone

Area 1 forest loss

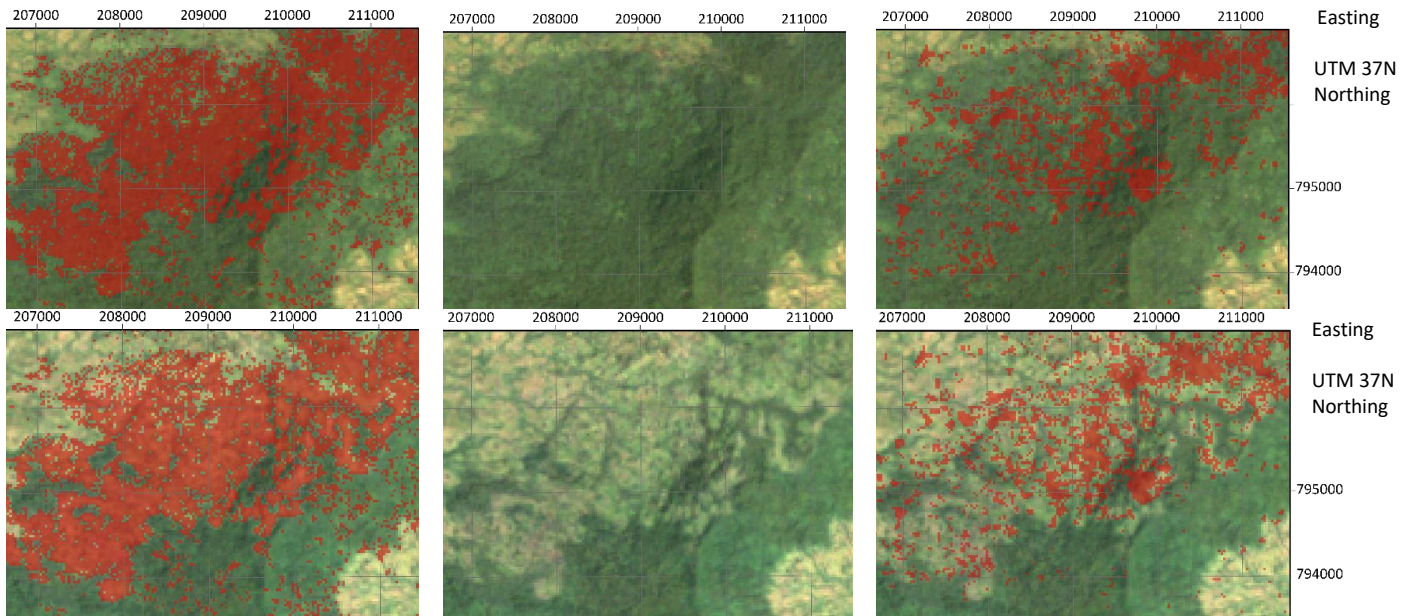


Figure 10-2 Area 1 forest loss: From left to right: Calculated forest loss areas in red overlaid on the composite 1995-2000 on top and on the composite 2015-2020 on the bottom, Landsat imagery composite 1995-2000 on top and composite 2015-2020 on the bottom, Hansen forest loss in red overlaid on the composite 1995-2000 on top and on the composite 2015-2020 on the bottom (Google Earth Engine 2020)

Area 2 forest loss

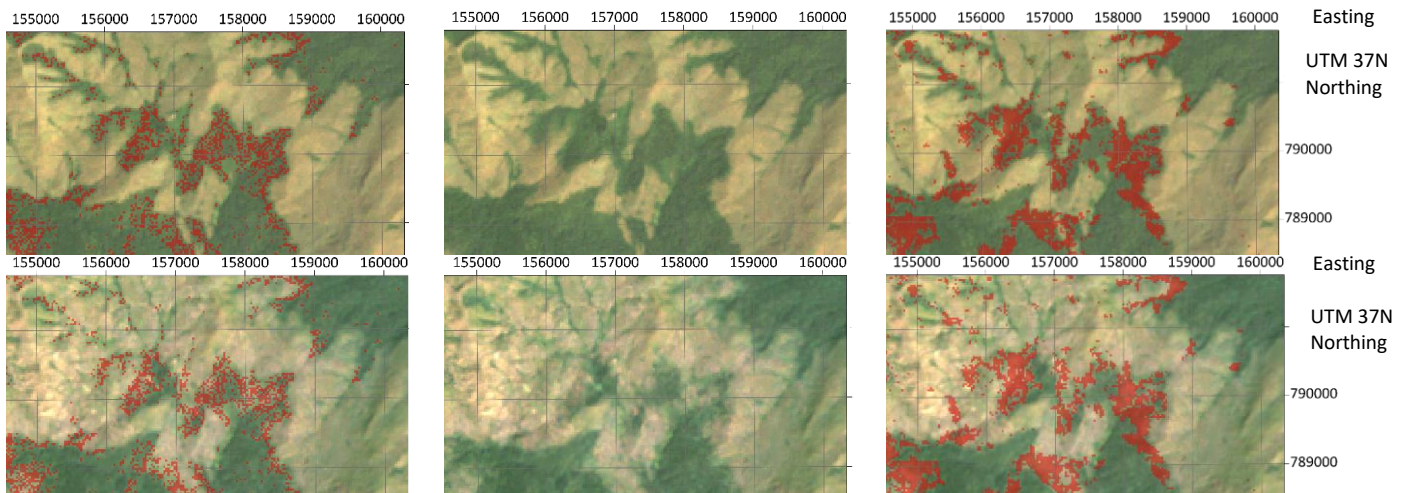


Figure 10-3 Area 2 forest loss: From left to right: Calculated forest loss areas in red overlaid on the composite 1995-2000 on top and on the composite 2015-2020 on the bottom, Landsat imagery composite 1995-2000 on top and composite 2015-2020 on the bottom, Hansen forest loss in red overlaid on the composite 1995-2000 on top and on the composite 2015-2020 on the bottom (Google Earth Engine 2020)

Area 3 forest loss

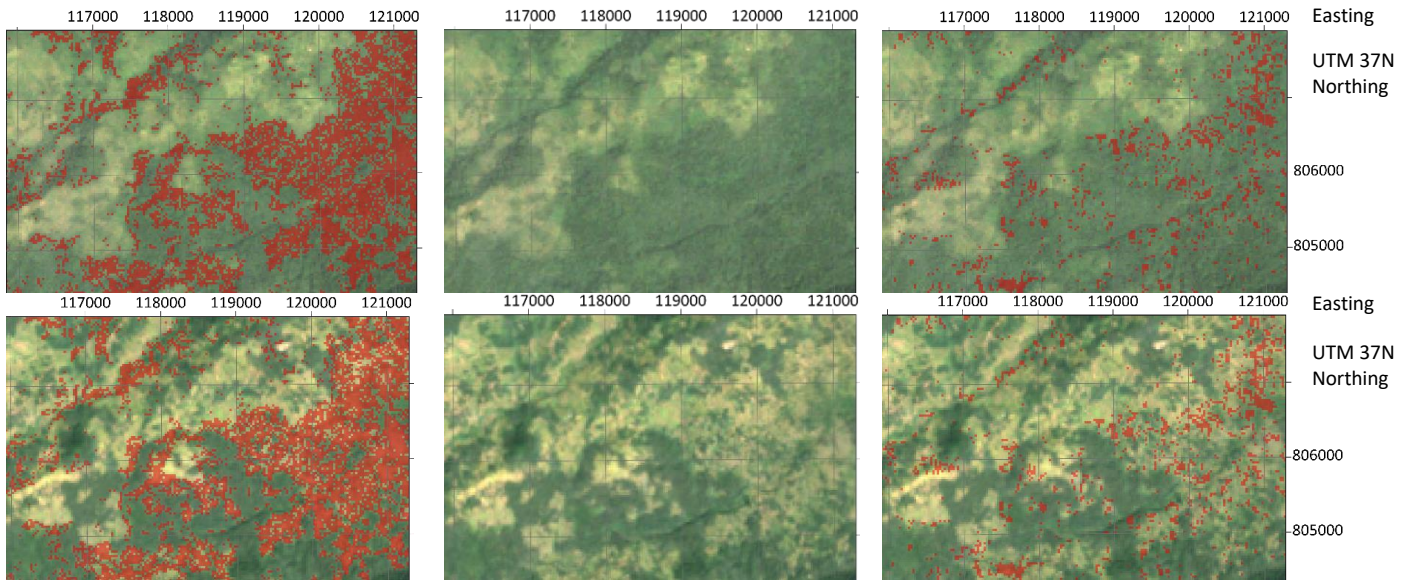


Figure 10-4 Area 3 forest loss: From left to right: Calculated forest loss areas in red overlaid on the composite 1995-2000 on top and on the composite 2015-2020 on the bottom, Landsat imagery composite 1995-2000 on top and composite 2015-2020 on the bottom, Hansen forest loss in red overlaid on the composite 1995-2000 on top and on the composite 2015-2020 on the bottom (Google Earth Engine 2020)

Area 4 forest loss

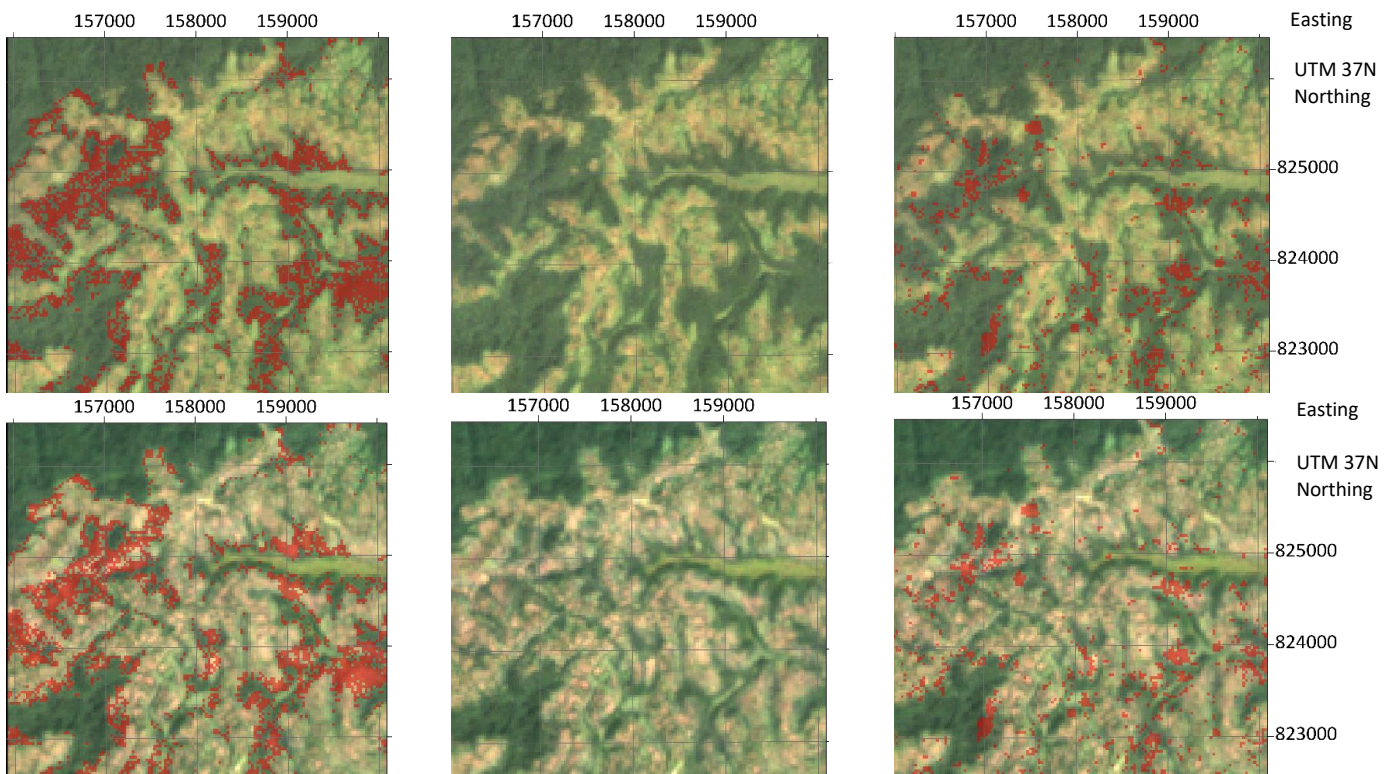


Figure 10-5 Area 4 forest loss: From left to right: Calculated forest loss areas in red overlaid on the composite 1995-2000 on top and on the composite 2015-2020 on the bottom, Landsat imagery composite 1995-2000 on top and composite 2015-2020 on the bottom, Hansen forest loss in red overlaid on the composite 1995-2000 on top and on the composite 2015-2020 on the bottom (Google Earth Engine 2020)

Area 5 forest loss

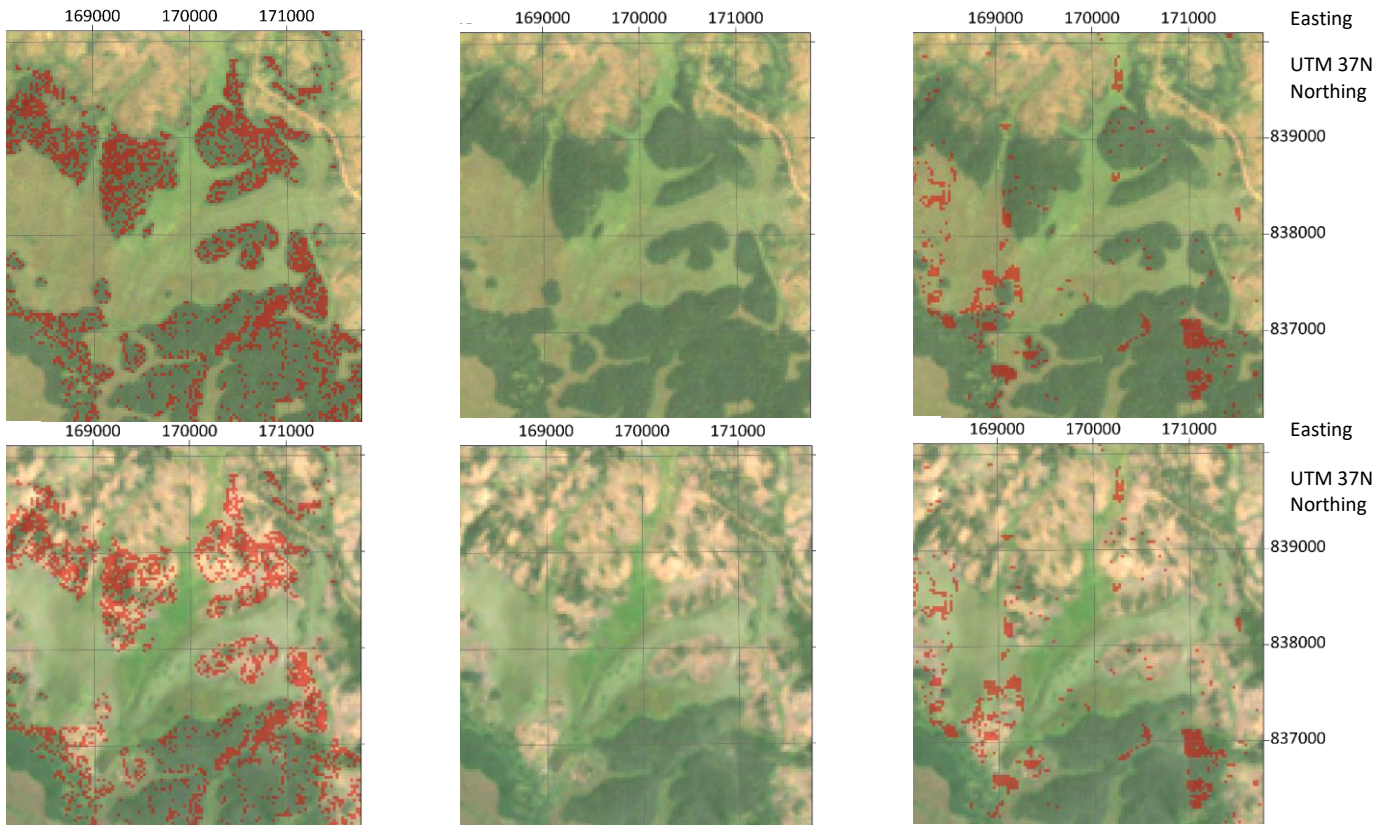


Figure 10-6 Area 5 forest loss: From left to right: Calculated forest loss areas in red overlaid on the composite 1995-2000 on top and on the composite 2015-2020 on the bottom, Landsat imagery composite 1995-2000 on top and composite 2015-2020 on the bottom, Hansen forest loss in red overlaid on the composite 1995-2000 on top and on the composite 2015-2020 on the bottom (Google Earth Engine 2020)

Area 6 forest loss

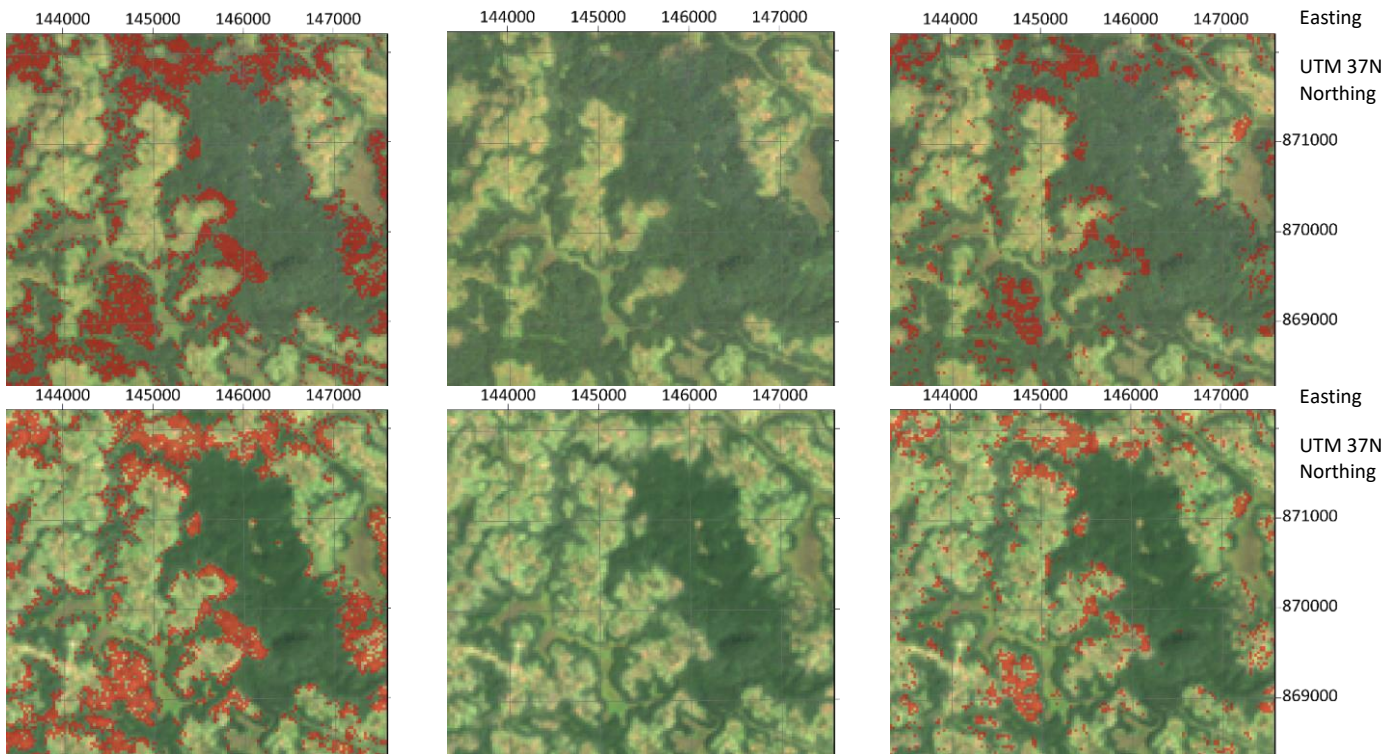


Figure 10-7 Area 6 forest loss: From left to right: Calculated forest loss areas in red overlaid on the composite 1995-2000 on top and on the composite 2015-2020 on the bottom, Landsat imagery composite 1995-2000 on top and composite 2015-2020 on the bottom, Hansen forest loss in red overlaid on the composite 1995-2000 on top and on the composite 2015-2020 on the bottom (Google Earth Engine 2020)

Area 1 forest gain

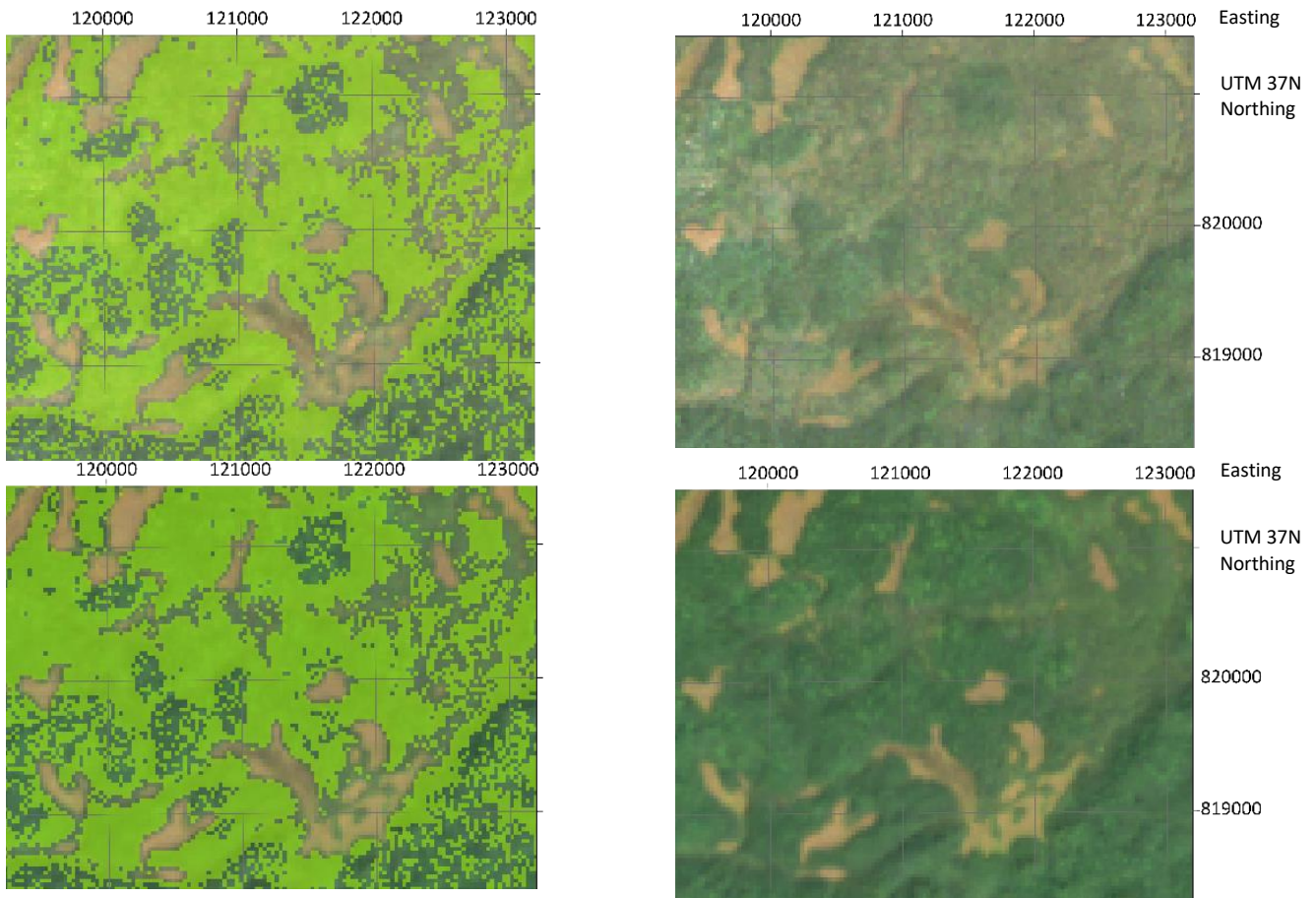


Figure 10-8 Area 1 forest gain: From left to right: Calculated forest loss areas in red overlaid on the composite 1995-2000 on top and on the composite 2015-2020 on the bottom, Landsat imagery composite 1995-2000 on top and composite 2015-2020 on the bottom, Hansen forest loss in red overlaid on the composite 1995-2000 on top and on the composite 2015-2020 on the bottom (Google Earth Engine 2020)

Area 2 forest gain

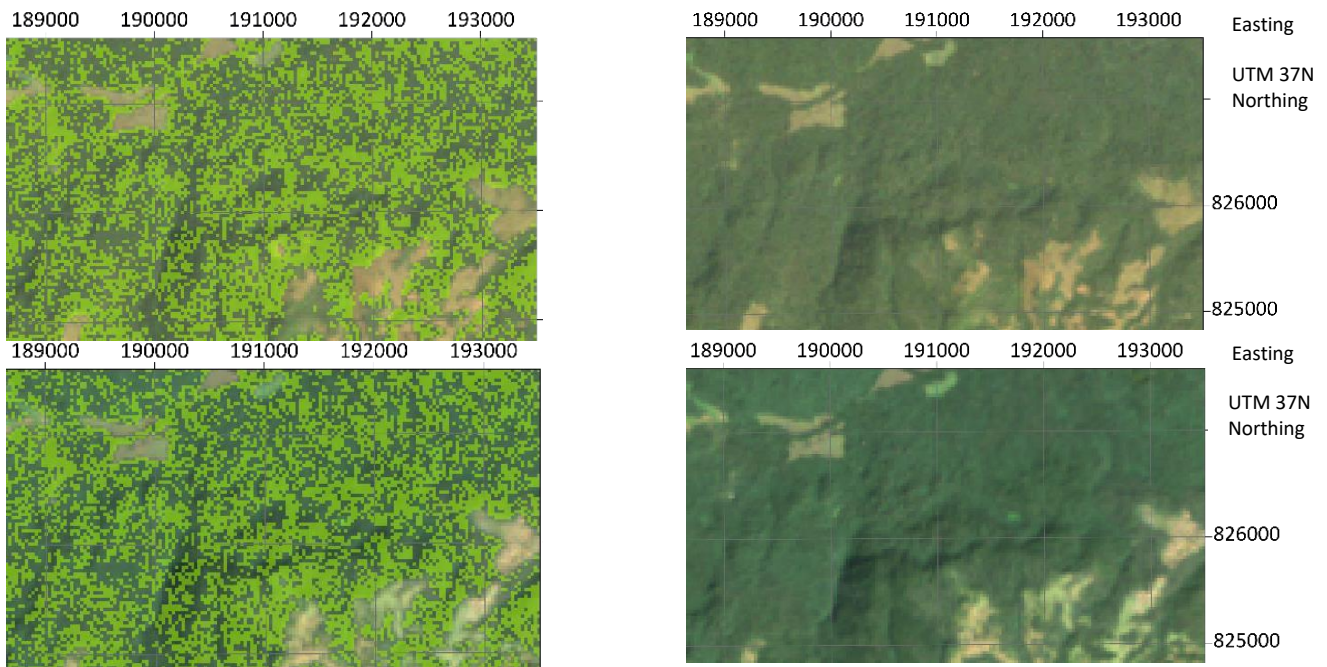


Figure 10-9 Area 2 forest gain: From left to right: Calculated forest loss areas in red overlaid on the composite 1995-2000 on top and on the composite 2015-2020 on the bottom, Landsat imagery composite 1995-2000 on top and composite 2015-2020 on the bottom, Hansen forest loss in red overlaid on the composite 1995-2000 on top and on the composite 2015-2020 on the bottom (Google Earth Engine 2020)

10.4.2 Sheka zone

Overview of the forest loss and forest gain validation areas

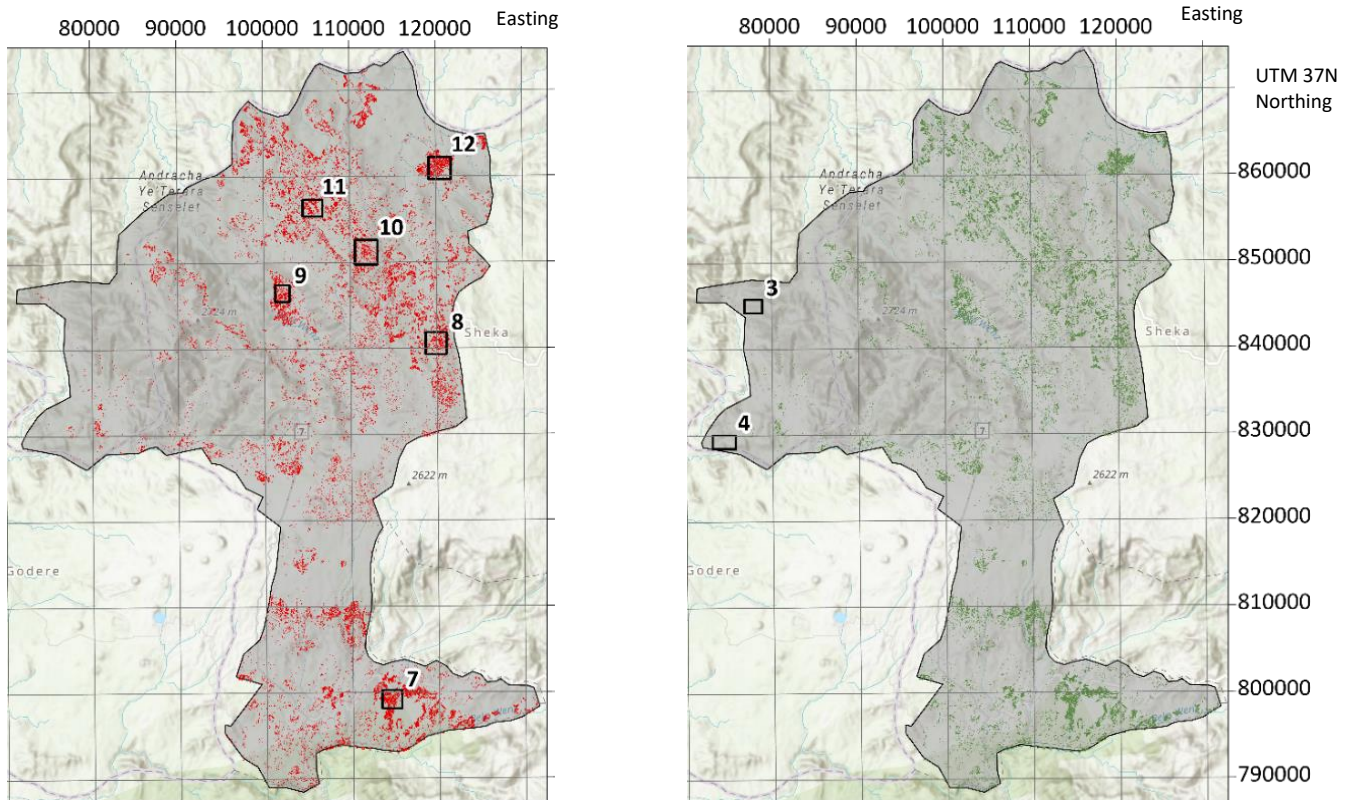


Figure 10-10 Left: Map of Sheka emphasizing the forest loss areas in red and the validation areas are framed with their corresponding number, Right: Map of Sheka emphasizing the forest gain areas in green and the validation areas are framed with their corresponding number

Area 7 forest loss

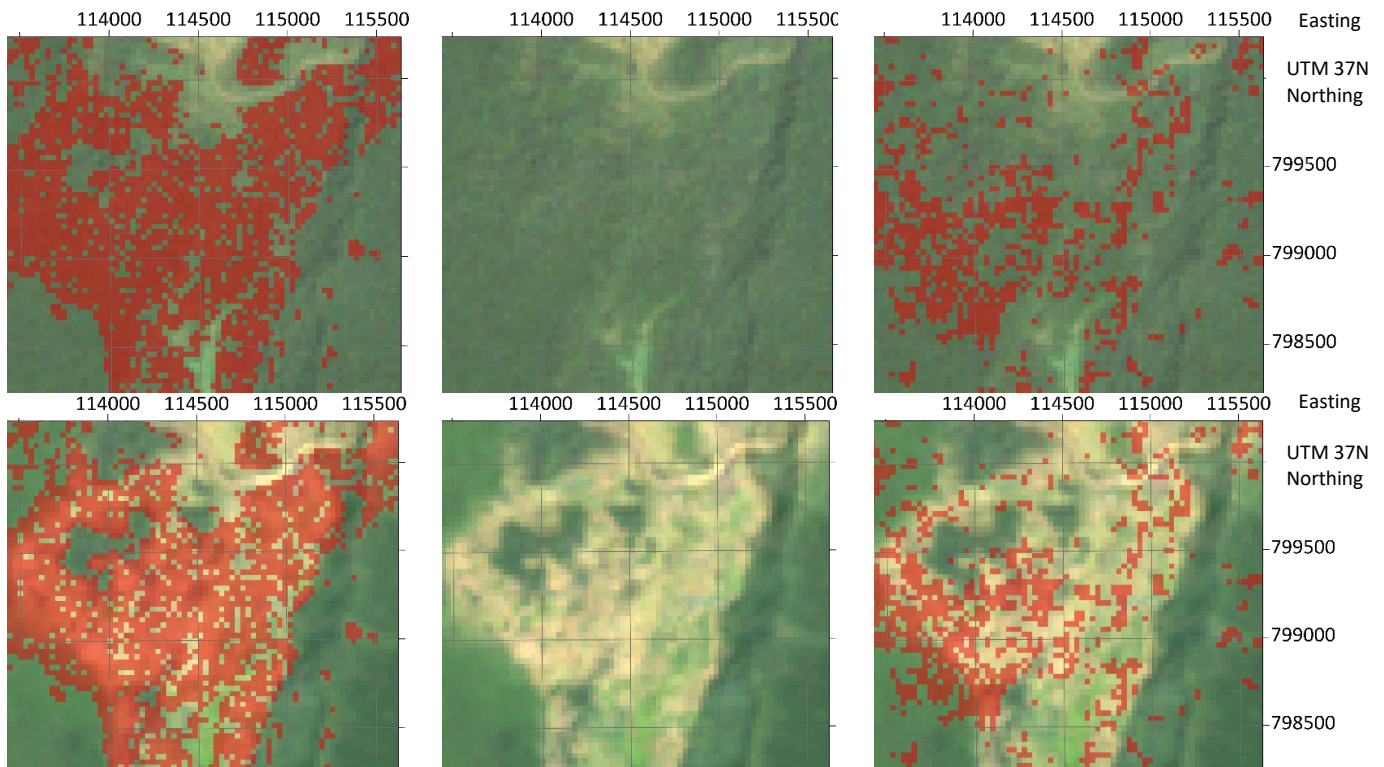


Figure 10-11 Area 7 forest loss: From left to right: Calculated forest loss areas in red overlaid on the composite 1995-2000 on top and on the composite 2015-2020 on the bottom, Landsat imagery composite 1995-2000 on top and composite 2015-2020 on the bottom, Hansen forest loss in red overlaid on the composite 1995-2000 on top and on the composite 2015-2020 on the bottom (Google Earth Engine 2020)

Area 8 forest loss

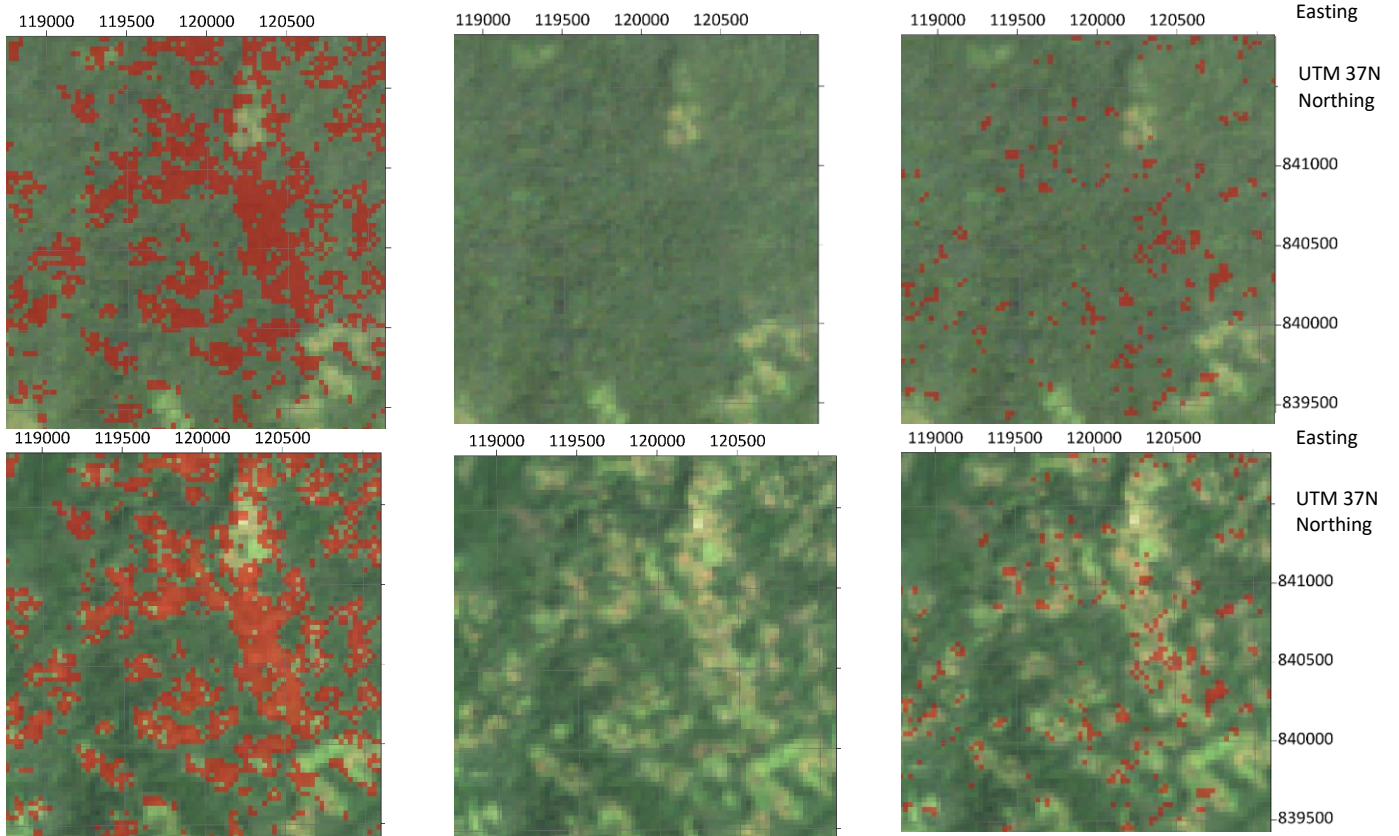


Figure 10-12 Area 8 forest loss: From left to right: Calculated forest loss areas in red overlaid on the composite 1995-2000 on top and on the composite 2015-2020 on the bottom, Landsat imagery composite 1995-2000 on top and composite 2015-2020 on the bottom, Hansen forest loss in red overlaid on the composite 1995-2000 on top and on the composite 2015-2020 on the bottom (Google Earth Engine 2020)

Area 9 forest loss

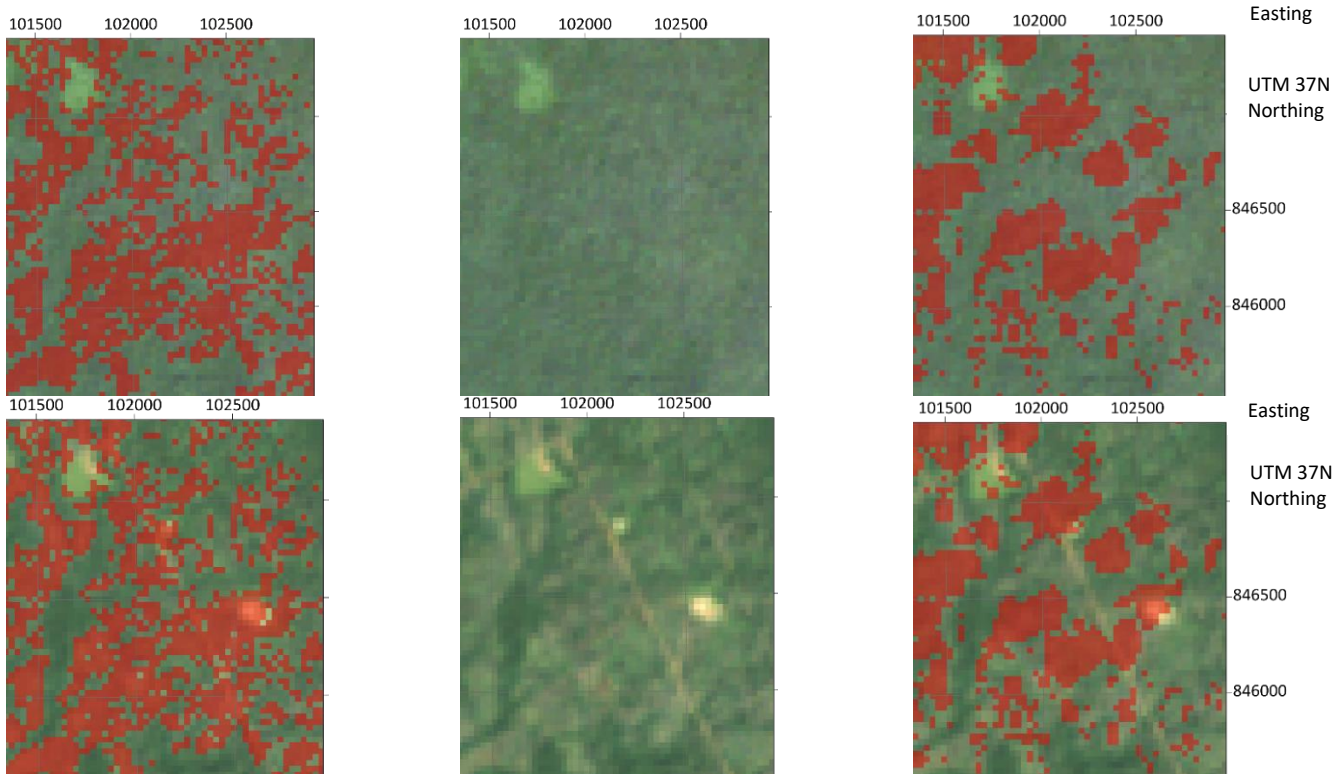


Figure 10-13 Area 9 forest loss: From left to right: Calculated forest loss areas in red overlaid on the composite 1995-2000 on top and on the composite 2015-2020 on the bottom, Landsat imagery composite 1995-2000 on top and composite 2015-2020 on the bottom, Hansen forest loss in red overlaid on the composite 1995-2000 on top and on the composite 2015-2020 on the bottom (Google Earth Engine 2020)

Area 10 forest loss

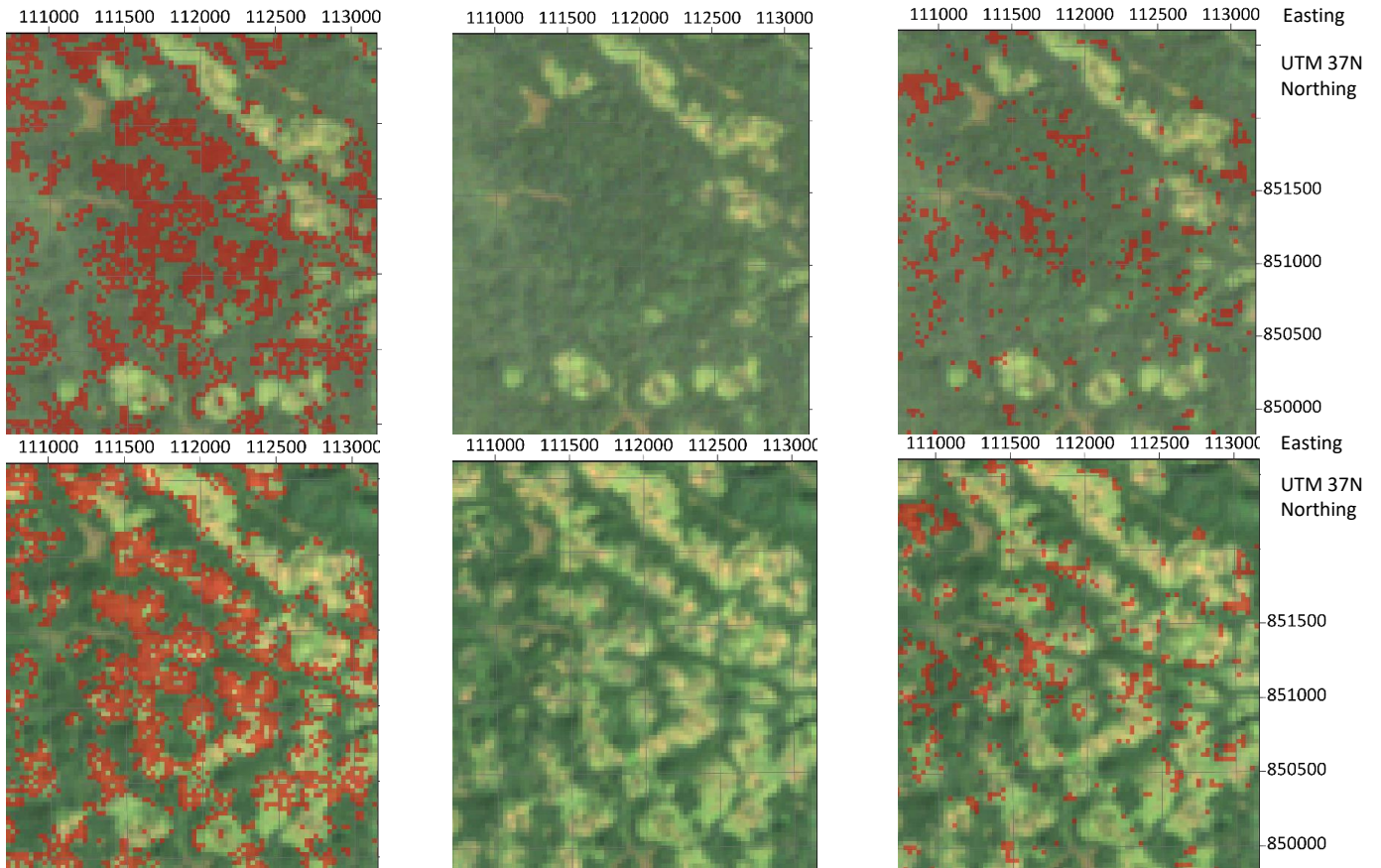


Figure 10-14 Area 10 forest loss: From left to right: Calculated forest loss areas in red overlaid on the composite 1995-2000 on top and on the composite 2015-2020 on the bottom, Landsat imagery composite 1995-2000 on top and composite 2015-2020 on the bottom, Hansen forest loss in red overlaid on the composite 1995-2000 on top and on the composite 2015-2020 on the bottom (Google Earth Engine 2020)

Area 11 forest loss

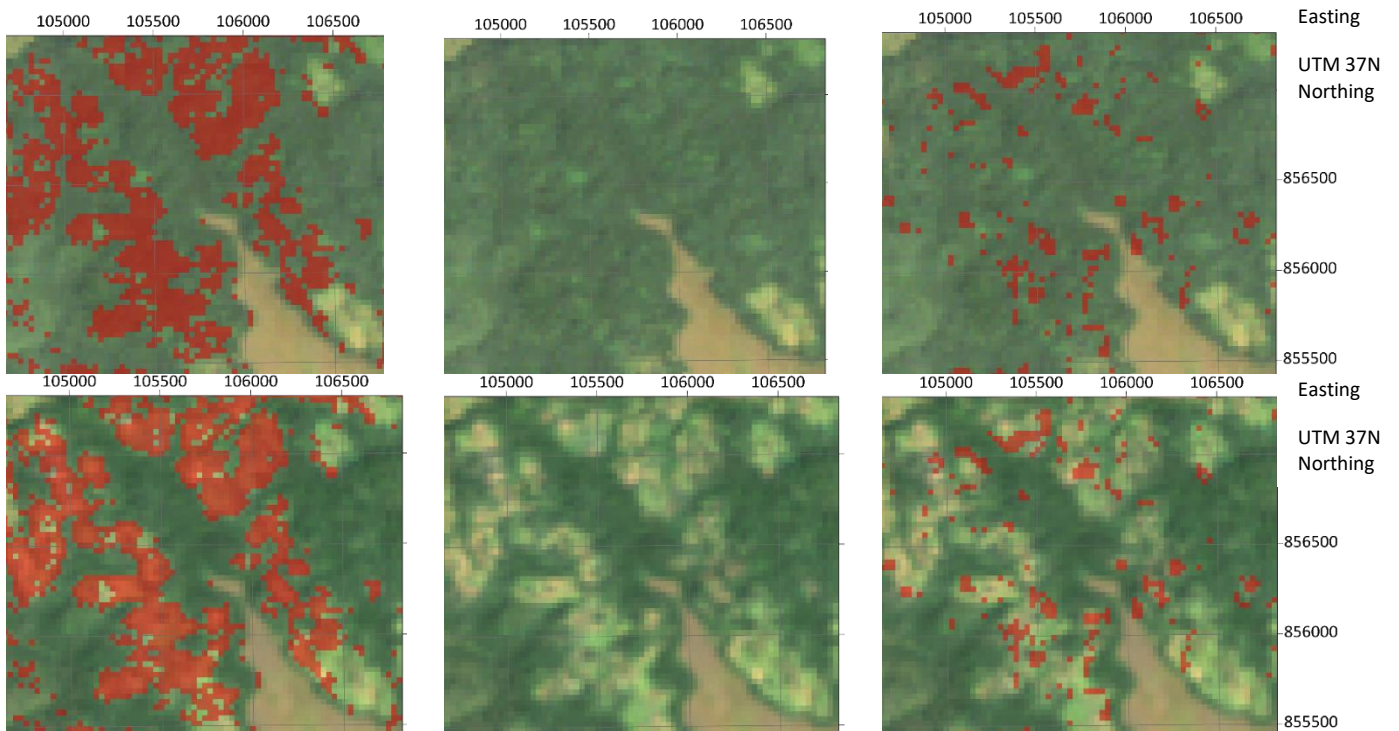


Figure 10-15 Area 11 forest loss: From left to right: Calculated forest loss areas in red overlaid on the composite 1995-2000 on top and on the composite 2015-2020 on the bottom, Landsat imagery composite 1995-2000 on top and composite 2015-2020 on the bottom, Hansen forest loss in red overlaid on the composite 1995-2000 on top and on the composite 2015-2020 on the bottom (Google Earth Engine 2020)

Area 12 forest loss

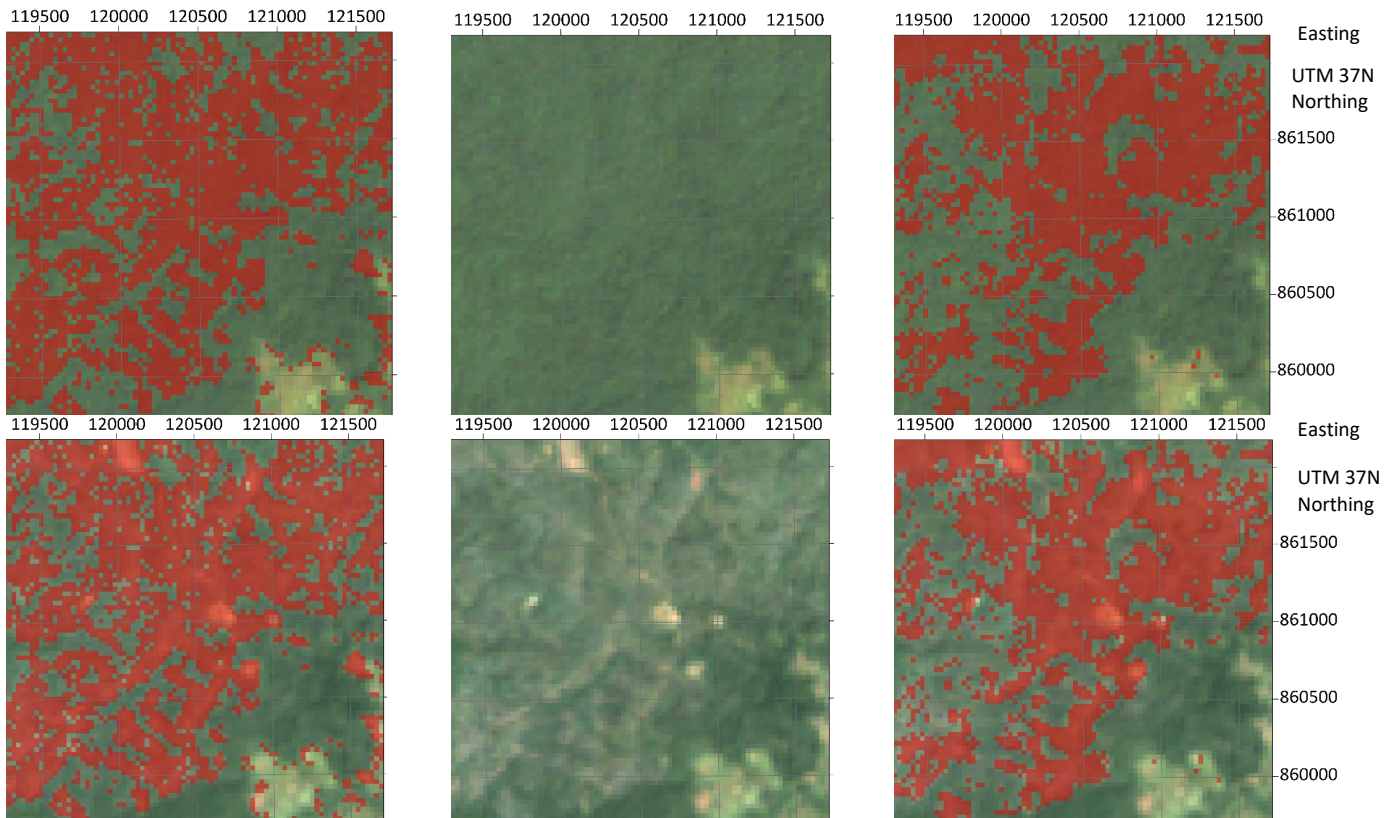


Figure 10-16 Area 12 forest loss: From left to right: Calculated forest loss areas in red overlaid on the composite 1995-2000 on top and on the composite 2015-2020 on the bottom, Landsat imagery composite 1995-2000 on top and composite 2015-2020 on the bottom, Hansen forest loss in red overlaid on the composite 1995-2000 on top and on the composite 2015-2020 on the bottom (Google Earth Engine 2020)

Area 3 forest gain

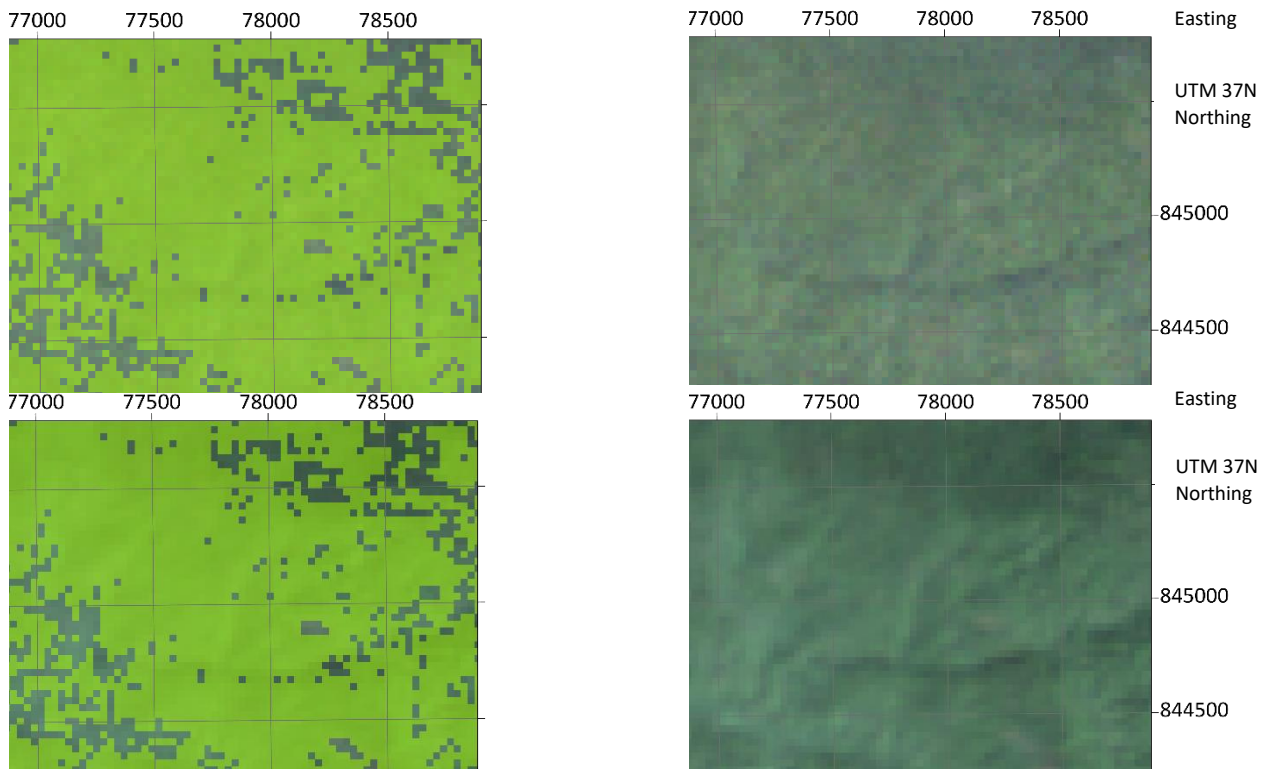


Figure 10-17 Area 3 forest gain: From left to right: Calculated forest gain areas in green overlaid on the composite 1995-2000 on top and on the composite 2015-2020 on the bottom, Landsat imagery composite 1995-2000 on top and composite 2015-2020 on the bottom, Hansen forest gain in green overlaid on the composite 1995-2000 on top and on the composite 2015-2020 on the bottom (Google Earth Engine 2020)

Area 4 forest gain

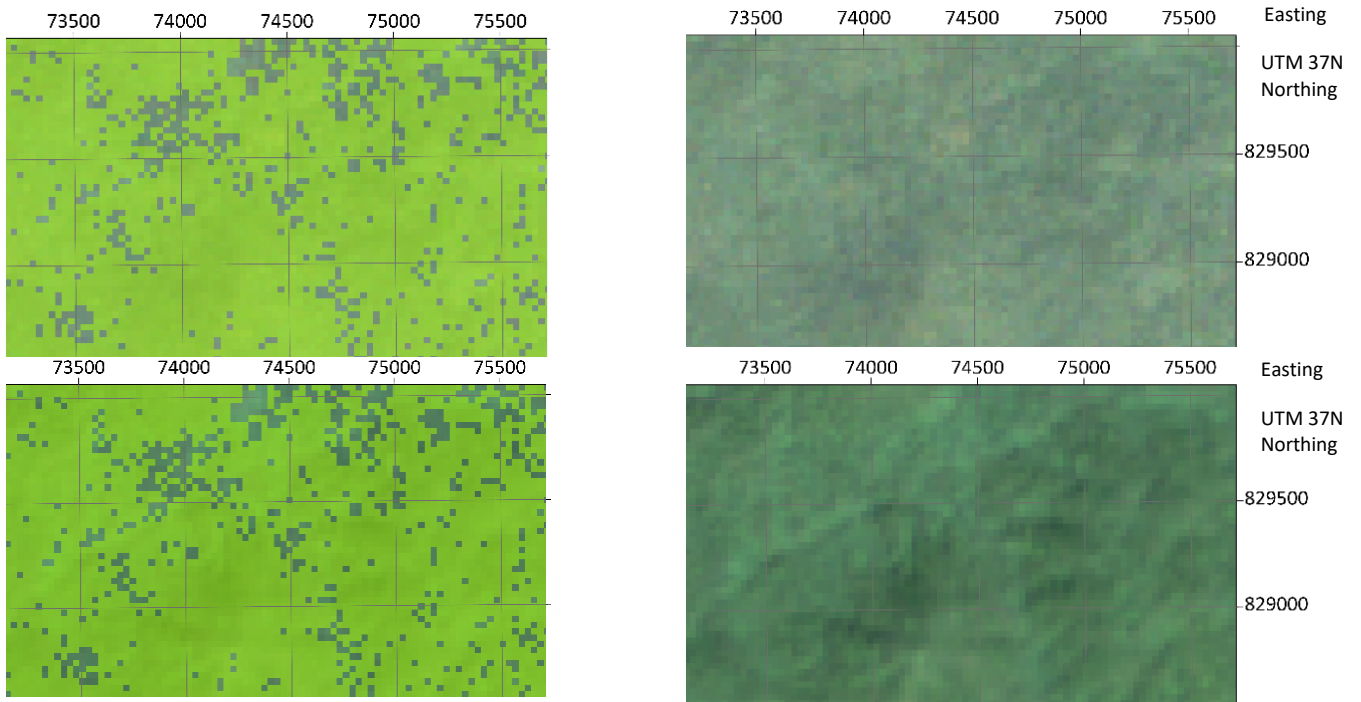


Figure 10-18 Area 4 forest gain: From left to right: Calculated forest loss areas in red overlaid on the composite 1995-2000 on top and on the composite 2015-2020 on the bottom, Landsat imagery composite 1995-2000 on top and composite 2015-2020 on the bottom, Hansen forest loss in red overlaid on the composite 1995-2000 on top and on the composite 2015-2020 on the bottom (Google Earth Engine 2020)

10.4.3 Illubabor zone

Overview of the forest loss and forest gain validation areas

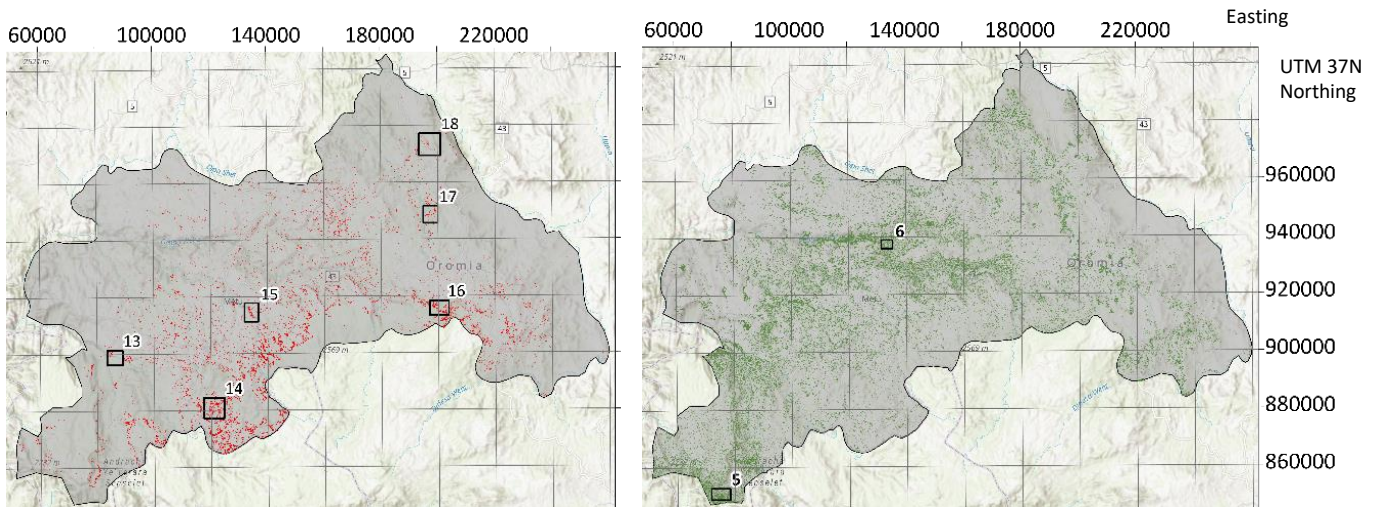


Figure 10-19 Left: Map of Illubabor emphasizing the forest loss areas in red and the validation areas are framed with their corresponding number, Right: Map of Illubabor emphasizing the forest gain areas in green and the validation areas are framed with their corresponding number

Area 13 forest loss

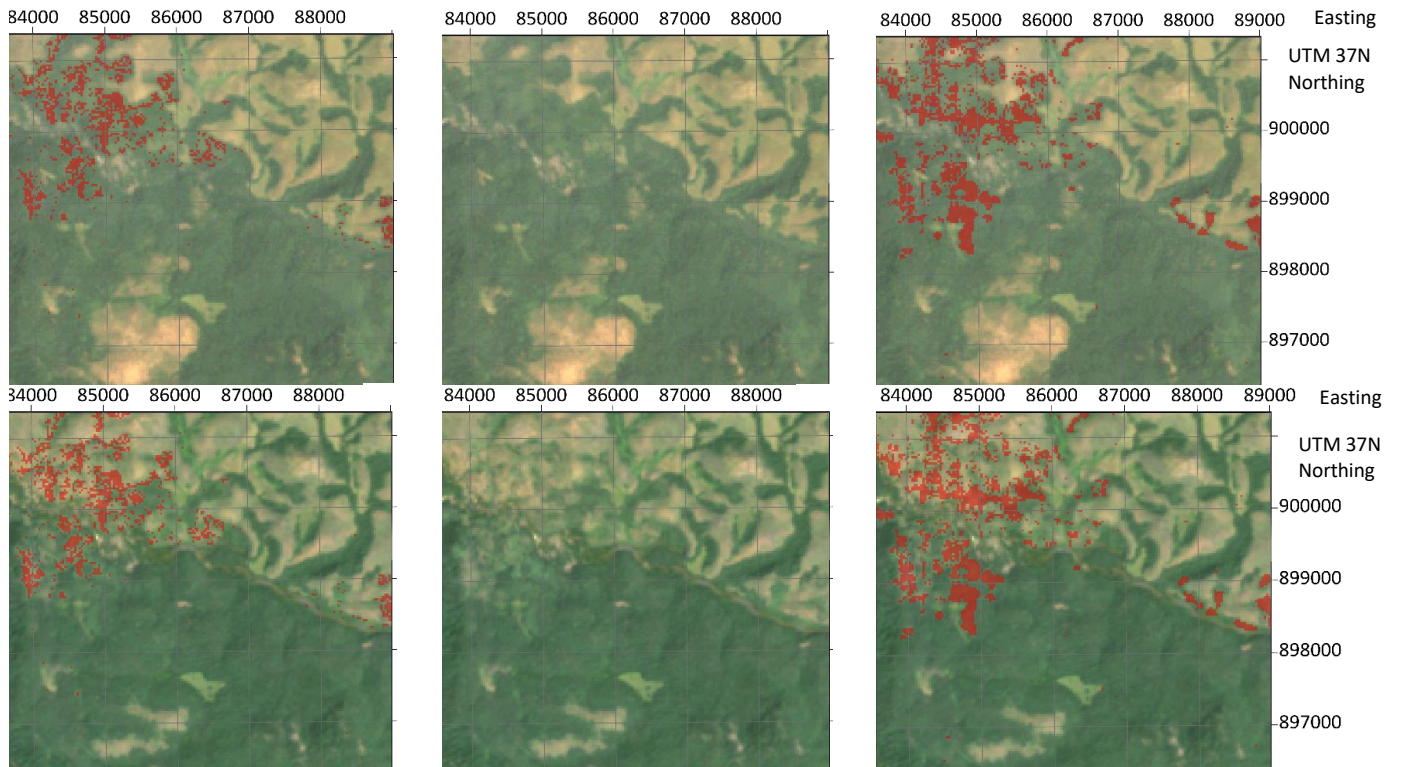


Figure 10-20 Area 13 forest loss: From left to right: Calculated forest loss areas in red overlaid on the composite 1995-2000 on top and on the composite 2015-2020 on the bottom, Landsat imagery composite 1995-2000 on top and composite 2015-2020 on the bottom, Hansen forest loss in red overlaid on the composite 1995-2000 on top and on the composite 2015-2020 on the bottom (Google Earth Engine 2020)

Area 14 forest loss

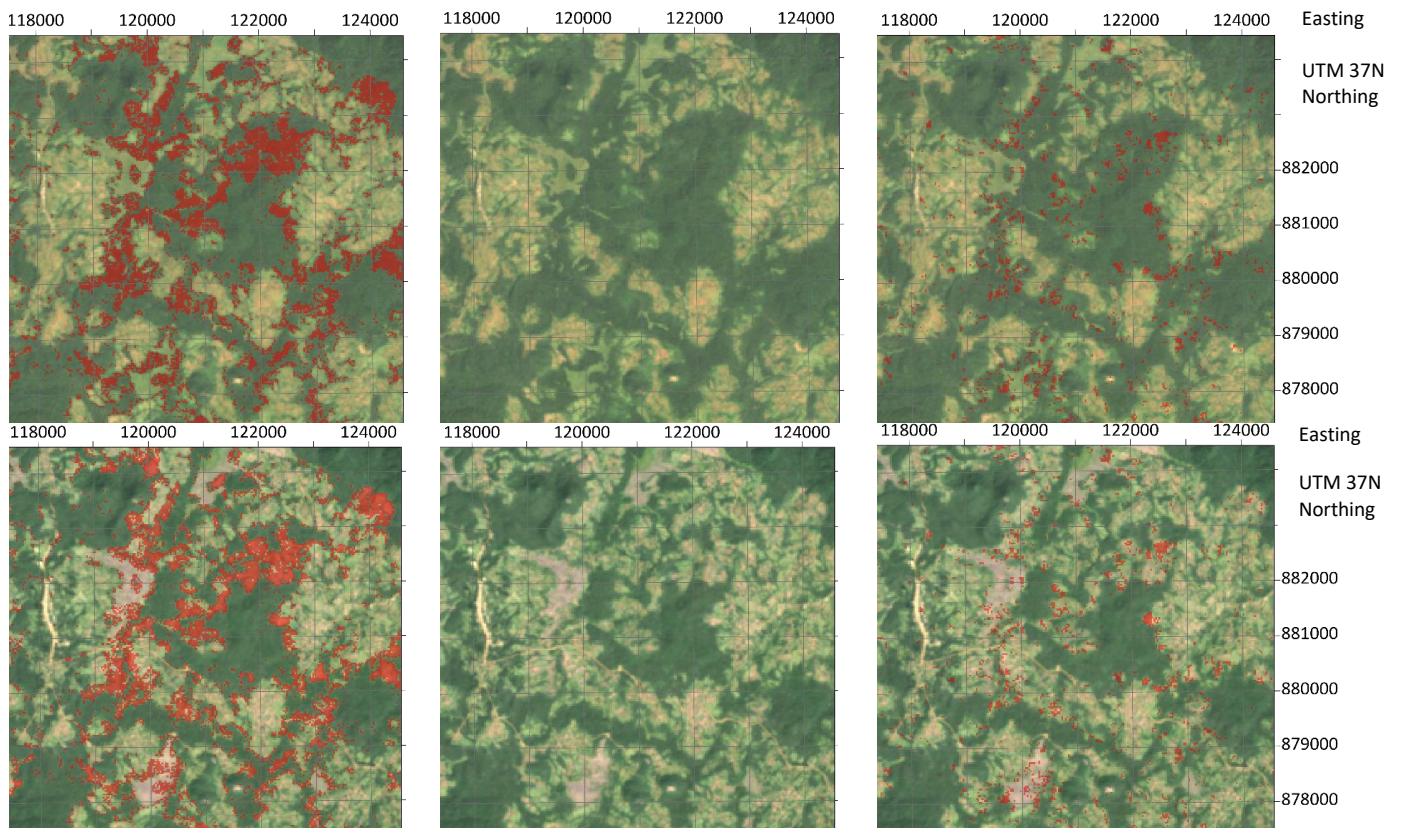


Figure 10-21 Area 42 forest loss: From left to right: Calculated forest loss areas in red overlaid on the composite 1995-2000 on top and on the composite 2015-2020 on the bottom, Landsat imagery composite 1995-2000 on top and composite 2015-2020 on the bottom, Hansen forest loss in red overlaid on the composite 1995-2000 on top and on the composite 2015-2020 on the bottom (Google Earth Engine 2020)

Area 15 forest loss

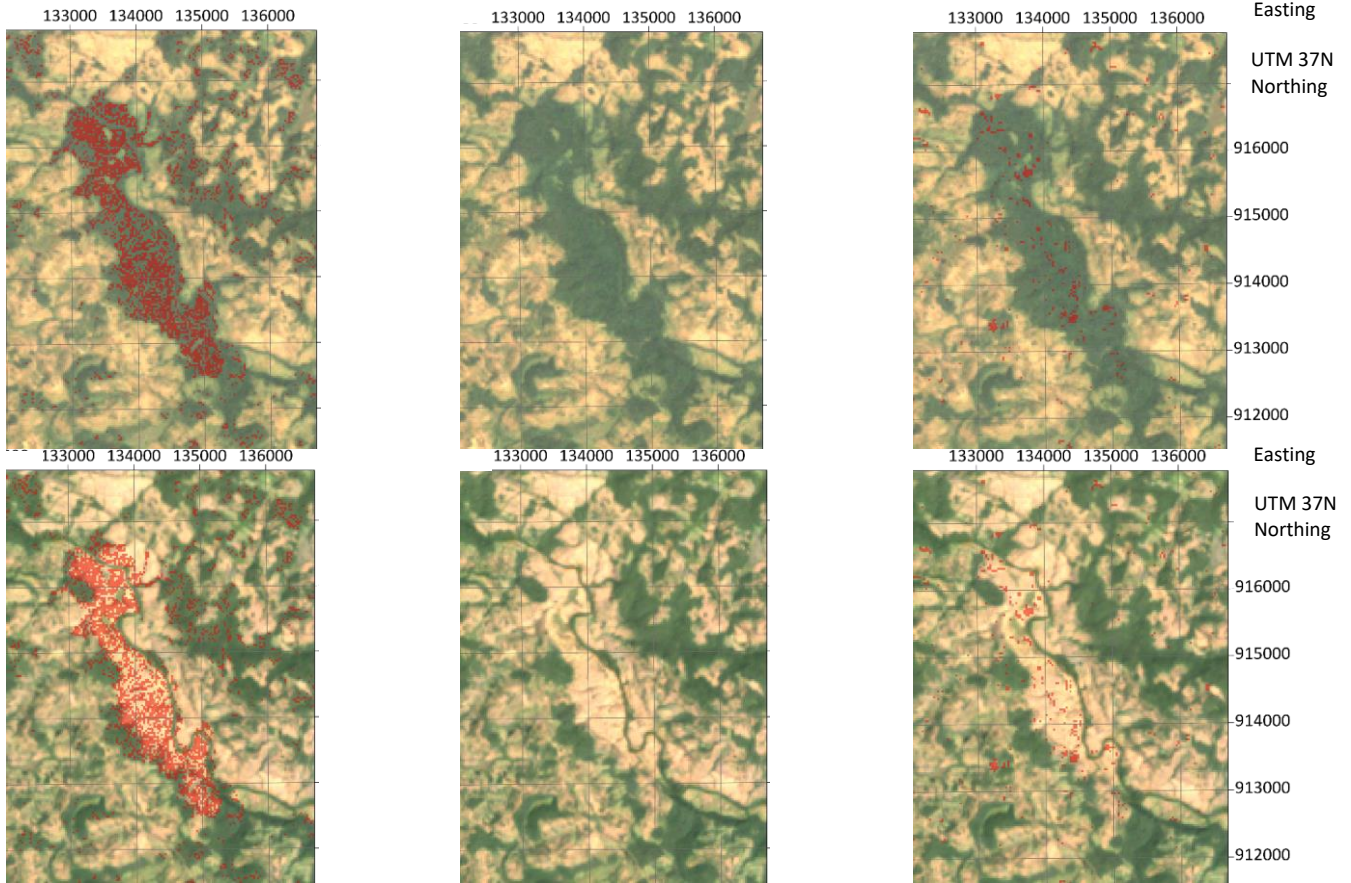


Figure 10-22 Area 15 forest loss: From left to right: Calculated forest loss areas in red overlaid on the composite 1995-2000 on top and on the composite 2015-2020 on the bottom, Landsat imagery composite 1995-2000 on top and composite 2015-2020 on the bottom, Hansen forest loss in red overlaid on the composite 1995-2000 on top and on the composite 2015-2020 on the bottom (Google Earth Engine 2020)

Area 16 forest loss

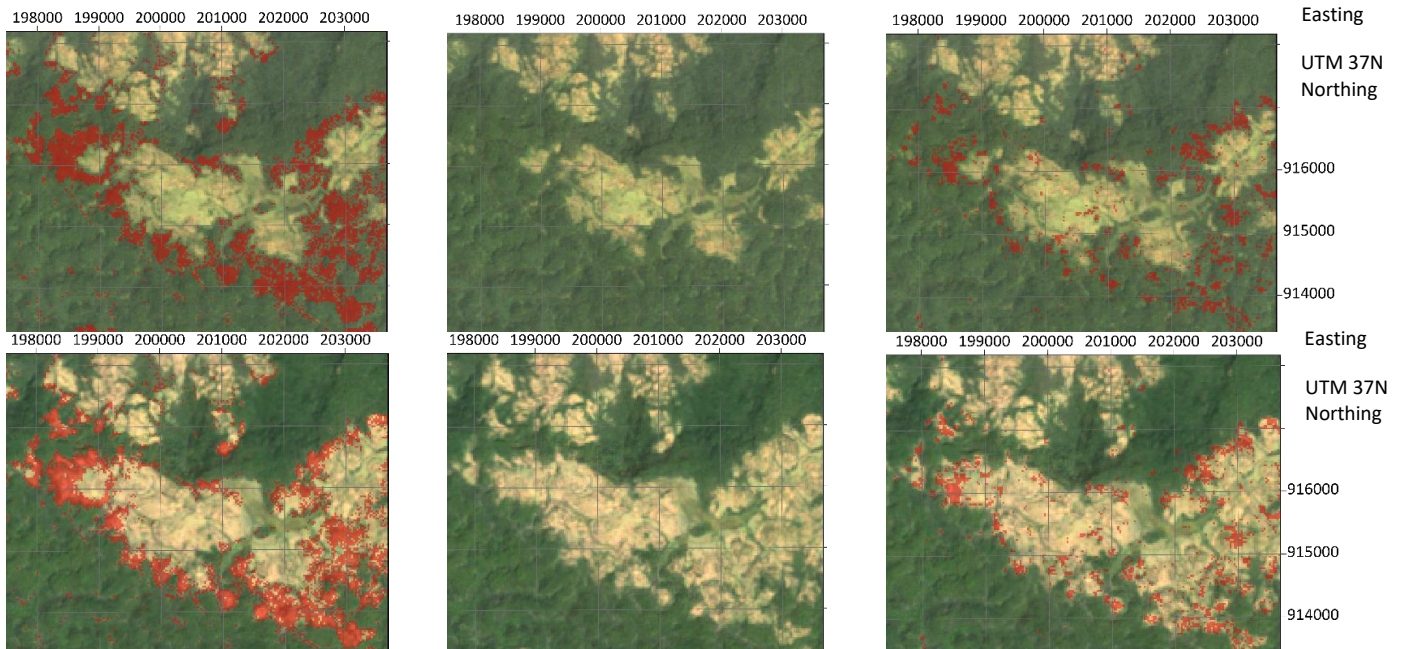


Figure 10-23 Area 62 forest loss: From left to right: Calculated forest loss areas in red overlaid on the composite 1995-2000 on top and on the composite 2015-2020 on the bottom, Landsat imagery composite 1995-2000 on top and composite 2015-2020 on the bottom, Hansen forest loss in red overlaid on the composite 1995-2000 on top and on the composite 2015-2020 on the bottom (Google Earth Engine 2020)

Area 17 forest loss

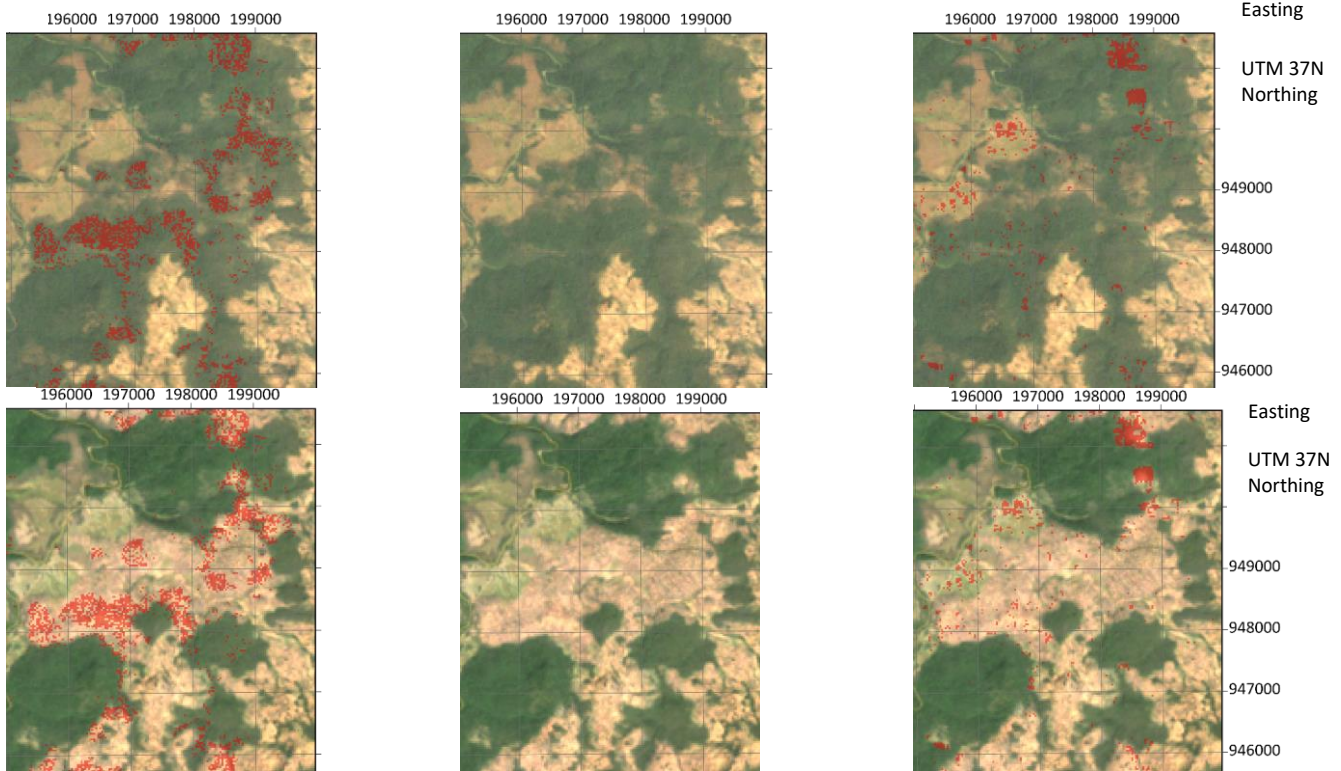


Figure 10-24 Area 72 forest loss: From left to right: Calculated forest loss areas in red overlaid on the composite 1995-2000 on top and on the composite 2015-2020 on the bottom, Landsat imagery composite 1995-2000 on top and composite 2015-2020 on the bottom, Hansen forest loss in red overlaid on the composite 1995-2000 on top and on the composite 2015-2020 on the bottom (Google Earth Engine 2020)

Area 18 forest loss

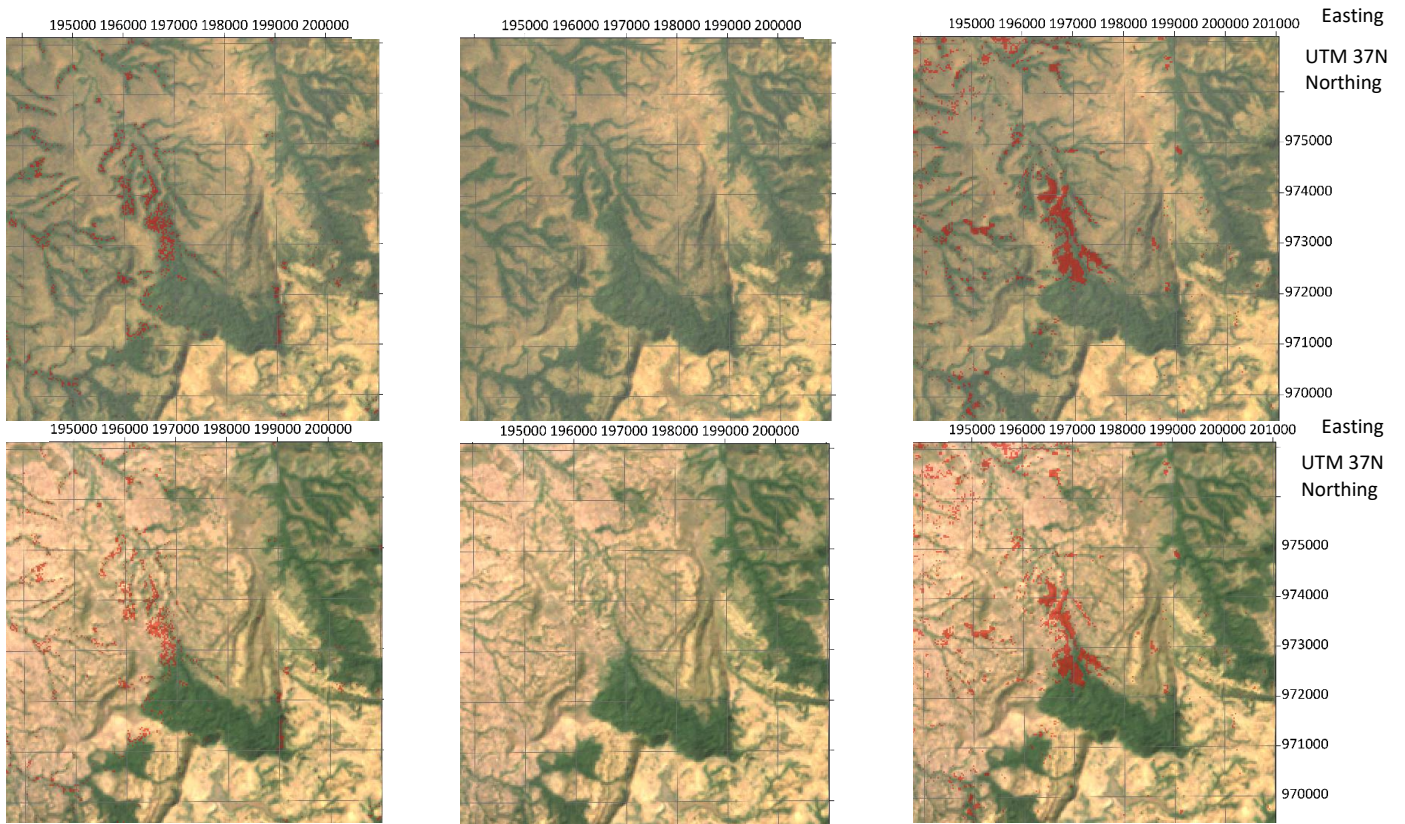


Figure 10-25 Area 18 forest loss: From left to right: Calculated forest loss areas in red overlaid on the composite 1995-2000 on top and on the composite 2015-2020 on the bottom, Landsat imagery composite 1995-2000 on top and composite 2015-2020 on the bottom, Hansen forest loss in red overlaid on the composite 1995-2000 on top and on the composite 2015-2020 on the bottom (Google Earth Engine 2020)

Area 5 forest gain

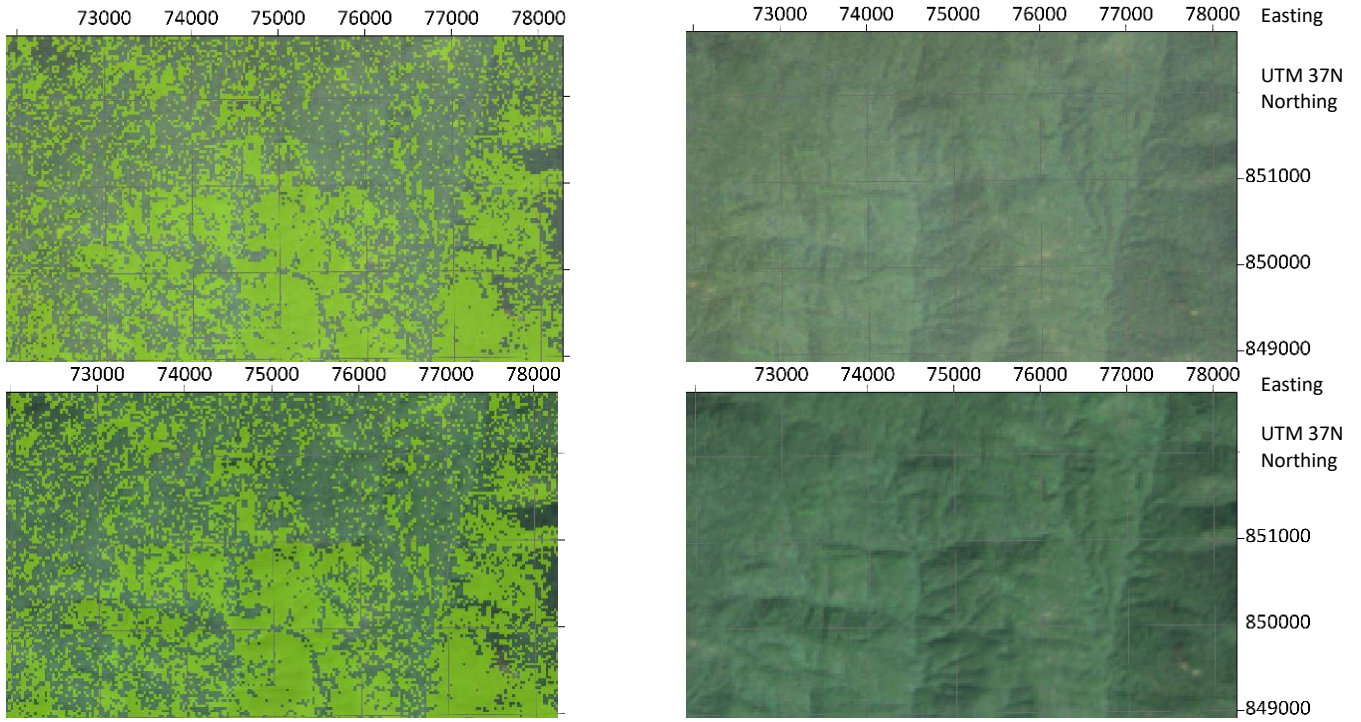


Figure 10-26 Area 5 forest gain: From left to right: Calculated forest loss areas in red overlaid on the composite 1995-2000 on top and on the composite 2015-2020 on the bottom, Landsat imagery composite 1995-2000 on top and composite 2015-2020 on the bottom, Hansen forest loss in red overlaid on the composite 1995-2000 on top and on the composite 2015-2020 on the bottom (Google Earth Engine 2020)

Area 6 forest gain

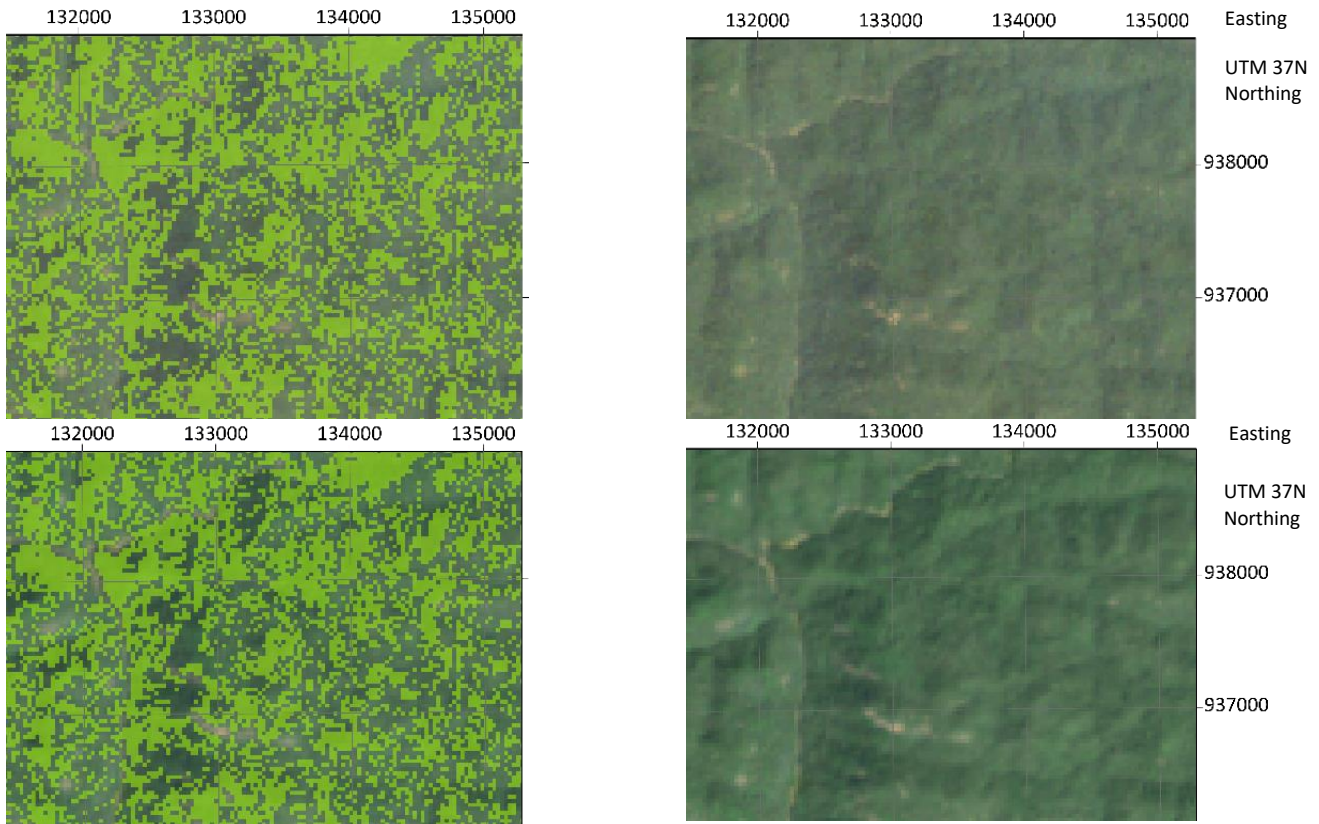


Figure 10-27 Area 6 forest gain: From left to right: Calculated forest loss areas in red overlaid on the composite 1995-2000 on top and on the composite 2015-2020 on the bottom, Landsat imagery composite 1995-2000 on top and composite 2015-2020 on the bottom, Hansen forest loss in red overlaid on the composite 1995-2000 on top and on the composite 2015-2020 on the bottom (Google Earth Engine 2020)

10.4.4 Bench Maji zone

Overview of the forest loss and forest gain validation areas

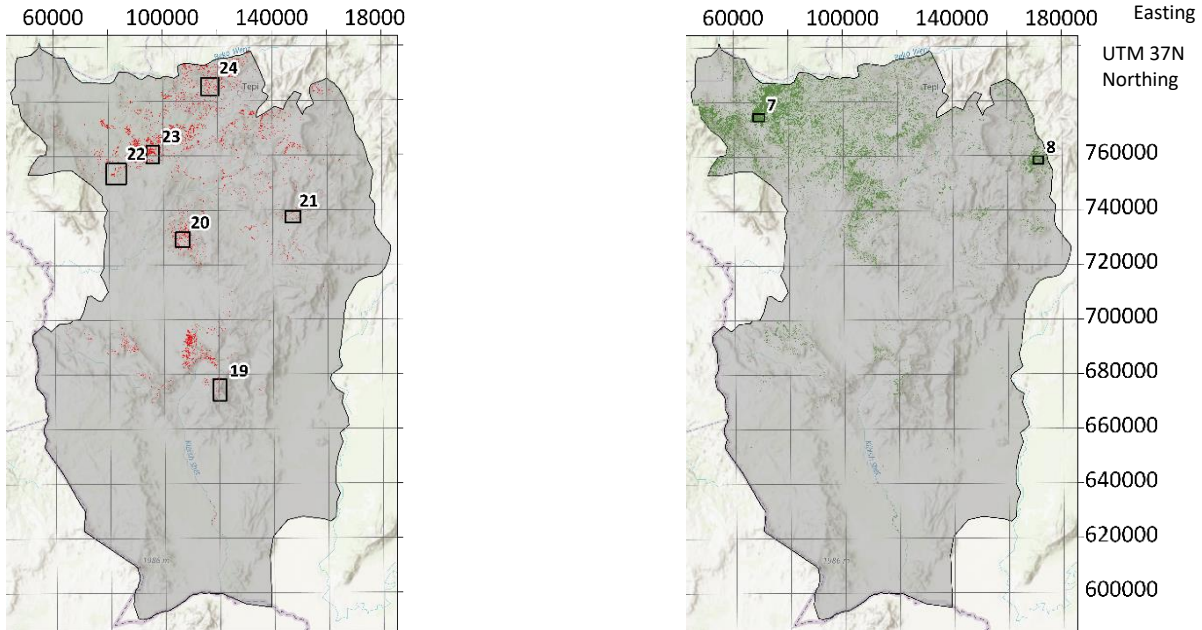


Figure 10-28 Left: Map of Bench Maji emphasizing the forest loss areas in red and the validation areas are framed with their corresponding number, Right: Map of Bench Maji emphasizing the forest gain areas in green and the validation areas are framed with their corresponding number

Area 19 forest loss

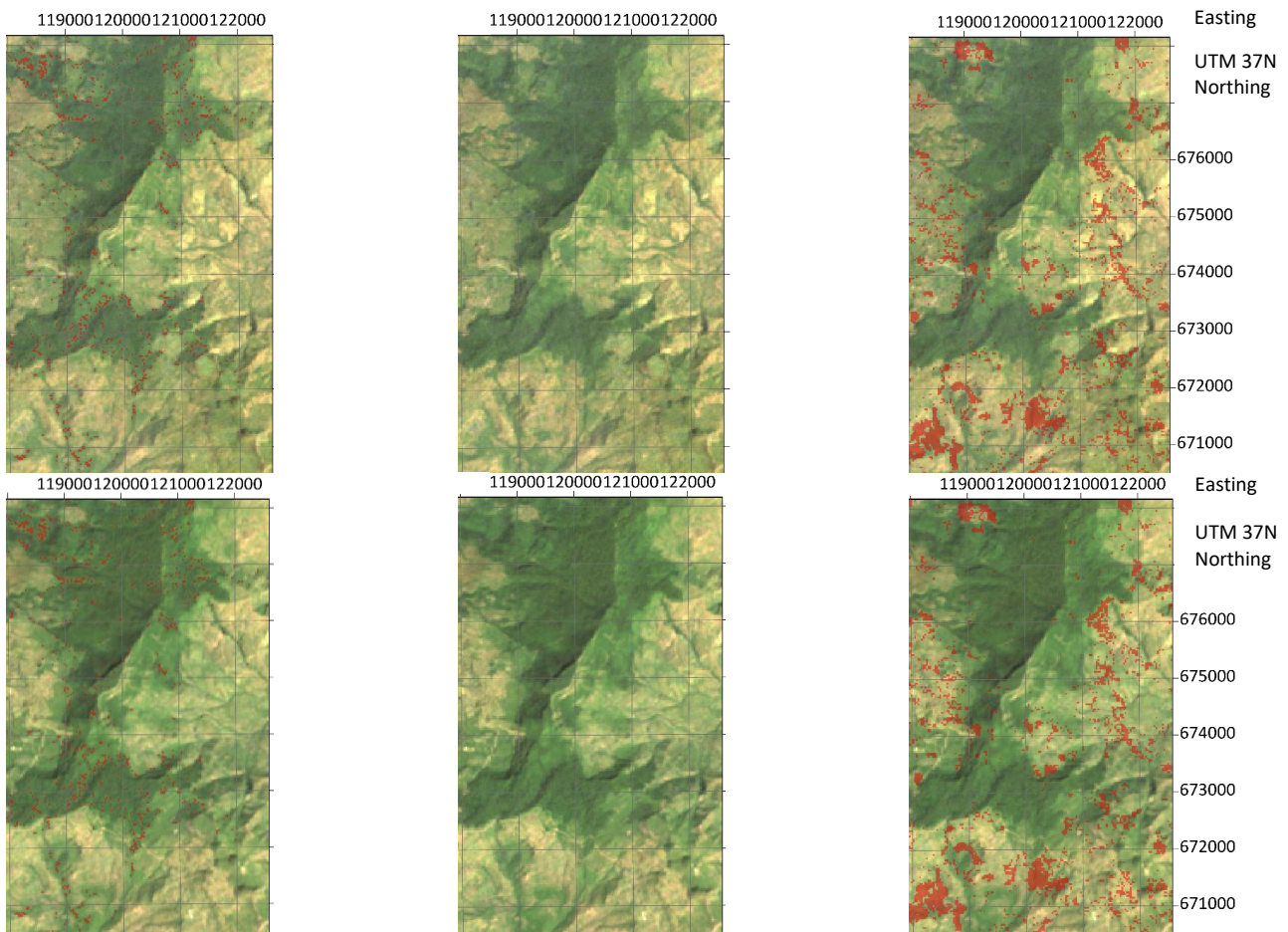


Figure 10-29 Area 19 forest loss: From left to right: Calculated forest loss areas in red overlaid on the composite 1995-2000 on top and on the composite 2015-2020 on the bottom, Landsat imagery composite 1995-2000 on top and composite 2015-2020 on the bottom, Hansen forest loss in red overlaid on the composite 1995-2000 on top and on the composite 2015-2020 on the bottom (Google Earth Engine 2020)

Area 20 forest loss

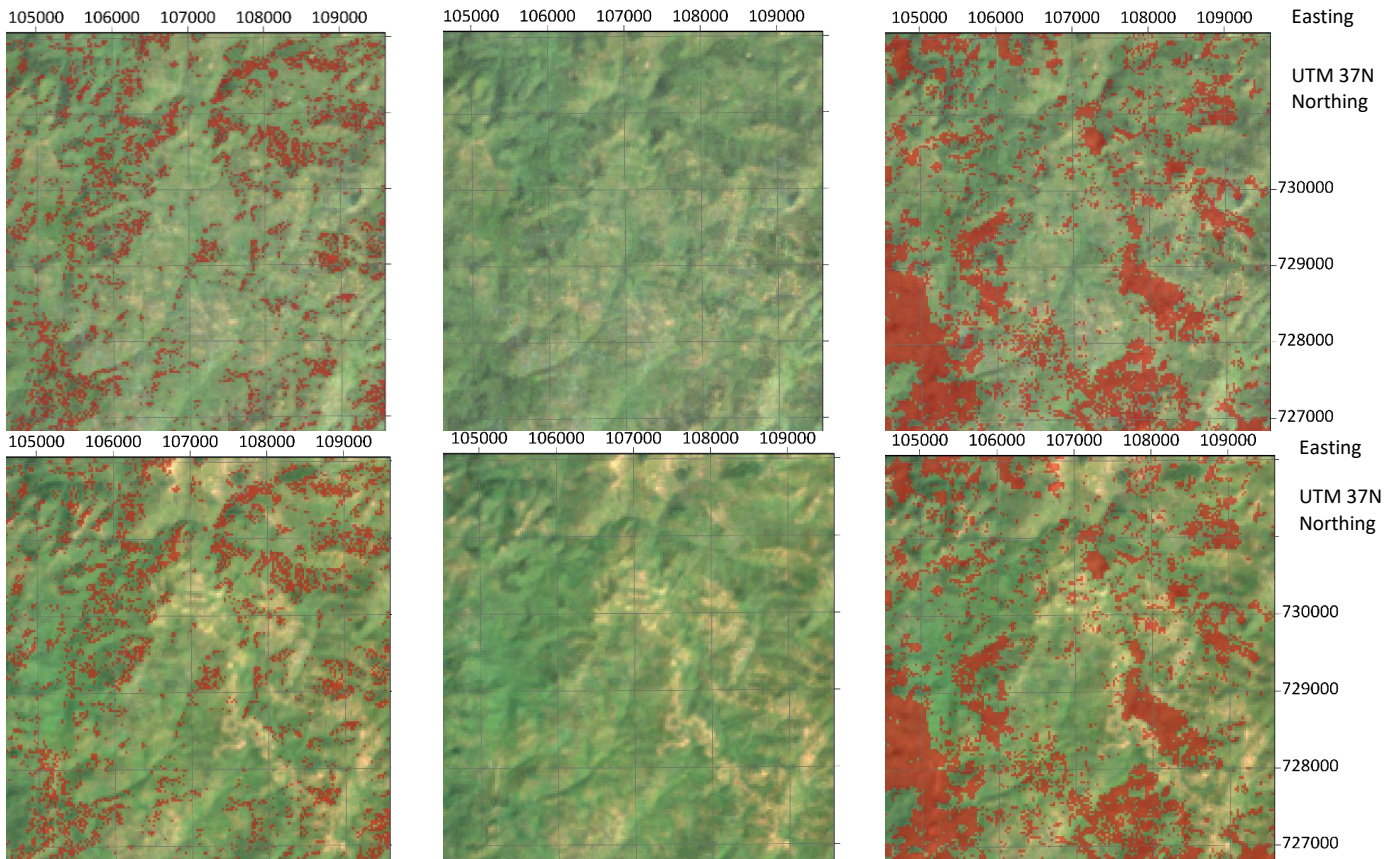


Figure 10-30 Area 20 forest loss: From left to right: Calculated forest loss areas in red overlaid on the composite 1995-2000 on top and on the composite 2015-2020 on the bottom, Landsat imagery composite 1995-2000 on top and composite 2015-2020 on the bottom, Hansen forest loss in red overlaid on the composite 1995-2000 on top and on the composite 2015-2020 on the bottom (Google Earth Engine 2020)

Area 21 forest loss

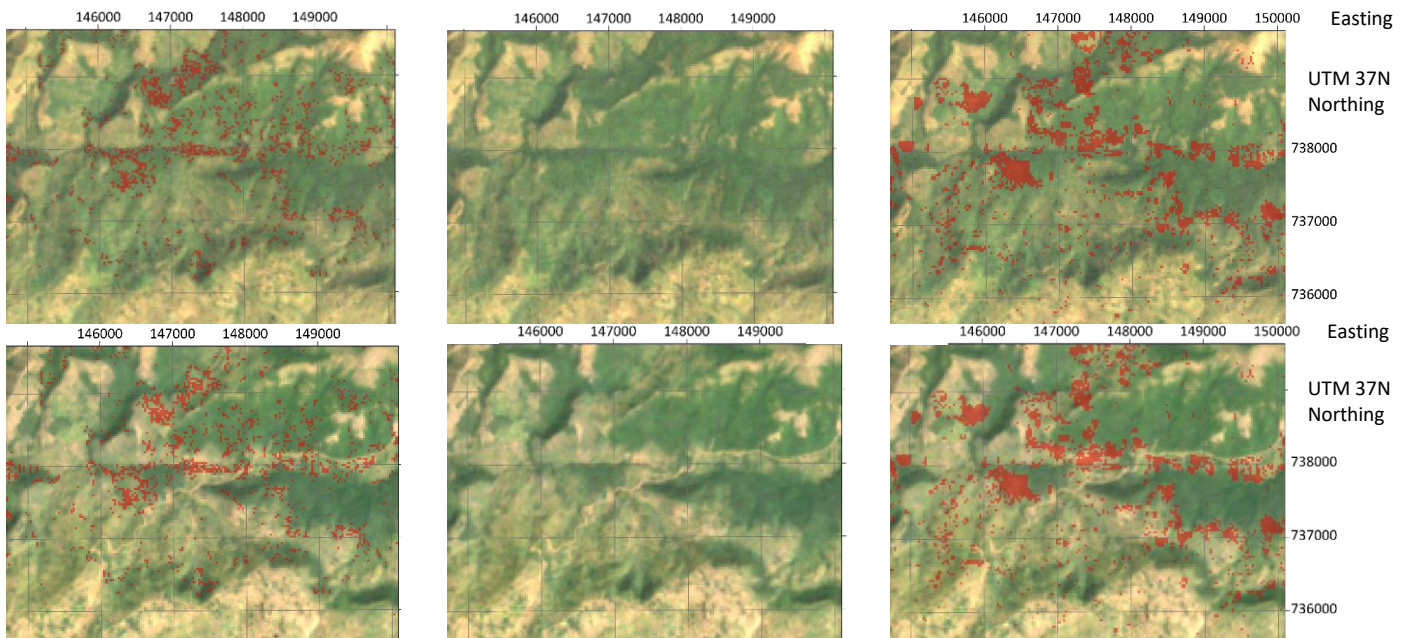


Figure 10-31 Area 21 forest loss: From left to right: Calculated forest loss areas in red overlaid on the composite 1995-2000 on top and on the composite 2015-2020 on the bottom, Landsat imagery composite 1995-2000 on top and composite 2015-2020 on the bottom, Hansen forest loss in red overlaid on the composite 1995-2000 on top and on the composite 2015-2020 on the bottom (Google Earth Engine 2020)

Area 22 forest loss

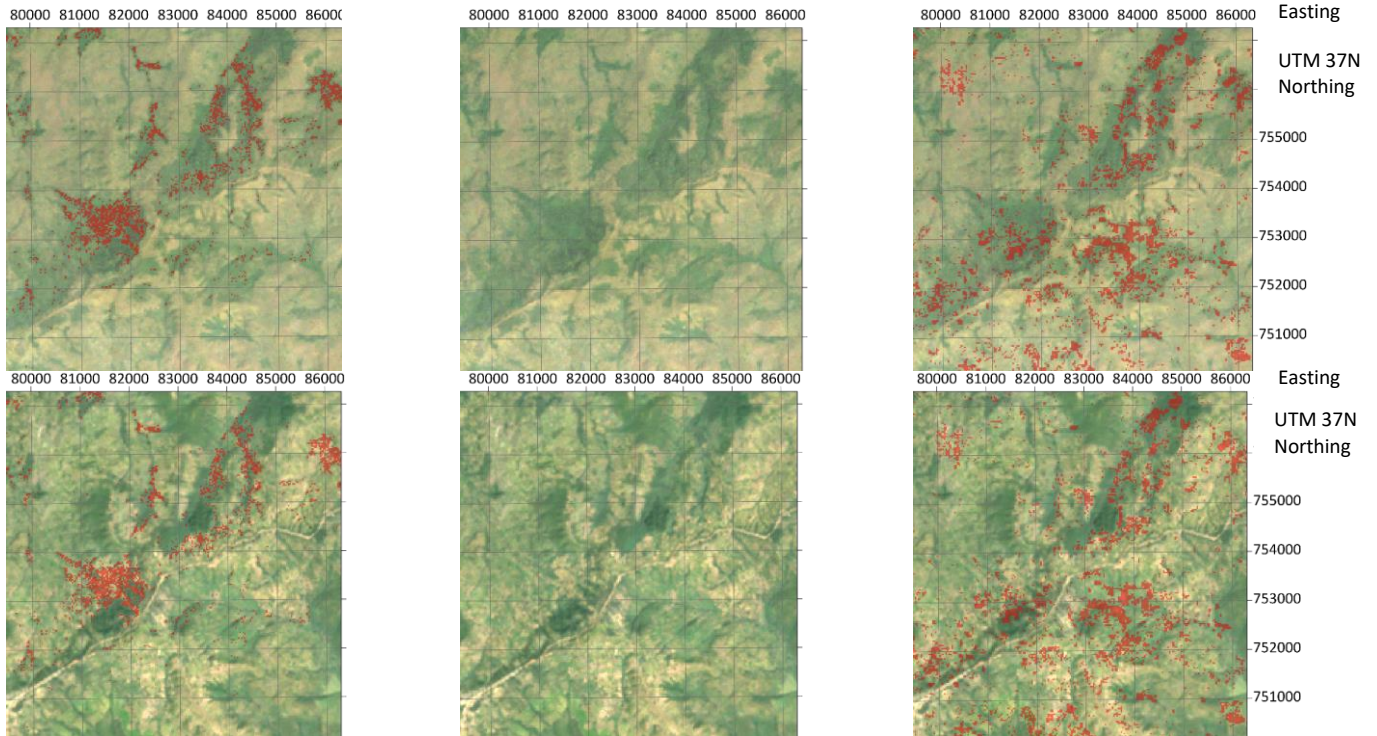


Figure 10-32 Area 22 forest loss: From left to right: Calculated forest loss areas in red overlaid on the composite 1995-2000 on top and on the composite 2015-2020 on the bottom, Landsat imagery composite 1995-2000 on top and composite 2015-2020 on the bottom, Hansen forest loss in red overlaid on the composite 1995-2000 on top and on the composite 2015-2020 on the bottom (Google Earth Engine 2020)

Area 23 forest loss

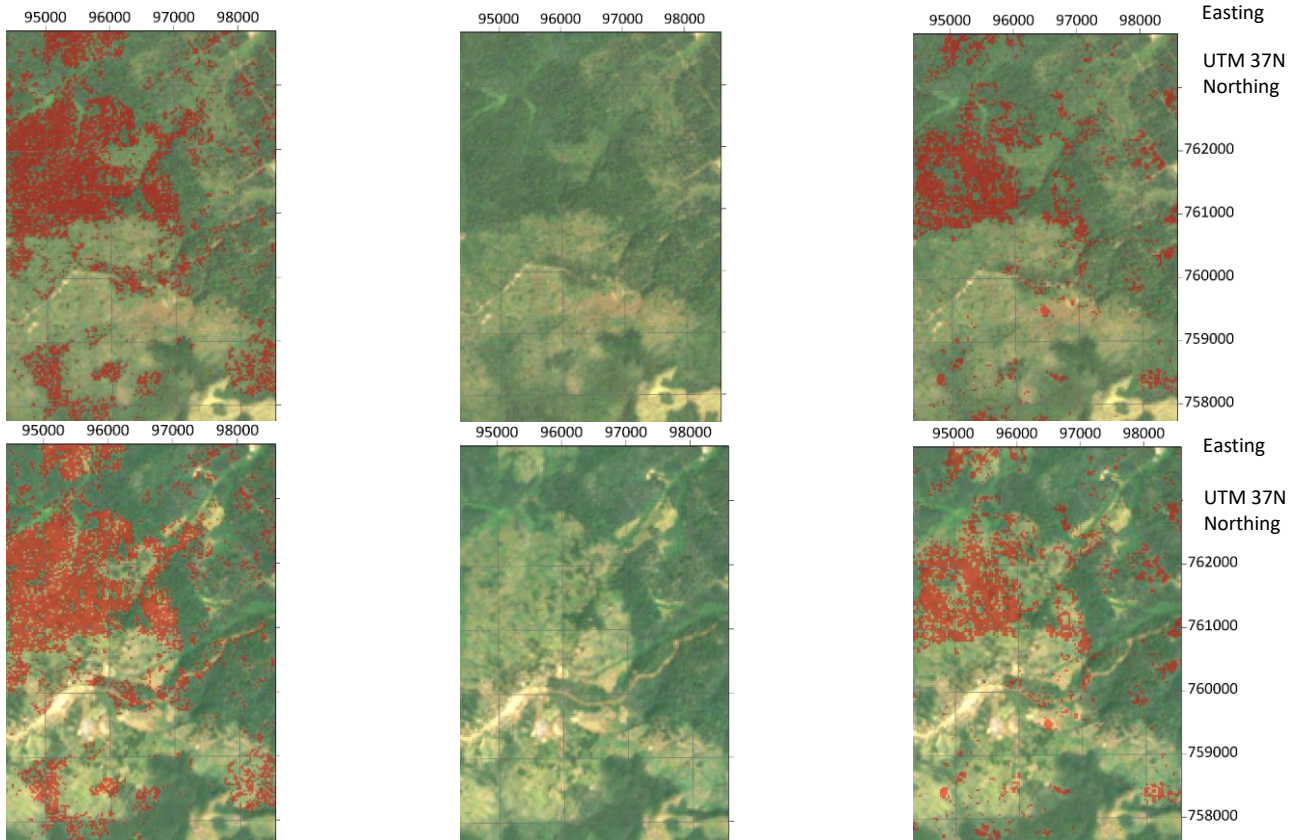


Figure 10-33 Area 23 forest loss: From left to right: Calculated forest loss areas in red overlaid on the composite 1995-2000 on top and on the composite 2015-2020 on the bottom, Landsat imagery composite 1995-2000 on top and composite 2015-2020 on the bottom, Hansen forest loss in red overlaid on the composite 1995-2000 on top and on the composite 2015-2020 on the bottom (Google Earth Engine 2020)

Area 24 forest loss

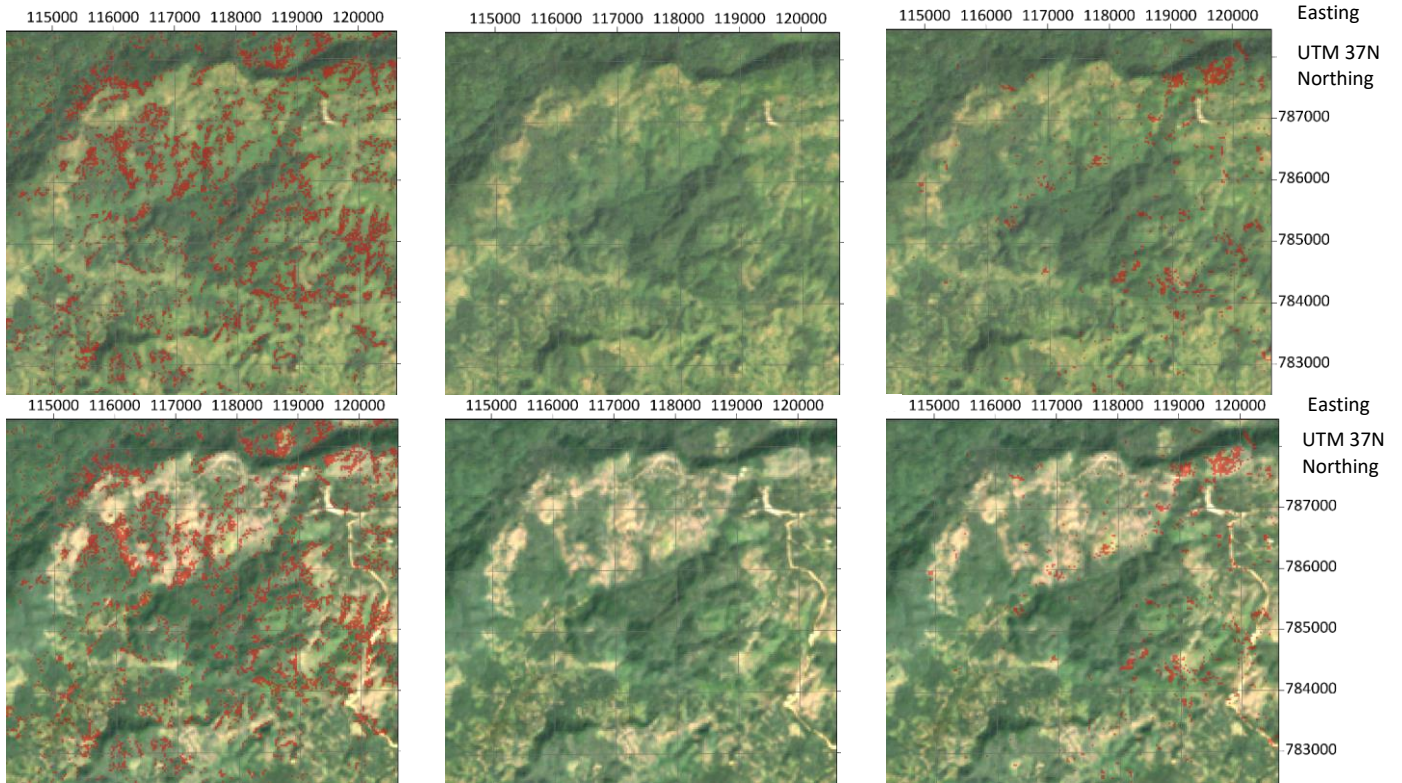


Figure 10-34 Area 24 forest loss: From left to right: Calculated forest loss areas in red overlaid on the composite 1995-2000 on top and on the composite 2015-2020 on the bottom, Landsat imagery composite 1995-2000 on top and composite 2015-2020 on the bottom, Hansen forest loss in red overlaid on the composite 1995-2000 on top and on the composite 2015-2020 on the bottom (Google Earth Engine 2020)

Area 7 forest gain

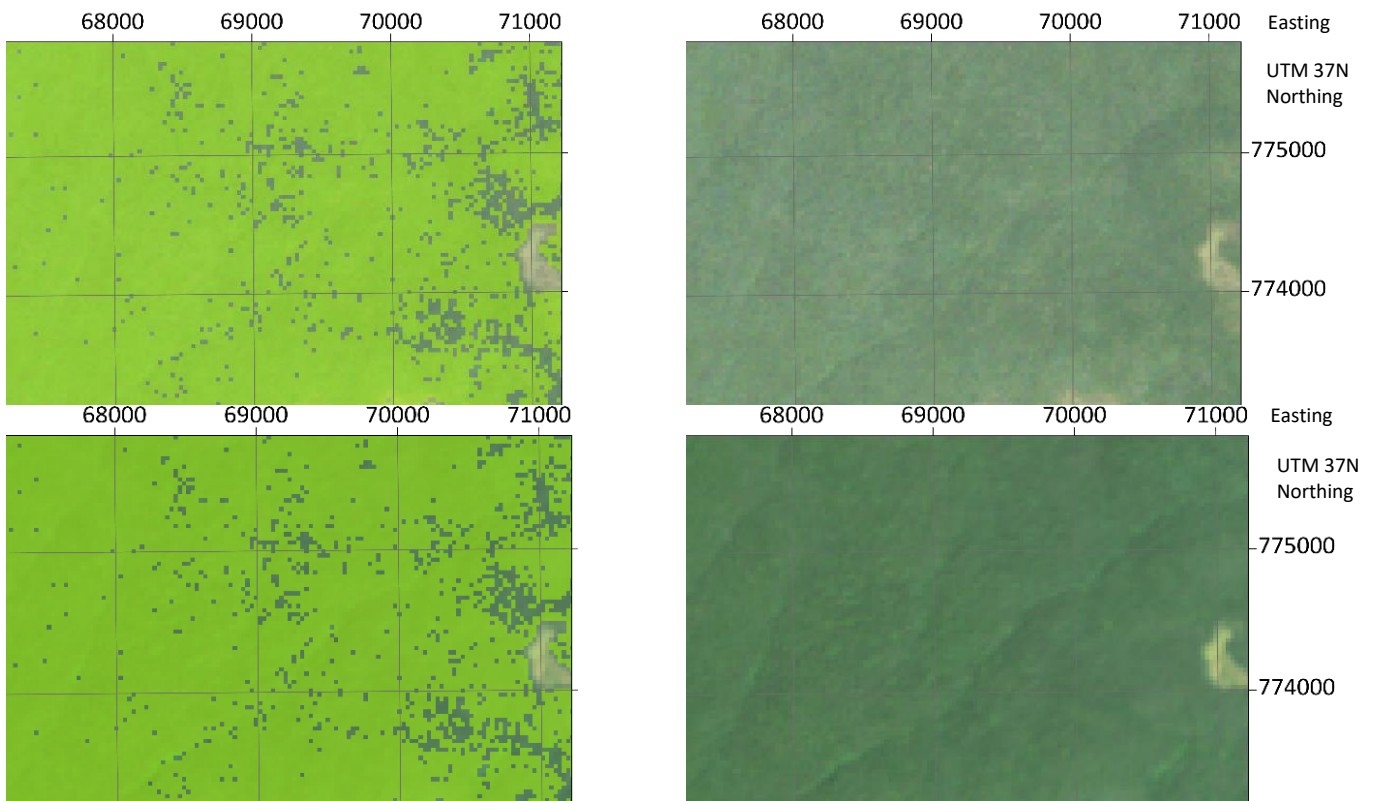


Figure 10-35 Area 7 forest gain: From left to right: Calculated forest gain areas in green overlaid on the composite 1995-2000 on top and on the composite 2015-2020 on the bottom, Landsat imagery composite 1995-2000 on top and composite 2015-2020 on the bottom, Hansen forest gain in green overlaid on the composite 1995-2000 on top and on the composite 2015-2020 on the bottom (Google Earth Engine 2020)

Area 8 forest gain

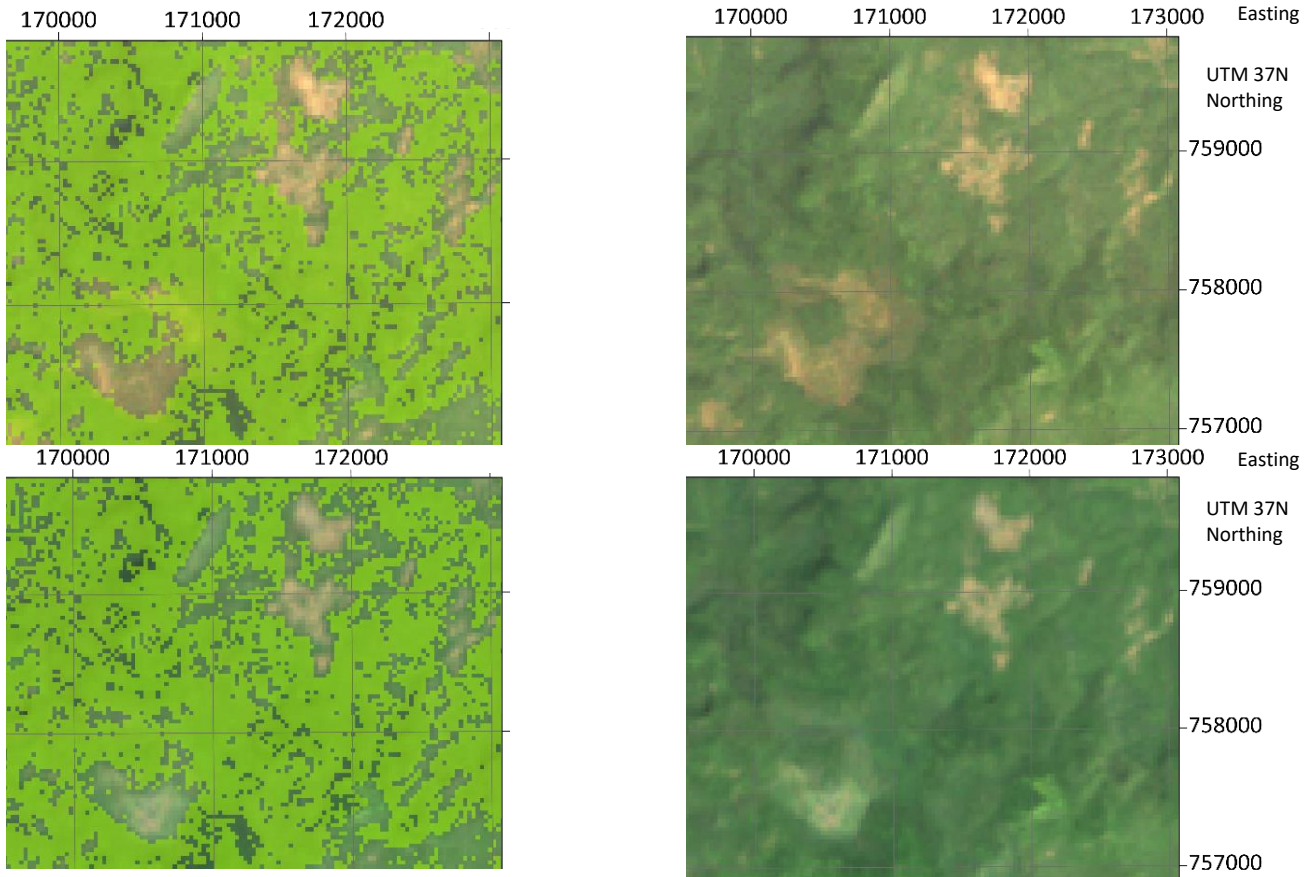


Figure 10-36 Area 8 forest gain: From left to right: Calculated forest loss areas in red overlaid on the composite 1995-2000 on top and on the composite 2015-2020 on the bottom, Landsat imagery composite 1995-2000 on top and composite 2015-2020 on the bottom, Hansen forest loss in red overlaid on the composite 1995-2000 on top and on the composite 2015-2020 on the bottom (Google Earth Engine 2020)

10.4.5 Bale zone

Overview of the forest gain and forest loss validation areas

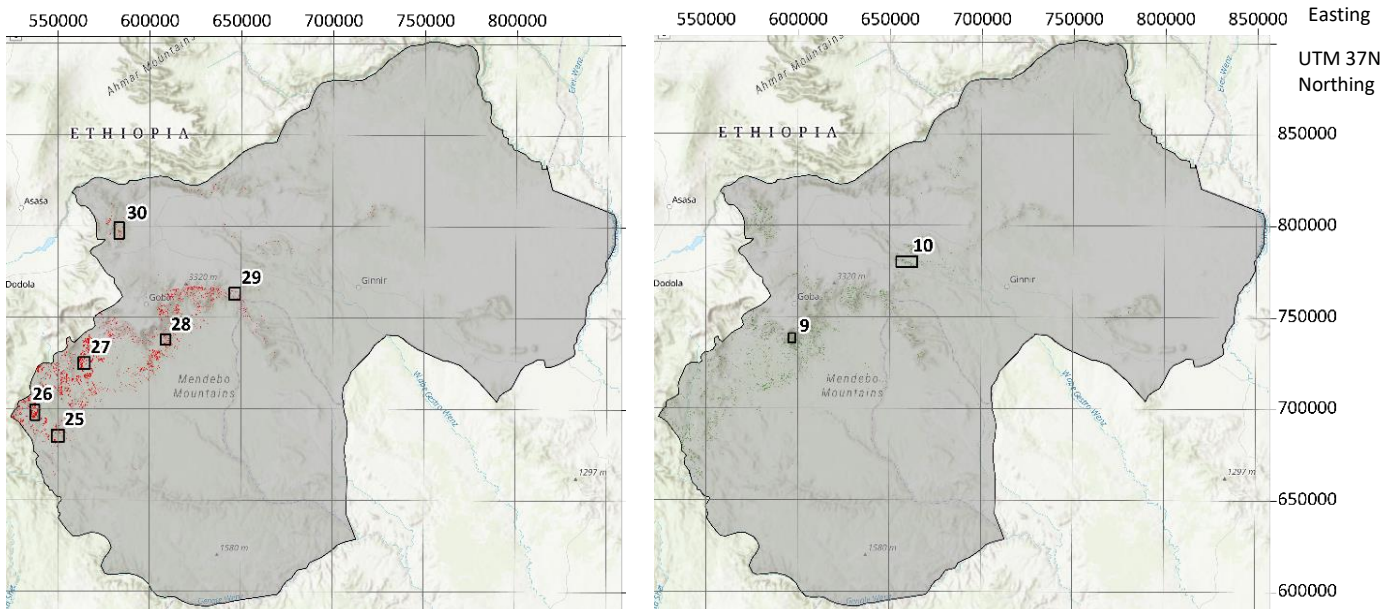


Figure 10-37 Left: Map of Bale emphasizing the forest loss areas in red and the validation areas are framed with their corresponding number, Right: Map of Bale emphasizing the forest gain areas in green and the validation areas are framed with their corresponding number

Area 25 forest loss

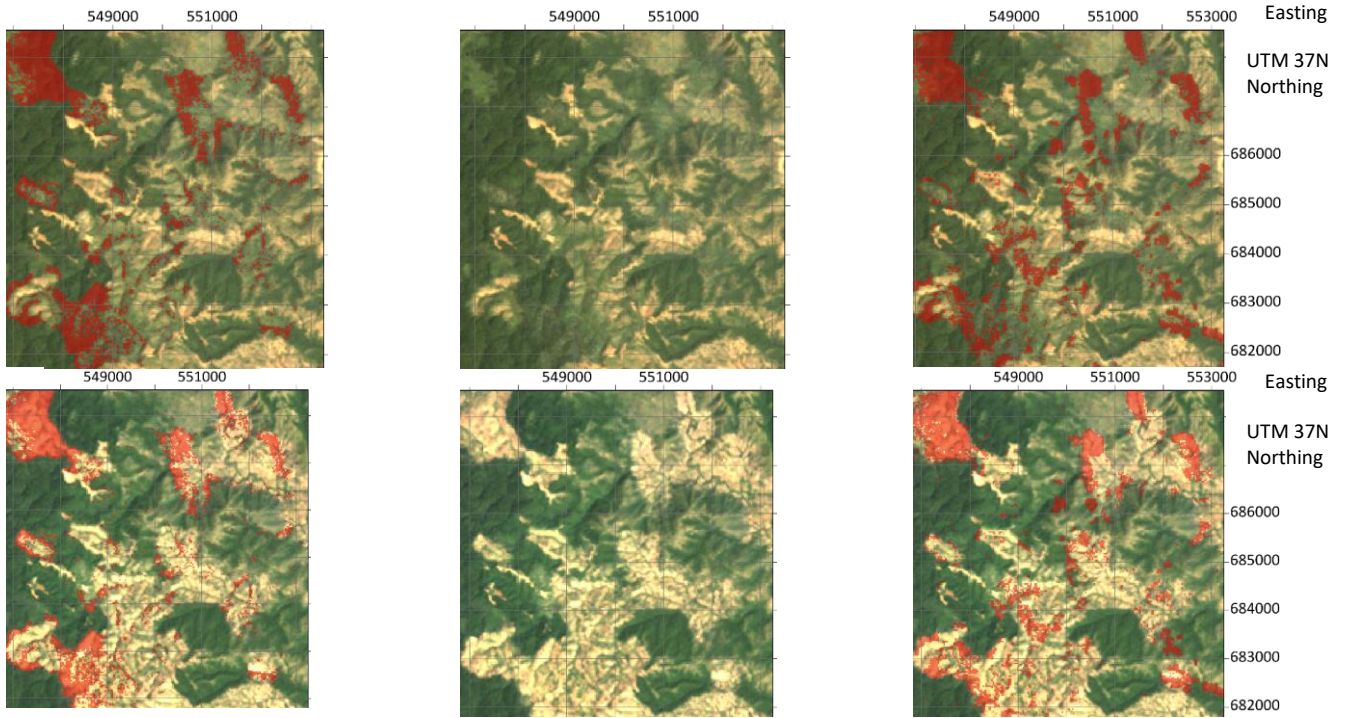


Figure 10-38 Area 25 forest loss: From left to right: Calculated forest loss areas in red overlaid on the composite 1995-2000 on top and on the composite 2015-2020 on the bottom, Landsat imagery composite 1995-2000 on top and composite 2015-2020 on the bottom, Hansen forest loss in red overlaid on the composite 1995-2000 on top and on the composite 2015-2020 on the bottom (Google Earth Engine 2020)

Area 26 forest loss

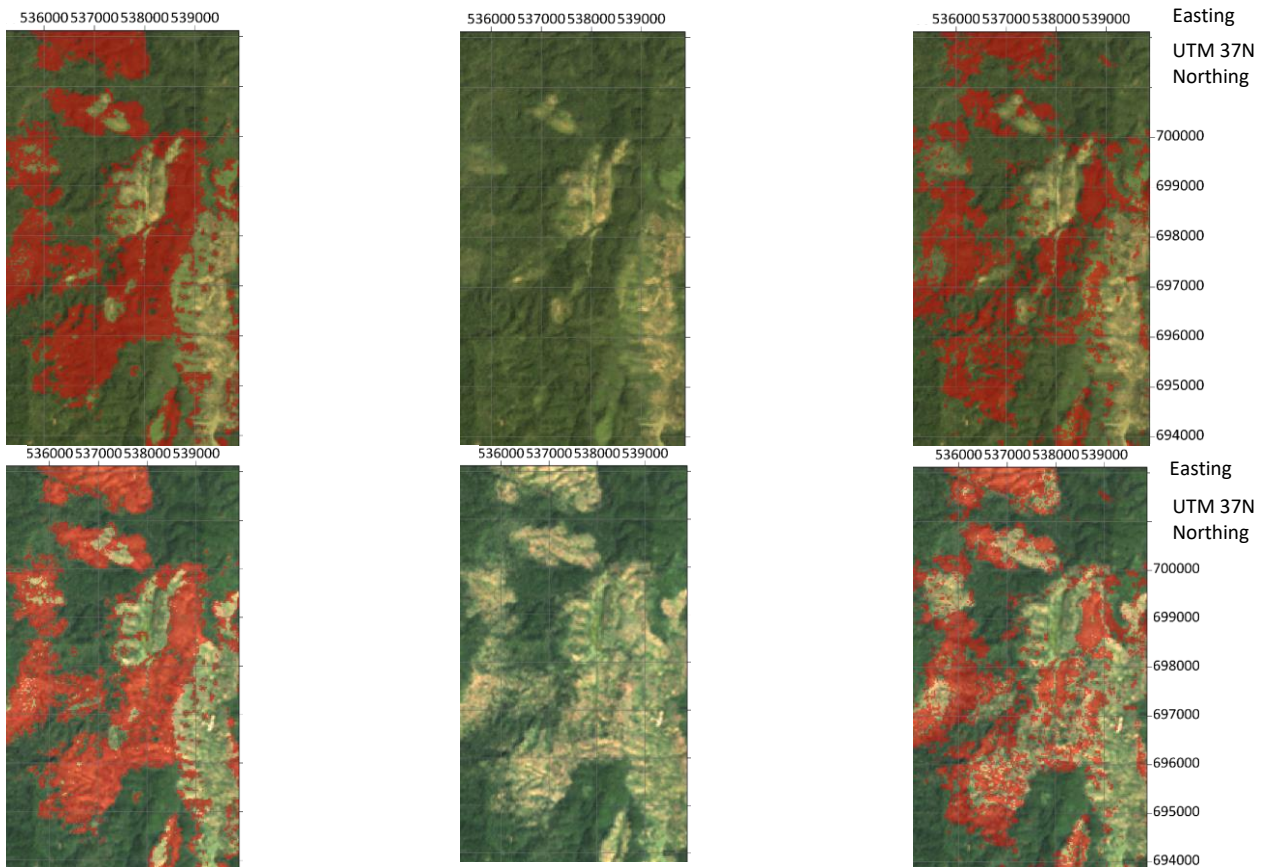


Figure 10-39 Area 26 forest loss: From left to right: Calculated forest loss areas in red overlaid on the composite 1995-2000 on top and on the composite 2015-2020 on the bottom, Landsat imagery composite 1995-2000 on top and composite 2015-2020 on the bottom, Hansen forest loss in red overlaid on the composite 1995-2000 on top and on the composite 2015-2020 on the bottom (Google Earth Engine 2020)

Area 27 forest loss

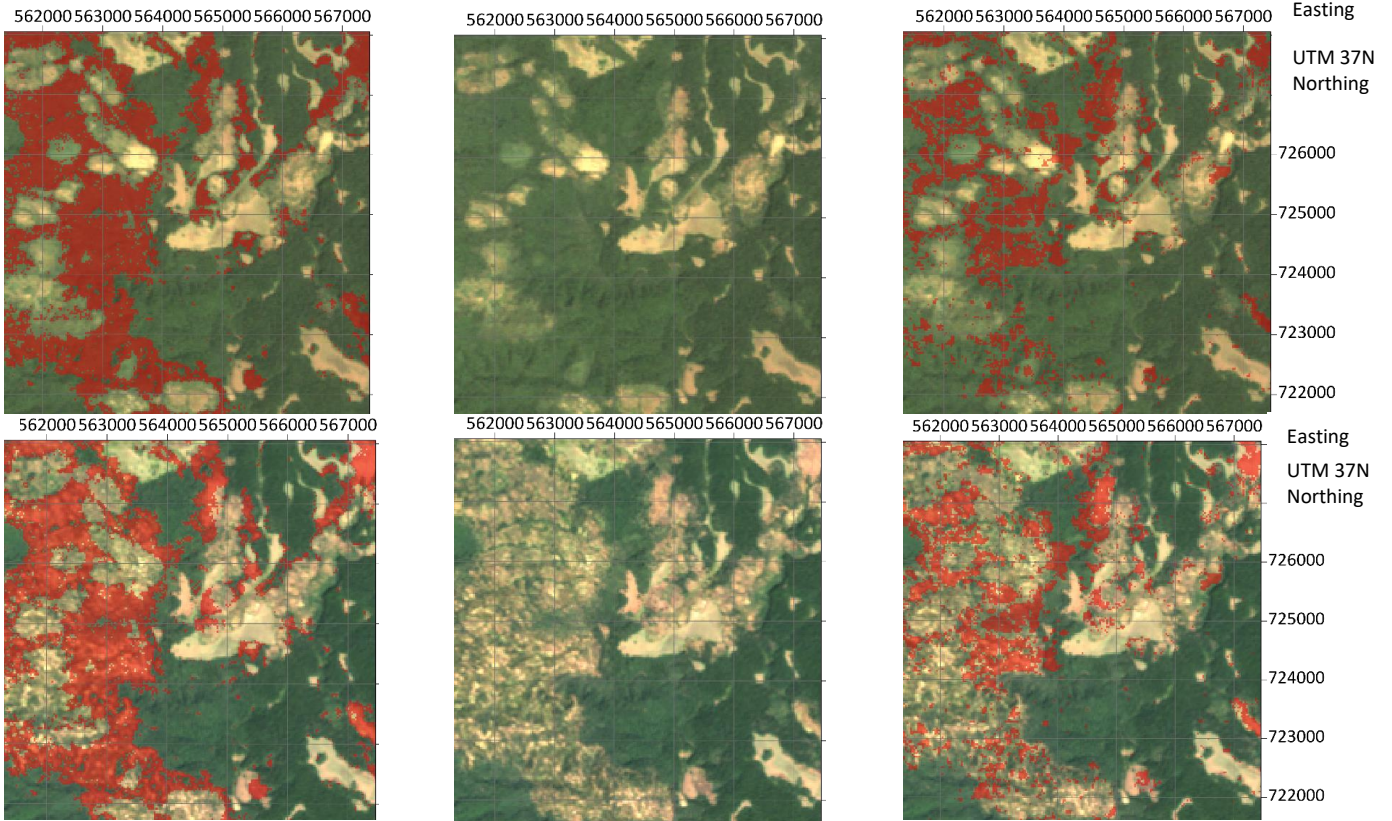


Figure 10-40 Area 27 forest loss: From left to right: Calculated forest loss areas in red overlaid on the composite 1995-2000 on top and on the composite 2015-2020 on the bottom, Landsat imagery composite 1995-2000 on top and composite 2015-2020 on the bottom, Hansen forest loss in red overlaid on the composite 1995-2000 on top and on the composite 2015-2020 on the bottom (Google Earth Engine 2020)

Area 28 forest loss

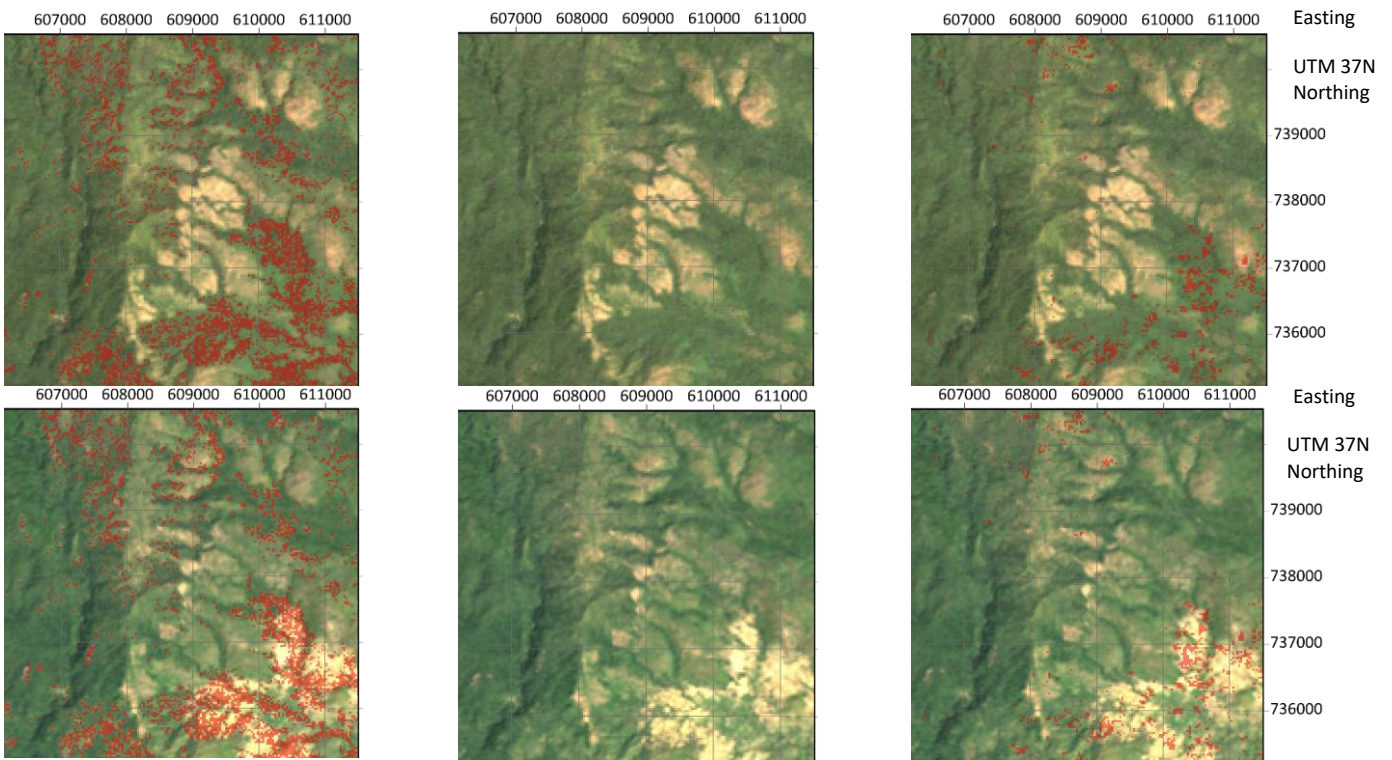


Figure 10-41 Area 28 forest loss: From left to right: Calculated forest loss areas in red overlaid on the composite 1995-2000 on top and on the composite 2015-2020 on the bottom, Landsat imagery composite 1995-2000 on top and composite 2015-2020 on the bottom, Hansen forest loss in red overlaid on the composite 1995-2000 on top and on the composite 2015-2020 on the bottom (Google Earth Engine 2020)

Area 29 forest loss

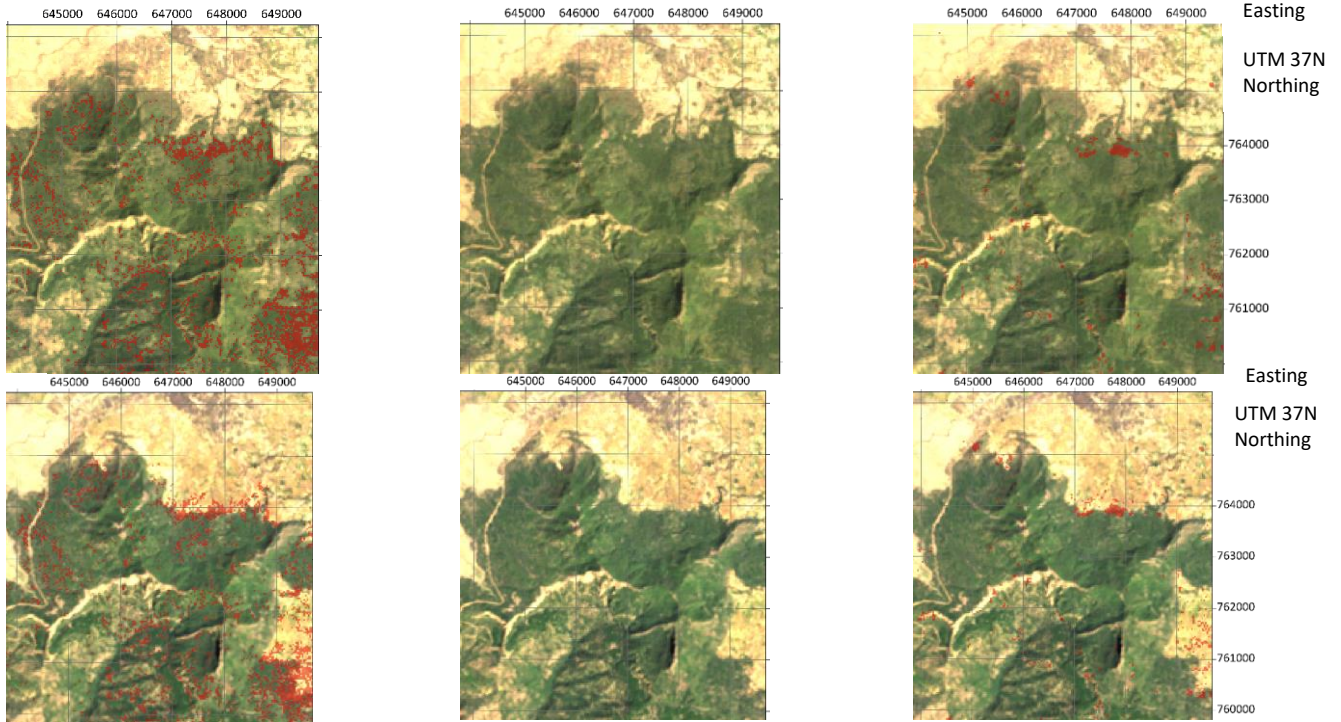


Figure 10-42 Area 29 forest loss: From left to right: Calculated forest loss areas in red overlaid on the composite 1995-2000 on top and on the composite 2015-2020 on the bottom, Landsat imagery composite 1995-2000 on top and composite 2015-2020 on the bottom, Hansen forest loss in red overlaid on the composite 1995-2000 on top and on the composite 2015-2020 on the bottom (Google Earth Engine 2020)

Area 30 forest loss

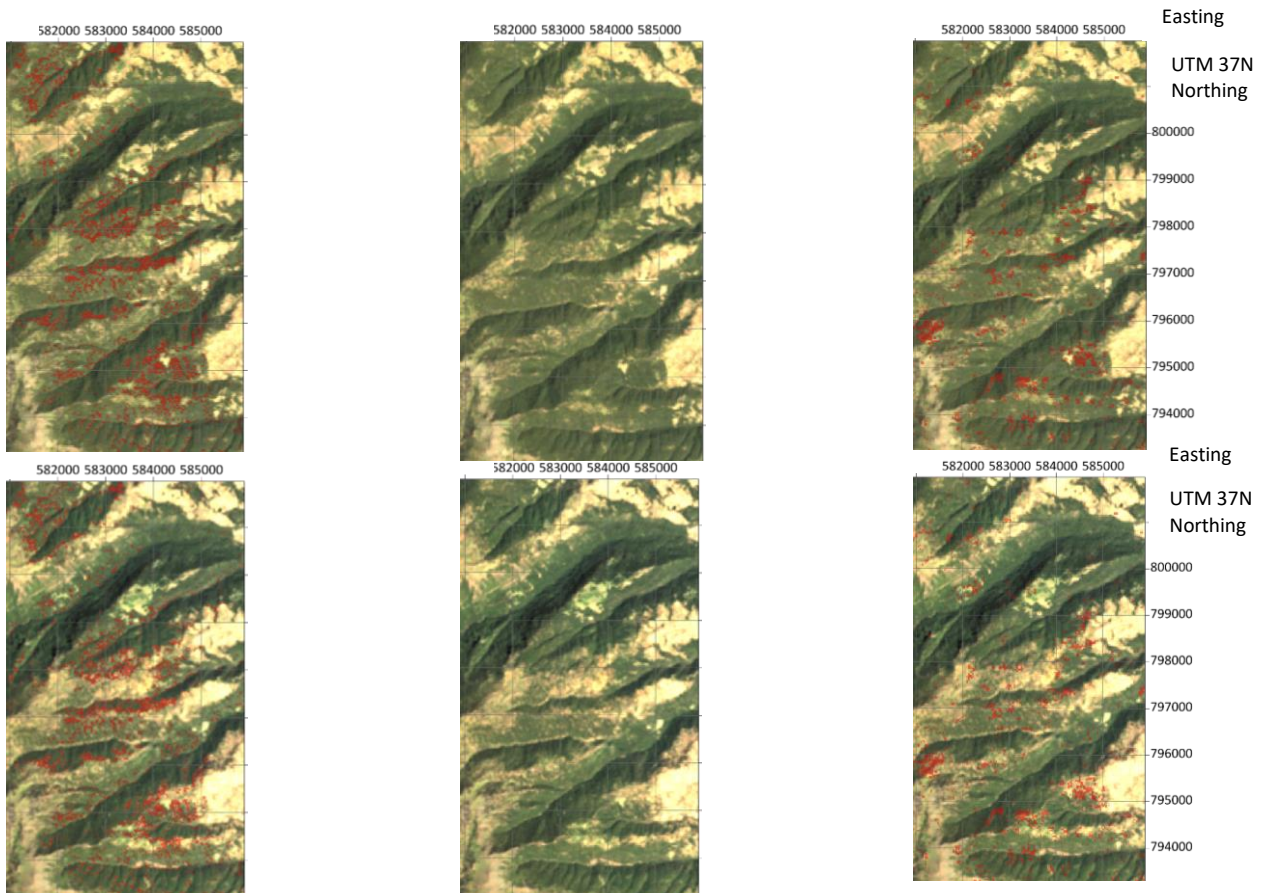


Figure 10-43 Area 30 forest loss: From left to right: Calculated forest loss areas in red overlaid on the composite 1995-2000 on top and on the composite 2015-2020 on the bottom, Landsat imagery composite 1995-2000 on top and composite 2015-2020 on the bottom, Hansen forest loss in red overlaid on the composite 1995-2000 on top and on the composite 2015-2020 on the bottom (Google Earth Engine 2020)

Area 9 forest gain

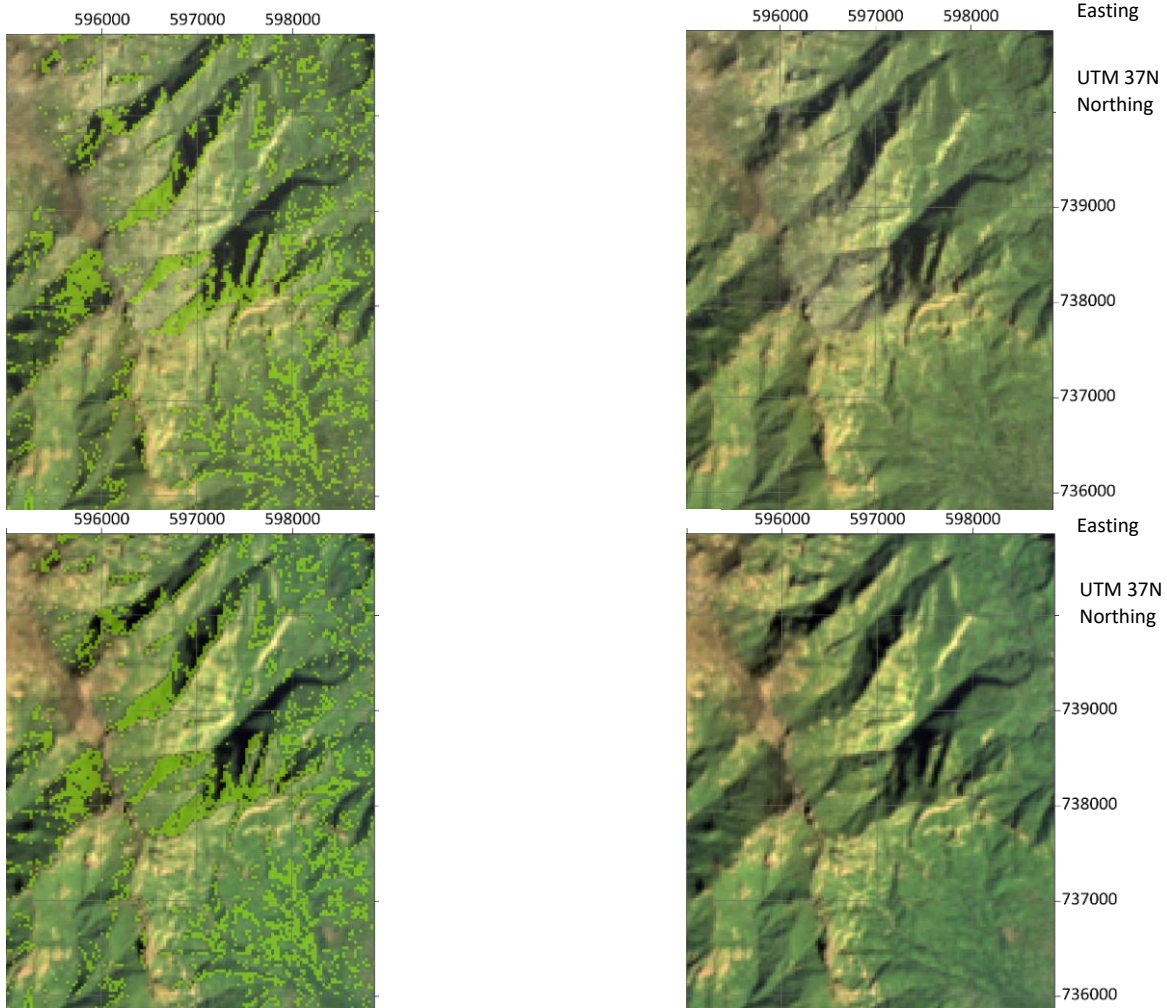


Figure 10-44 Area 9 forest gain: From left to right: Calculated forest loss areas in red overlaid on the composite 1995-2000 on top and on the composite 2015-2020 on the bottom, Landsat imagery composite 1995-2000 on top and composite 2015-2020 on the bottom, Hansen forest loss in red overlaid on the composite 1995-2000 on top and on the composite 2015-2020 on the bottom (Google Earth Engine 2020)

Area 10 forest gain

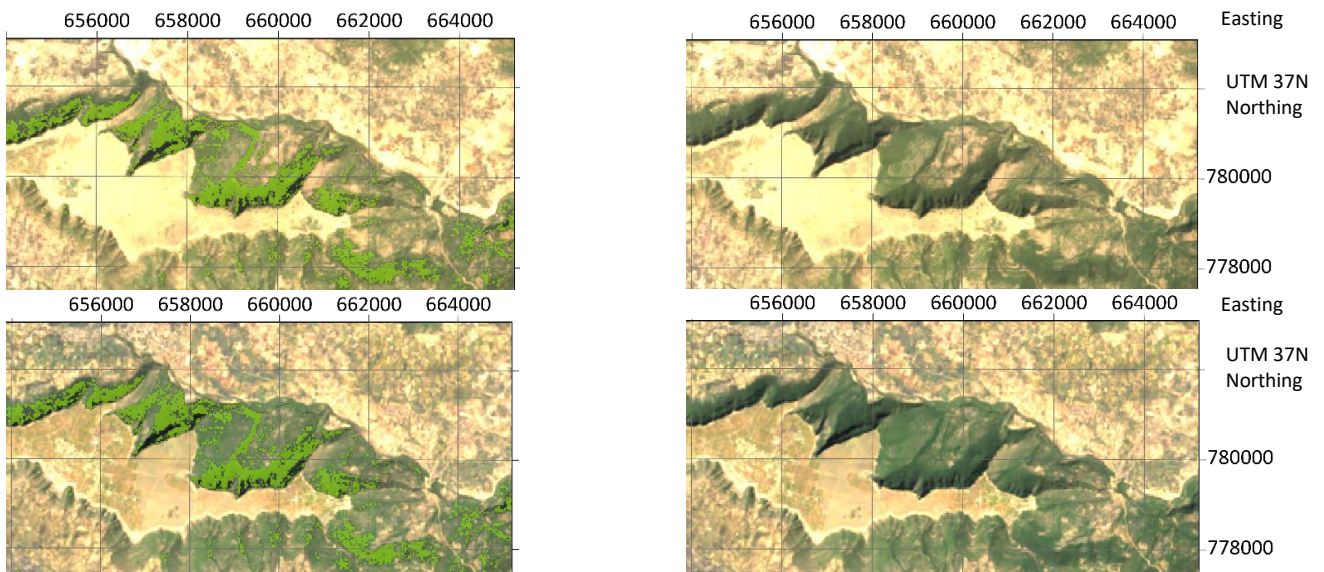


Figure 10-45 Area 10 forest gain: From left to right: Calculated forest loss areas in red overlaid on the composite 1995-2000 on top and on the composite 2015-2020 on the bottom, Landsat imagery composite 1995-2000 on top and composite 2015-2020 on the bottom, Hansen forest loss in red overlaid on the composite 1995-2000 on top and on the composite 2015-2020 on the bottom (Google Earth Engine 2020)

Evaluation of the forest loss and forest gain validation areas

Table 10-5 List depicting the loss validation areas with the zone name, their performance and related to that the explanation. Highlighted with a frame are the areas where the calculated loss performed better than the Hansen forest loss.

Area number and study zone	Performance	Explanation
1- Keffa	the loss calculation works better	it detects the shape and the amount of forest loss, Hansen detects the shape but not enough forest loss area
2- Keffa	both are similar	in shape and forest loss area detection
3- Keffa	the loss calculation works better	Hansen misses some forest loss places
4- Keffa	both are similar	in shape and forest loss area detection
5- Keffa	both are similar	in shape and forest loss area detection
6- Keffa	the loss calculation works better	Hansen detects not all forest loss areas
7- Sheka	the loss calculation works better	Hansen underestimates the forest loss
8- Sheka	the loss calculation works better	Hansen underestimates the forest loss areas but detects the shape correctly
9- Sheka	both are similar	in shape and forest loss area detection
10- Sheka	the loss calculation works better	Hansen underestimates the forest loss areas
11- Sheka	the loss calculation works better	Hansen underestimates the forest loss areas
12- Sheka	both are similar	in shape and forest loss area detection
13- Illubabor	both are similar	in shape and forest loss area detection
14- Illubabor	the loss calculation works better	Hansen underestimates the forest loss areas
15- Illubabor	the loss calculation works better	Hansen underestimates the forest loss areas
16- Illubabor	both are similar	in shape and forest loss area detection
17- Illubabor	the loss calculation works better	Hansen misses some forest loss areas
18- Illubabor	both are similar	in shape and forest loss area detection
19- Bench Maji	unclear	whether there is forest loss or not
20- Bench Maji	unclear	both are almost the same, do not see clear differences between the two datasets
21- Bench Maji	both are similar	in shape and forest loss area detection
22- Bench Maji	Hansen works better	The calculated forest loss detection misses some forest loss places
23- Bench Maji	Hansen works better	too many forest loss places are detected
24- Bench Maji	the loss calculation works better	Hansen misses some forest loss areas
25- Bale	both are similar	in shape and forest loss area detection
26- Bale	both are similar	in shape and forest loss area detection
27- Bale	both are similar	in shape and forest loss area detection
28- Bale	unclear	both do not detect the forest loss areas correctly
29- Bale	unclear	both do not detect the forest loss areas correctly
30- Bale	both are similar	in shape and forest loss area detection

Table 10-6 List depicting the gain validation areas with the zone name, their performance and related to that the explanation. Highlighted with a frame are the two real gain areas

Area number and study zone	Performance	Explanation
1- Keffa	appears to be no real gain	greyish brownish colour on the forest
2- Keffa	appears to be no real gain	greyish brownish colour on the forest
3- Sheka	appears to be no real gain	greyish brownish colour on the forest
4- Sheka	appears to be no real gain	greyish brownish colour on the forest
5- Illubabor	appears to be no real gain	greyish brownish colour on the forest
6- Illubabor	appears to be no real gain	greyish brownish colour on the forest
7- Bench Maji	appears to be no real gain	greyish brownish colour on the forest
8- Bench Maji	seems to be real gain	more forest cover is detected
9- Bale	seems to be real gain	more forest cover is detected
10- Bale	appears to be no real gain	greyish brownish colour on the forest

10.5 Google Earth Engine scripts

Unsupervised Classification

<https://code.earthengine.google.com/b91a3f487169f95ed0eedc60a2d697f1>

Supervised Classification (yearly composites)

<https://code.earthengine.google.com/03fe4011346ff05e6b5e060f7df9fbc1>

5-year dry season composites and change detection

<https://code.earthengine.google.com/9eca94f7fa9550b6df3cd2ab30f46b50>

CODED Calculation

<https://code.earthengine.google.com/4abe2dbdb7e7cc203c065ca5efff1cf1>

CODED Visualization study zones

<https://code.earthengine.google.com/980767e75054cd58e44d193f722d7aa2>

CODED Visualization study kebeles

<https://code.earthengine.google.com/00a4e72b010005213af2acae42be1ca8>

Hansen forest loss

<https://code.earthengine.google.com/2b7d388a81d804336c3c6f9f1d2ab505>

CHIRPS precipitation data

<https://code.earthengine.google.com/ad93fa5c67b04b052f8ef0c892d16cdd>

Sentinel-2 supervised classification

<https://code.earthengine.google.com/0202f858753e0cb40f421de9c485bbb1>

11 Appendix II Results

11.1 Sheka zone

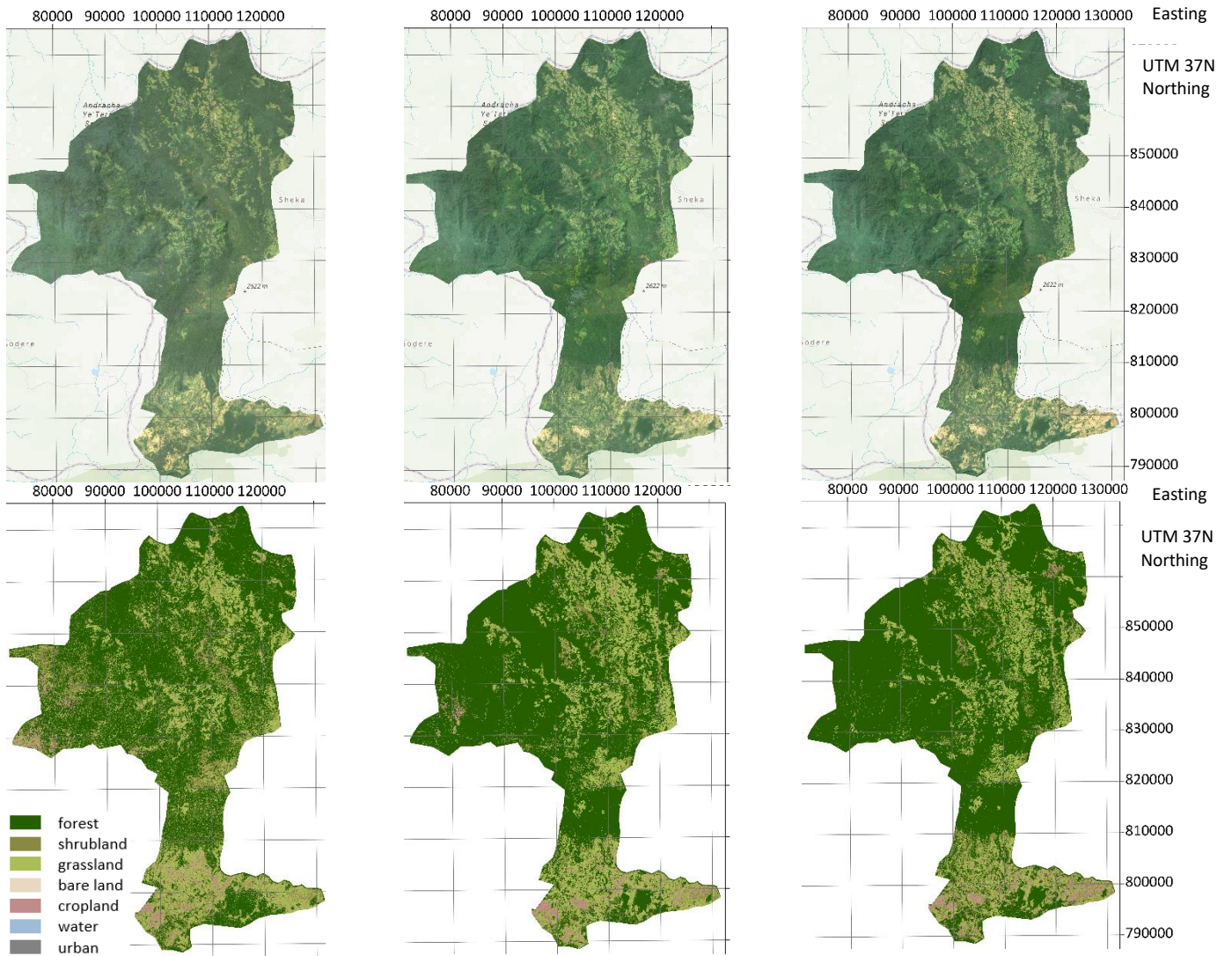


Figure 11-1 Top: Landsat imagery composites 1995-2000, 2010-2015 and 2015-2020 for Sheka zone (Google Earth Engine 2020), Bottom: Classified composites 1995-2000, 2010-2015 and 2015-2020

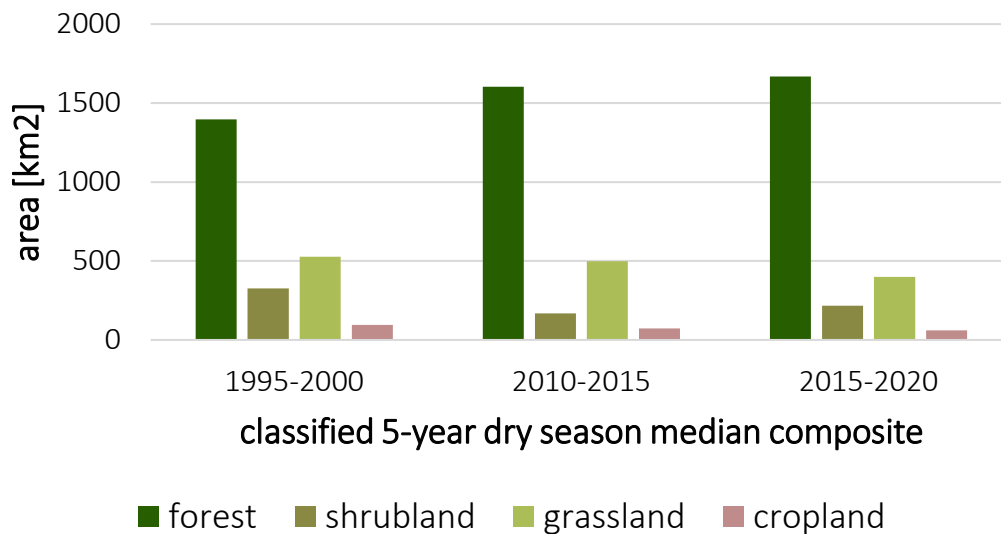


Figure 11-2 Graphic illustrating the areal size of the different land cover classes per classified composite for Sheka zone

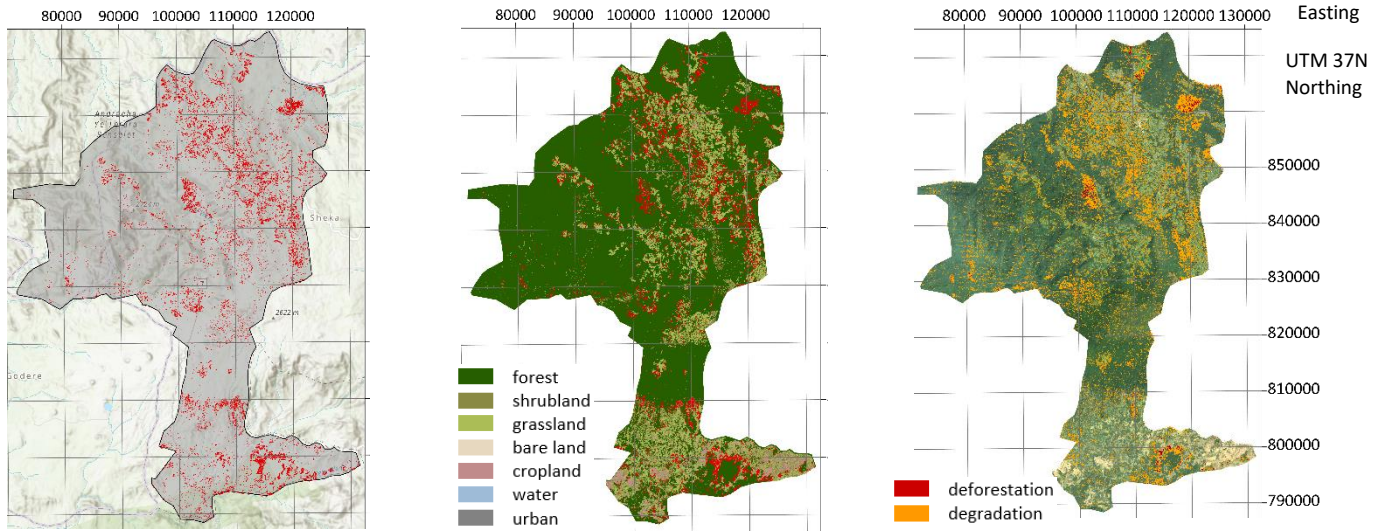


Figure 11-3 From left to right: Calculated forest loss displayed in red for Sheka zone, calculated loss in red overlaid on the classified composite 2015-2020, degradation in orange and deforestation in red calculated with the CODED algorithm overlaid on the Landsat imagery composite 2015-2020

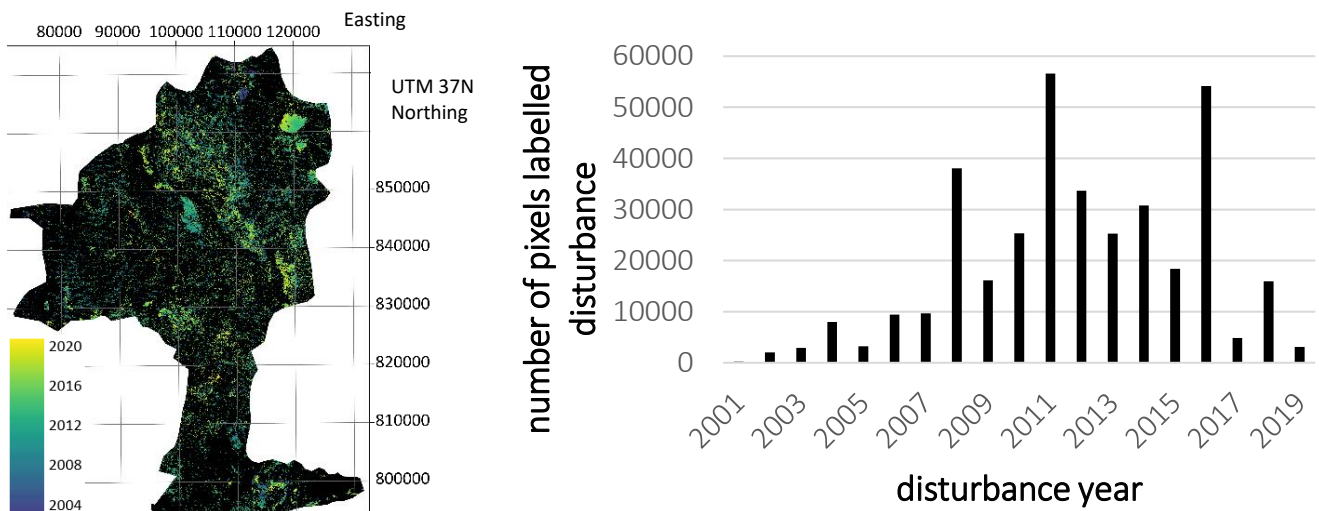


Figure 11-4 Left: Disturbance dates calculated with the CODED algorithm for Sheka zone, Right: Corresponding histogram showing the number of pixels labelled as disturbance for every year during the study period

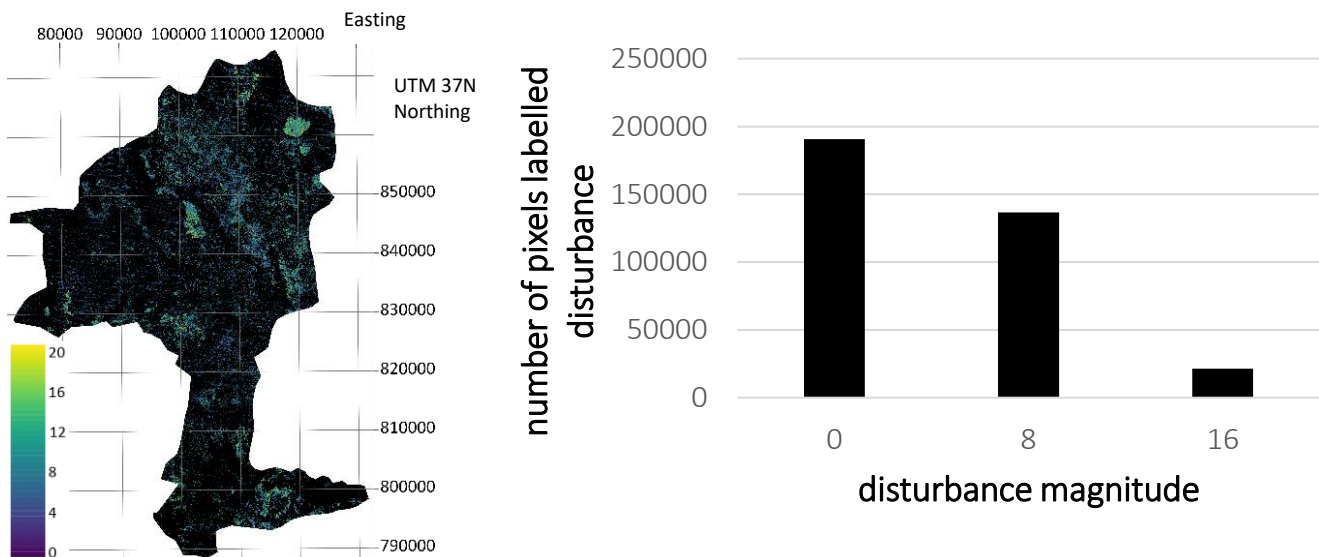


Figure 11-5 Left: Disturbance magnitudes calculated with the CODED algorithm for Sheka zone, Right: Corresponding histogram showing the number of pixels labelled as disturbance for the different magnitudes

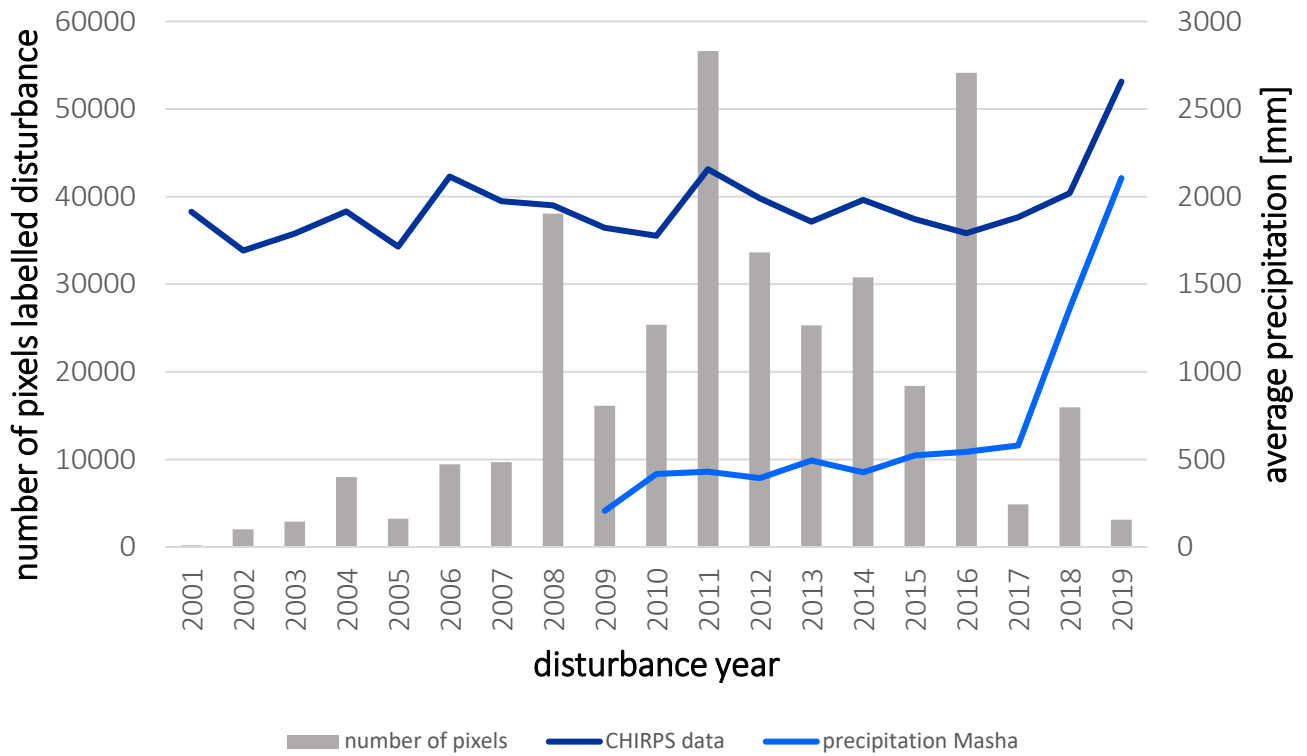


Figure 11-6 Histogram showing the number of pixels labelled as disturbance for every year during the analysis period for Sheka zone, the light blue line demonstrates the precipitation data from world weather for the city of Masha (World Weather Online 2020), the dark blue line refers to the average precipitation extracted from the Chirps data (Google Earth Engine 2020)

11.2 Illubabor zone

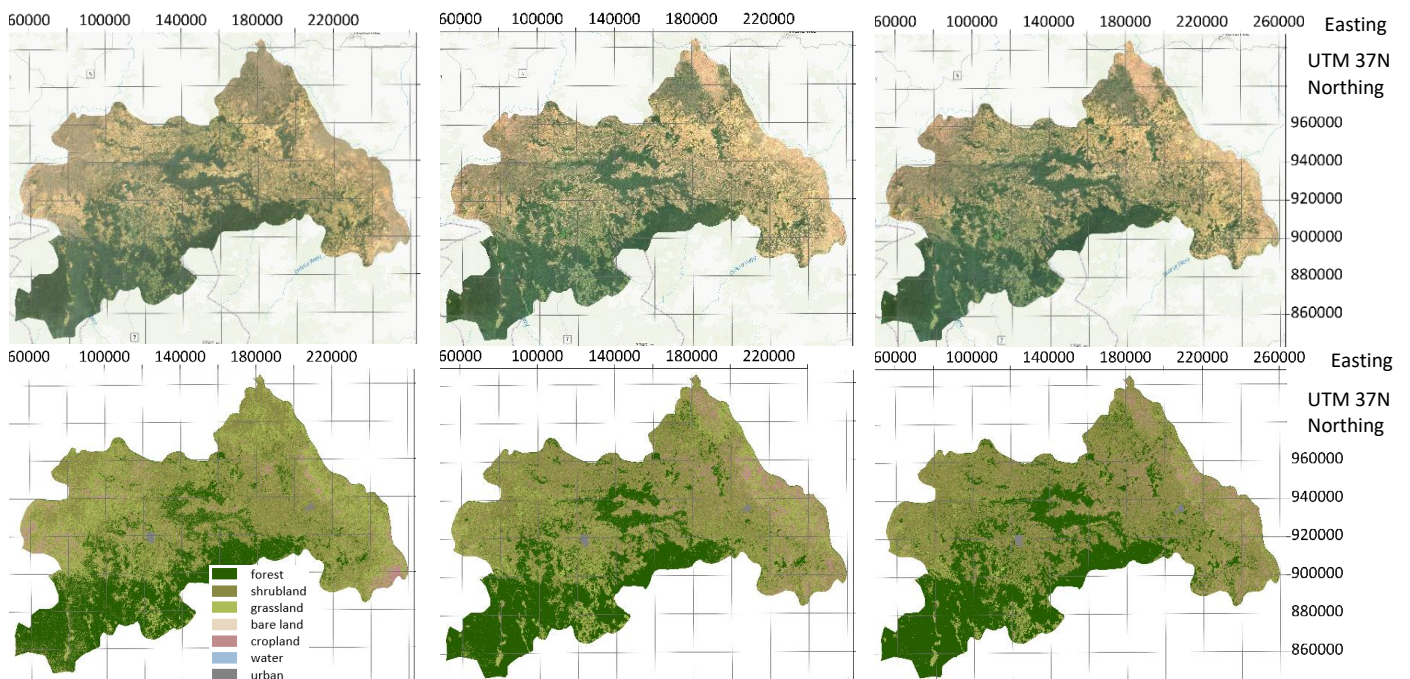


Figure 11-7 Top: Landsat imagery composites 1995-2000, 2010-2015 and 2015-2020 for Illubabor zone (Google Earth Engine 2020), Bottom: Classified composites 1995-2000, 2010-2015 and 2015-2020

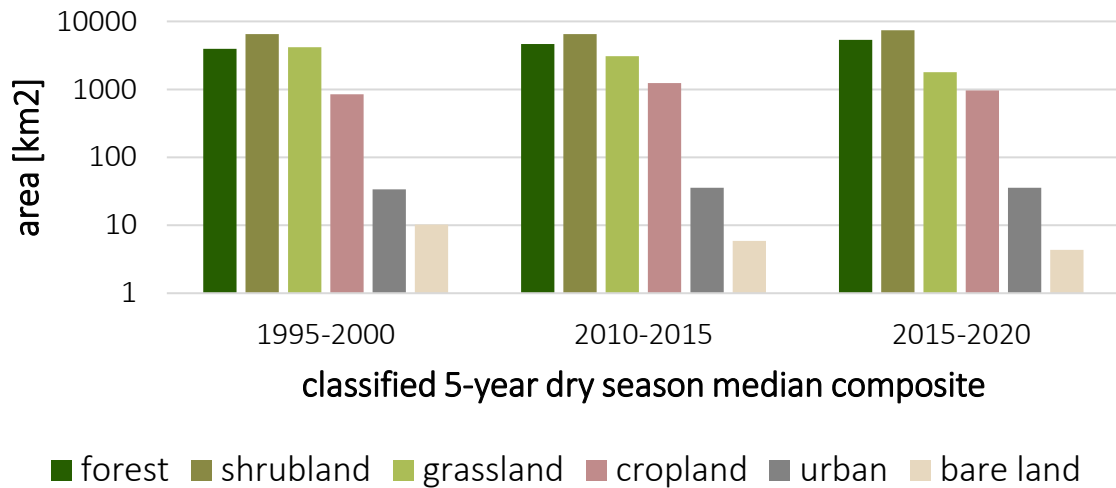


Figure 11-8 Graphic illustrating the areal size of the different land cover classes per classified composite for Illubabor zone

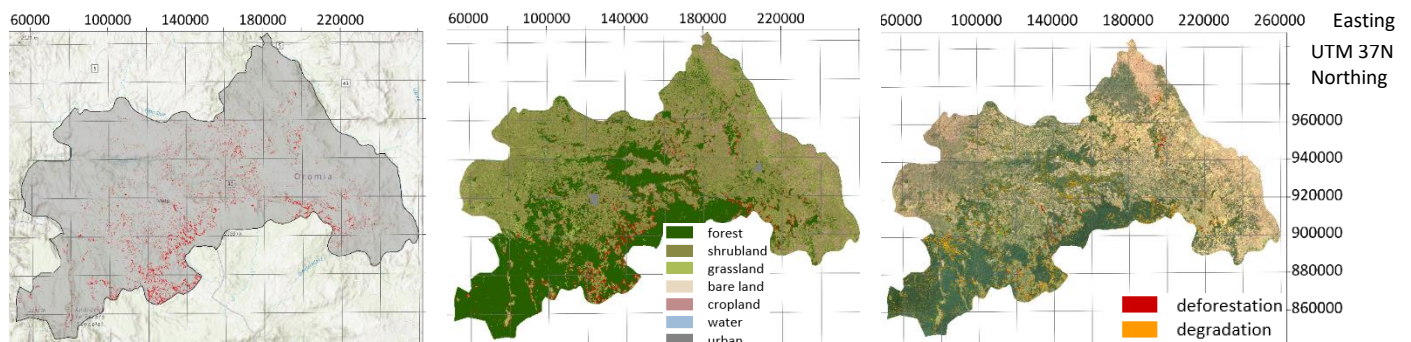


Figure 11-9 From left to right: Calculated forest loss displayed in red for Illubabor zone, calculated loss in red overlaid on the classified composite 2015-2020, degradation in orange and deforestation in red calculated with the CODED algorithm overlaid on the Landsat imagery composite 2015-2020

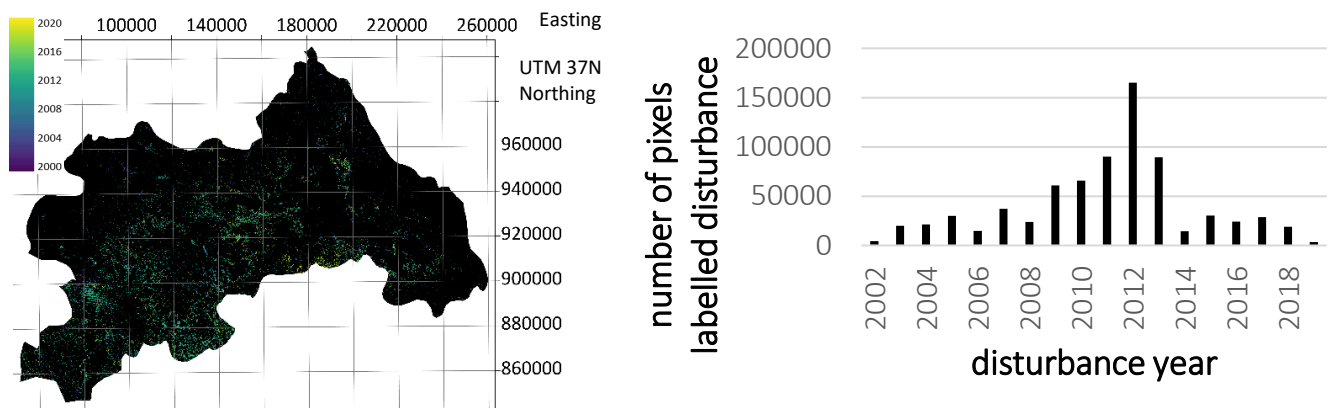


Figure 11-10 Left: Disturbance dates calculated with the CODED algorithm for Illubabor zone, Right: Corresponding histogram showing the number of pixels labelled as disturbance for every year during the study period

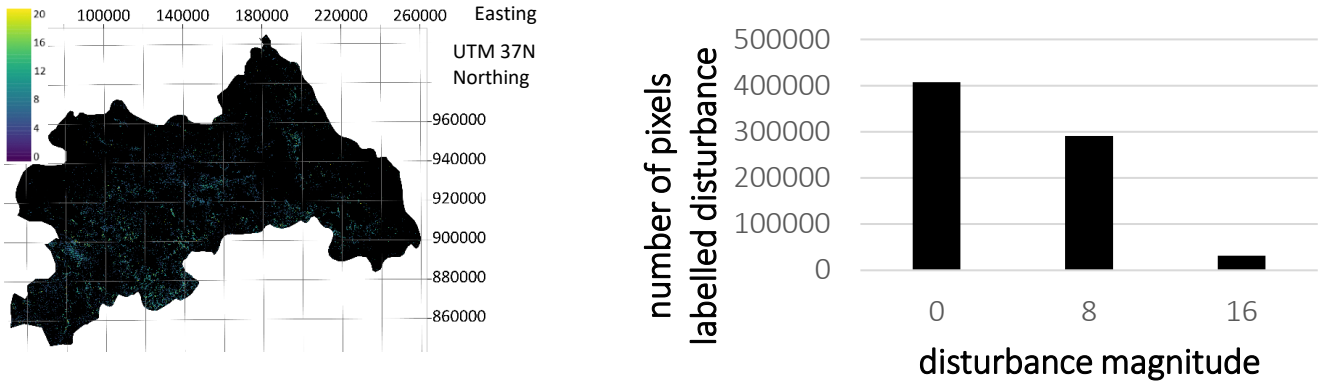


Figure 11-11 Left: Disturbance magnitudes calculated with the CODED algorithm for Illubabor zone, Right: Corresponding histogram showing the number of pixels labelled as disturbance for the different magnitudes

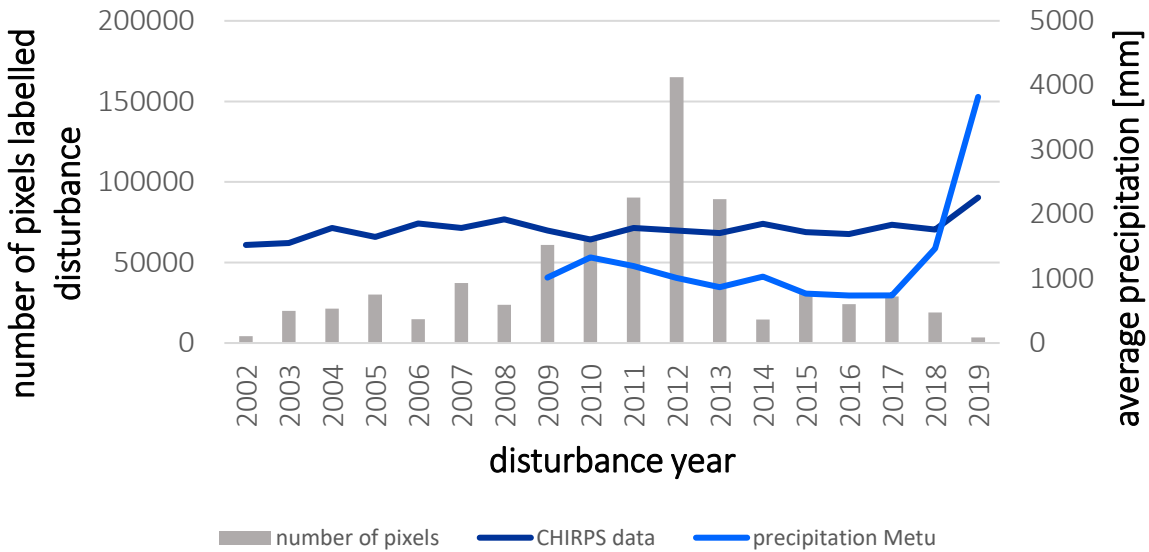


Figure 11-12 Histogram showing the number of pixels labelled as disturbance for every year during the analysis period for Illubabor zone, the light blue line demonstrates the precipitation data from world weather for the city of Metu (World Weather Online 2020), the dark blue line refers to the average precipitation extracted from the Chirps data (Google Earth Engine 2020)

11.3 Bench Maji zone

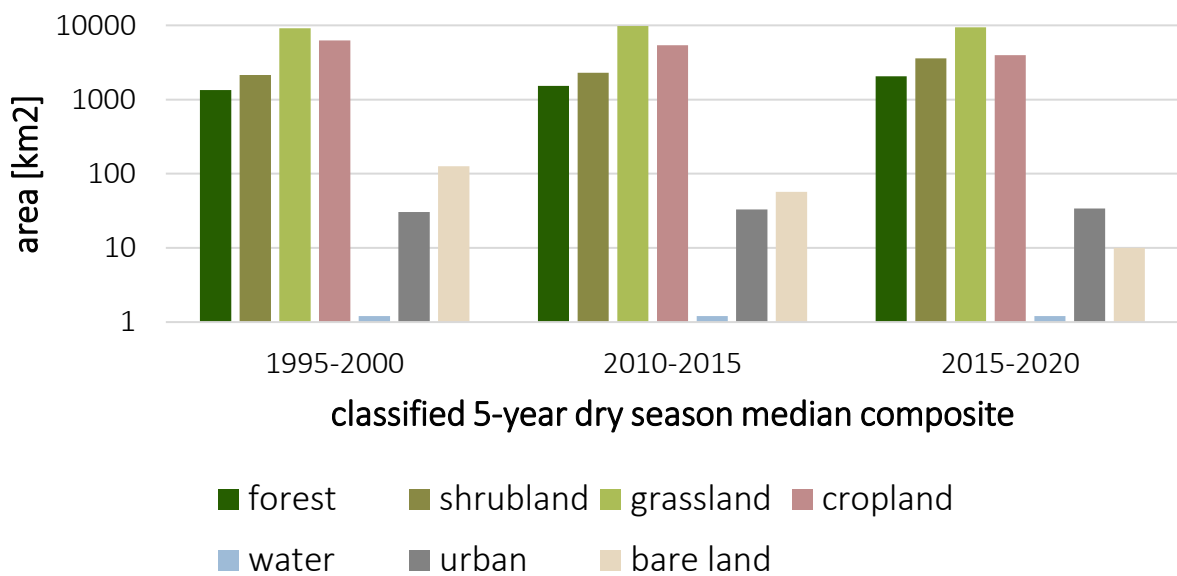


Figure 11-13 Graphic illustrating the areal size of the different land cover classes per classified composite for Bench Maji zone

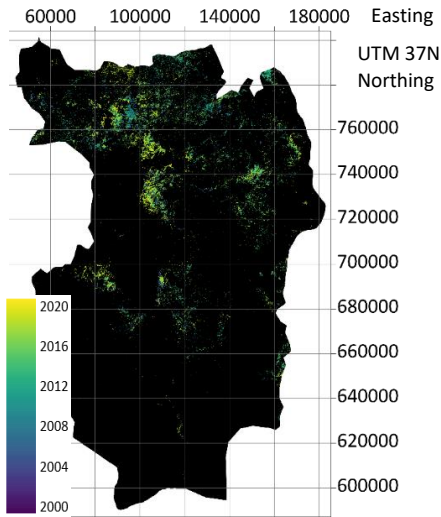


Figure 11-14 Disturbance dates calculated with the CODED algorithm for Bench Maji zone

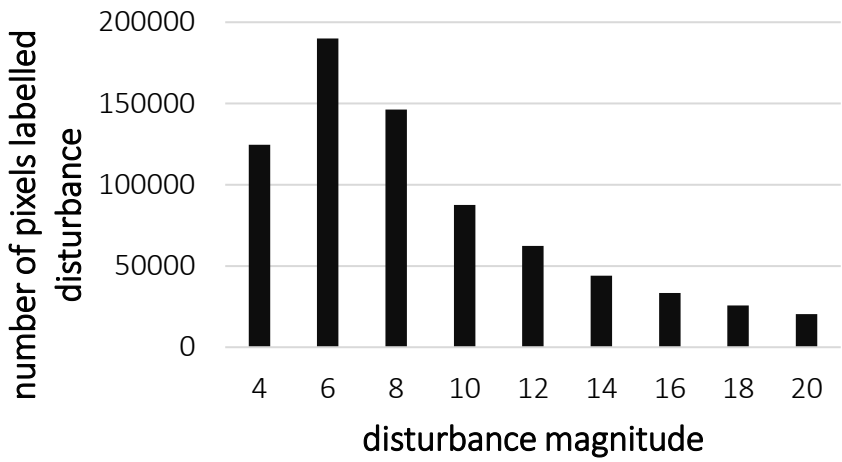
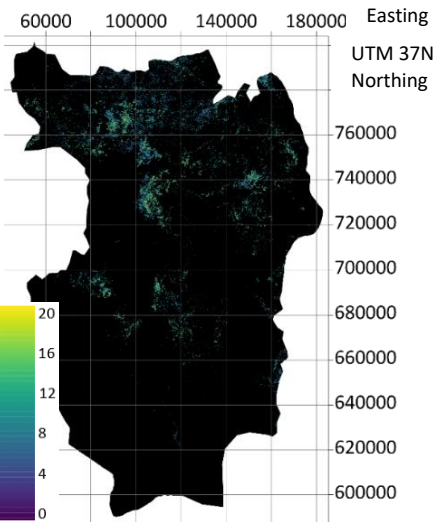


Figure 11-15 Left: Disturbance magnitudes calculated with the CODED algorithm for Bench Maji zone, Right: Corresponding histogram showing the number of pixels labelled as disturbance for the different magnitudes

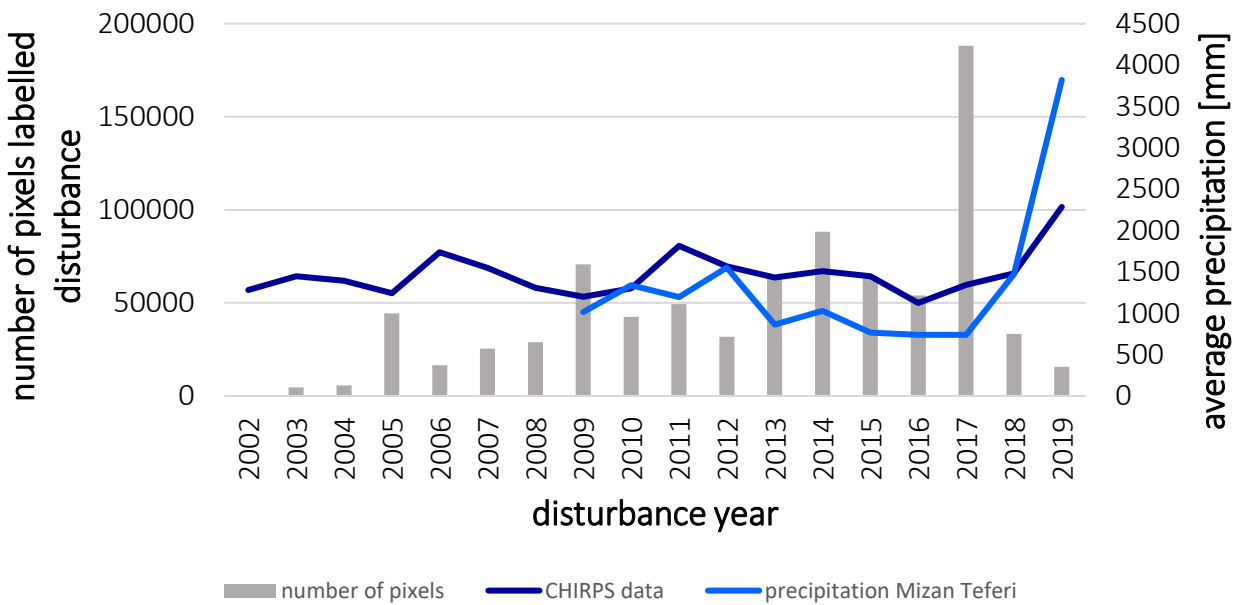


Figure 11-16 Histogram showing the number of pixels labelled as disturbance for every year during the analysis period for Bench Maji zone, the light blue line demonstrates the precipitation data from world weather for the city of Mizan Teferi (World Weather Online 2020), the dark blue line refers to the average precipitation extracted from the Chirps data (Google Earth Engine 2020)

11.4 Bale zone

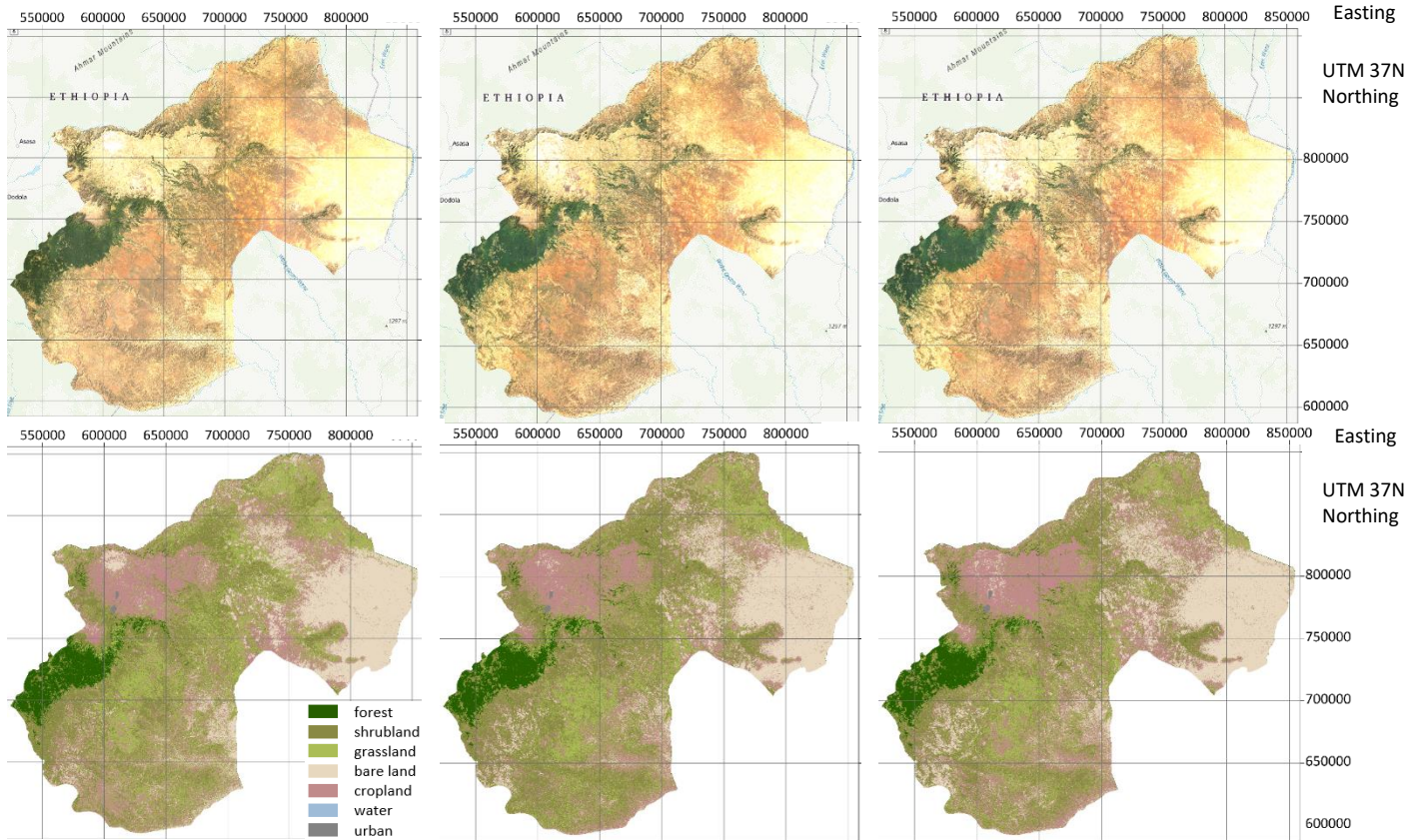


Figure 11-17 Top: Landsat imagery composites 1995-2000, 2010-2015 and 2015-2020 for Bale zone (Google Earth Engine 2020), Bottom: Classified composites 1995-2000, 2010-2015 and 2015-2020

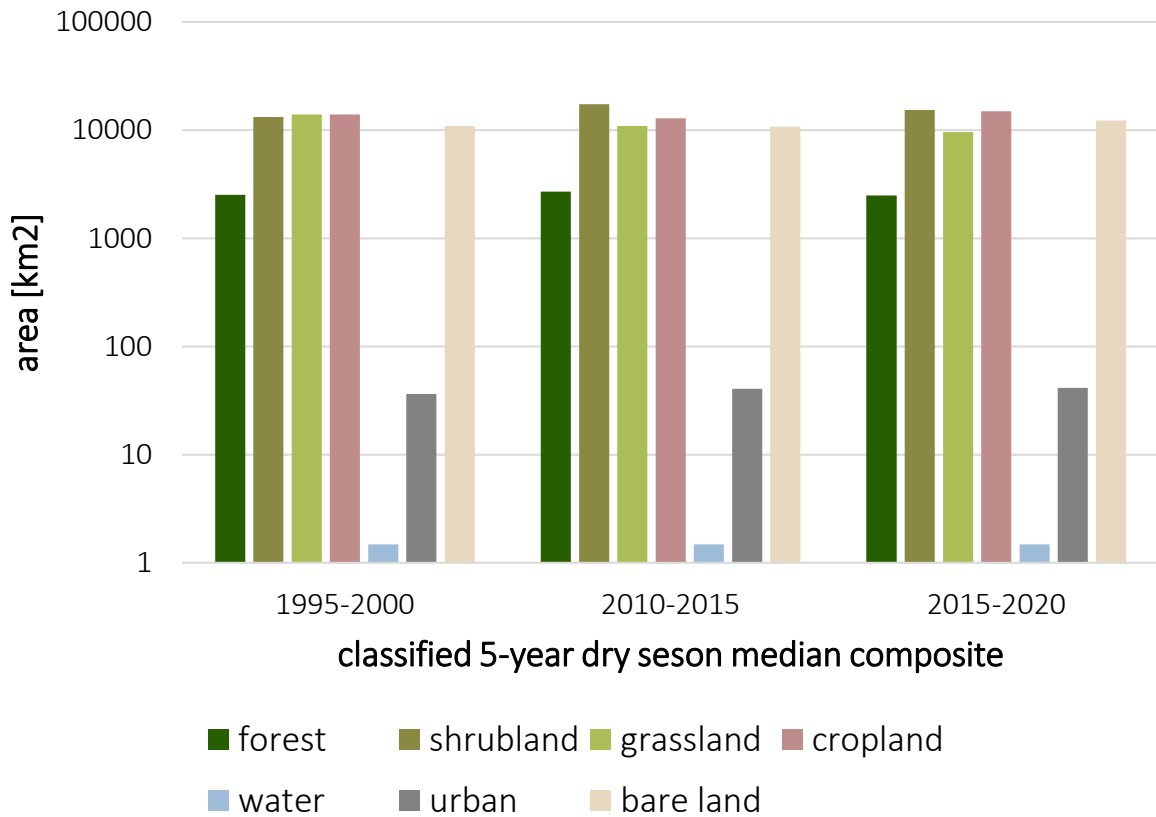


Figure 11-18 Graphic illustrating the areal size of the different land cover classes per classified composite for Bale zone

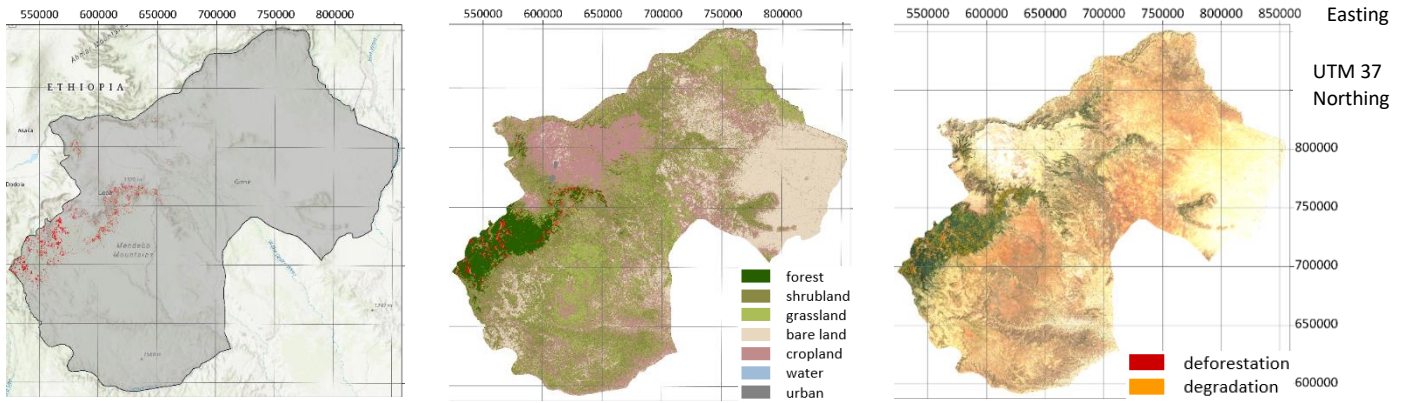


Figure 11-19 From left to right: Calculated forest loss displayed in red for Bale zone, calculated loss in red overlaid on the classified composite 2015-2020, degradation in orange and deforestation in red calculated with the CODED algorithm overlaid on the Landsat imagery composite 2015-2020

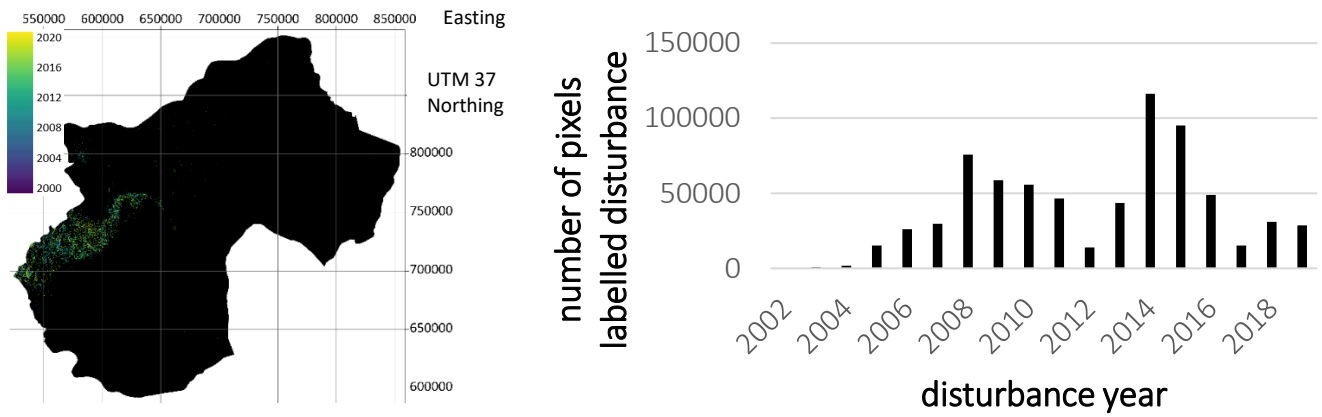


Figure 11-20 Left: Disturbance dates calculated with the CODED algorithm for Bale zone, Right: Corresponding histogram showing the number of pixels labelled as disturbance for every year during the study period

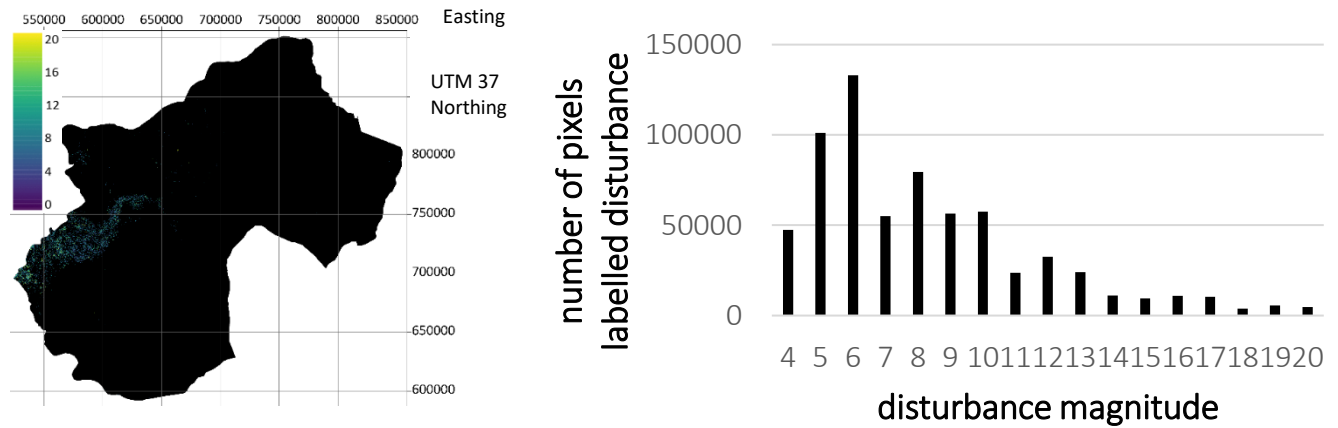


Figure 11-21 Left: Disturbance magnitudes calculated with the CODED algorithm for Bale zone, Right: Corresponding histogram showing the number of pixels labelled as disturbance for the different magnitudes

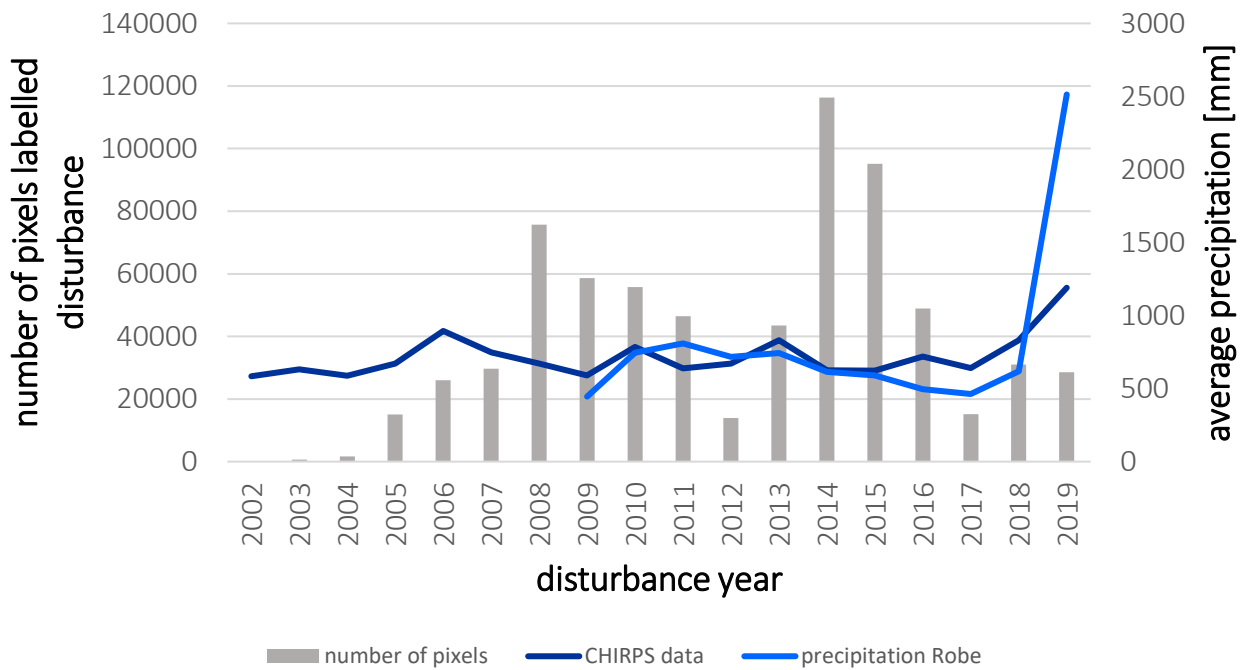


Figure 11-22 Histogram showing the number of pixels labelled as disturbance for every year during the analysis period for Bale zone, the light blue line demonstrates the precipitation data from world weather for the city of Robe (World Weather Online 2020), the dark blue line refers to the average precipitation extracted from the Chirps data (Google Earth Engine 2020)

11.5 Keshi kebele

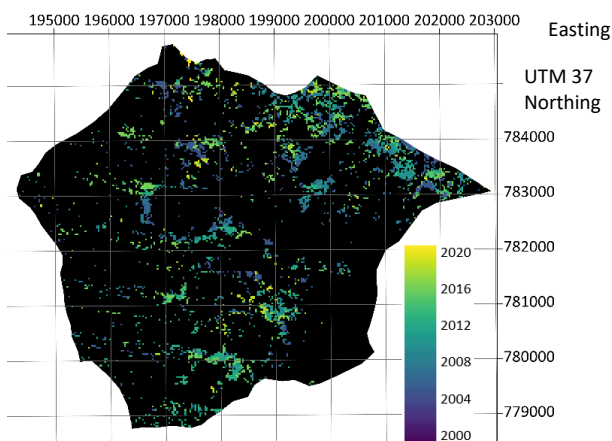


Figure 11-23 Left: Disturbance dates calculated with the CODED algorithm for Keshi kebele

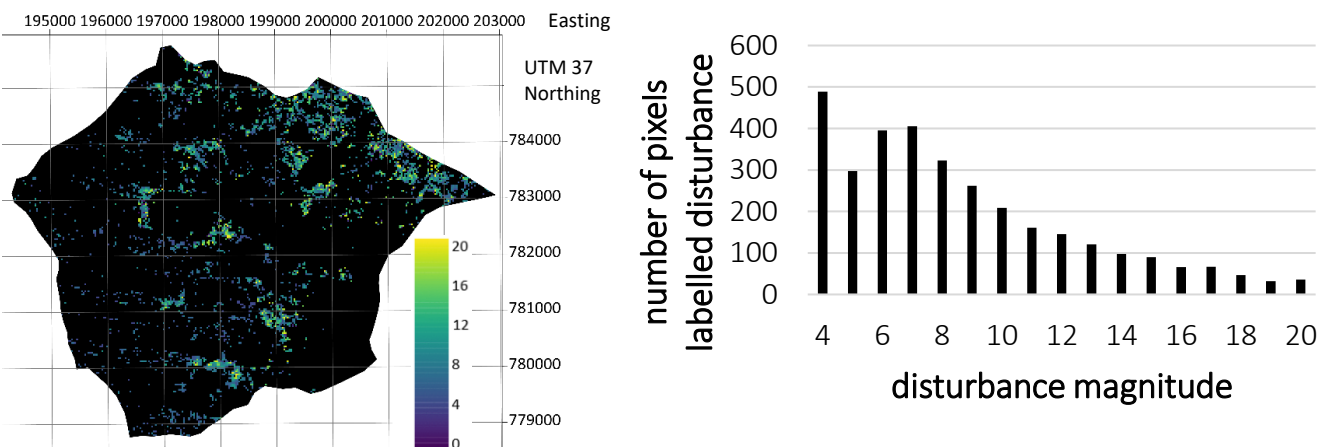


Figure 11-24 Left: Disturbance magnitudes calculated with the CODED algorithm for Keshi kebele, Right: Corresponding histogram showing the number of pixels labelled as disturbance for the different magnitudes

11.6 Chebere kebele

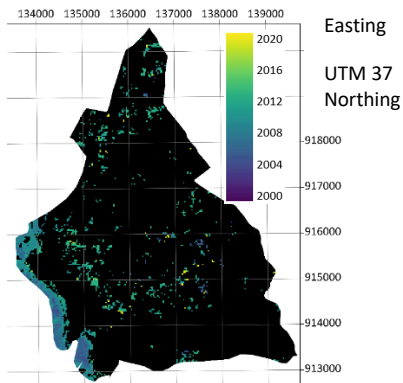


Figure 11-25 Disturbance dates calculated with the CODED algorithm for Chebere kebele

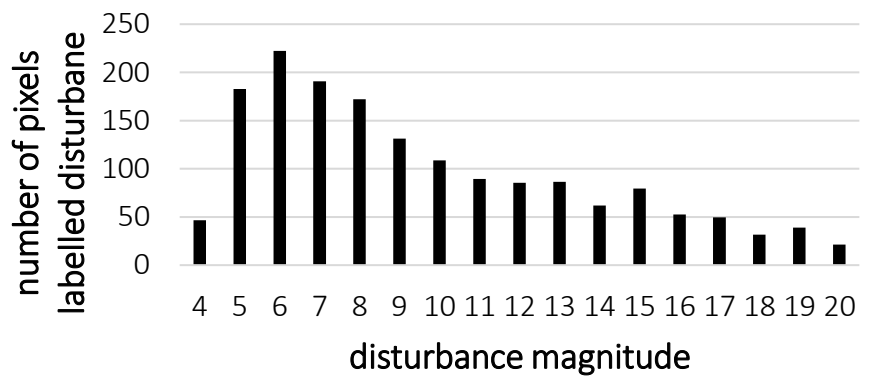
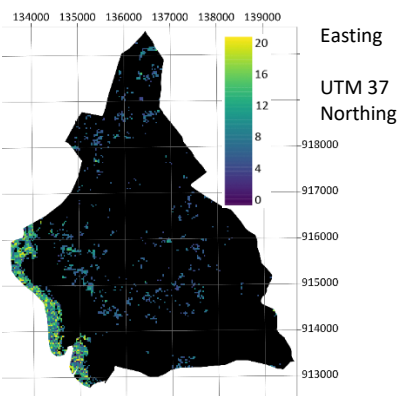


Figure 11-26 Left: Disturbance magnitudes calculated with the CODED algorithm for Chebere kebele, Right: Corresponding histogram showing the number of pixels labelled as disturbance for the different magnitudes

11.7 Giz Meret kebele

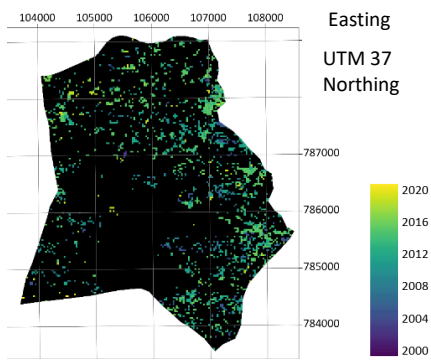


Figure 11-27 Disturbance dates calculated with the CODED algorithm for Giz Meret kebele

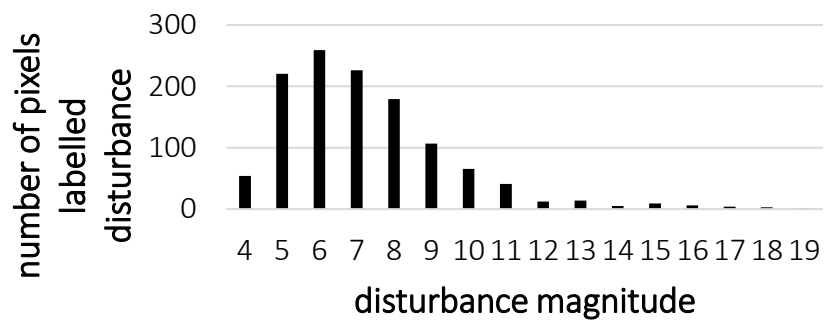
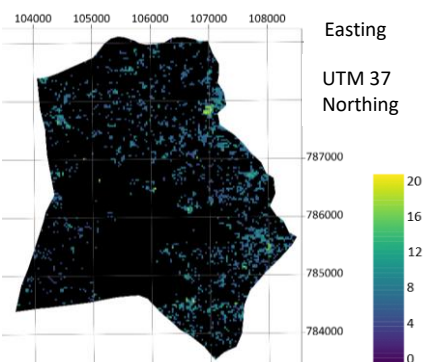


Figure 11-28 Left: Disturbance magnitudes calculated with the CODED algorithm for Giz Meret kebele, Right: Corresponding histogram showing the number of pixels labelled as disturbance for the different magnitudes

11.8 Sodu Lelaftu kebele

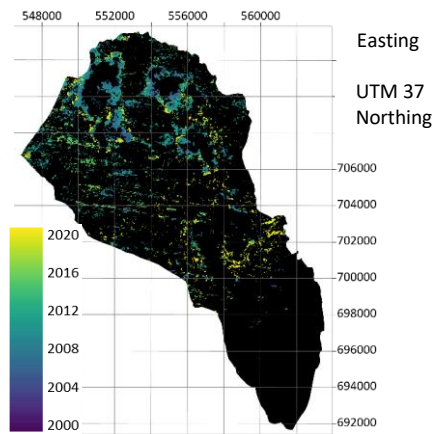


Figure 11-29 Disturbance dates calculated with the CODED algorithm for Sodu Lelaftu kebele

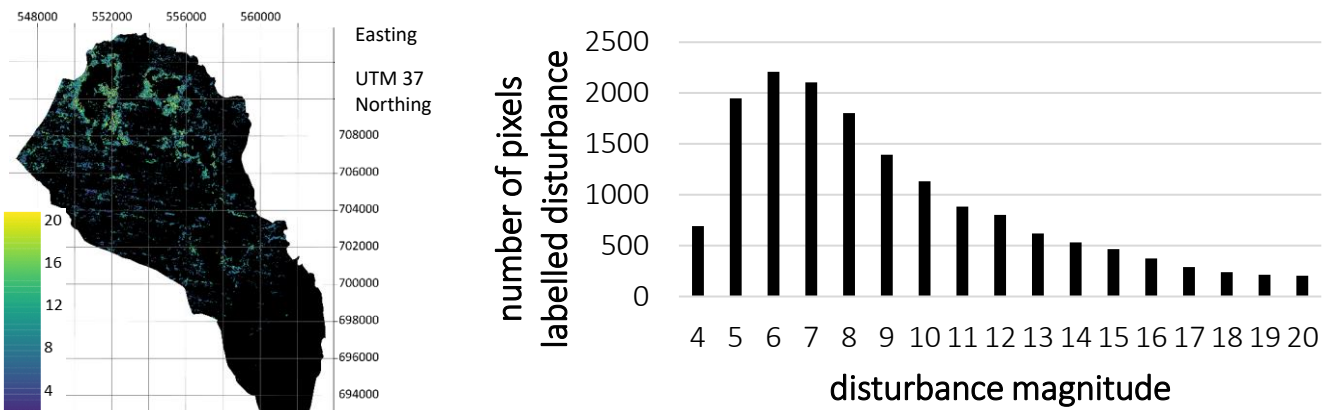


Figure 11-30 Left: Disturbance magnitudes calculated with the CODED algorithm for Sodu Lelaftu kebele, Right: Corresponding histogram showing the number of pixels labelled as disturbance for the different magnitudes

11.9 Bergi kebele

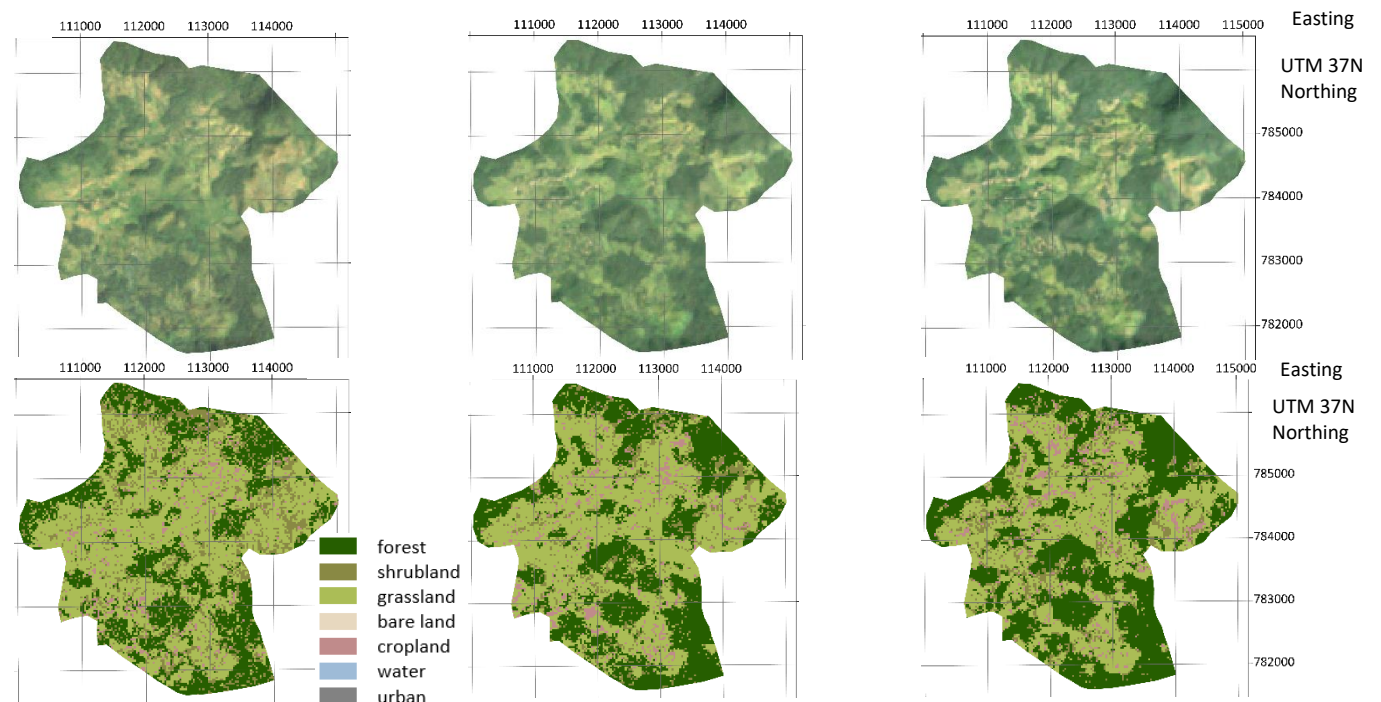


Figure 11-31 Top: Landsat imagery composites 1995-2000, 2010-2015 and 2015-2020 for Bergi kebele (Google Earth Engine 2020), Bottom: Classified composites 1995-2000, 2010-2015 and 2015-2020

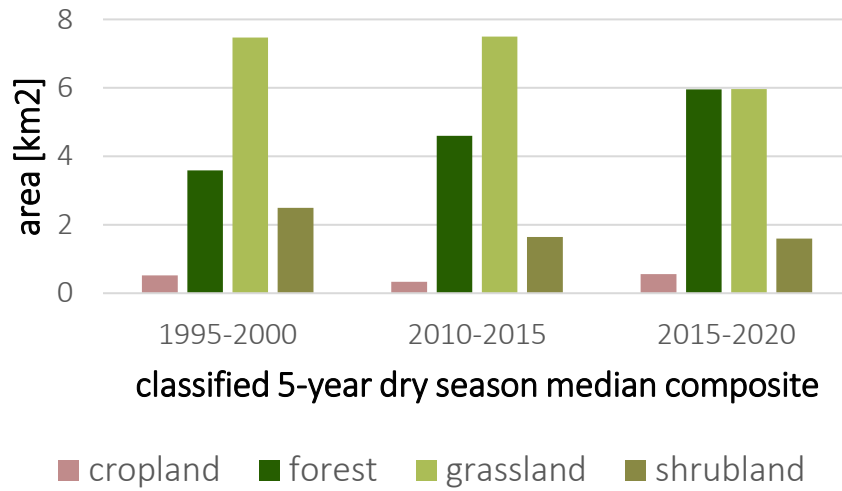


Figure 11-32 Graphic illustrating the areal size of the different land cover classes per classified composite for Bergi kebele

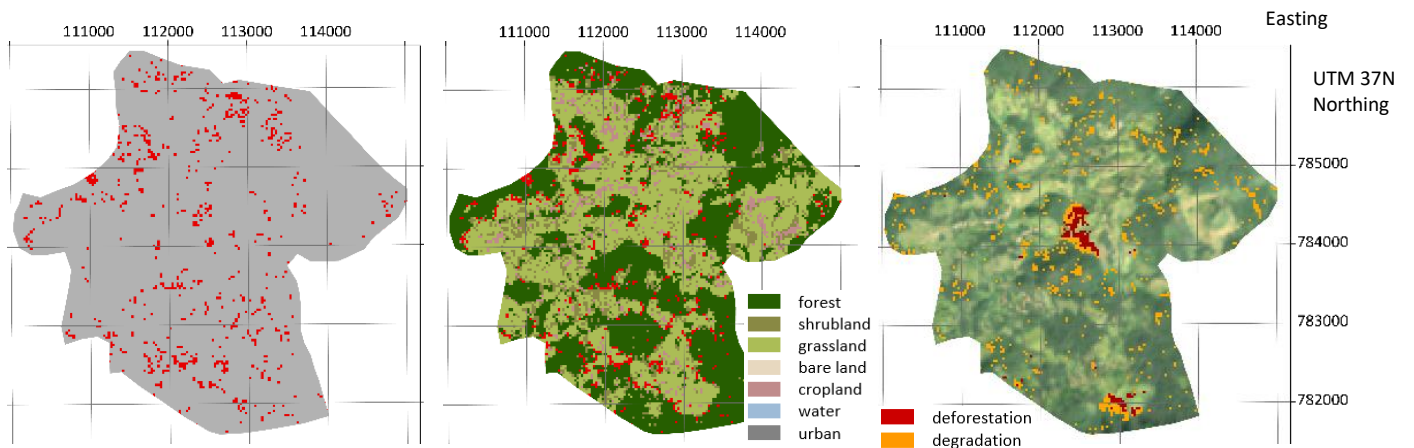


Figure 11-33 From left to right: Calculated forest loss displayed in red for Bergi kebele, calculated loss in red overlaid on the classified composite 2015-2020, degradation in orange and deforestation in red calculated with the CODED algorithm overlaid on the Landsat imagery composite 2015-2020

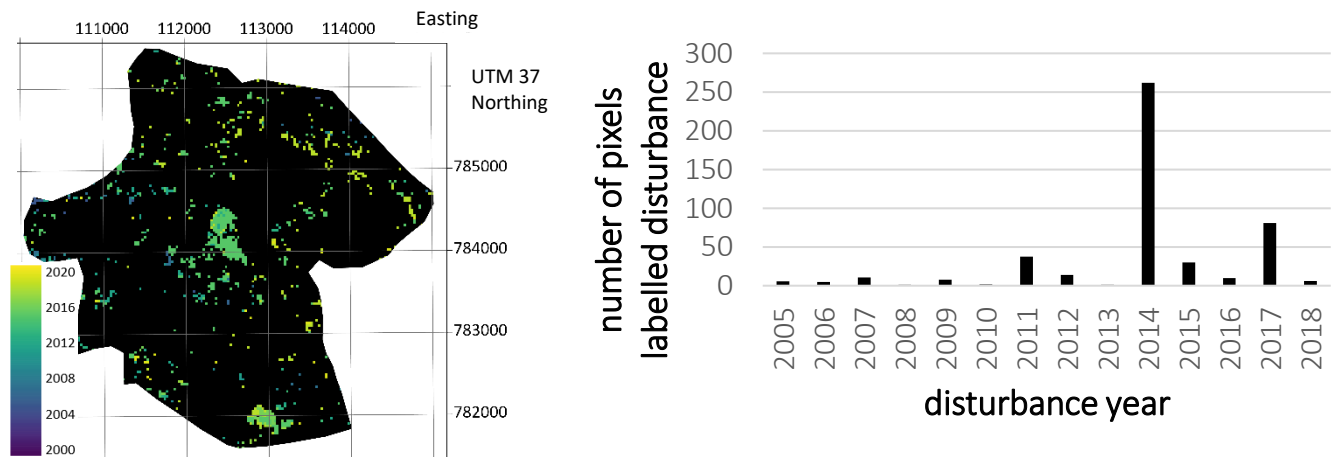


Figure 11-34 Disturbance dates calculated with the CODED algorithm for Bergi kebele, Right: Corresponding histogram showing the number of pixels labelled as disturbance for every year during the study period

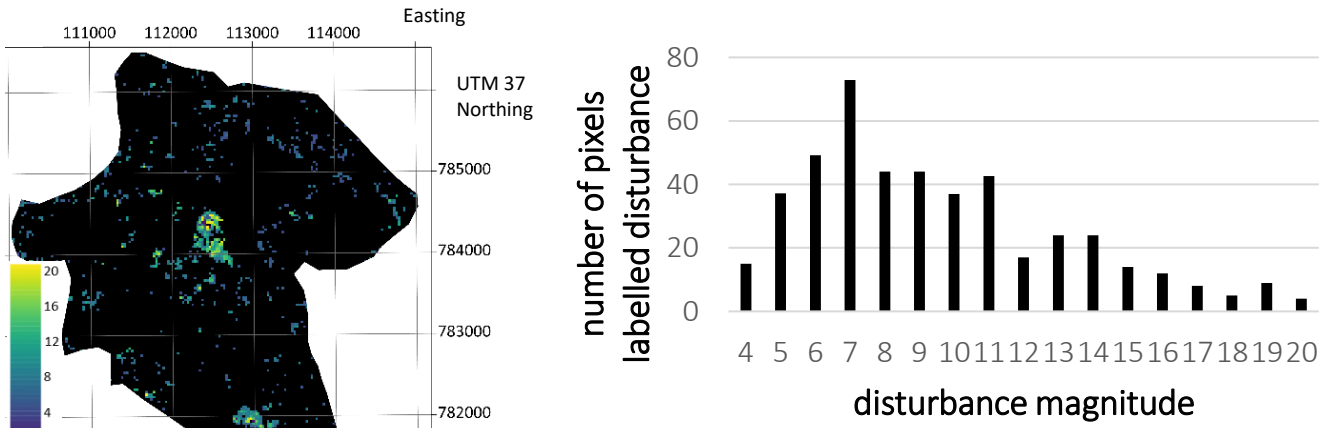


Figure 11-35 Left: Disturbance magnitudes calculated with the CODED algorithm for Keffa zone, Right: Corresponding histogram showing the number of pixels labelled as disturbance for the different magnitudes

11.10 Mankira kebele

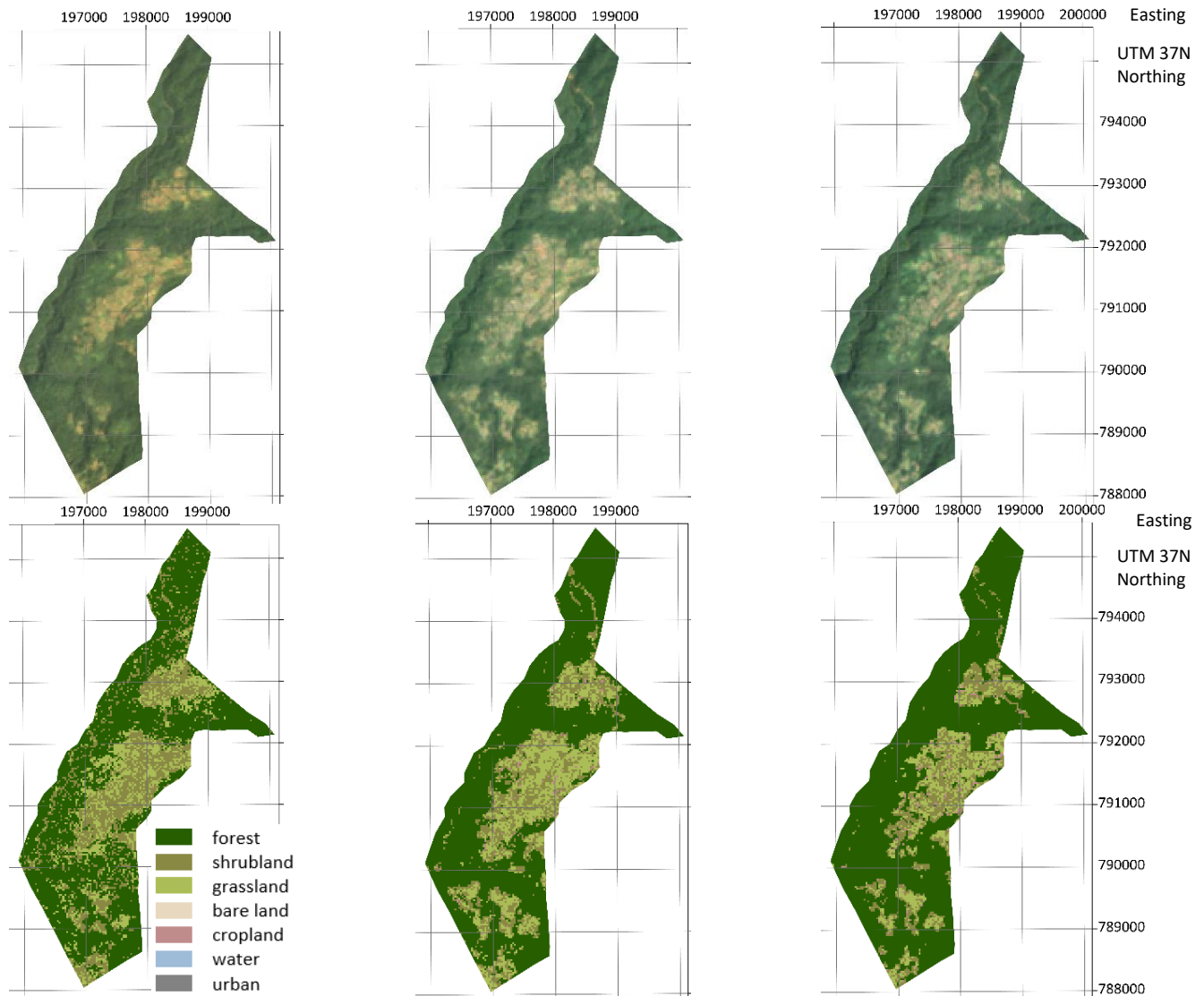


Figure 11-36 Top: Landsat imagery composites 1995-2000, 2010-2015 and 2015-2020 for Mankira kebele (Google Earth Engine 2020), Bottom: Classified composites 1995-2000, 2010-2015 and 2015-2020

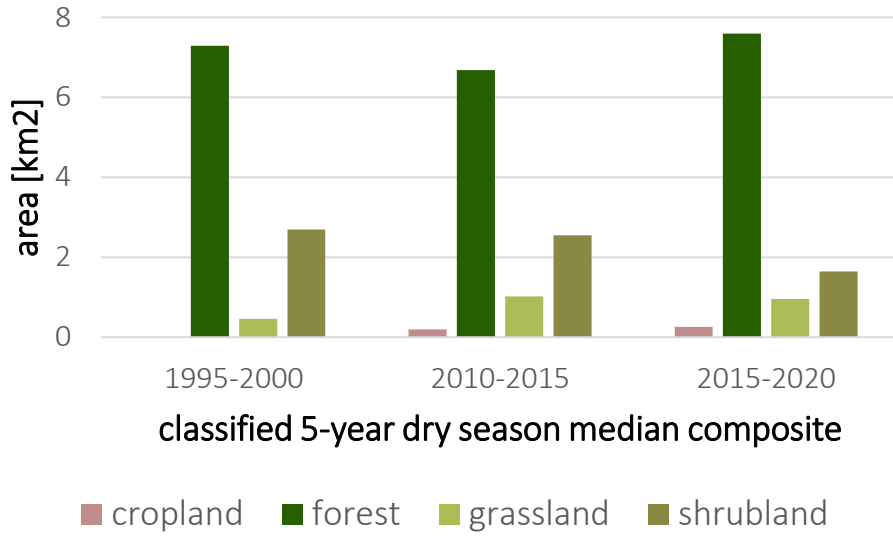


Figure 11-37 Graphic illustrating the areal size of the different land cover classes per classified composite for Mankira kebele

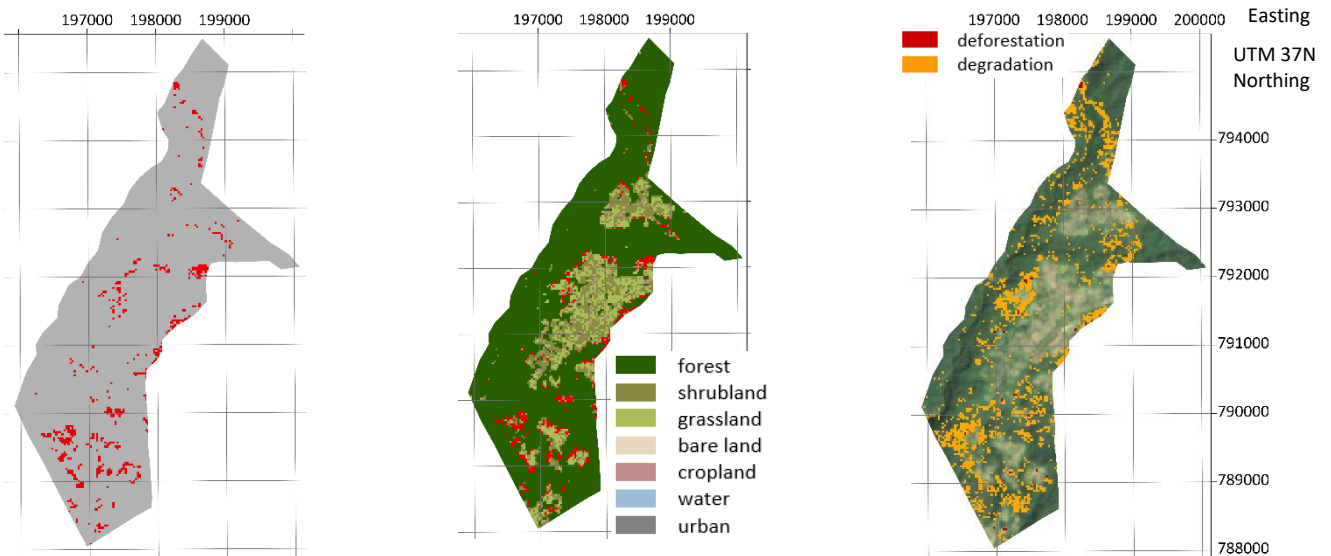


Figure 11-38 From left to right: Calculated forest loss displayed in red for Mankira kebele, calculated loss in red overlaid on the classified composite 2015-2020, degradation in orange and deforestation in red calculated with the CODED algorithm overlaid on the Landsat imagery composite 2015-2020

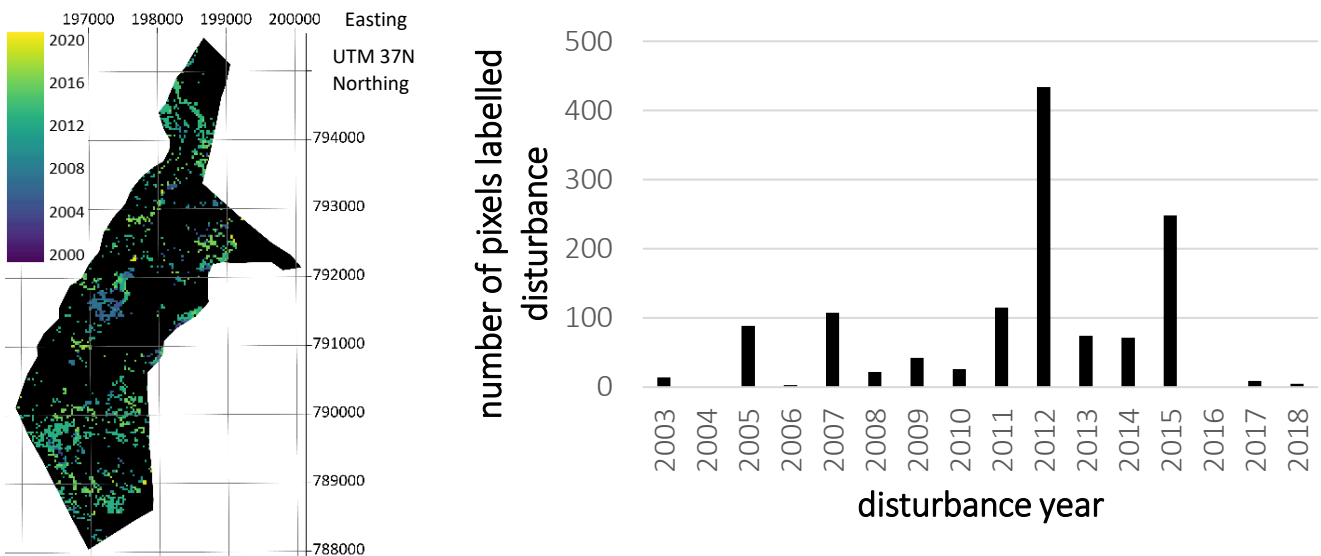


Figure 11-39 Left: Disturbance dates calculated with the CODED algorithm for Mankira kebele, Right: Corresponding histogram showing the number of pixels labelled as disturbance for every year during the study period

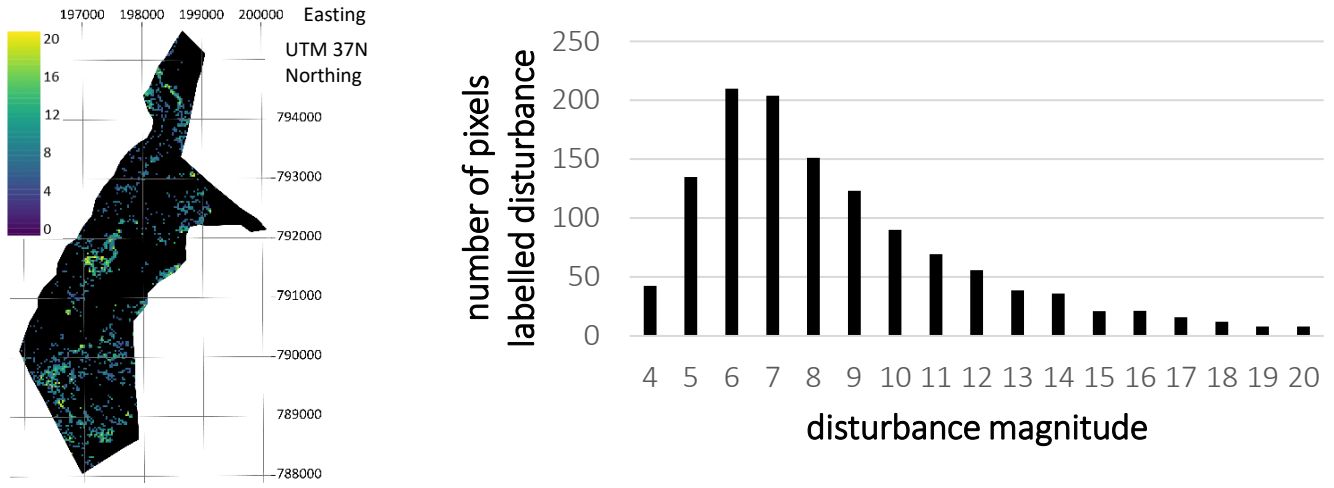


Figure 11-40 Left: Disturbance magnitudes calculated with the CODED algorithm for Mankira kebele, Right: Corresponding histogram showing the number of pixels labelled as disturbance for the different magnitudes

11.11 Keja Araba kebele

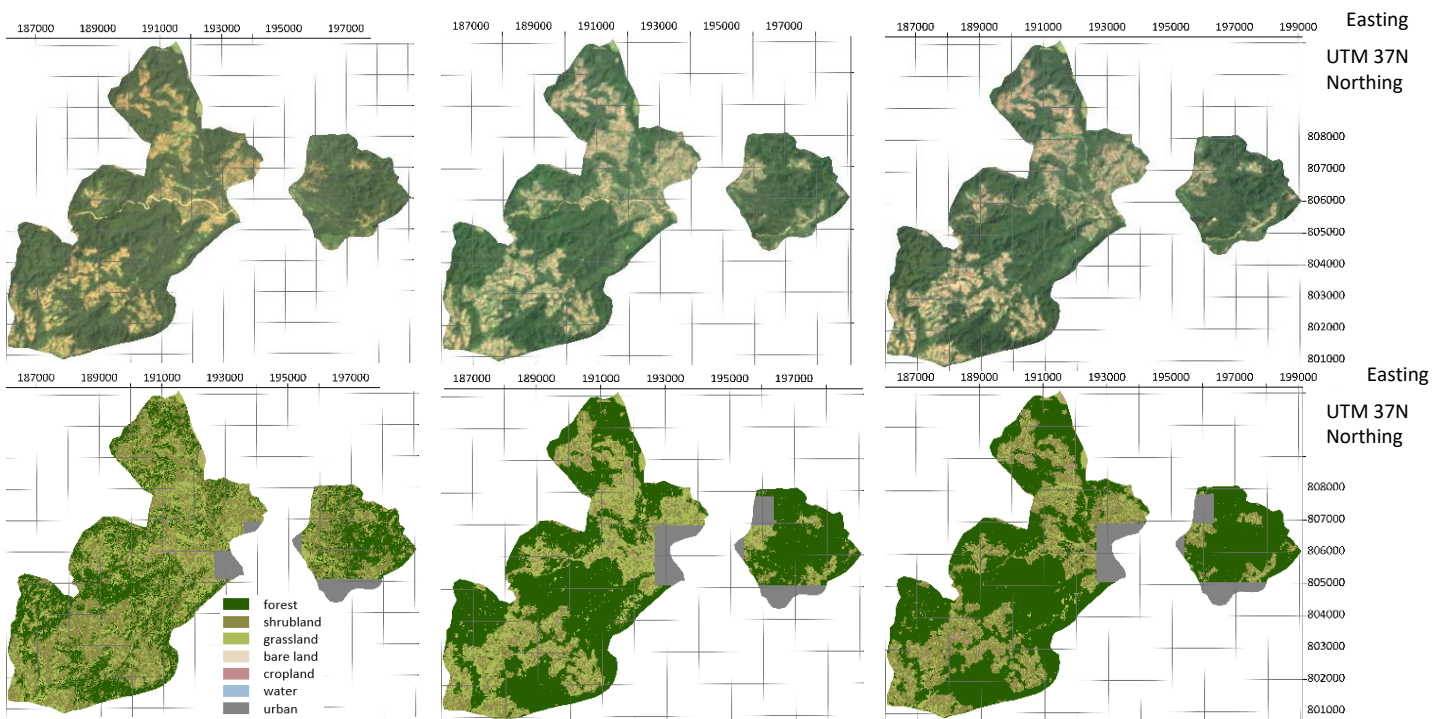


Figure 11-41 Top: Landsat imagery composites 1995-2000, 2010-2015 and 2015-2020 for Keja Araba kebele (Google Earth Engine 2020), Bottom: Classified composites 1995-2000, 2010-2015 and 2015-2020

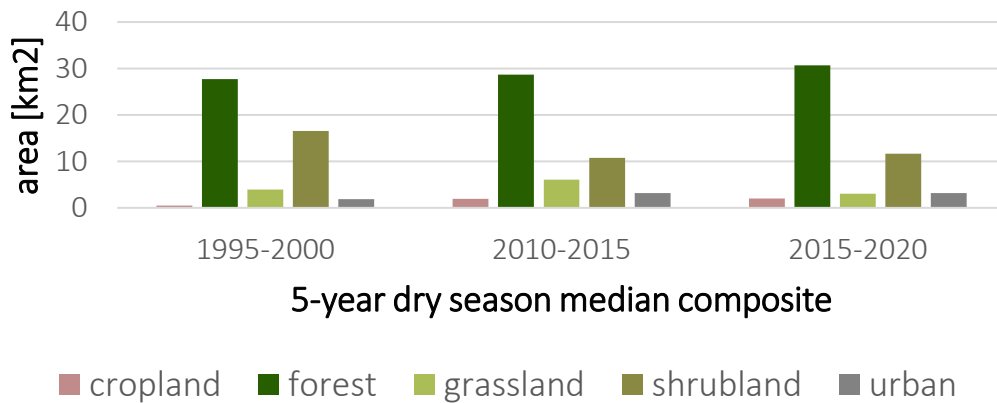


Figure 11-42 Graphic illustrating the areal size of the different land cover classes per classified composite for Keja Araba kebele

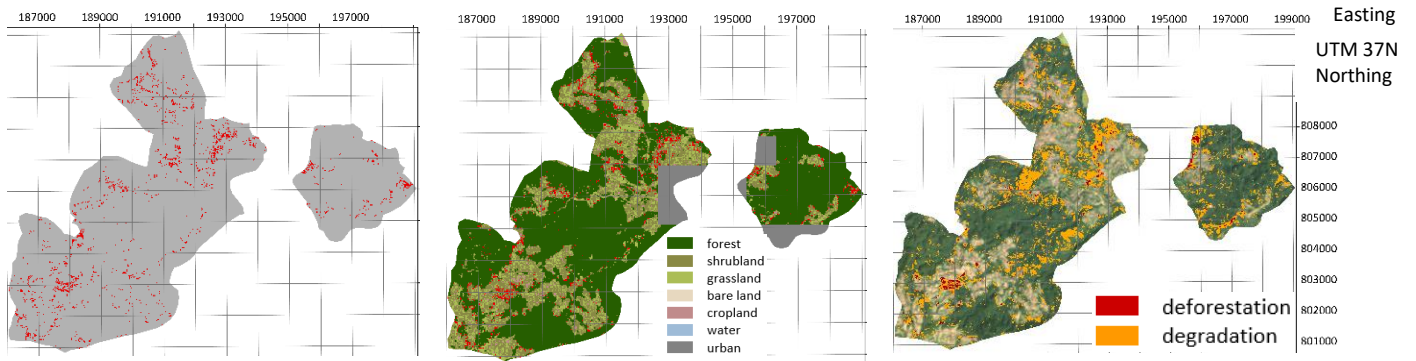


Figure 11-43 From left to right: Calculated forest loss displayed in red for Keja Araba kebele, calculated loss in red overlaid on the classified composite 2015-2020, degradation in orange and deforestation in red calculated with the CODED algorithm overlaid on the Landsat imagery composite 2015-2020

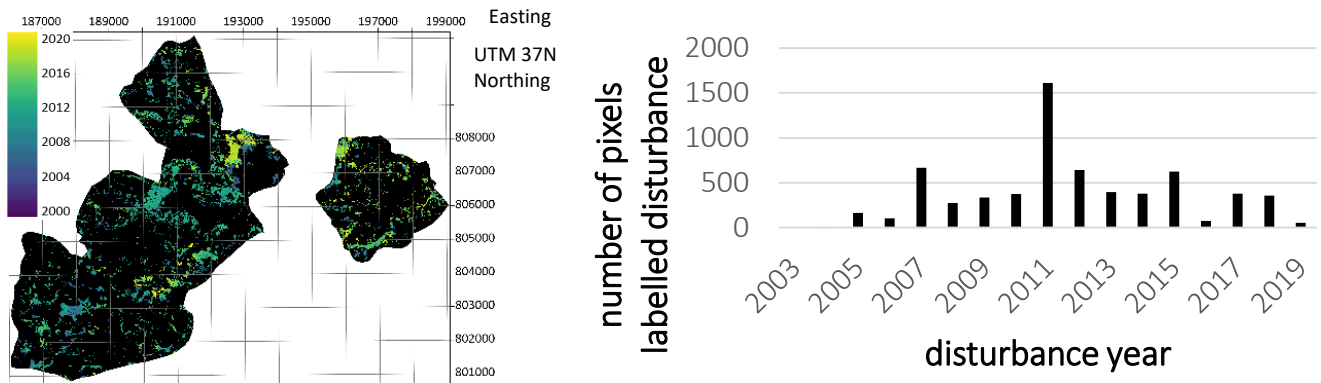


Figure 11-44 Left: Disturbance dates calculated with the CODED algorithm for Keja Araba kebele, Right: Corresponding histogram showing the number of pixels labelled as disturbance for every year during the study period

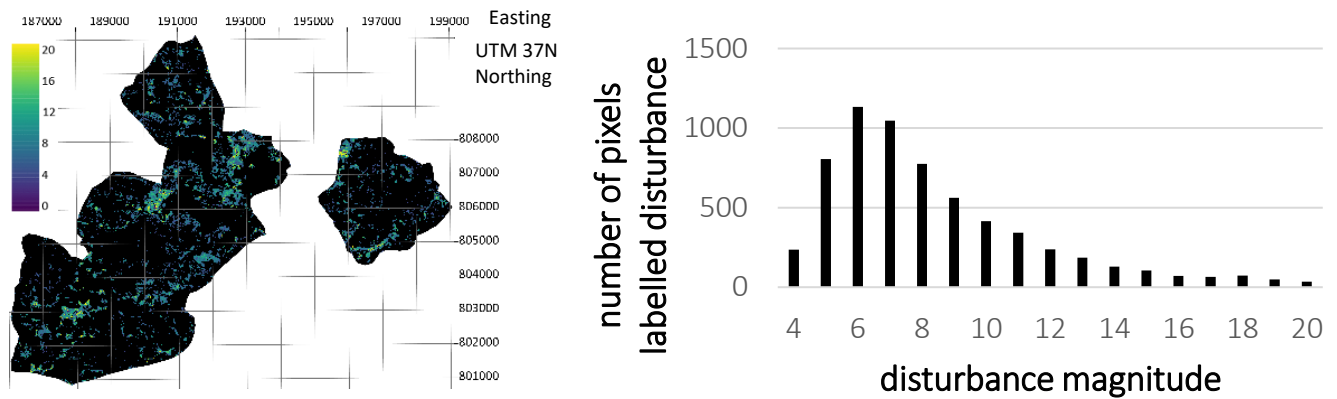
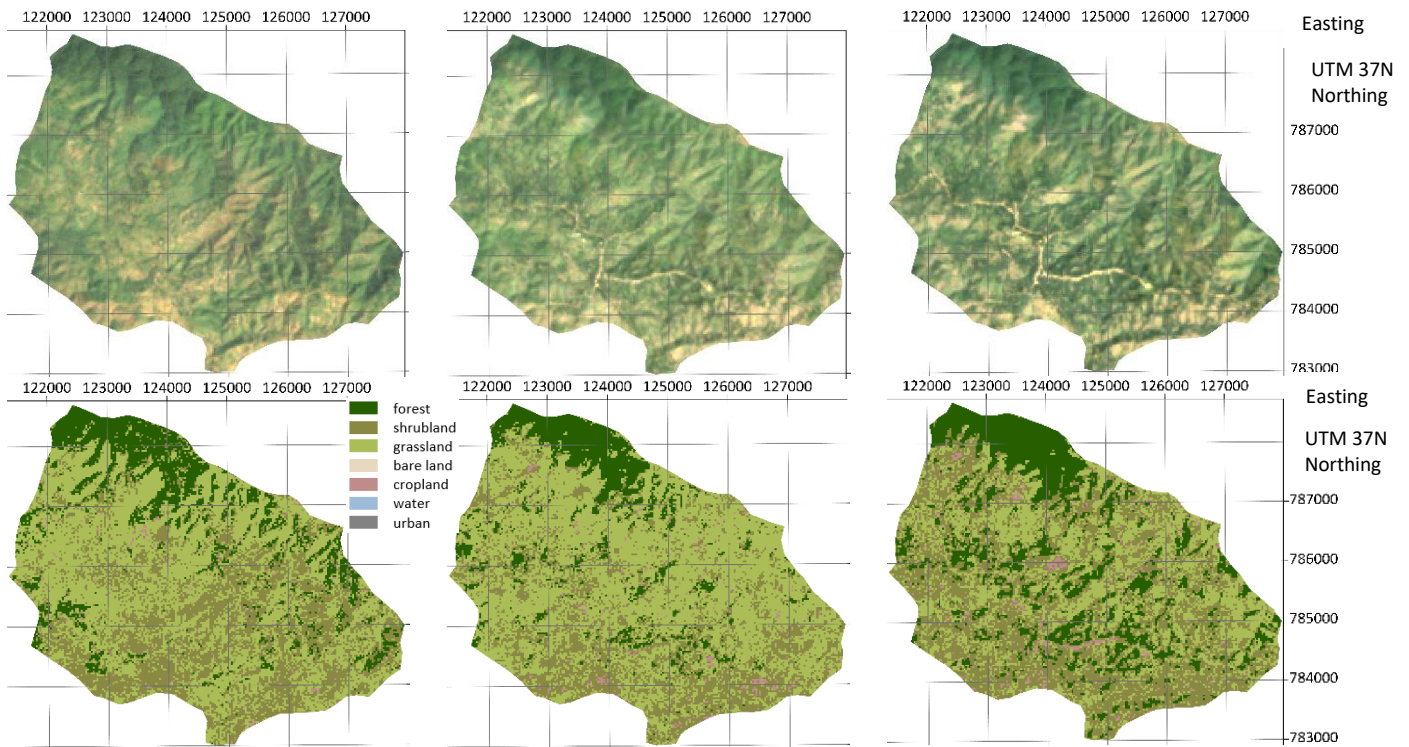


Figure 11-45 Left: Disturbance magnitudes calculated with the CODED algorithm for Keja Araba kebele, Right: Corresponding histogram showing the number of pixels labelled as disturbance for the different magnitudes

11.12 Seriti kebele



Appendix Figure 11-46 Top: Landsat imagery composites 1995-2000, 2010-2015 and 2015-2020 for Seriti kebele (Google Earth Engine 2020), Bottom: Classified composites 1995-2000, 2010-2015 and 2015-2020

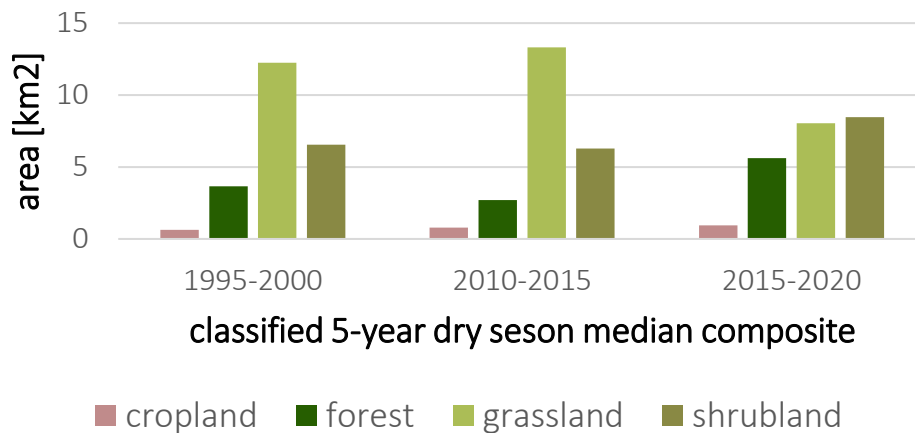


Figure 11-47 Graphic illustrating the areal size of the different land cover classes per classified composite for Seriti kebele

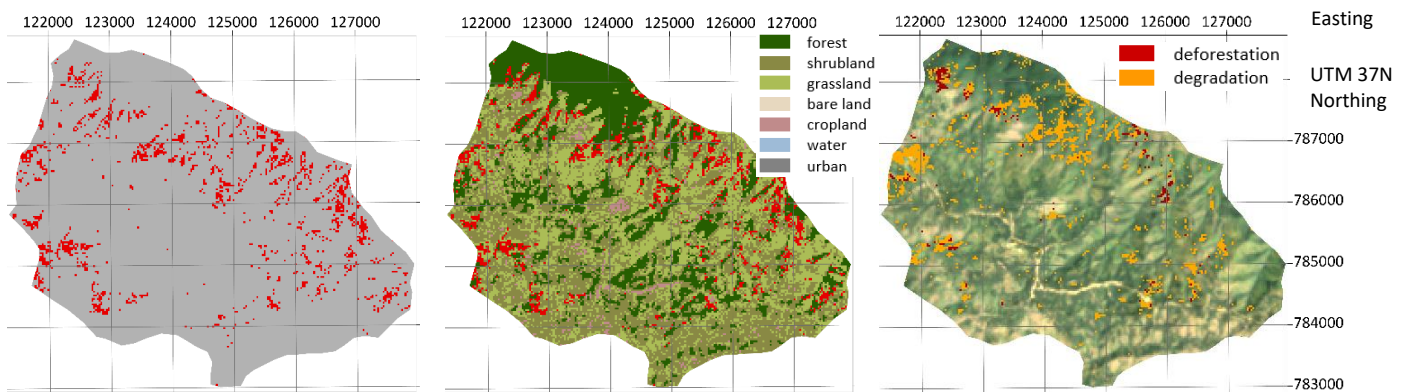


Figure 11-48 From left to right: Calculated forest loss displayed in red for Seriti kebele, calculated loss in red overlaid on the classified composite 2015-2020, degradation in orange and deforestation in red calculated with the CODED algorithm overlaid on the Landsat imagery composite 2015-2020

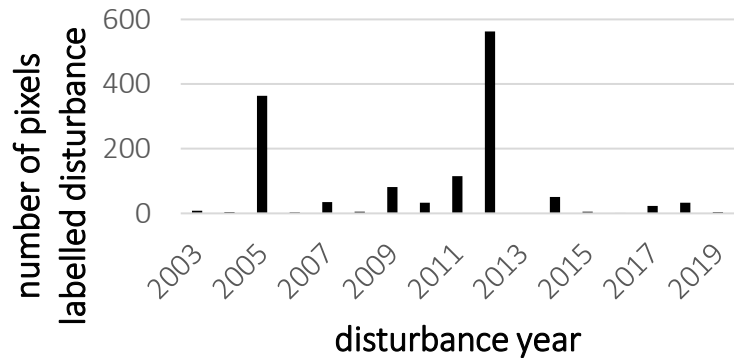
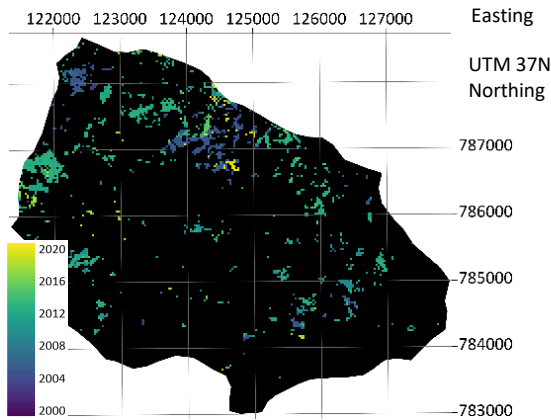


Figure 11-49 Disturbance dates calculated with the CODED algorithm for Seriti kebele, Right: Corresponding histogram showing the number of pixels labelled as disturbance for every year during the study period

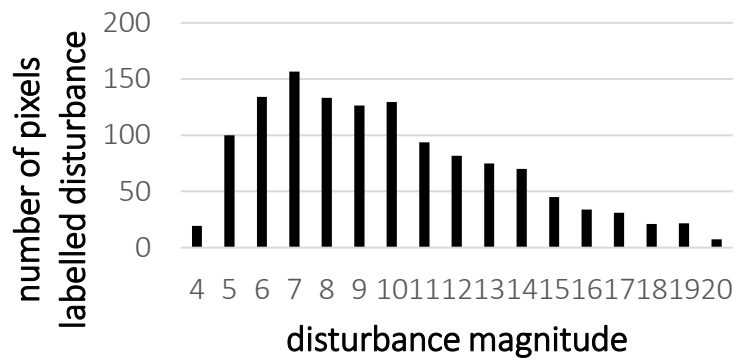
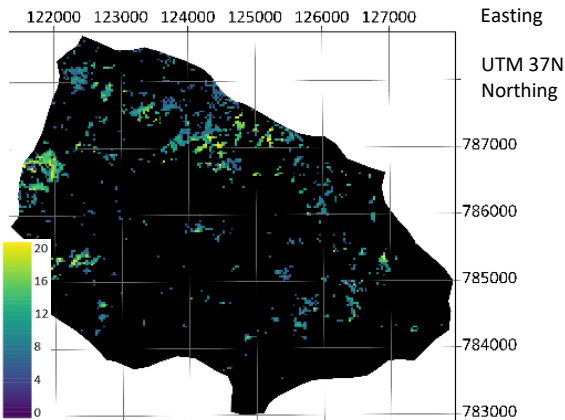


Figure 11-50 Left: Disturbance magnitudes calculated with the CODED algorithm for Seriti kebele, Right: Corresponding histogram showing the number of pixels labelled as disturbance for the different magnitudes

11.13 Muti kebele

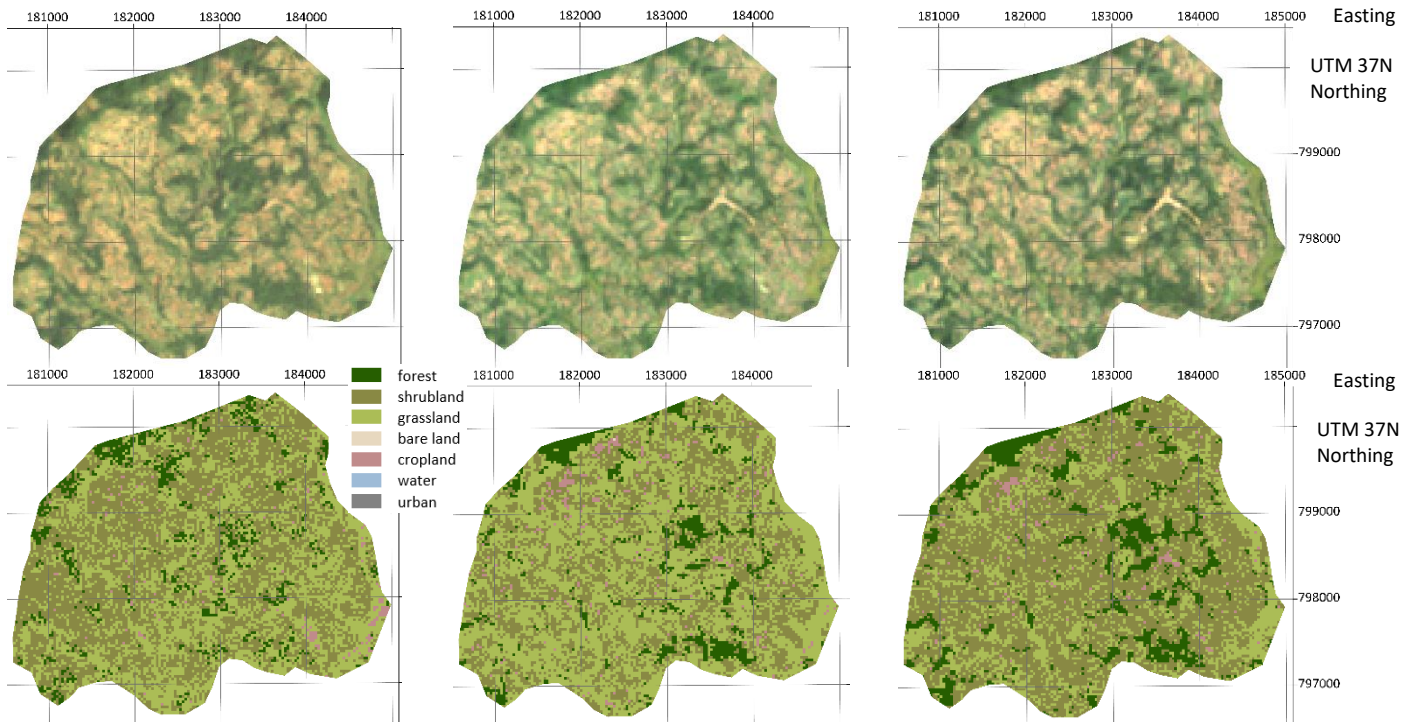


Figure 11-51 Top: Landsat imagery composites 1995-2000, 2010-2015 and 2015-2020 for Muti kebele (Google Earth Engine 2020), Bottom: Classified composites 1995-2000, 2010-2015 and 2015-2020

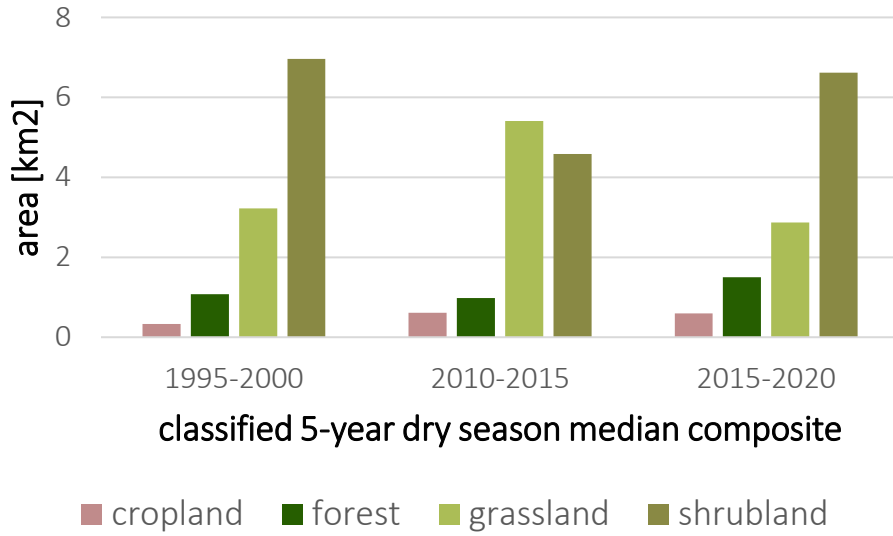


Figure 11-52 Graphic illustrating the areal size of the different land cover classes per classified composite for Muti kebele

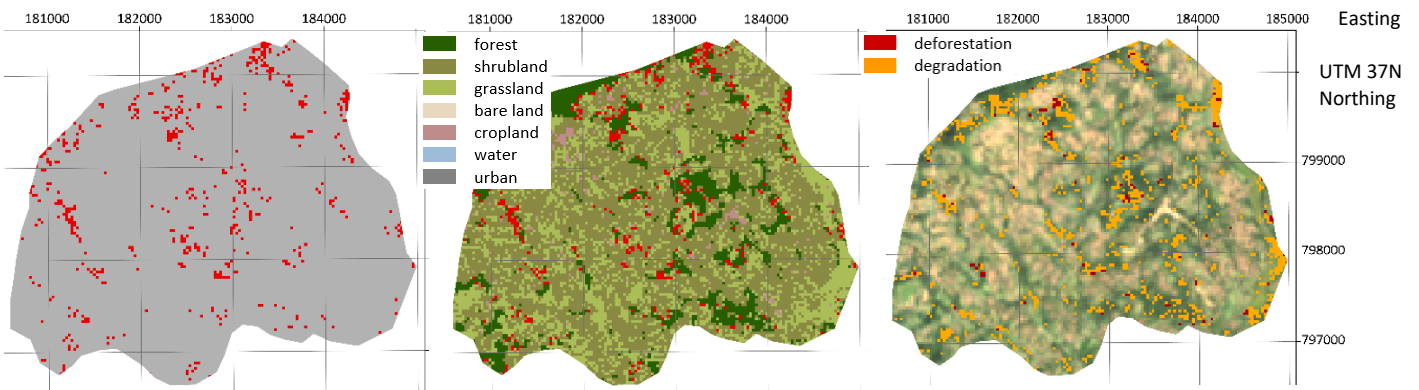


Figure 11-53 From left to right: Calculated forest loss displayed in red for Muti kebele, calculated loss in red overlaid on the classified composite 2015-2020, degradation in orange and deforestation in red calculated with the CODED algorithm overlaid on the Landsat imagery composite 2015-2020

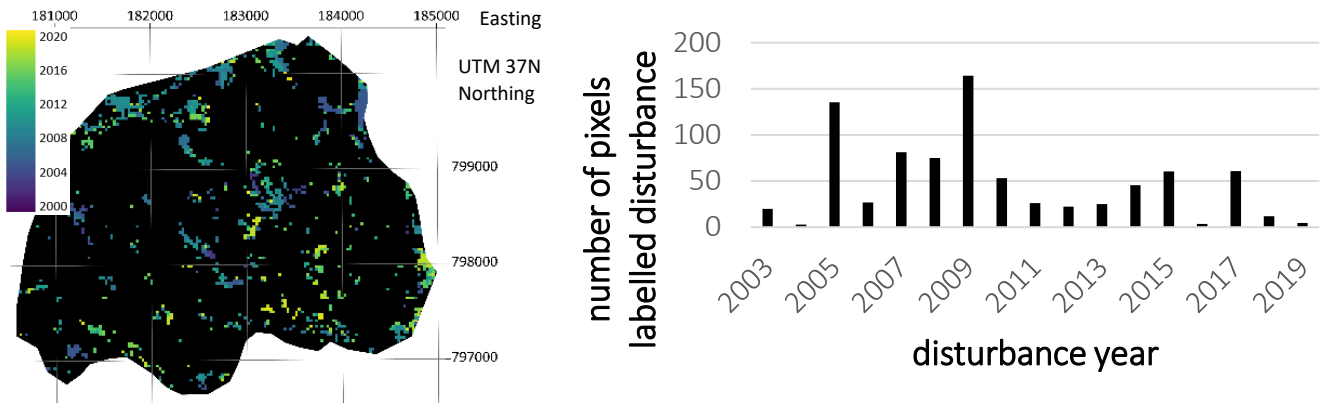


Figure 11-54 Left: Disturbance dates calculated with the CODED algorithm for Muti kebele, Right: Corresponding histogram showing the number of pixels labelled as disturbance for every year during the study period

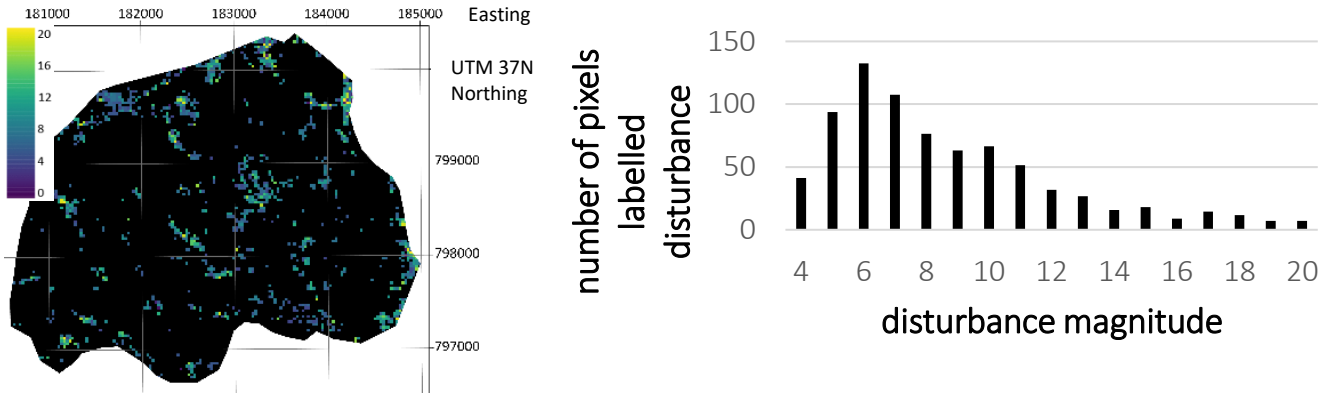


Figure 11-55 Left: Disturbance magnitudes calculated with the CODED algorithm for Muti kebele, Right: Corresponding histogram showing the number of pixels labelled as disturbance for the different magnitudes

11.14 Ganga kebele

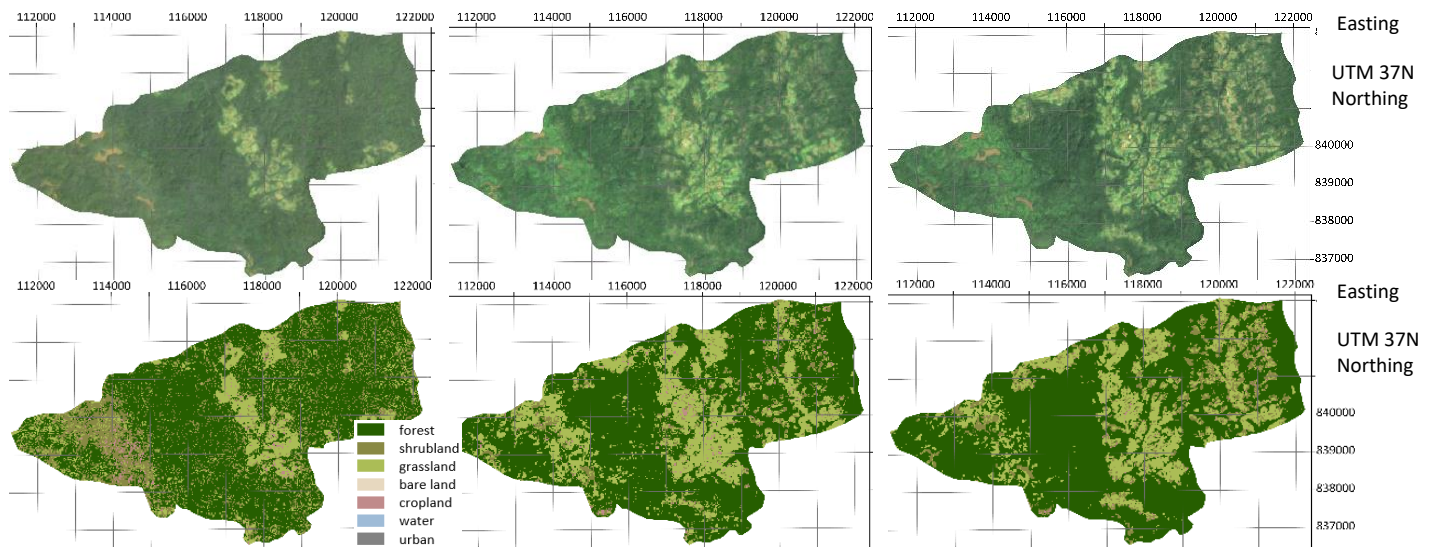


Figure 11-56 Top: Landsat imagery composites 1995-2000, 2010-2015 and 2015-2020 for Ganga kebele (Google Earth Engine 2020), Bottom: Classified composites 1995-2000, 2010-2015 and 2015-2020

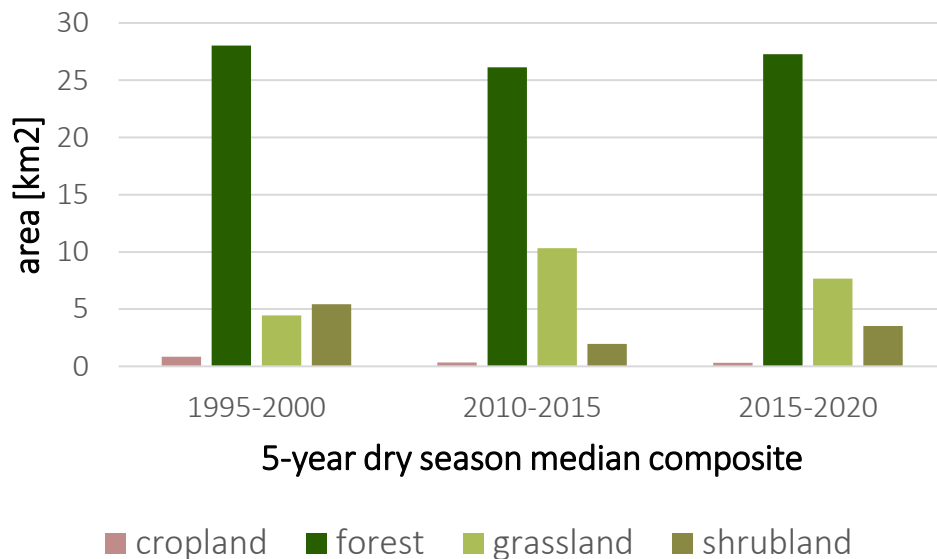


Figure 11-57 Graphic illustrating the areal size of the different land cover classes per classified composite for Ganga kebele

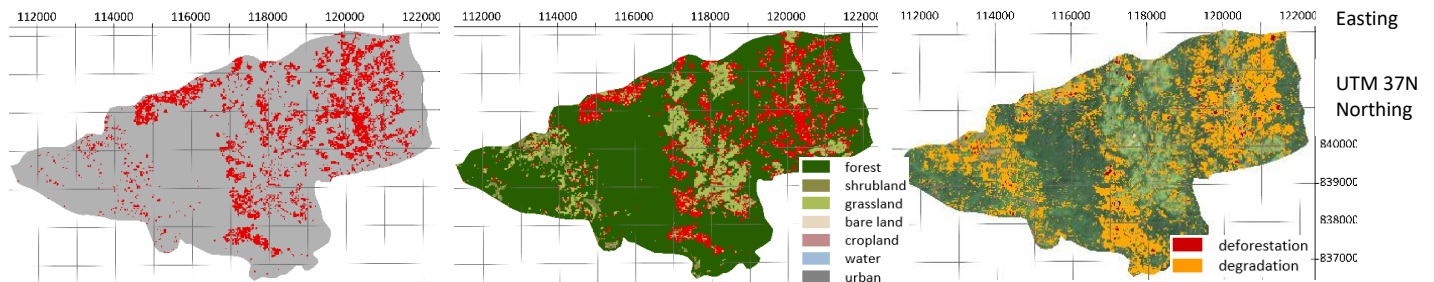


Figure 11-58 From left to right: Calculated forest loss displayed in red for Ganga kebele, calculated loss in red overlaid on the classified composite 2015-2020, degradation in orange and deforestation in red calculated with the CODED algorithm overlaid on the Landsat imagery composite 2015-2020

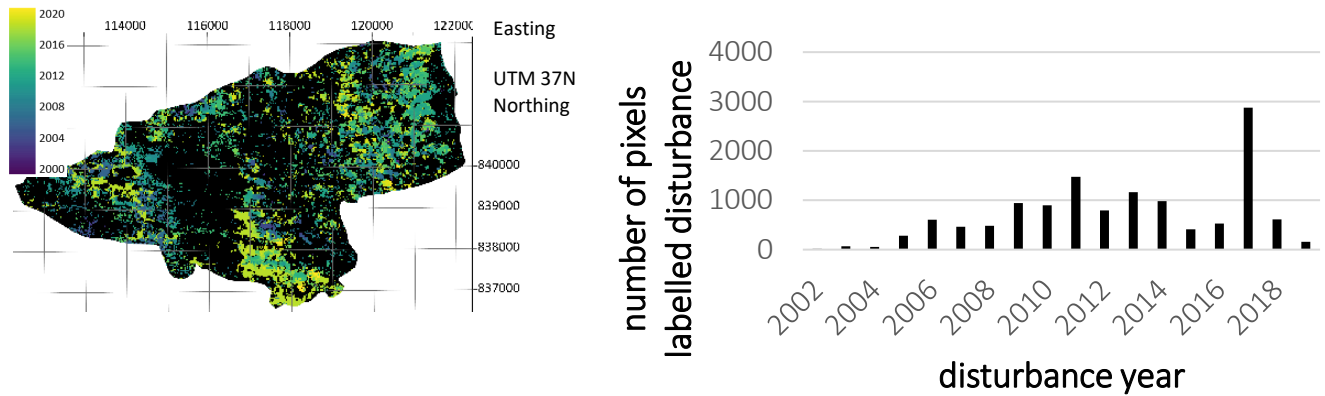


Figure 11-59 Left: Disturbance dates calculated with the CODED algorithm for Ganga kebele, Right: Corresponding histogram showing the number of pixels labelled as disturbance for every year during the study period

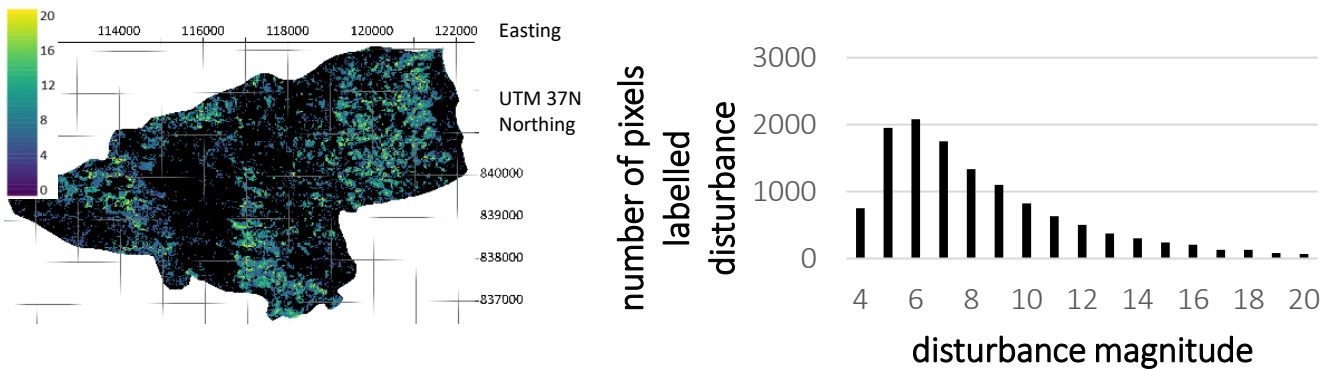


Figure 11-60 Left: Disturbance magnitudes calculated with the CODED algorithm for Ganga kebele, Right: Corresponding histogram showing the number of pixels labelled as disturbance for the different magnitudes

11.15 All study kebeles

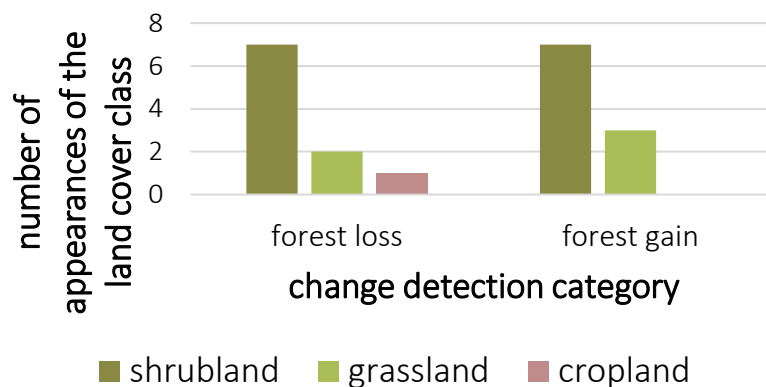


Figure 11-61 Graphic visualizing the number of appearances of the land cover class with the highest proportion on the categories forest loss, forest gain and to urban

12 Personal declaration

« I hereby declare that the submitted thesis is the result of my own, independent work. All external sources are explicitly acknowledged in the thesis.»

A handwritten signature in black ink, appearing to read 'M. Müller', written over a horizontal line.

Michelle Müller, Freienbach 28.09.20